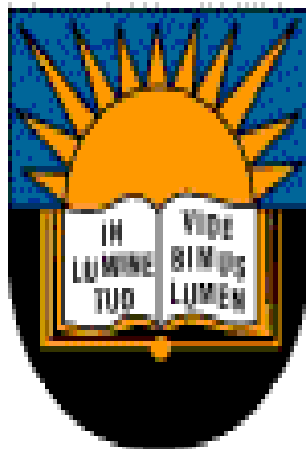


**Synthesis and evaluation of pyrene grafted onto zinc oxide nanoparticles for the removal
of organic contaminants from wastewater**



University of Fort Hare
Together in Excellence



Masters Research

By
University of Fort Hare
Together in Excellence
Zipho Samuel

Department of Chemistry

UNIVERSITY OF FORT HARE

SUPERVISOR: Prof. Omobola O. Okoh

CO-SUPERVISOR: Dr. Mike O. Ojemaye

March 2022

Preface

I performed the experimental work described in this dissertation at the Department of Chemistry, University of Fort Hare, Alice, from February 2020 to August 2021, under the supervision of Professor O Okoh and Doctor M.O Ojemaye.

The presented studies in this dissertation are my original work and have not been submitted in any form for any degree or diploma to any institution of higher learning. Where other works have been used, they have been duly acknowledged or adequately cited in this dissertation.

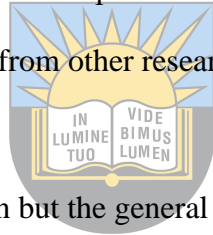


University of Fort Hare
Together in Excellence

Declaration 1 - Plagiarism

I, Zipho Samuel, declare that:

1. The research reported in this dissertation, except where indicated is my original work.
2. This dissertation has not been submitted at any other university for any degree or examination purposes.
3. This dissertation does not contain other person's data, pictures, graphs or other information, unless specifically acknowledged as being sourced from other people's work.
4. This dissertation does not contain other person's writing, unless specifically acknowledged as being sourced from other researchers. Where other written sources have been quoted, then:
 - a. Their words have been re-written but the general information attributed to them has been referenced.
5. This dissertation does not contain text, graphics or tables copied and pasted from the internet or any other source.



University of Fort Hare
Together in Excellence

Signature

A handwritten signature in black ink, appearing to read 'Zipho Samuel', is written over a dotted line.

Declaration 2 - Publications

Details of manuscripts that form part of this dissertation are provided herein:

Manuscript 1

Zipho Samuel, Mike O. Ojemaye, Omobola O. Okoh and Anthony I. Okoh: Adsorption of simazine herbicide from aqueous solution by novel pyrene functionalized zinc oxide nanoparticles: Kinetics and isotherm studies (unpublished).

I synthesized the novel adsorbent and evaluated its efficiency for the removal of simazine from aqueous medium. I also wrote the initial and final drafts of this manuscript under the supervision of Prof O. Okoh and Dr M.O Ojemaye. Prof A.I Okoh provided the funding. This work is presented in **chapter three** of this dissertation.

Manuscript 2

Zipho Samuel, Mike O. Ojemaye, Omobola O. Okoh and Anthony I. Zinc oxide nanoparticles functionalized with chelating nitrogenous groups for the adsorption of methyl violet in aqueous solutions (unpublished).



University of Fort Hare
Together in Excellence

I carried out synthesis and removal efficiency study of the adsorbent. Prof O. Okoh and Dr M.O Ojemaye guided me up to the final draft of this manuscript, with funding from Prof A.I Okoh. This manuscript is reported in **chapter four** of this dissertation.

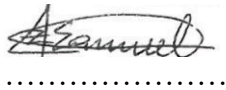
Manuscript 3

Zipho Samuel, Mike O. Ojemaye, Omobola O. Okoh and Anthony I. Okoh: Pyrene ligand grafted onto zinc oxide nanoparticles for the removal of brilliant green from aqueous solutions (unpublished).

Previously synthesised adsorbent in manuscript 2 was accessed for the removal of brilliant green from aqueous solutions. This work was done under the supervision of Prof O. Okoh and Dr M.O

Ojemaye. Prof A.I Okoh provided the funding. This work is reported in **chapter five** of this dissertation.

Signature:



.....



University of Fort Hare
Together in Excellence

Conference contributions

1. Oral presentation

Zipho Samuel, Mike O. Ojemaye, Omobola O. Okoh and Anthony I. Okoh. Zinc oxide nanoparticles functionalized with chelating nitrogenous groups for the adsorption of methyl violet in aqueous solutions. Presented at the International Conference on Water Resources Management and Sustainability: Solutions for Arid Regions, United Arab Emirate (22-24 March 2022).



University of Fort Hare
Together in Excellence

Certification

This is to certify that this research is a record of the original work carried out by Zipho Samuel under our supervision in the Department of Chemistry, University of Fort Hare in fulfilment of the requirements for the award of Masters of Science degree in Chemistry.

Supervisor's signature

Date

.....

.....

Co-supervisor's signature

Date

.....

.....



University of Fort Hare
Together in Excellence

Acknowledgements

I will like to acknowledge the below mentioned contributors to the success of this work:

- God for giving me strength to accomplish this work.
- My supervisors Prof O.O Okoh and Dr M.O Ojemaye who showed me great support throughout this study.
- South African Medical Research Council Microbial Water Monitoring Center based in the University of Fort Hare Alice campus (South Africa) for their financial support and facilities provided in the course of this study through Prof AI Okoh.
- Sasol Foundation based in South Africa for their bursary received during this study.
- Department of Chemistry for the opportunity and the offering of their laboratory facilities.
- Friends and family who were supportive throughout.



University of Fort Hare
Together in Excellence

Dedication

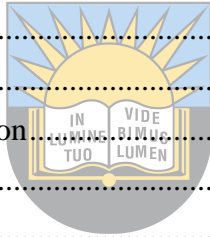
I will like to dedicate my master's degree to my parents, Mr Vusumzi Mbi and Miss Fezeka Samuel. I also like to dedicate this degree to my late high school principal, Mr Lizwe Ngalo for his contribution to the person I am today.



University of Fort Hare
Together in Excellence

Table of Contents

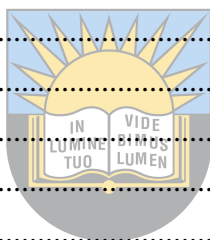
Preface.....	ii
Declaration 1 - Plagiarism	iii
Declaration 2 - Publications.....	iv
Conference contributions	vi
Certification	vii
Acknowledgements.....	viii
Dedication	ix
Table of Contents.....	x
List of Tables	xv
List of Figures.....	xvii
List of acronyms and abbreviations	xx
Abstract.....	xxiii
Chapter One	1
Introduction.....	1
1.1. Problem statement and justification.....	2
1.2. Null hypotheses.....	4
1.3. Aim	4
1.4. Objectives	5
1.5. Dissertation overview	5
References.....	6
Chapter Two.....	11
Literature review.....	11
2.1. Pesticides and their classifications.....	11
2.1.1. Target organism based classifications	11
2.1.1.1. Herbicides.....	11
2.1.1.2. Insecticides	13
2.1.1.3. Fungicides	14
2.1.2. Classification based on their chemical composition.....	16
2.1.2.1. Organochlorine pesticides	16
2.1.2.2. Organophosphorus pesticides.....	18
2.1.2.3. Organonitrogen pesticides.....	21
2.1.2.4. Pyrethroid pesticides	23



University of Fort Hare
Together in Excellence

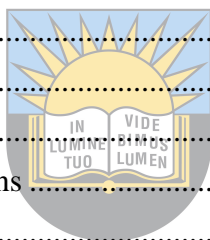
2.2.	Dyes and their classifications.....	25
2.2.1.	Classifications based on origin.....	26
2.2.1.1.	Natural dyes.....	26
2.2.1.2.	Synthetic dyes	27
2.2.2.	Classifications based on solution behaviour.....	29
2.3.	Effect and fate of pesticides in wastewater.....	33
2.3.1.	Cancer.....	34
2.3.2.	Asthma.....	35
2.3.3.	Dermatological problems	36
2.3.4.	Diabetes	37
2.3.5.	Endocrine disorders	38
2.4.	Effect and fate of dyes in wastewater	39
2.5.	Removal of pesticides from wastewater	40
2.6.	Dye removal techniques from polluted water.....	41
2.7.	Zinc oxide nanoparticles global industrial usage.....	42
2.8.	Metallic nanoparticles (MNPs) as potent materials for pesticides and dyes removal	43
2.9.	Metallic nanoparticles synthesis methods.....	48
2.9.1.	Sol – gel method.....	48
2.9.2.	Co-precipitation method.....	48
2.9.3.	Sonothermal method.....	48
2.9.4.	Microemulsion.....	49
2.9.5.	Green synthesis.....	49
2.10.	Most common metal oxide nanoparticles characterization techniques.....	50
	References.....	51
	Chapter Three.....	76
	Adsorption of simazine herbicide from aqueous solution by novel pyrene functionalized zinc oxide nanoparticles: Kinetics and isotherm studies.....	76
	Abstract.....	76
3.1.	Introduction.....	78
3.2.	Experimental	80
3.2.1.	Materials and chemicals	80
3.2.2.	Synthesis.....	81
3.2.2.1.	Synthesis of 1-(4-hydroxyphenyl)-4-phenyl-2,3-diazabutadiene (Pyrene).....	81
3.2.2.2.	Synthesis of zinc oxide nanoparticles (ZnO NPs).....	81
3.2.2.3.	Zinc oxide nanoparticles functionalization	82

3.2.3.	Characterization.....	83
3.2.4.	Adsorbate preparation.....	84
3.2.5.	Surface charge determination	84
3.2.6.	Adsorption studies	84
3.2.7.	Solid phase extraction (SPE)	85
3.2.8.	GC/ECD analysis.....	85
3.2.9.	Quality Assurance.....	86
3.2.10.	Desorption and reusability studies	86
3.2.11.	Data analysis	86
3.3.	Results and discussion	87
3.3.1.	Characterization.....	87
3.3.1.1.	FTIR analysis	87
3.3.1.2.	EDX analysis.....	88
3.3.1.3.	SEM analysis.....	89
3.3.1.4.	TEM analysis.....	89
3.3.1.5.	XRD analysis.....	90
3.3.1.6.	TGA analysis.....	91
3.3.2.	Adsorption studies	92
3.3.2.1.	pH effect.....	92
3.3.2.2.	Effect of contact time.....	93
3.3.2.3.	Effect of adsorbent amount	94
3.3.2.4.	Effect of adsorbate concentration.....	94
3.3.3.	Adsorption isotherms.....	95
3.3.4.	Adsorption kinetics.....	96
3.3.5.	Reusability and desorption studies	98
3.4.	Conclusion	98
	References.....	99
	Chapter Four	106
	Zinc oxide nanoparticles functionalized with chelating nitrogenous groups for the adsorption of methyl violet in aqueous solutions.....	106
	Abstract.....	106
4.1.	Introduction.....	108
4.2.	Methodology	110
4.2.1.	Materials and reagents	110
4.2.2.	Syntheses of materials	110



4.2.2.1.	Silica coated zinc oxide nanoparticles (ZnO-Si NPs)	110
4.2.2.2.	1-(4-hydroxyphenyl)-4-pyrenyl-2,3-diazabutadiene (Pyrene) synthesis	111
4.2.2.3.	Pyrene grafted onto zinc oxide nanoparticles (ZnO-Pyrene NPs) synthesis.....	112
4.2.3.	Characterization.....	113
4.2.4.	Adsorbate preparation.....	114
4.2.5.	Surface charge determination	114
4.2.6.	Adsorption studies	114
4.2.7.	Desorption and reusability studies.....	115
4.2.8.	Data analysis.....	116
4.3.	Results and discussion	116
4.3.1.	Characterization.....	116
4.3.1.1.	Functional group identification	116
4.3.1.2.	Morphology and composition of synthesized materials.....	117
4.3.1.3.	Particle size determination and shape confirmation.....	119
4.3.1.4.	Crystal information determination.....	120
4.3.1.5.	Purity and thermal stability of the materials	122
4.3.2.	Adsorption studies	123
4.3.2.1.	pH effect.....	123
4.3.2.2.	Effect of contact time	124
4.3.2.3.	Dose effect.....	124
4.3.2.4.	Effect of dye concentration	125
4.3.3.	Kinetic studies	126
4.3.4.	Adsorption isotherms.....	127
4.3.5.	Desorption and reusability studies.....	128
4.4.	Conclusion	129
	References.....	129
	Chapter Five.....	138
	Pyrene ligand grafted onto zinc oxide nanoparticles for the removal of brilliant green from aqueous solutions	138
	Abstract.....	138
5.1.	Introduction.....	139
5.2.	Methodology	141
5.2.1.	Materials and chemicals	141
5.2.2.	Synthesis and characterization of pyrene grafted zinc oxide nanoparticles	141
5.2.3.	Preparation of adsorbate solutions.....	141

5.2.4.	Point of zero charge	141
5.2.5.	Adsorbate removal experiment.....	142
5.2.6.	Reusability and desorption studies	143
5.2.7.	Data analysis.....	143
5.3.	Results and discussion	143
5.3.1.	Characterization.....	143
5.3.2.	Adsorption studies	144
5.3.2.1.	Influence of pH.....	144
5.3.2.2.	Influence of contact time.....	144
5.3.2.3.	Influence of adsorbent dose.....	145
5.3.2.4.	Influence of adsorbate concentration	145
5.3.3.	Kinetic studies	146
5.3.4.	Adsorption isotherms.....	148
5.3.5.	Reusability and desorption studies	149
5.4.	Conclusion	150
References	150
Chapter Six	157
General conclusion and recommendations	157
Appendix I	159
Data for simazine removal	159
Appendix II	168
Data for methyl violet removal	168
Appendix III	175
Data for brilliant green removal	175
Ethics clearance	182



University of Fort Hare
Together in Excellence

List of Tables

Table	Description	Page
Table 2.1	Show some commonly used organochlorine pesticides across the world.	17
Table 2.2	Show some commonly used organophosphorus pesticides across the world.	20
Table 2.3	Show some commonly used organonitrogen pesticides across the world.	22
Table 2.4	Show some commonly used pyrethroid pesticides across the world.	24
Table 2.5	Show some of the common global industrial usage of zinc oxide.	43
Table 2.6	Show some of commonly used metallic nanoparticles for pesticides' removal.	44
Table 2.7	Show some of previously adsorbents for various dyes' removal.	45
Table 2.8	Show commonly used adsorption kinetic models.	47
Table 2.9	Show commonly used adsorption isotherms.	47
Table 3.1	Show calibration data and quality assurance parameters.	86
Table 3.2	Show simazine adsorption isotherms' parameters.	96
Table 3.3	Show simazine adsorption onto the novel adsorbent kinetic models' parameters.	97
Table 4.1	Show methyl violet adsorption onto the novel adsorbent kinetic models' parameters.	126
Table 4.2	Show methyl violet adsorption isotherms' parameters.	128

Table 4.3	Show comparison of adsorption capacities of various methyl violet adsorbents from aqueous medium.	128
Table 5.1	Show brilliant green adsorption onto pyrene-ZnO nanoparticles kinetic models' parameters.	147
Table 5.2	Show brilliant green adsorption isotherms' parameters.	149



University of Fort Hare
Together in Excellence

List of Figures

Figure	Description	Page
Figure 2.1	Show chemical structures of common herbicides.	12 - 13
Figure 2.2	Show chemical structures of some common insecticides.	14
Figure 2.3	Show chemical structures of common fungicides.	15
Figure 2.4	Show chemical structures of common natural dyes.	27
Figure 2.5	Show chemical structures of some common synthetic dyes.	28
Figure 2.6	Show chemical structures of commonly studied cationic dyes.	30
Figure 2.7	Show chemical structures of some commonly studied anionic dyes.	31
Figure 2.8	Show commonly used non-ionic dyes chemical structures.	32
Figure 3.1	Show chemical structure of simazine.	78
Figure 3.2	Show synthesis of 1-(4-hydroxyphenyl)-4-pyrenyl-2,3-diaza-1,3-butadiene.	81
Figure 3.3	Show preparation of novel pyrene functionalized ZnO NPs.	83
Figure 3.4	Show FTIR spectra of ZnO, ZnO-Pyrene and Pyrene ligand.	87
Figure 3.5	Show EDX spectra of (a) ZnO (b) ZnO-Pyrene and (c) Pyrene ligand.	88
Figure 3.6	Show SEM images of (a) ZnO (b) ZnO-Pyrene and (c) Pyrene ligand.	89
Figure 3.7	Show synthesized NPs TEM images (a) ZnO NPs and (b) ZnO-Pyrene NPs and their particle size distributions.	90
Figure 3.8	Show XRD diffractograms of ZnO and pyrene functionalized ZnO nanoparticles.	91
Figure 3.9	Show TGA curves of (a) ZnO and (b) ZnO-Pyrene nanoparticles.	92

Figure 3.10	Show (a) Point zero charge curve of ZnO-Pyrene nanoparticles and (b) pH effect.	93
Figure 3.11	Show effect of contact time.	93
Figure 3.12	Show effect of adsorbent amount.	94
Figure 3.13	Show effect of adsorbate concentration.	95
Figure 3.14	Show reusability and desorption studies.	98
Figure 4.1	Show chemical structure of methyl violet.	108
Figure 4.2	Show preparation of silica coated ZnO NPs.	111
Figure 4.3	Show synthesis of 1-(4-hydroxyphenyl)-4-pyrenyl-2,3-diaza-1,3-butadiene.	111
Figure 4.4	Show preparation of amine modified ZnO NPs.	112
Figure 4.5	Show preparation of carboxylic modified ZnO NPs.	112
Figure 4.6	Show preparation of pyrene grafted onto ZnO NPs.	113
Figure 4.7	Show FTIR spectra of ZnO-Si, ZnO-NH ₂ , ZnO-COOH and ZnO-Pyrene.	117
Figure 4.8	Show SEM images of (a) ZnO-Si, (b) ZnO-NH ₂ , (c) ZnO-COOH and (d) ZnO-Pyrene NPs.	118
Figure 4.9	Show EDX spectra of (a) ZnO-Si, (b) ZnO-NH ₃ , (c) ZnO-COOH and (d) ZnO-Pyrene NPs.	119
Figure 4.10	Show TEM images of (a) ZnO-Si, (b) ZnO-NH ₂ , (c) ZnO-COOH and ZnO-Pyrene nanoparticles and their particle distributions.	120
Figure 4.11	Show XRD spectra of ZnO-Si, ZnO-NH ₂ , ZnO-COOH and ZnO-Pyrene.	121
Figure 4.12	Show TGA curve of (a) ZnO-Si (b) ZnO-NH ₂ (c) ZnO-COOH and (d) ZnO-Pyrene NPs.	122

Figure 4.13	Show pH effect curve on MV adsorption.	123
Figure 4.14	Show contact time effect curve on MV adsorption capacity.	124
Figure 4.15	Show adsorbent dose effect curve on MV adsorption.	125
Figure 4.16	Show adsorbate concentration effect on adsorption capacity of MV onto the adsorbent.	125
Figure 4.17	Show adsorption and desorption of methyl violet.	129
Figure 5.1	Show (a) point of zero charge (b) influence of pH (c) influence of contact time (d) influence of adsorbent dose and (e) influence of adsorbate concentration.	146
Figure 5.2	Show adsorption and desorption of BG onto ZnO-Pyrene.	150



University of Fort Hare
Together in Excellence

List of acronyms and abbreviations

^{13}C NMR - carbon 13 nuclear magnetic resonance

^1H NMR - proton nuclear magnetic resonance

AEMRG – Applied Environmental and Microbiology Research Group

AL – Alachlor

ALD – Aldicarb

APTES – 3-aminopropyltriethoxysilane

ATR – Atrazine

AU – Arbitrary units

Ave – Average

BF – Bifenthrin

BG - Brilliant green

BHR – Bronchial hyper-reactivity

CBL – Carbaryl

CLD – Chlordane

CVP – Chlorfenvinphos

DCC – Dicyclohexylcarbodiimide

DDT – Dichlorodiphenyltrichloroethane

DLM – Deltamethrin

DMAP – 4-dimethylaminopyridine

DMDT – Methoxychlor

DMF – Dimethylformide

DZ – Diazinon



University of Fort Hare
Together in Excellence

EDCs - Endocrine Disruptive Chemicals

EDX - Energy Dispersive X-ray

FEN – Fenvalerate

FNP – Fenpropathrin

FTIR - Fourier-Transform Infra-Red spectroscopy

GAC – Granular activated carbon

GC/ECD – Gas chromatograph equipped with electron capture detector

HCH – Hexachlorocyclohexane

IARC - International Agency for Research on Cancer

LOD - Limit of detection

LOQ - Limit of quantification

ML – Metolachlor

MLT – Malathion

MP – Methyl parathion

MV - Methyl violet

NPs – Nanoparticles

OCPs – Organochlorine pesticides

ONPs – Organonitrogen pesticides

OP – Organophosphorus

OPPs – Organophosphorus pesticides

PAC – Powder activated carbon

SAMRC – South Africa Medical Research Council

SbS – Shell-by-Shell



University of Fort Hare
Together in Excellence

SDG - Sustainable development goals

SEM - Scanning Electron Microscopy

SPE – Solid Phase Extraction

T₁D – Type 1 diabetes

T₂D – Type 2 diabetes

TCDD - 2,3,7,8- tetrachlorodibenzo-p-dioxin

TEM - Transmission Electron Microscopy

TEOS - Tetraorthosilicate

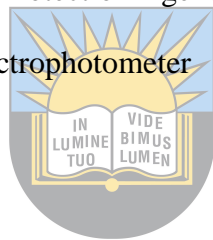
TGA - Thermo-Gravimetric Analyser

USEPA – United States Environmental Protection Agency

UV-Vis – Ultra Violet-Visible light spectrophotometer

XRD - X-Ray Diffractometer

γ – HCH – Lindane



University of Fort Hare
Together in Excellence

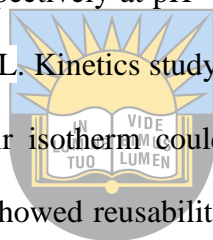
Abstract

Drinking water scarcity is a global crisis even though water covers about three quarters of the earth. One of the major causes of this scarcity is water pollution, which is a result of human activities. This has been noticed and reported for a number of years but is still unsolved and intensifying. Hence, scientists are busy trying to find solutions to this global menace. In this study, zinc oxide nanoparticles were synthesised via co-precipitation, a cost reasonable method and functionalized by grafting a pyrene ligand on its surface in order to provide a scaffold to which many other functionalities can be adsorbed. By so doing, the efficiency and capacity of bare nanoparticles is improved. The synthesised pyrene ligand was successfully characterised with nuclear magnetic resonance (NMR) and Fourier transform infrared spectroscopy (FTIR). The adsorbent was characterized using X-ray diffractometer (XRD), scanning electron microscope (SEM), transmission electron microscope (TEM), FTIR, energy dispersive x-ray (EDX) and thermogravimetric analyzer (TGA). The choice of zinc oxide nanoparticles as preferred adsorbent was due to their exceptional properties including large surface area, thermal and chemical stabilities. These properties are the reason zinc oxide nanoparticles possess high adsorption efficiency and capacity.

The results of characterization indicated a decreased particle size and improved thermal stabilities of the pyrene grafted zinc oxide nanoparticles compared to the zinc oxide nanoparticles, showing that this material can be employed even at higher temperatures. The average particle size of the bare nanoparticles decreased from 290 to 181 nm after functionalization. Thermal stability increased from 550°C in the bare nanoparticles to 650°C in the functionalized nanoparticles. Characteristic reflections of zinc oxide nanoparticles in the XRD analysis were maintained even after functionalization (i.e. 31.8 °, 34.5 °, 36.3 °, 47.6 °, 56.6 °, 62.9 °, 66.5 °, 68.0 ° and 69.2 °).

However, diffractogram roughness was noticed for the functionalized nanoparticles due to the introduction of the amorphous layer from the ligand.

This novel material was employed for the removal of an herbicide, simazine as well as two dyes, methyl violet and brilliant green from aqueous solutions by batch adsorption experiments. The kinetics and isotherm studies of the different adsorption processes were carried out by using three of the commonly used kinetic and isotherm models (pseudo-first order, intraparticle diffusion and pseudo-second order) and (Langmuir, Temkin isotherms and Freundlich) respectively. From all batch adsorption experiments conducted for simazine removal, the adsorbent showed effectiveness and high adsorption capacity for the removal of simazine. The highest observed efficiency and capacity were 71.3% and 137 mg/g respectively at pH = 2, time = 60 minutes, adsorbent dose = 20 mg and adsorbate conc = 0.281 mg/L. Kinetics study for the adsorption of simazine favoured pseudo-first order. However, Langmuir isotherm could also be applicable to understand the adsorption process. The material also showed reusability potential of up to three cycles for this contaminant indicating that this material can be re-used.



University of East Hare
Together in Excellence

In the case of the removal of methyl violet from aqueous solution, the adsorbent showed a reasonable adsorption maximum capacity (q_{\max}) (31.5 mg/g) at contact time = 360 min, adsorbent dose approximately = 40 mg, temperature = $20 \pm 2^\circ\text{C}$ and pH = 6.5, when compared to other adsorbents previously reported for the removal of methyl violet (MV) in literature. Kinetics and isotherm studies indicated that the process for the removal of this pollutant with this pyrene grafted onto zinc oxide nanoparticles proceeded via pseudo-first order ($R^2 = 0.931$) and Langmuir isotherm models ($R^2 = 0.980$) respectively. These results indicated that this material could serve as alternate material to already established materials for the removal of recalcitrant organic

pollutants from aqueous solutions. Moreover, the adsorbent also showed reusability potential for this contaminant.

Similarly, the adsorbent showed high removal efficiency and capacity in all batch adsorption experiments for brilliant green (BG) adsorption. The highest adsorption efficiency of 88.8% was accomplished with 79.8 mg at pH 6.50 and temperature of $20 \pm 2^\circ\text{C}$ within 360 minutes. BG adsorption rate mechanism was best explained by the pseudo-first order kinetic model ($R^2 = 0.903$). Dye adsorption behaviour was best explained using Langmuir isotherm ($R^2 = 0.980$). Reusability of the adsorbent showed that the adsorbent is efficient after three runs. The overall results of adsorption by a way of comparison of the adsorption capacity of this novel material with respect to the contaminants is in this trend: brilliant green > methyl violet > simazine. This study indicates that this novel material can serve as new material for the removal of herbicides and dyes as well as vast variety of pollutants from wastewater considering its high adsorption efficiency and its recyclability. Thus, industries can explore the use of this material for the removal of varying pollutants from wastewater.

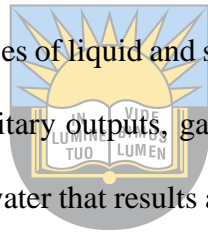


University of Fort Hare
Together in Excellence

Chapter One

Introduction

Water is the most fundamental substance of life on this planet, and a valuable resource for human survival. One of the key sustainable development goals (SDG) is to ensure availability and sustainable management of water and sanitation for all, and this is considered, and remains a major global crisis as a result of global climate change, industrialization, population growth and water quality deterioration (Sandia, 2003; Tyagi, 2016). Water covers about 70% of the earth's surface and is a principal receiver of the discharges of both organic and inorganic pollutants. Wastewater can be defined as used contaminated or polluted water. Generally, it is classified as domestic or industrial wastewater (Carolin *et al.*, 2017). This classification is based on the source of origin. Domestic wastewater comprises of liquid and solid discharges from non-manufacturing processes, which includes sewage, sanitary outputs, garbage, detergents etc (Tee *et al.*, 2016). However, the industrial wastewater is water that results after an industrial process. The release of untreated industrial wastewater has been reported as a major source of water pollution (Carolin *et al.*, 2017).



University of Fort Hare
Together in Excellence

Organic pollutants are carbon-based chemicals like pharmaceuticals, solvents, dyes and pesticides, which end up in water streams because of farmlands runoff, factories and wastewater discharge. However, inorganic pollutants include toxic heavy metals, which are not carbon-based. Both groups of pollutants affect the chemical and physical properties of water and cause a significant threat to human well-being. Dyes from industrial effluents (e.g., leather, paper, textiles and cosmetics industries) are one of the hazardous materials to water sources specifically and environment in general (Yu *et al.*, 2014). Most dyes are highly recalcitrant to conventional physical (ion exchange, irradiation, membrane filtration) and biological water treatment (aerobic and anaerobic digestion) methods (Zhang and Wu, 2014). These substances are highly resistant to biodegradation since their compounds contain complex aromatic structures. Untreated

effluents containing dyes when released to large water bodies lead to colour increase in water even at low amounts (less than 1 ppb), therefore making polluted water more detrimental (Zhang and Wu, 2014). Since water colouration prevents sunlight penetration in water, the dissolved oxygen levels are reduced and vice versa for biological oxygen demand (BOD) (Carmen and Daniela, 2012). Because of the latter effects, aquatic biota are exposed to greater environmental hazard due to dyes' disposal (Shanker *et al.*, 2017). These substances are also persistent; therefore, they can accumulate and cause serious health problems in human through direct exposure or food chain. On the other hand, pesticides are various agents that are classified based on their potential of killing different types of living creatures (Ahmad *et al.*, 2010). Pesticides are distinct from other chemical substances since they are purposely dispersed in the environment (e.g. agricultural farmlands) (Corsini *et al.*, 2008). Moreover, they are synthesised to disrupt specific living organisms and predictably characterized by variable levels of toxicity (Corsini *et al.*, 2008). They are mainly classified by taking into consideration two criteria: target organism and chemical classes (Ahmad *et al.*, 2010). Pesticides are used intentionally to protect agricultural farmlands from pests; however, their remains can reach beyond their target areas through overland, groundwater, atmospheric and subsurface routes as stated by Groenendijk *et al.* (1994). As a result, they have been associated with human health problems. Due to these negative effects of the aforementioned pollutants in water and the environment, there is an urgent need for studies to be conducted to device means for the removal of these pollutants from water. This serves as the motivation of this study.

1.1. Problem statement and justification

Availability of water is a global concern as mentioned in the introduction and reported by other researchers (Sandia, 2003; Tyagi, 2016) because water is a critical feedstock for many industries and homes (Savage and Diallo, 2005). Moreover, water is also essential for all life on earth. It is also worth to mention that majority of developing countries heavily rely on agriculture (Praburaj

et al., 2018), which uses more water. However, because of water scarcity they struggle to maximize their profits. This is why many African countries are still undeveloped. Hence, sustainable development goal 6 was developed to counteract this. Water scarcity leads to poverty and unemployment since farmers employ fewer workers even though aiming for maximum production, which is hardly met because of the aforementioned crisis. Thus, farmers use more of supplementary substances such as fertilizers and pesticides to overcome failure to maximize production. The use of these supplementary substances contributes to water pollution and indirectly intensifies water scarcity as these substances reach up to water stream and pollute them (Norse, 2005; Adeyemo, 2003). Water pollution also leads to the growth of illnesses and fatal diseases like cancer and endocrine disorders, which has been associated with pesticides (Kim *et al.*, 2017; Sanborn *et al.*, 2007). For a number of years, cancer has been reported amongst top 10 causes of death globally (Rana *et al.*, 2021). Just like pesticides, organic dyes have also been associated with cancer due to their carcinogenicity (Decouple, 1979). Even so, their use is still intensifying because of population and industrialization growth. Owing to their persistence these substances persist in environmental matrices thus causing imbalances on the ecosystem and affects people directly or indirectly. Due to these concerns, several methods/techniques have been developed and adopted for the removal of these pollutants in water/wastewater.

Adsorption has gained more recommendation from these techniques (Esposito *et al.*, 2013; Sannino *et al.*, 2013; Auta and Hameed, 2012; Chen *et al.*, 2011). Hence, many adsorbents have been developed and adopted for both pesticides and dyes removal from water/wastewater. Even though these adsorbent materials including magnetic metal-ceramic nanocomposites (Pansini *et al.*, 2018), iron oxide nanoparticles (Eshete *et al.*, 2018), hydroxypropyl- β -cyclodextrin-polyurethane magnetic nanoconjugates (Nasiri and Alizadeh, 2019), AgI modified TiO₂ nanoparticles (Jafari *et al.*, 2012), ZnS nanoparticles loaded activated carbon (Jamshidi *et al.*, 2016), graphite oxide nanoparticle (Ghaedi *et al.*, 2014) and so on have shown promises for the removal of diverse types of contaminants/ pollutants from water. Their applicability has been

ascribed to their surface area and high porosity, their widespread use is limited because of poor adsorption capabilities, high cost of preparation, difficulty in disposing and regenerating them. Thus other more efficient, easily disposable and regenerated alternatives should be established. Literature search revealed that some adsorbent materials and nanoparticles, which have been mostly employed for the elimination of contaminants from wastewater especially dyes, have concerns such as particle aggregation and agglomeration (Mahl *et al.*, 2013), which leads to particle size increase thus decreasing their adsorption capability. Zinc oxide nanoparticles have been reported to be more efficient as a result of their increased surface area, great chemical and thermal stabilities and ability to graft other functionalities on their surface (Ozgür *et al.*, 2005; Kango *et al.*, 2013; Wang *et al.*, 2021). Moreover, zinc oxide nanoparticles are non-magnetic in nature therefore they usually experience lesser aggregation compared to magnetic nanoparticles thus making their particle size easily controllable. In addition, introducing multidentate ligands such as 1-(4-hydroxyphenyl)-4-pyrenyl-2,3-diaza-1,3-butadiene on their surfaces may improve their adsorbing capabilities, since these ligands provide them a scaffold onto which other organic functionalities can be attached. By doing so, these introduced ligands also reduce aggregation of bare nanoparticles even more.

1.2. Null hypotheses

- I. Pyrene grafted onto zinc oxide nanoparticles will not adsorb organic herbicide.
- II. Pyrene grafted onto zinc oxide nanoparticles will not adsorb organic dyes.
- III. The rate of adsorption will not differ for different organic contaminants.
- IV. The rate of adsorption will not decrease with increasing time.

1.3. Aim

The aim of this research is to synthesize and characterize pyrene grafted onto zinc oxide nanoparticles and determine their effectiveness for the removal of organic contaminants (herbicide simazine and organic dyes; methyl violet and brilliant green) from wastewater.

1.4. Objectives

- I. To synthesize and characterize zinc oxide nanoparticles.
- II. To synthesize and characterize 1-(4-hydroxyphenyl)-4-pyrenyl-2,3-diaza-1,3-butadiene (pyrene ligand).
- III. To synthesize and characterize pyrene ligand grafted onto zinc oxide nanoparticles.
- IV. To determine the efficiency of pyrene grafted onto zinc oxide nanoparticles for the removal of organic contaminants including one herbicide and two dye compounds from wastewater through batch adsorption experiments.
- V. To carry out desorption studies for the used adsorbents in order to ascertain their reusability.

1.5. Dissertation overview

This dissertation contains six chapters that are described briefly below. The novelty of this project includes the synthesis of 1-(4-hydroxyphenyl)-4-phenyl-2,3-diaza-1,3-butadiene ligand grafted onto zinc oxide nanoparticles by using covalent bonding. It also includes their first time application for the removal of one herbicide, simazine and two dye compounds; methyl violet and brilliant green from water. In this dissertation, isotherm and kinetic studies were also carried out to bring about the understanding of the mechanism of each adsorption process; desorption and reusability studies were as well carried out to determine the recyclability and reusability potentials respectively of this novel adsorbent. This dissertation is in manuscript format and consists of a number of stand-alone chapters. However, the entire dissertation is coherent with the objectives of the entire project.

Chapter 1 includes a brief introduction on water scarcity, causes of water scarcity including water pollution. It further highlights the contributing substances/chemicals to water pollution especially the ones that are subjects of this research study. Justification of this study, null hypotheses, aim and specific objectives are also presented in this chapter.

Chapter 2 gives literature review on the topic of the study, description of types and classifications of organic dyes and pesticides. It also gives description of their effect and fate, remediation techniques, metallic nanoparticles as potent adsorbents. Furthermore, metallic nanoparticles synthesis methods and characterization techniques were also discussed under this chapter.

Chapter 3 includes synthesis and characterization of the novel material synthesized from zinc oxide nanoparticles and 1-(4-hydroxyphenyl)-4-phenyl-2,3-diaza-1,3-butadiene ligand, evaluation of its efficiency for the removal of simazine through batch adsorption experiments, kinetic and isotherm studies. In addition, this chapter also presents the desorption and reusability studies of the adsorbent accordingly.

Chapter 4 presents the synthesis of novel zinc oxide nanoparticles functionalized with chelating nitrogenous groups (1-(4-hydroxyphenyl)-4-phenyl-2,3-diazo-1,3-butadiene ligand) and the characterization of the synthesized materials. It also includes adsorption, kinetic, isotherm, desorption and reusability studies for the removal of methyl violet from aqueous solutions.

Chapter 5 presents the adsorption, isotherm, kinetic studies, and desorption studies of pyrene ligand grafted onto zinc oxide nanoparticles for the sequestering of brilliant green from water.

Chapter 6 gives the general conclusions and recommendations on this study.

References

- Adeyemo, O.K., 2003. Consequences of pollution and degradation of Nigerian aquatic environment on fisheries resources. *Environmentalist*, 23(4), pp.297-306.
- Ahmad, T., Rafatullah, M., Ghazali, A., Sulaiman, O., Hashim, R. and Ahmad, A., 2010. Removal of pesticides from water and wastewater by different adsorbents: a review. *Journal of Environmental Science and Health, Part C*, 28(4), pp.231-271.
- Auta, M. and Hameed, B.H., 2012. Modified mesoporous clay adsorbent for adsorption isotherm and kinetics of methylene blue. *Chemical Engineering Journal*, 198, pp.219-227.

Carmen, Z. and Daniela, S., 2012. *Textile organic dyes-characteristics, polluting effects and separation/elimination procedures from industrial effluents-a critical overview* (Vol. 3, pp. 55-86). Rijeka: IntechOpen.

Carolyn, C.F., Kumar, P.S., Saravanan, A., Joshiba, G.J. and Naushad, M., 2017. Efficient techniques for the removal of toxic heavy metals from aquatic environment: a review. *Journal of Environmental Chemical Engineering*, 5(3), pp.2782-2799.

Chen, D., Chen, J., Luan, X., Ji, H. and Xia, Z., 2011. Characterization of anion-cationic surfactants modified montmorillonite and its application for the removal of methyl orange. *Chemical Engineering Journal*, 171(3), pp.1150-1158.

Corsini, E., Liesivuori, J., Vergieva, T., Van Loveren, H. and Colosio, C., 2008. Effects of pesticide exposure on the human immune system. *Human & Experimental Toxicology*, 27(9), pp.671-680.

Decouple, P., 1979. Cancer risks associated with employment in the leather and leather products industry. *Archives of Environmental Health: An International Journal*, 34(1), pp.33-37.



University of Fort Hare
Together in Excellence

Eshete, M., Bowleg, J., Perales, S.G., Okunrobo, M., Watkins, D. and Spencer, H., 2018. Adsorption of propazine, simazine and bisphenol A on the surface of nanoparticles of iron oxide nanoparticles of carbon and metallic oxides. *Journal of Environmental Protection*, 9(1), pp.13.

Esposito, S., Sannino, F., Pansini, M., Bonelli, B. and Garrone, E., 2013. Modes of interaction of simazine with the surface of model amorphous silicas in water. *The Journal of Physical Chemistry C*, 117(21), pp.11203-11210.

Ghaedi, M., Zeinali, N., Ghaedi, A.M., Teimuori, M. and Tashkhourian, J., 2014. Artificial neural network-genetic algorithm based optimization for the adsorption of methylene blue and brilliant green from aqueous solution by graphite oxide nanoparticle. *Spectrochimica Acta Part A: Molecular and Biomolecular Spectroscopy*, 125, pp.264-277.

Groenendijk, P., van der Kolk, J.W. and Travis, K.Z., 1994. Prediction of exposure concentration in surface waters. *Freshwater Field Tests for Hazard Assessment of Chemicals*, pp.105-125.

Jafari, S., Azizian, S. and Jaleh, B., 2012. Enhancement of methyl violet removal by modification of TiO₂ nanoparticles with AgI. *Journal of Industrial and Engineering Chemistry*, 18(6), pp.2124-2128.

Jamshidi, M., Ghaedi, M., Dashtian, K., Ghaedi, A.M., Hajati, S., Goudarzi, A. and Alipanahpour, E., 2016. Highly efficient simultaneous ultrasonic assisted adsorption of brilliant green and eosin B onto ZnS nanoparticles loaded activated carbon: artificial neural network modeling and central composite design optimization. *Spectrochimica Acta Part A: Molecular and Biomolecular Spectroscopy*, 153, pp.257-267.

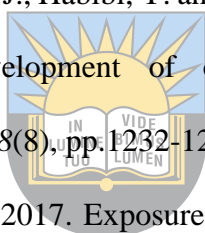
Kango, S., Kalia, S., Celli, A., Njuguna, J., Habibi, Y. and Kumar, R., 2013. Surface modification of inorganic nanoparticles for development of organic–inorganic nanocomposites—A review. *Progress in Polymer Science*, 38(8), pp.1232-1261.

Kim, K.H., Kabir, E. and Jahan, S.A., 2017. Exposure to pesticides and the associated human health effects. *Science of the Total Environment*, 575, pp.525-535.

Mahl, D., Diendorf, J., Meyer-Zaika, W. and Epple, M., 2011. Possibilities and limitations of different analytical methods for the size determination of a bimodal dispersion of metallic nanoparticles. *Colloids and Surfaces A: Physicochemical and Engineering Aspects*, 377(1-3), pp.386-392.

Nasiri, S. and Alizadeh, N., 2019. Synthesis and adsorption behavior of hydroxypropyl- β -cyclodextrin–polyurethane magnetic nanoconjugates for crystal and methyl violet dyes removal from aqueous solutions. *Royal Society of Chemistry Advances*, 9(42), pp.24603-24616.

Norse, D., 2005. Non-point pollution from crop production: Global, regional and national issues. *Pedosphere*, 15(4), pp.499-508.



University of Fort Hare
Together in Excellence

Özgür, Ü., Alivov, Y.I., Liu, C., Teke, A., Reshchikov, M., Doğan, S., Avrutin, V.C.S.J., Cho, S.J. and Morkoç, A.H., 2005. A comprehensive review of ZnO materials and devices. *Journal of Applied Physics*, 98(4), p.11.

Pansini, M., Sannino, F., Marocco, A., Allia, P., Tiberto, P., Barrera, G., Polisi, M., Battista, E., Netti, P.A. and Esposito, S., 2018. Novel process to prepare magnetic metal-ceramic nanocomposites from zeolite precursor and their use as adsorbent of agrochemicals from water. *Journal of Environmental Chemical Engineering*, 6(1), pp.527-538.

Praburaj, L., Design, F. and Nadu, T., 2018. Role of agriculture in the economic development of a country. *Shanlax International Journal of Commerce*, 6(3), pp.1-5.

Rana, J.S., Khan, S.S., Lloyd-Jones, D.M. and Sidney, S., 2021. Changes in mortality in top 10 causes of death from 2011 to 2018. *Journal of General Internal Medicine*, 36(8), pp.2517-2518.

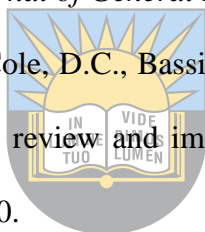
Sanborn, M., Kerr, K.J., Sanin, L.H., Cole, D.C., Bassil, K.L. and Vakil, C., 2007. Non-cancer health effects of pesticides: systematic review and implications for family doctors. *Canadian Family Physician*, 53(10), pp.1712-1720.

Sandia, D., 2003. Water purification roadmap—a report of the executive committee, US Department of the Interior, Bureau of Reclamation and Sandia National Laboratories. Report 2003.

Sannino, F., Ruocco, S., Marocco, A., Esposito, S. and Pansini, M., 2013. Simazine removal from waters by adsorption on porous silicas tailored by sol–gel technique. *Microporous and Mesoporous Materials*, 180, pp.178-186.

Savage, N. and Diallo, M.S., 2005. Nanomaterials and water purification: opportunities and challenges. *Journal of Nanoparticle Research*, 7(4-5), pp.331-342.

Shanker, U., Rani, M. and Jassal, V., 2017. Degradation of hazardous organic dyes in water by nanomaterials. *Environmental Chemistry Letters*, 15(4), pp.623-642.



University of Fort Hare
Together in Excellence

Tee, P.F., Abdullah, M.O., Tan, I.A.W., Rashid, N.K.A., Amin, M.A.M., NolascoHipolito, C. and Bujang, K., 2016. Review on hybrid energy systems for wastewater treatment and bio-energy production. *Renewable and Sustainable Energy Reviews*, 54, pp.235-246.

Tyagi, P.K., 2016. Nanotechnology helps to save water for developed a multitier Tdistribution pipe system on wastewater exit point in multistory buildings. *International Journal of Current Microbiology and Applied Sciences*, 5(5), pp.816-821.

Wang, Z., Bockstaller, M.R. and Matyjaszewski, K., 2021. Synthesis and applications of ZnO/polymer nanohybrids. *American Chemistry Society Materials Letters*, 3(5), pp.599-621.

Yu, J.G., Zhao, X.H., Yang, H., Chen, X.H., Yang, Q., Yu, L.Y., Jiang, J.H. and Chen, X.Q., 2014. Aqueous adsorption and removal of organic contaminants by carbon nanotubes. *Science of the Total Environment*, 482, pp.241-251.

Zhang, W. and Wu, C.W., 2014. Dyeing of multiple types of fabrics with a single reactive azo disperse dye. *Chemical Papers*, 68(3), pp.330-335.



University of Fort Hare
Together in Excellence

Chapter Two

Literature review

Due to the negative effects of dyes and pesticides in the environment and human, in this chapter, detailed discussion on dyes and pesticides together with their classifications, their effects and fate in wastewater will be reported as well as their remediation techniques. In addition, owing to the importance of adsorption techniques including their high efficiency, simplicity and flexibility, adsorption will be discussed in relation to metallic nanoparticles for the removal of the pollutants under consideration in this study. The synthesis routes and characterizations techniques for zinc oxide nanoparticles and their functionalization will also be discussed in depth herein.

2.1. Pesticides and their classifications

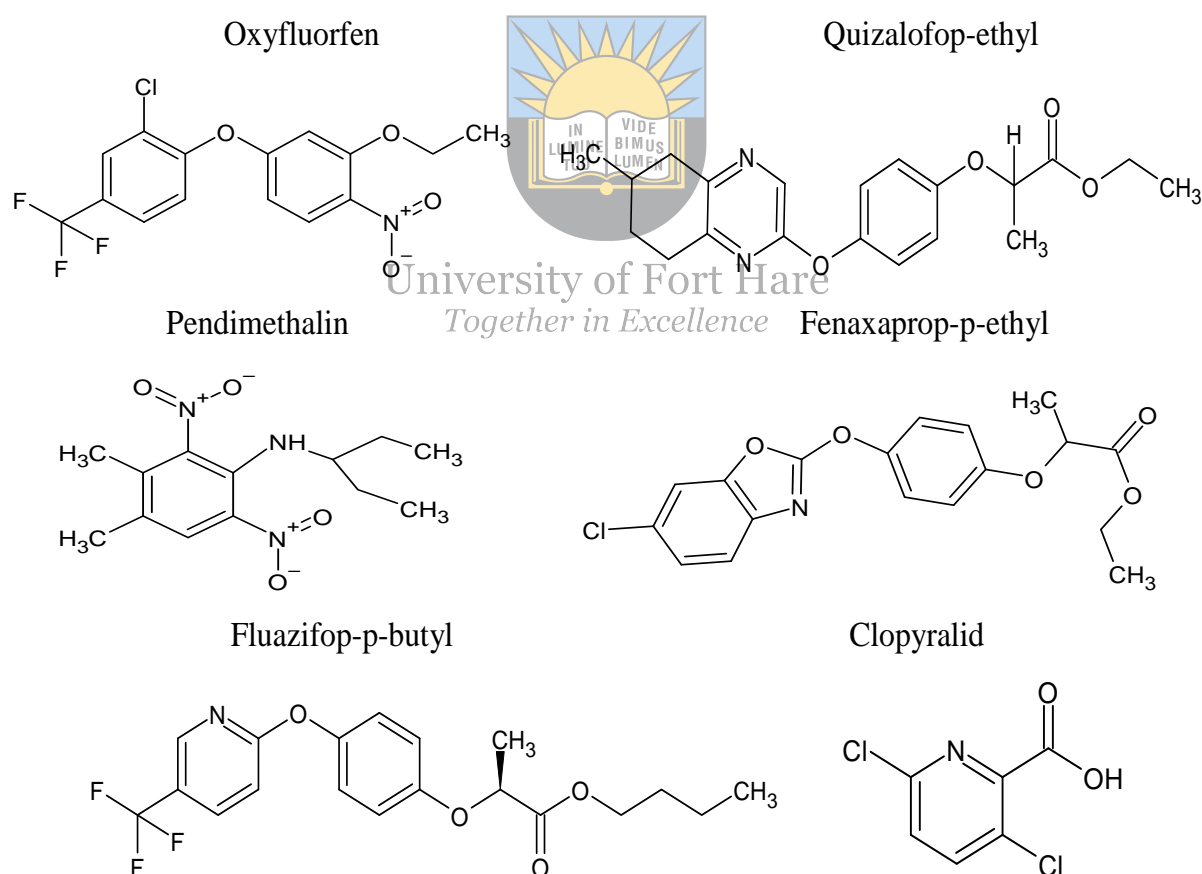
Pesticides are numerous and diverse groups of chemical compounds, with the primary goal of eliminating pests in households and agricultural farmlands (Fenik *et al.*, 2011). Their diversity in chemical composition results in different physicochemical properties within a chemical class (e.g. organochlorine pesticides) and across different chemical classifications. As a result, their use in agricultural systems is probably the most important factor, which has contributed to the national (Quinn *et al.*, 2011) and worldwide increase in food production (Kim and Smith, 2001). Despite their advantages, they are regarded among the most environmentally stable, mobile and toxic substances (Fenik *et al.*, 2011).

2.1.1. Target organism based classifications

2.1.1.1. Herbicides

Herbicides are chemicals that are mainly used to kill weeds without causing any harm to the crops when properly selected and applied (Qasem, 2011). Herbicides inhibit weeds through metabolic processes by interaction with the specific protein (Dayan *et al.*, 2010). Kughur (2012) reported that herbicide application is not only limited to crop production, they can also be used in animal

production to control infectious diseases and parasites that emerge under extremely crowded conditions. Herbicides can either be organic or inorganic chemicals (California Weed Conference, 1985). They can be easily selected from botanicals or mycoherbicides (Mo and He, 2005). However, they are of high public concerns and have received high criticism nowadays (Qasem, 2011). Qasem (2011) also reported that synthetic herbicides are still intensively applied in developing and developed countries for weed control. Tamang *et al.* (2015) reported that in India, yield loss due to weeds can vary from 40-68% and this is quite high. The authors further reported that already existing pre and post emergence herbicides such as oxyfluorfen, quizalofop-ethyl, pendimethalin and fenaxaprop-p-ethyl (Figure 2.1) can be used to monitor the emergence and growth of broadleaved weeds and annual grasses.



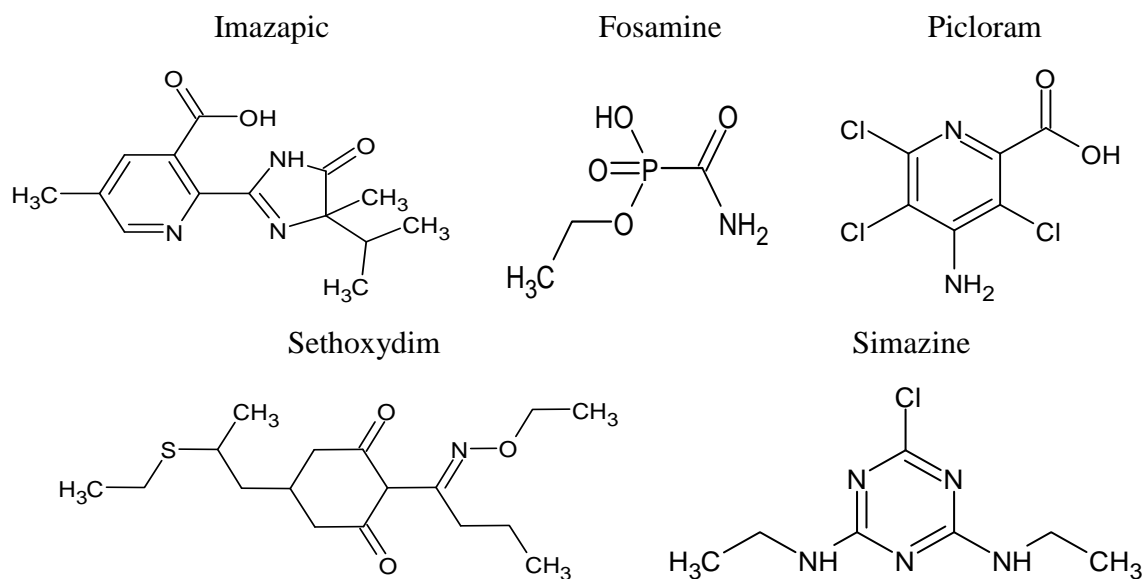


Figure 2.1: Chemical structures of some common herbicides.

2.1.1.2. Insecticides

Insecticides are agents of biological or chemical origins that are used in agriculture, forestry, horticulture and domestically to control pests, which may be vectors for animal and human diseases (Gupta *et al.*, 2019). Mossa *et al.* (2018) reported two major types of insecticides, synthetic and natural insecticides. Synthetic insecticides, referring to groups of chemicals based on their mode of toxic action (i.e. organochlorines, carbamates, organophosphates, and pyrethroids) (Figure 2.2) and the natural insecticides including azadirachtin, spinosad, abamectin and rotenone. As a result of the widespread and long-term application of synthetic insecticides, their residues have accumulated in food, milk, soil, water and other environmental compartments (Mossa *et al.*, 2018). Natural insecticides include mineral, chemical and biological materials, which may be found in the markets (i.e. pyrethrum, spinosad, neem, abamectin, rotenone, bacillus thuringiensis (Bt), garlic, pepper, cinnamon, and some essential oil products) (Kaya and Vega, 2012). Natural insecticides' safety and selectivity are not exact and some of the natural compounds are toxic; for instance, nicotine and arsenic, these insecticides have been banned in most countries (Mossa *et al.*, 2018).

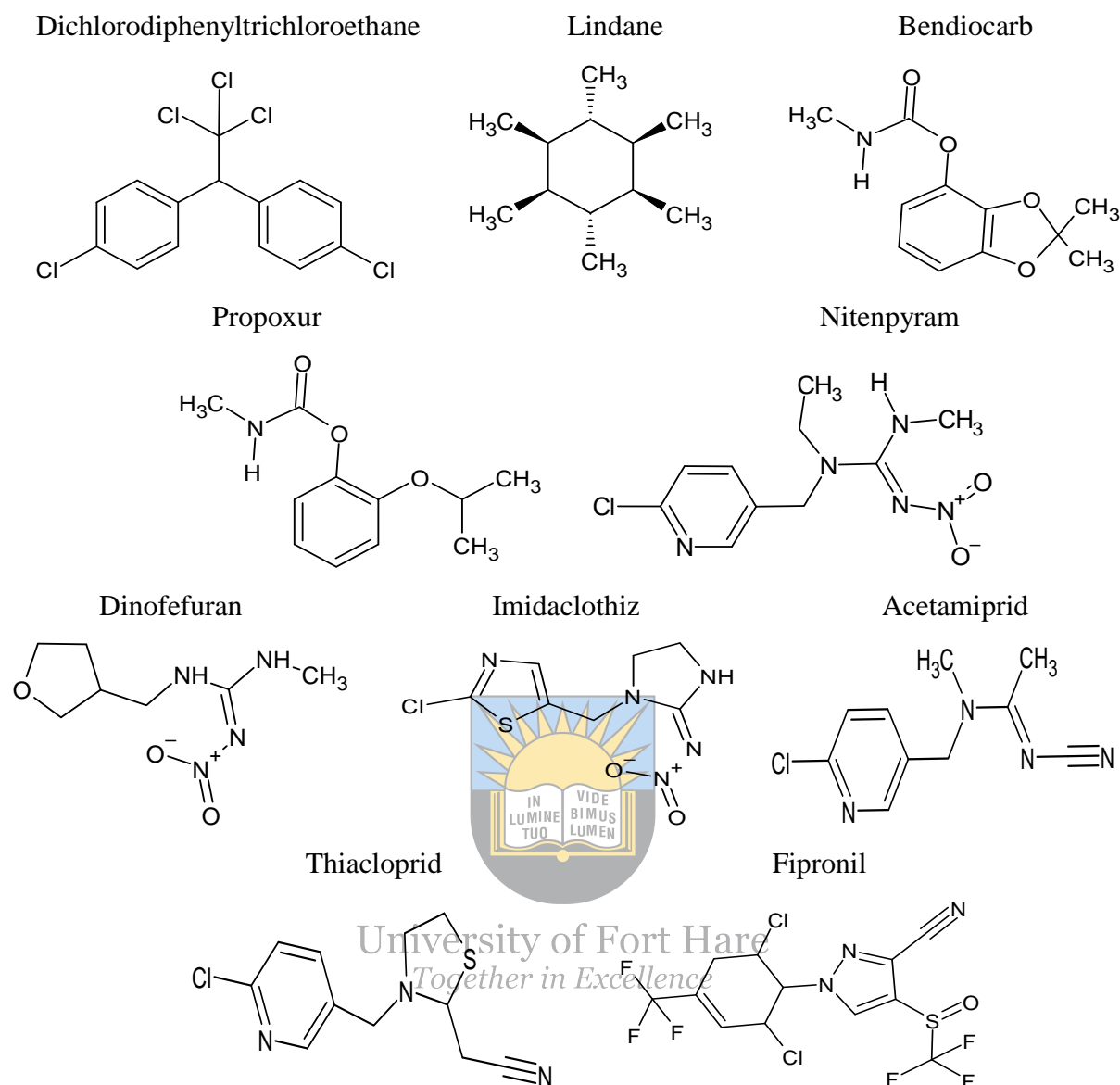


Figure 2.2: Chemical structures of some common insecticides.

2.1.1.3. Fungicides

Fungicides are biological organisms or chemical compounds that terminate or prevent the development of fungal spores or fungi (Gullino *et al.*, 2000). The chemical structures of some commonly used fungicides across the world are shown in Figure 2.3. According to Saladin *et al.* (2003), this happens when fungicides are able to improve plant defence mechanisms through cell wall lignification or stimulation of enzymes involved in phenolic and flavonoids compounds syntheses.

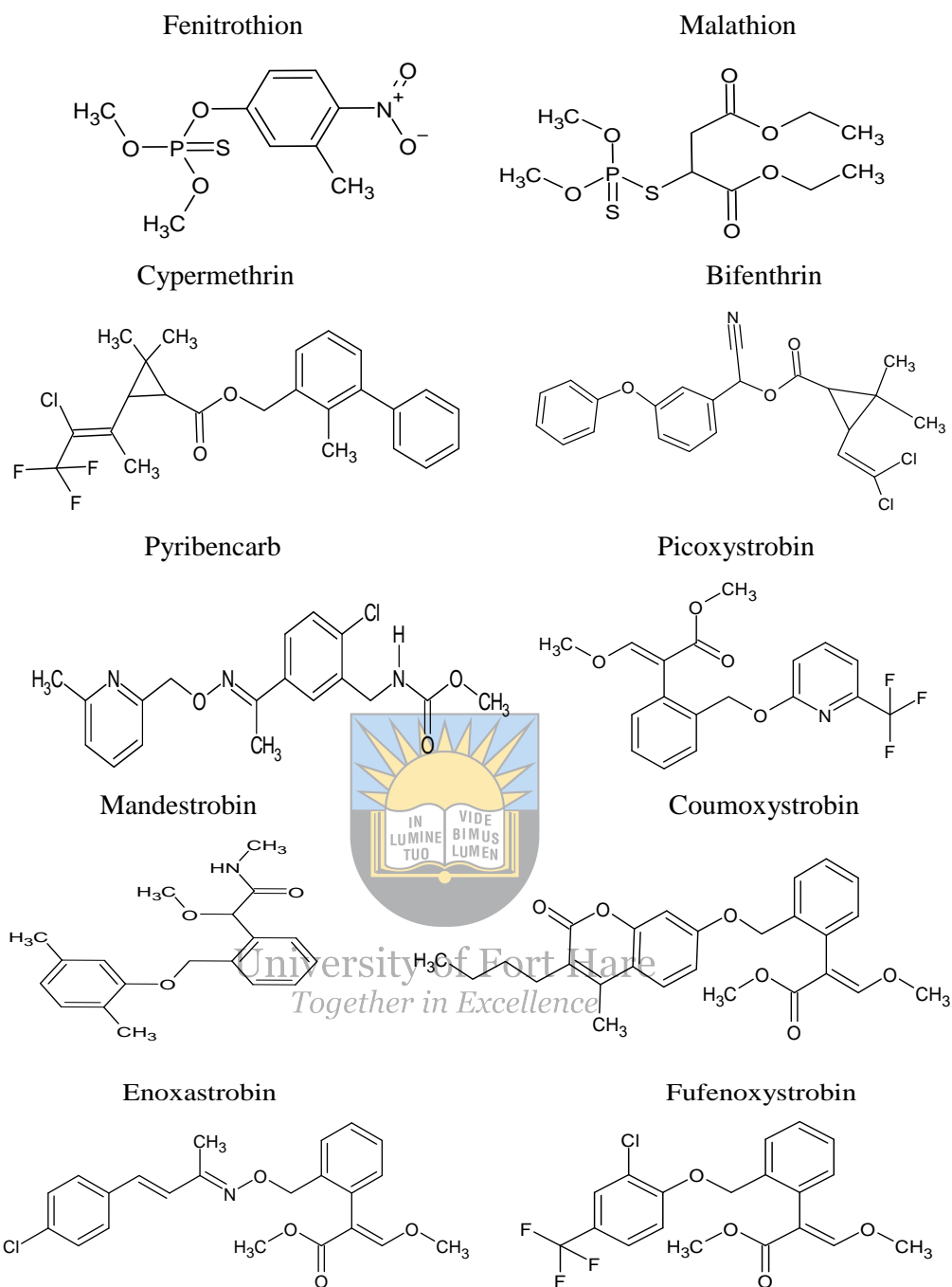


Figure 2.3: Chemical structures of some common fungicides.

In agriculture, the effectiveness of fungicides has been mainly focused on fungal pathogens or their residues in crops (Saladin *et al.*, 2003). Fungi infections contribute to approximately 20% of worldwide yield loss (Gullino *et al.*, 2000). Xia *et al.* (2006) reported that in the past decades, fungicides have become the primary fungi control means on account of their easy application, low cost and effectiveness. Mohamed and Akladios (2017) categorized them into systematic and

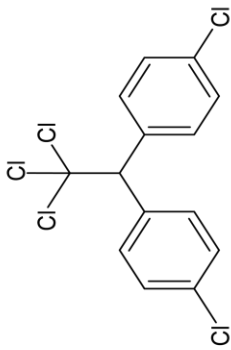
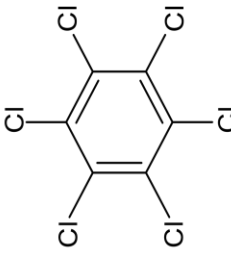
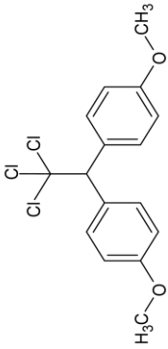
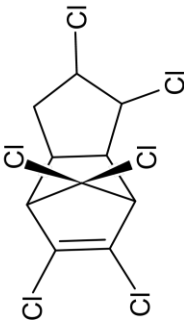
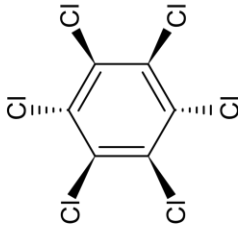
non-systematic fungicides (also referred to as contact fungicides). Systematic fungicides have lethal ability to fungus after the parenchyma penetration by the mycelia and the ability to stop infection spread within the plant, whereas non-systematic fungicides (e.g. sulphur or copper) have defensive action by preventing or killing fungal spores' prior the mycelia growth and development within the plant tissues (Mohamed and Akladious, 2017).

2.1.2. Classification based on their chemical composition

2.1.2.1. Organochlorine pesticides

Organochlorine pesticides (OCPs) fall under the primary subcategory of chemical pesticides (Mohamed and Akladious, 2017). Huang and Lee (2015) reported that they have been of great use in agriculture, domestic households and industries in the past. This group of pesticides include dimethyldiphenyltrichloroethane, hexachlorocyclohexane, methoxychlor, chlordane, dieldrin, toxaphene, kepone, mirex and lindane (Table 2.1) (Isegbe *et al.*, 2016). As a result of their persistence and bioaccumulation properties, these types of pesticides were banned from the market (Huang and Lee, 2015) and their usage has decreased (de Boer *et al.*, 2010). Nevertheless, OCPs and their metabolites are still detected in different environmental matrices such as soil (Lin *et al.*, 2012), water (Quinete *et al.*, 2011) and air as a result of human activities (Kosikowska and Biziuk, 2010). On top of the aforementioned properties of organochlorine pesticides, Kim and Smith (2001) mentioned their hydrophobicity and lipophilicity, low vapour pressure and photo-oxidation stability to be the main features for their efficacy as pesticides and their persistence in the environment. During the period 1946 to 1980, the use of organochlorines was extensive in South Korea for rice crops yield improvement (Mansourieh *et al.*, 2019). For a number of decades OCPs have been used against adults and larvae of malaria vectors in some areas of the world (Omer *et al.*, 1980). Omer *et al.* (1980) reported dichlorodiphenyltrichloroethane as the first chlorinated hydrocarbon to control malaria and louse borne typhus; this was noticed during Second World War.

Table 2.1: Some commonly used organochlorine pesticides across the world.

Chemical class	Name of pesticide	Acronym	Chemical formula	Molar mass	Chemical Structure
Organochlorine pesticide	Dichlorodiphenyltrichloroethane	DDT	$C_{14}H_9Cl_5$	354,49 g/mol	
	Hexachlorocyclohexane	HCH	$C_6H_6Cl_6$	290,83 g/mol	
	Methoxychlor		$C_{16}H_{15}Cl_3O_2$	345,65 g/mol	
	Chlordane	CLD	$C_{10}H_6Cl_8$	409,779 g/mol	
	Lindane	γ -HCH	$C_6H_6Cl_6$	290,83 g/mol	



University of Fort Hare
Together in Excellence

However, just like most chlorinated hydrocarbons, this pesticide was banned in 1972 in many nations due to its negative effects on the environment (Omer *et al.*, 1980). Benzene hexachloride is one of the popular insecticides, which have been broadly used in 20th century, even in this

century it is still in use in some developing countries (Yang *et al.*, 2015). Methoxychlor has been reported to induce reproductive defects in male rats. However, that has not been well proven (Latchoumycandane *et al.*, 2002). Chlordane was broadly used in both agricultural and residential applications and about 70,000 metric tons of chlordane was produced from 1948 to 1988 (Xiao *et al.*, 2011). Xiao *et al.* (2011) further stated that due to their long half-life they still exist in some environments. According to Kanthasamy *et al.* (2005), dieldrin was first synthesized in the laboratories of Julius Hyman & Company in Denver, United States of America in 1946 and was extensively used as an insecticide mainly for soil pests, grasshoppers, termites, etc.

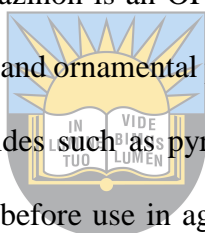
However, just like most chlorinated hydrocarbons, this pesticide was banned in 1972 in many nations due to its negative effects on the environment (Omer *et al.*, 1980). Benzene hexachloride is one of the popular insecticides, which have been broadly used in 20th century, even in this century it is still in use in some developing countries (Yang *et al.*, 2015). Methoxychlor has been reported to induce reproductive defects in male rats. However, that has not been well proven (Latchoumycandane *et al.*, 2002). Chlordane was broadly used in both agricultural and residential applications and about 70,000 metric tons of chlordane was produced from 1948 to 1988 (Xiao *et al.*, 2011). Xiao *et al.* (2011) further stated that due to their long half-life they still exist in some environments. According to Kanthasamy *et al.* (2005), dieldrin was first synthesized in the laboratories of Julius Hyman & Company in Denver, United States of America in 1946 and was extensively used as an insecticide mainly for soil pests, grasshoppers, termites, etc.

2.1.2.2. Organophosphorus pesticides

In the 1980s, a new group of pesticides called organophosphorus (OPPs) became a headline in pest management (Mansouriieh *et al.*, 2019). According to Jokanović (2009), OPPs cater for all organic compounds with phosphorus in their chemical structure and are applied to kill pests in orchards, industrial plantations and vegetable cultivation. They are characterized by their ester structure, easy decomposition on plant surfaces and interiors as well as in soils (Jaffrezic-Renault,

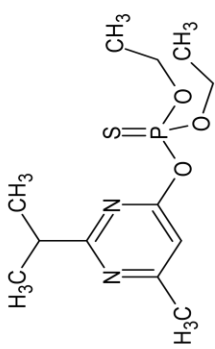
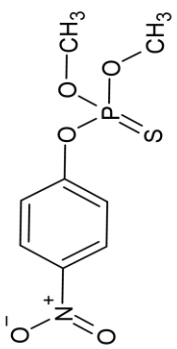
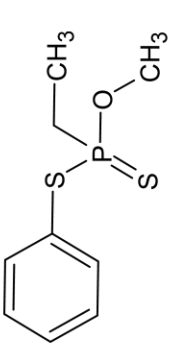
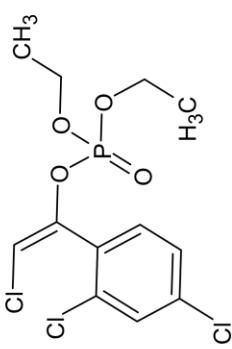
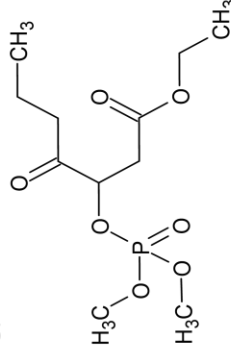
2001). Organophosphorus pesticides include diazinon, methyl parathion, fonofos, chlorfenvinphos, malathion, dichlorvos, metamidofos, chlorpyrifos, phosalone, fenitrothion, demeton-S-methyl and monocrotophos, their primary use is to protect plants (Fenik *et al.*, 2011). Some these OPPs are presented in Table 2.2. Their use is a result of their insecticidal activity based on the inhibition of acetylcholinesterase, which may cause hyperactivity, death and asphyxia of pests (Jiao *et al.*, 2018). As a result of their high persistence in the environment and high toxicity on exposed organisms, organophosphorus (OP) pesticides are considered as a constant hazard to non-target species (Roex *et al.*, 2003).

OP compounds are one of the toxic compounds known up-to-date. Because of their widespread application in modern agriculture and high toxicity of their neurotoxins public concerns has increased (Jaffrezic-Renault, 2001). Diazinon is an OP insecticide used to control soil insects, fruit and vegetables, field crops insects, and ornamental plant insects (Jiao *et al.*, 2018). Diazinon may be found in mixtures with pesticides such as pyrethrins, lindane, and disulfoton as it is normally diluted with other chemicals before use in agriculture (Matouq *et al.*, 2008). Methyl parathion (MP) was firstly introduced in the agricultural market seven decades ago as an organophosphorous pesticide (Diagne *et al.*, 2007). This insecticide is commonly used to control sucking and chewing insects in a broad scope of crops, including cereals, vegetables, vines, fruits, ornamentals, cotton and other field crops (Arapoglou *et al.*, 2003). Fonofos (O-ethyl-S-phenylethylphosphonodithioate) that was firstly registered for use with the United States Environmental Protection Agency (USEPA) in 1967 as an organophosphate insecticide is used to protect plants, most commonly corn but also sugarcane, tobacco, peanuts, and many various crops from diverse worms and it is applied to soils (USEPA, 1999). Fonofos has no domestic applications (Mahajan *et al.*, 2006).



University of Fort Hare
Together in Excellence

Table 2.2: Some commonly used organophosphorus pesticides across the world.

Chemical class	Name of pesticide	Acronym	Chemical formula	Molar mass	Chemical structure
Organophosphorus pesticide	Diazinon	DZ	$C_{12}H_{21}N_2O_3PS$	304.35 g/mol	
	Methyl parathion	MP	$C_8H_{10}NO_5PS$	263.21 g/mol	
	Fonofos		$C_{10}H_{15}OPS_2$	246.30 g/mol	
	Chlorfenvinphos	CVP	$C_{12}H_{14}Cl_3O_4P$	359.60 g/mol	
	Malathion	MLT	$C_{10}H_{19}O_6PS_2$	330.40 g/mol	

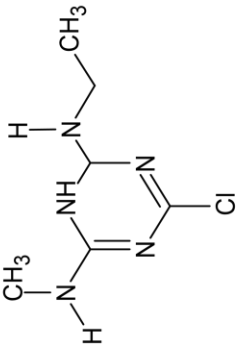
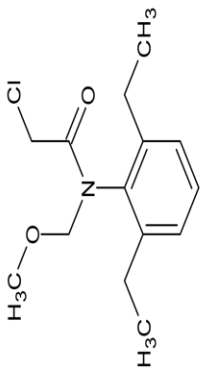
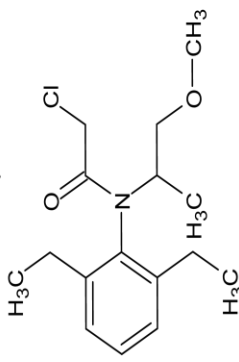
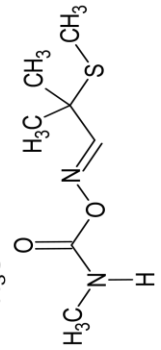
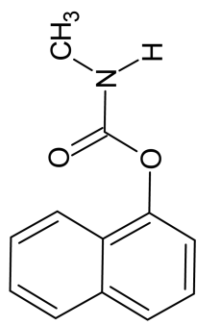
Malathion (O,O-dimethyl-S-1,2-bis-ethoxycarbonylethylphosphorodithioate), is regarded as a widely used organophosphorus pesticides for public health programmes and agriculture (Ahmed *et al.*, 2007). Chlorfenvinphos [2-chloro-1-(2,4-dichlorophenyl)vinyl-diethylphosphate] an organophosphorus insecticide used for the control of insect pests in livestock and domestic pests

such as flies, mites and fleas (Roselló-Márquez *et al.*, 2019). It was banned in United States in 1991 (Azab and Kamel, 2016).

2.1.2.3. Organonitrogen pesticides

Organonitrogen pesticides (ONPs) also play a key part in fighting pests (Zhang and Lee, 2006). The term organonitrogen pesticides, is an umbrella name for a large number of organic pesticides containing nitrogen (Tankiewicz *et al.*, 2011). These type of pesticides are known by the names of several chemical groups. In literature the term ‘organonitrogen pesticides’ normally refers to triazines, carbamates and their derivatives (Fenik *et al.*, 2011). ONPs also include phenylureas in addition to carbamates, and triazines. Carbamates and OPPs are listed with the most crucial chemicals used for agricultural and household pest protection (Fenik *et al.*, 2011). They are less stable in the environment compared to OCPs, but however, they can get into the human digestive system, thus posing severe health hazard to humans (Fenik *et al.*, 2011). The organonitrogen herbicides, alachlor, atrazine and metolachlor (Table 2.3) are among the most widely used and sensed pesticides in water streams worldwide (Gascón, 1998). Moreover, they are among the top ten most used herbicides in the United States and Europe (Thurman and Meyer, 1996). Their widespread application together with their over-use, runoff from mixing and loading areas, accidental spills and breakdown waste discharge create environmental threats (Gascón, 1998). Their solubility, in water, mobility in surface and ground water, and half-life in soil give organonitrogen herbicides capability to reach estuaries whereby they are carried to the sea resulting to contamination (Gascón, 1998).

Table 2.3: Some commonly used organonitrogen pesticides across the world.

Chemical class	Name of pesticide	Acronym	Chemical formula	Molar mass	Chemical structure
Organonitrogen pesticide	Atrazine	ATR	$C_8H_{14}ClN_5$	215.68g/mol	
	Alachlor	AL	$C_{14}H_{20}ClNO_2$	269.77g/mol	
	Metolachlor	ML	$C_{15}H_{22}ClNO_2$	283.79g/mol	
	Aldicarb	ALD	$C_7H_{14}N_2O_2S$	190.27g/mol	
	Carbaryl	CBL	$C_{12}H_{11}NO_2$	201.22g/mol	

Even though carbamates fall under organonitrogen pesticides (Fenik *et al.*, 2011), they are also a class of highly effective commercial pesticides, which are widely used against fungi, insects and weeds globally (Zhang and Lee, 2006). Their usage has been increasing due to their lower environmental persistence compared to organochlorine and organophosphorous pesticides (Zhang and Lee, 2006). According to Wu *et al.* (2009) their low bioaccumulation potentials, broad biological activity, and relatively low mammalian toxicities are the factors that are enhancing their usage in agriculture. However, since they are acetylcholinesterase inhibitors, they are suspected carcinogens and mutagens. Some carbamate insecticides like carbaryl can be teratogenic in large amounts and nitrosated to form strongly carcinogenic nitroso-compounds (Fenik *et al.*, 2011).

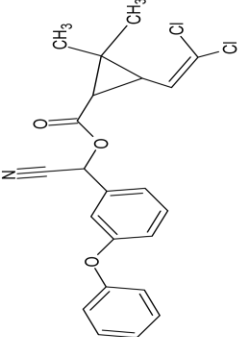
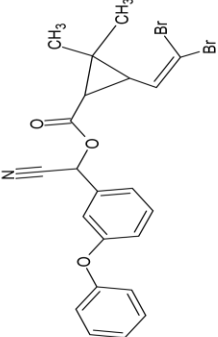
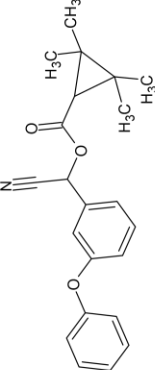
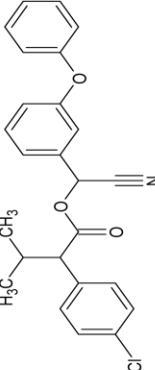
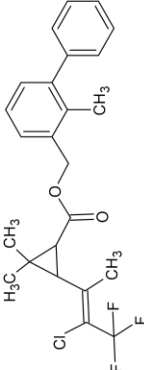
2.1.2.4. Pyrethroid pesticides

Pyrethroids, a synthetic organic insecticides class made from pyrethrins, which have been broadly used throughout the world since the 1980s. This is because of their low toxicity and high effectiveness in comparison to other insecticides including carbamic ester compounds and organophosphorus (Yoo *et al.*, 2016). Pyrethroid pesticides are currently among the three major kinds of pesticides (Ying *et al.*, 2012). Based on their molecular structures, they can be divided into urban pyrethroids referring to those that are containing no alpha-, characterized by low toxicity and agricultural pyrethroids referring to those with an alpha-, with average toxicity. They are primarily used for non-agricultural and agriculture pest control, respectively.

In addition, they also play a critical role in domestic products such as mosquito-repellent perfumes and shampoos (Tang *et al.*, 2018). Cypermethrin, fenpropathrin, deltamethrin, bifenthrin, permethrin, fenvalerate, lcyhalothrin, and cyfluthrin are examples of this pesticide (Table 2.4) and are widely used in these days (Gong, 2013). At present, pyrethroids are the most predominant household insecticides for both outdoor and indoor applications, based on their

selective insecticidal activity, relatively lower mammalian toxicity and low persistence in the environment than OPPs (Ye *et al.*, 2006).

Table 2.4: Some commonly used pyrethroid pesticides across the world.

Chemical class	Name of pesticide	Acronym	Chemical formula	Molar mass	Chemical structure
Pyrethroids	Cypermethrin	CP	$C_{22}H_{19}Cl_2NO_3$	416.30g/mol	
	Deltamethrin	DLM	$C_{22}H_{19}Br_2NO_3$	505.20g/mol	
	Fenpropathrin	FNP	$C_{22}H_{22}NO_3$	349.40g/mol	
	Fenvalerate	FEN	$C_{25}H_{22}ClNO_3$	419.90g/mol	
	Bifenthrin	BF	$C_{23}H_{22}ClF_3O_2$	422.90g/mol	

Nevertheless, the OPPs and ONPs are still the most used pesticides nowadays and their usage is still intensifying, because of their reliability, prices and wide range of applications. After the decision of the United States EPA about stopping specific applications of the OP insecticides such as chlorpyrifos based on their toxicity to humans, the sales of insecticides containing pyrethroids eventually increased sharply (Feo *et al.*, 2010).

2.2. Dyes and their classifications

A dye can be defined as a substance characterized by absorbing part (chromophore) which absorbs part of the visible light (Benkhaya *et al.*, 2020) and that has colouring ability in solutions. Dyes are characterized by a capacity of absorbing radiation within the visible spectrum (380 - 750 nm) (Benkhaya *et al.*, 2020). The fraction of light reflected by the dye is what is considered colour. The colour intensity of the different dyes is associated with their chemical composition (Nozet and Majault, 1976). Nowadays, dyes are known as organic compounds that are artificially synthesized and that are hydro or oil-soluble whereas it is the opposite for pigments and they maintain their particulate form even in solutions (Vazquez-Ortega *et al.*, 2020). Dyes are mostly used in textile industry, which emerged in more than 4000 years ago (Benkhaya *et al.*, 2020). From the last 150 years of those years, dyes were obtained from natural sources (Ferreira *et al.*, 2004). A big change in dye industry came after William Henry Perking obtained Mauveine, in 1856, when trying to synthesize quinine, a medicinal drug used to treat malaria (Abel, 2012). Then from that failure, a new generation of dyes emerged (synthetic dyes) (Saratale *et al.*, 2011), which are the most commonly used dyes presently. Dyes can be classified into two broad groups, which have their own subcategories (i.e. classification based on origin and classification based on solution behaviour).

2.2.1. Classifications based on origin

2.2.1.1. Natural dyes

Natural dyes are those that are derived from natural sources. Minerals, plants, and insects/animals are usually used to synthesize natural dyes (Zerin *et al.*, 2019). Natural dyes have been applicable to dye textile fabrics and clothes for thousands of years. Presently these types of dyes are considered as positive dyes since natural sounds green whereas sometimes as negative due to lesser reliability compared to synthetic dyes (Fröse *et al.*, 2019). According to dos Santos Silva *et al.* (2020), natural dyes are generally less toxic and allergenic in comparison to synthetic dyes and usually produce biodegradable wastewater, which is not the case for many synthetic dyes. However, Hussein *et al.* (1997) reported plants used for dye extraction to have antimicrobial activity. Furthermore, common natural dyes have been considered as potent antimicrobial agents because of their high content of tannins. Plant derived dyes that are naphthoquinone rich such as lawsone from henna, lapachol from alkanet and juglone from walnut exhibit both antifungal and antibacterial activity (Gershon and Shanks, 1975; Wagner *et al.*, 1989).



University of Fort Hare

This implies that the antimicrobial activity of plants that are used to derive natural dyes are a result of the latter, not other chemical species available in these plants. Natural dyes are normally used in the colouring of cosmetics, textile, drugs, foods, etc., and their use is a result of their low or non-toxicity (Siva, 2007). Even though plants as common sources of natural dyes show a variety of colours, not all of their extracts and materials can be considered as dyes. Because some of their extracts do not dissolve in water hence can be rather considered as pigments. While others dissolve but do not get adsorbed onto fibres which makes up many textile materials. Whereas some do dissolve but fade when exposed to air, sunlight or washed (Siva, 2007), which is not usually the case with known dyes. These dyes can be classified into indigoids, flavones, carotenoids, anthraquinones, alpha naphthoquinones, anthocyanidin and dihydropyrans based on their functional groups. Due to paucity of information on their extraction, application methods

and disadvantages, these dyes were overtaken by synthetic dyes. Figure 2.4 shows the chemical structures of some natural dyes.

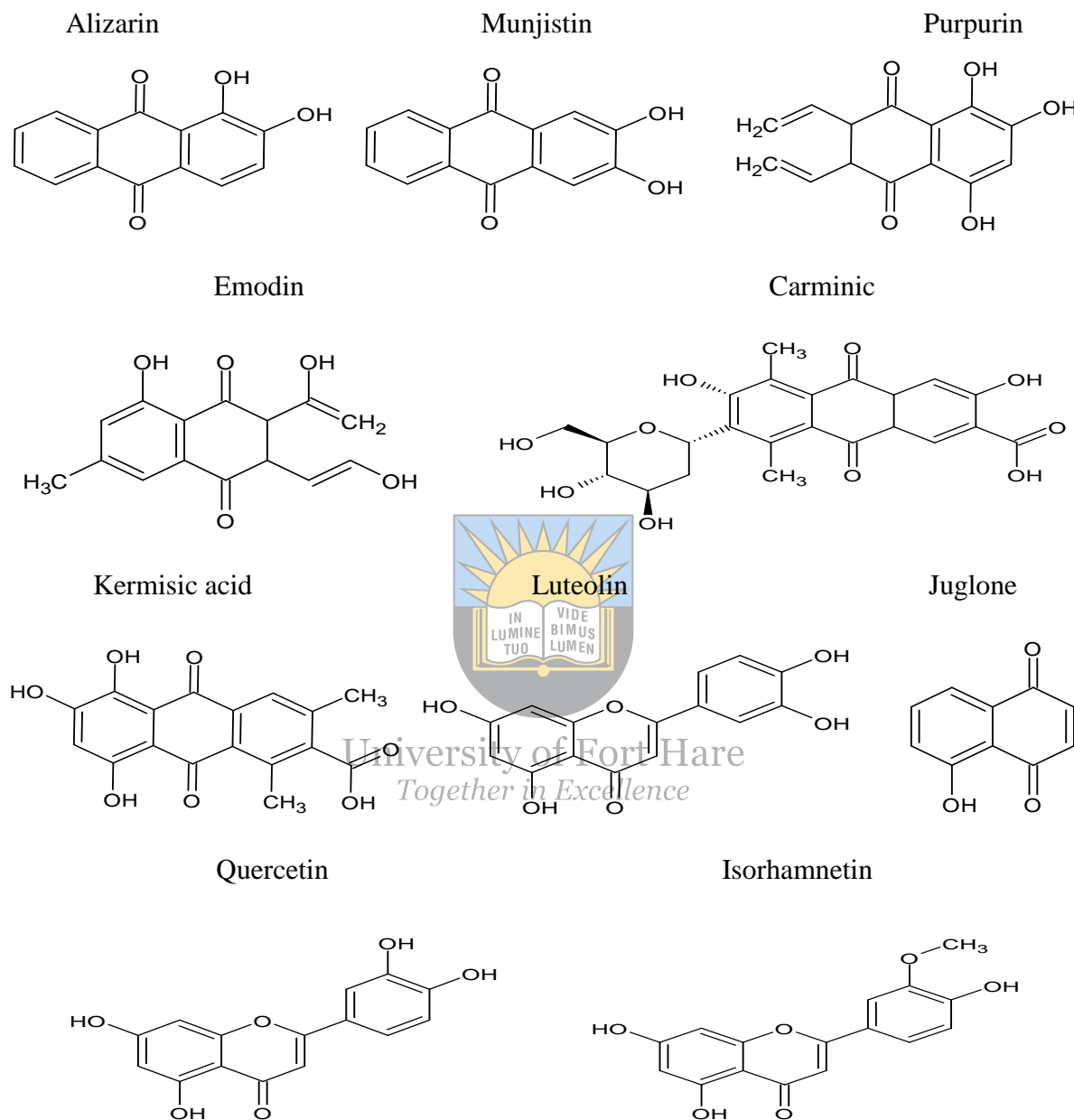


Figure 2.4: Chemical structures of common natural dyes.

2.2.1.2. Synthetic dyes

Synthetic dyes are dyes that are prepared in the laboratories using chemicals. Synthetic dyes are structurally diverse (Figure 2.5). However, the industry frequently used dyes can be chemically

classified into azo, sulphur, phthalocyanine, anthraquinone and triphenylmethyl (trityl) derivatives (Forgacs *et al.*, 2004).

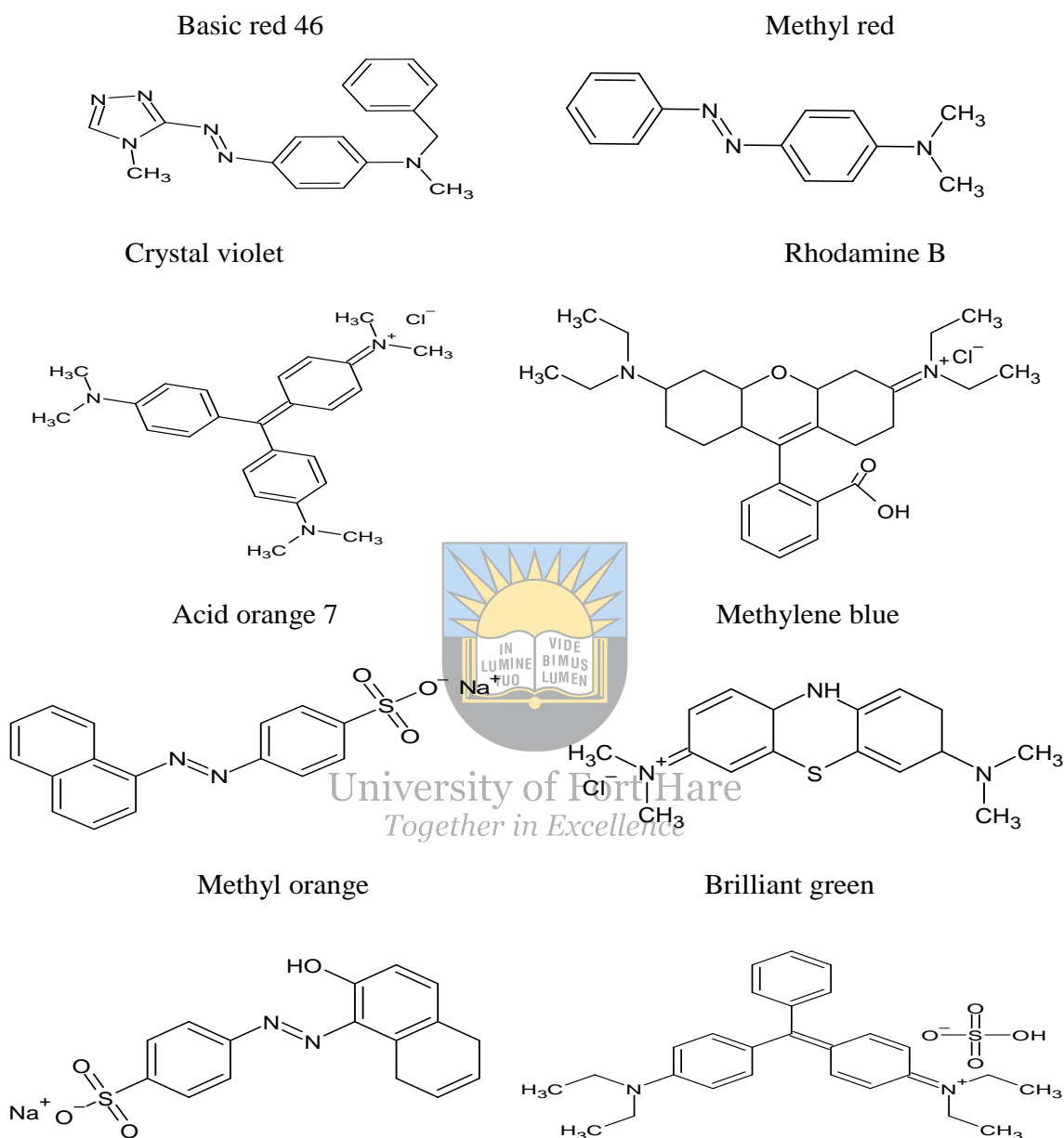


Figure 2.5: Chemical structures of some common synthetic dyes.

Nevertheless, the exact number of synthetic dyes produced worldwide is unknown but is estimated to be more than 10 000 tons per year. These types of dyes are characterized by multiple potentialities, which include fast and consistent coloration with different classes of fabrics (Slama

et al., 2021). Other common properties of synthetic dyes are their optical, physicochemical and thermal stabilities together with their recalcitrance on microbial degradation, which allows them to persist in the environment for prolonged periods (Velić *et al.*, 2017). When compared to other types of dyes, azo dyes attribute for the largest number of synthetic dyes extensively used in numerous industries including textile, cosmetics, food and paper printing (Pandey *et al.*, 2007). Based on literature, these dyes are aromatic and consist of one or more $-N=N-$ group(s) structurally. However, sulphur dyes are employed for textile cellulosic materials dyeing or blends of cellulosic fibres and normally a cheap and traditional reducing agent (Sodium sulfide) is used in sulphur dyeing (Nguyen and Juang, 2013). Even though “traditional” sounds friendly, sodium sulphide is toxic and hazardous to handle. Phthalocyanine dyes are a class of dyes, which are formed via a reaction of dicyobenzene and transition metals such as Cu, Ni, Co and Pt (Berradi *et al.*, 2019). Berradi *et al.* (2019) also stated that the phthalocyanine nucleus allows the dye molecules to be sensitive to light. The most commonly used in this class is copper phthalocyanine owing to its high chemical stability (Yamagami *et al.*, 2017). This class is often used in electrochemistry. After azo dyes, anthraquinone are the most important class and their general formula is derived from anthracene hence its chromophore group is quinone (Franciscon *et al.*, 2009). Triphenylmethanes are the least important category in textile industries and are the oldest synthetic dyes including fuchsin and malachite green (Wang *et al.*, 2011).

2.2.2. Classifications based on solution behaviour

To merge the earlier discussed broader classifications (classifications based on origin), dyes can also be grouped based on their solution behaviour i.e. cationic, anionic and non-ionic dyes. This classification is based on the charge that dyes possessed on aqueous solutions. Some dyes bare a positive charge in aqueous solutions (cationic dyes) (Figure 2.6), whereas some bare a negative charge in aqueous solutions (anionic dyes) (Figure 2.7) and others bare a neutral charge or no charge (non-ionic dyes) (Figure 2.8). This phenomenon helps scientist to predict the suitable

adsorbent for each class of dyes or the materials to which these classes can be easily attached. This also makes it easy for their industrial applications. Some cationic dyes in which extensive studies have been performed include rhodamine 6G (Jarrah, 2017), methylene blue (Yao *et al.*, 2010), basic yellow (El Qada *et al.*, 2008), malachite green (Yu *et al.*, 2017).

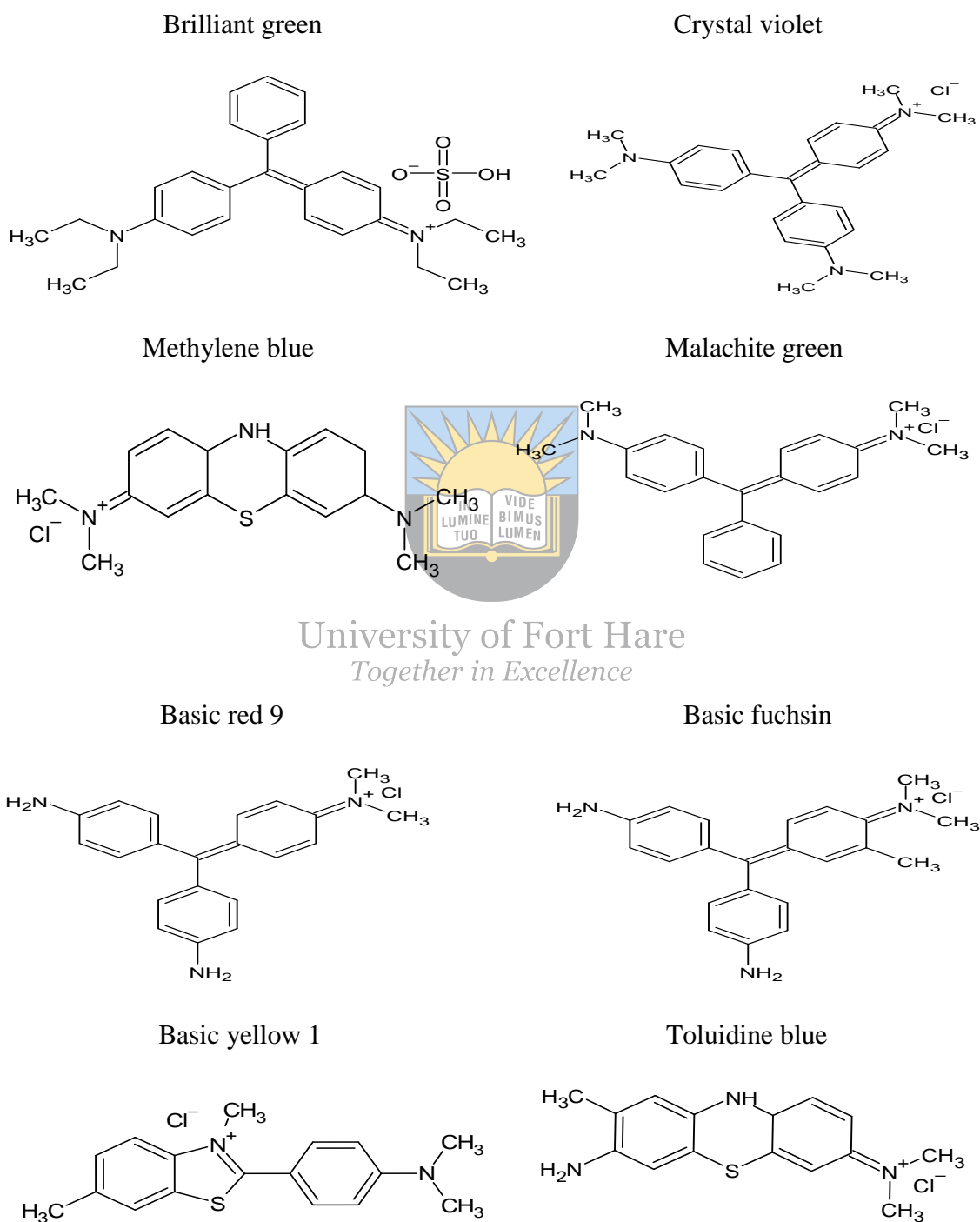


Figure 2.6: Chemical structures of commonly studied cationic dyes.

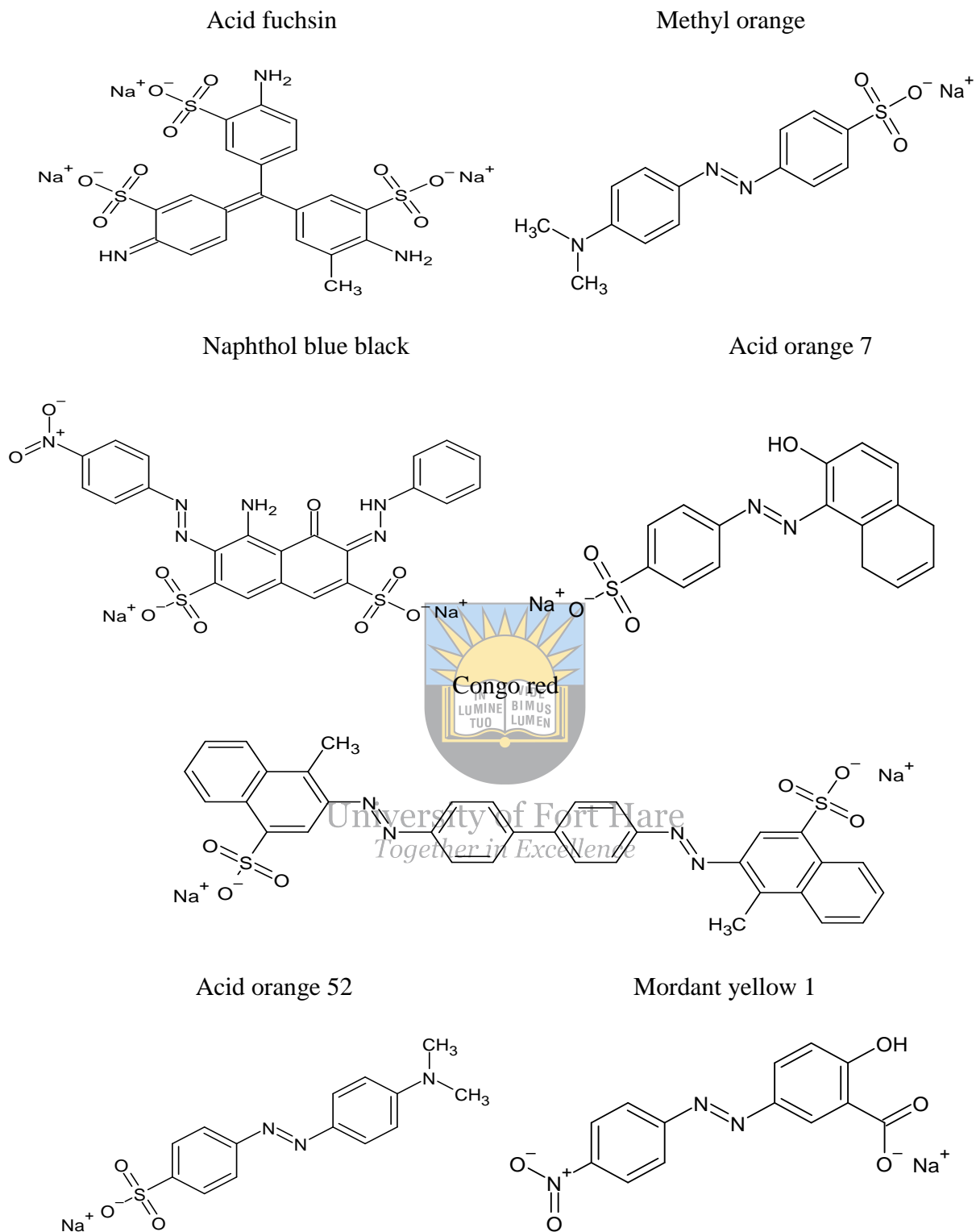


Figure 2.7: Chemical structures of some commonly studied anionic dyes.

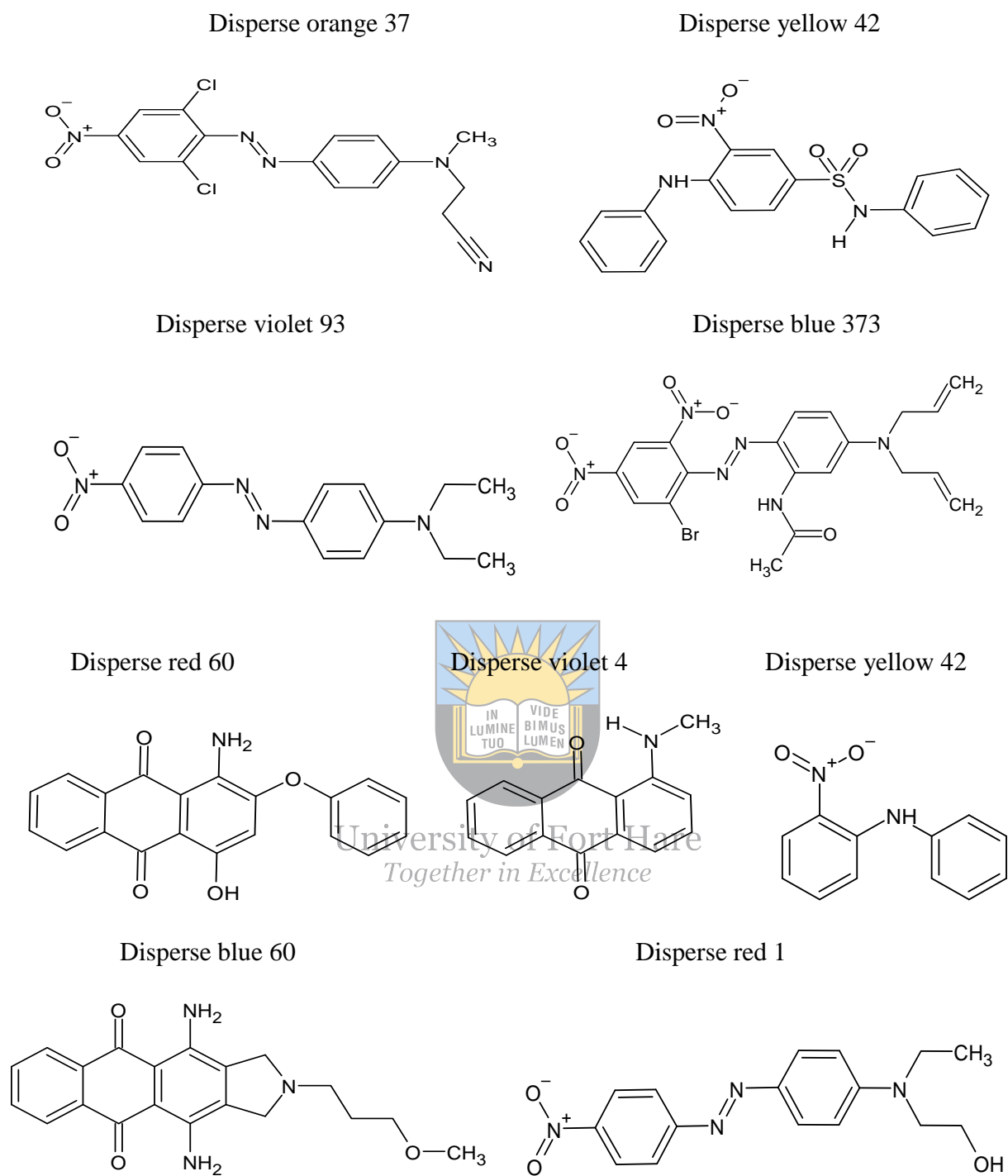


Figure 2.8: Commonly used non-ionic dyes chemical structures.

Cationic dyes are mostly used in silk wool, acrylic and nylon dyeing. Based on different substitution on their aromatic groups these dyes possess different chemical structures (Eren and Afsin, 2007). Cationic dyes regarded as toxic colorants has ability of causing negative effects

such as allergic dermatitis, mutations, cancer and skin irritation (Eren and Afsin, 2009). These dyes are also referred to as basic dyes. Anionic dyes also include a large number of different dyes possessing different structures, for example, azoic, triphenylmethane, nitro and anthraquinone dyes sharing common features like ionic substitutions and water-solubilizing. Anionic azo dyes consist quite a large amount of the reactive dyes (Hunger, 2007). The latter uses their reactive groups to interact with wool, cotton and more to form covalent bond and their release to the surrounding is undesirable, as they possess low fixation in the hydrolysis of their reactive groups in water (Salleh *et al.*, 2011). Some of the anionic dyes that have been studied by other researchers include acid turquoise blue 2G (Ren *et al.*, 2016), brilliant red (Yu *et al.*, 2020), methyl orange (Yao *et al.*, 2011) and brilliant yellow (Pourfaraj *et al.*, 2017).

2.3. Effect and fate of pesticides in wastewater

According to Gavrilesco (2005), the extent to which pesticides can contaminate surface water or underground water is dependant on several factors like the properties of the soil, crop management practices, hydraulic loading on the soil and the properties of the pesticides. Gavrilesco (2005) also reported that the pesticides chemical structural variations do not only tell their target organisms but also tell the way they will move in the environment from one point to another. Subsequently, these variations also affect the volatility and water solubility of these pesticides. Volatile compounds will prefer air medium as a result, they will spread over a wide range thus posing treat to more organisms especially terrestrials. However, the water-soluble compounds will prefer water and will spread through water streams flow and food chain. Hydrophobic pesticides on the other hand will prefer sediments and will spread through the food chain. During the degradation of these pesticides, less harmful chemicals or rather more, may form in comparison to the original chemical (Gavrilesco, 2005). Reddy *et al.* (2015) reported that O,O-diethyl-O-3,5,6-trichloro-2-pyridyl phosphorothionate (a crystalline organophosphate) is water insoluble, however its metabolites have high water solubility. As a result of chemical

structural variations, rates of degradation for different pesticides on soil vary and this is also influenced by the soil organisms present (Gavrilescu, 2005). This means that some pesticides may persist for years while degrading whereas some may not (Ryoo *et al.*, 2013), leading to leaching to water streams. Sometimes the effect of pesticides cannot be directly observed from wastewater rather it can be observed because of wastewater distribution to the environment. As a result of industrial wastewater discharges and farmlands surface runoff estuaries and coastal waters are often polluted by pesticides and other substances (Bhuvaneshwari *et al.*, 2015). These pesticides then possess their effects in wastewater through exposed organisms depending on their individual properties. Their negative effect in human health varies from short-term illness (e.g., skin and eye irritation, dizziness, headaches and nausea) to diseases that are chronic (e.g. cancer, asthma, dermatological problems and diabetes) (Kim *et al.*, 2017; Sanborn *et al.*, 2007).

2.3.1. Cancer

Cancer is a chronic disease that results from uncontrolled division of abnormal cells in a body part. It emerges when cancer cells build-up several genetic modifications that provide them several capabilities (Cahill *et al.*, 1999). The latter, according to Hanahan and Weinberg (2000), comprises the ability to escape normal growth control, evasion of the suicidal apoptotic mechanism, metastasis, and development of prolonged angiogenesis. The full understanding of cancer has not yet been met due to its complexity (Anand *et al.*, 2008). Cancer continues to be considered as one of worldwide killers regardless of the large amount of research and quick developments made in this field in the past decades (Anand *et al.*, 2008). United States of America (USA) statistics revealed that about 23% of the total deaths in the USA are due to cancer following heart disease (Jemal *et al.*, 2007). On top of natural genetic disorders, exposure to pesticides have been counted as one of its causes. Koutros *et al.* (2016) associated imazethapyr and imazaquin (imidazolinone herbicides) to bladder cancer. Carcinogenic pesticides may intensify the risk of cancer through various mechanisms, such as genotoxicity, hormonal action,

tumor promotion and immunotoxicity (Dich *et al.*, 1997). In contrast to genotoxic compounds, carcinogens acting through other mechanisms like tumour promotion are said to have a threshold, i.e., minimum level at which their effects can be detected or observed (Dich *et al.*, 1997). According to Dich *et al.* (1997), complete carcinogens possess both genotoxic and tumour-promotive potentials. Some non-genotoxic insecticides, such as arsenic compounds, have been assessed as human carcinogens. Their report went on to state that weak genotoxic chemicals including 2,3,7,8- tetrachlorodibenzo-p-dioxin (TCDD) and chlordane have been evaluated as carcinogenic based on their tumour promotion potential (Dich *et al.*, 1997).

2.3.2. Asthma

Asthma can be defined as a chronic inflammatory disease occurring in the conducting airways (i.e. trachea, the two stem bronchi, the bronchi and the bronchioles). When this happens, bronchial hyper-reactivity (BHR) (the tendency of asthmatic people's smooth muscle cells to react to non-specific stimuli such as intense exercise and cold air), airway wall remodelling, excessive mucus production, and airway narrowing result (Lambrecht and Hammad, 2015). Conventionally, two classifications of asthma have been clinically defined (Lambrecht and Hammad, 2015). Asthma has been linked to factors such as allergies, tobacco smoking, viral and bacterial infections, air pollution, obesity, changes in sex hormone levels, and occupational exposures. However, association between bronchial hyper-reactivity, asthma symptoms and pesticide exposure have also been revealed by numerous epidemiological and clinical studies (Kim *et al.*, 2017). Exacerbation of asthma due to pesticide exposure may be via several mechanisms such as irritation, immunosuppression, inflammation, or endocrine disruption (Hernández *et al.*, 2011; Amaral, 2014). In a study conducted by Raanan *et al.* (2015), it was concluded that early life exposure to OP pesticides could possibly cause respiratory symptoms consistent with childhood asthma. The study was conducted among 359 mothers and children in the United State of America. In a cross sectional study involving 211 female farm workers, a

positive relationship between entering a pesticide-sprayed field and ocular-nasal symptoms was deduced (Ndlovu *et al.*, 2014).

2.3.3. Dermatological problems

Primarily, exposure to pesticides is through the skin for handlers, sprayers, and people using repellents. With the exception of acute poisonings, contact dermatitis is said to be the most common health effect of pesticides, either through allergic or irritant mechanisms (Śpiewak, 2001). Certain pesticide components have ability of intensifying the skin sensitivity to light, leading to phototoxic reactions (Hindson and Diffey, 1984), or may result into photo-allergy caused by photo-activated chemical reaction on the skin (Savitt, 1972). Dermatoses due to pesticides can be categorized into contact dermatitis, erythema multiforme-like eruptions, ashy dermatosis, chloracne and skin cancer (Mothemela, 2010). Contact dermatitis is a commonly occurring skin disease related to pesticides exposure, occurring both allergic and irritant. Most often, it occurs more likely on hands, feet, legs (front) than forearms, thighs (front) and legs (back), which are normally covered with clothes (Śpiewak, 2001). Erythema multiforme-like eruptions are considered as a form of allergic contact dermatitis.

Mendoza *et al.* (2008) reported eruptions that are due to glyphosate pesticide which occur after an irritant contact dermatitis. Both dimethoate and methyl parathion have been reported to cause erythema multiforme in a space of few hours after contact (Rademaker, 1998). Ashy dermatosis mostly occurs in individuals with dark skin and it is usually noticed by single or multiple ashen maculae of different size and shape. Penagos *et al.* (2004) reported ashy dermatosis on 39 banana farm workers to be caused by chlorothalonil in Panama. Bleiberg *et al.* (1964) described pesticide-related porphyria cutanea tarda in three workers in association with herbicides such as 2,4-dichlorophenol and 2,4,5-trichlorophenol. Chloracne is associated with chlorinated polycyclic aromatic hydrocarbons. Skin cancer risk has intensified in professional pesticide sprayers. The International Agency for Research on Cancer (IARC) has reported a growing lip

and skin cancer risk among their group participants (IARC Working Group, 1991). Although arsenic pesticides that were banned 40-50 years ago are still associated with skin cancer owing that to their strong carcinogenic properties.

2.3.4. Diabetes

Diabetes mellitus involves a collection of diseases known for causing hyperglycaemia as a result of reduced insulin action, insulin production, or both (Evangelou *et al.*, 2016). It is categorized into two types (i.e. Type 1 (T₁D) and Type 2 diabetes (T₂D)). The most common type of diabetes is type 2, which accounts for approximately 90% of all diabetes cases (Nolan *et al.*, 2011). Diabetes, as a global epidemic, is presently affecting more than 350 million people and by 2050 expected to have reached 550 million (Whiting *et al.*, 2011). Bradfield *et al.* (2011) and Morris *et al.* (2012) reported diabetes to be known for its multifactorial pathogenesis as a result of its strong genetic component. However, according to Nolan *et al.* (2011) it is equally influenced by different lifestyles. The increasing diabetes cases, specifically T₂D, has been mostly linked with lifestyle factors including choice of diet and obesity in the past.

However, in the past decade environmental contaminants were also noticed as prime factors. Pesticides has gained a lot of attention as environmental contaminants particularly as organochlorines, which have potential to bio-accumulate in exposed organisms from contact exposure or via the food chain. Organochlorines and other diverse types of pesticides have been directly linked to increasing T₂D risk (Lee *et al.*, 2010), as well as factors like insulin resistance, adiposity and dyslipidaemia (Lee *et al.*, 2011). Many studies suggested that pesticides cause diabetes by disrupting insulin release or tissues' response to insulin via multiple mechanisms including oxidative/nitrosative stress, mitochondrial dysfunction, inflammatory pathways and peroxisome alteration. Pesticides may also alter body's defence axis such as autonomic nervous and immune-neuroendocrine systems (Mostafalou *et al.*, 2012; Karami-Mohajeri and Abdollahi, 2011).

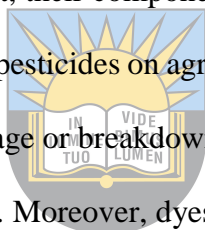
2.3.5. Endocrine disorders

Following the discovery of DDT, a number of various pesticides have been developed and broadly used across the world with some limited governing restrictions. Even though they have shown efficiency in pest control in order to maximize food production, they have possessed some negative health effects to exposed organisms including humans (Mnif *et al.*, 2011). These effects include endocrine disruption, which has been linked with several chemicals called endocrine disruptive chemicals (EDCs). Pesticides form majority of these chemicals (Sugiyama *et al.*, 2005; Lemaire *et al.*, 2006; Tabb and Blumberg, 2006; Leghait *et al.*, 2009). Their percentage ratios of comparison is as follows, herbicides (21%), fungicides (31%) and insecticides (46%) (Mnif *et al.*, 2011). It is also worth to mention that some of them were banned so long ago but are still detected in the environments of several countries (i.e. atrazine and DDT) (Mnif *et al.*, 2011).

EDCs act primarily by interfering with natural hormones because of their strong capability to bind to estrogen or androgen receptors (Tabb and Blumberg, 2006). Specifically, they can bind to and activate various hormone receptors (i.e. androgen receptor, aryl hydrocarbon receptor, estrogen receptor, constitutive androstane receptor, pregnane x receptor and estrogen related receptor) and fake their natural action (agonist action) (Mnif *et al.*, 2011). These chemicals are also capable of binding to the aforementioned receptors without activation (Mnif *et al.*, 2011). The latter, antagonist action hinders the receptors and inhibits their action. In addition, EDCs may also interfere with the buildup and elimination of hormones causing concentration decrease of natural hormones (Mnif *et al.*, 2011). The effects linked to endocrine disruption have been noted in both invertebrates (Gooding *et al.*, 2003) and vertebrates (with humans included) (Oskam *et al.*, 2003).

2.4. Effect and fate of dyes in wastewater

Textile industries are amongst the major sources of dye pollution in the environment worldwide (Mani and Bharagava, 2018). Approximately, more than 7×10^5 metric tons per annum are produced worldwide (Chen *et al.*, 2003). Their application is mainly in textile, paper, pharmaceutical, food, and cosmetics industries (Chandra and Bharagava, 2013). However, textile industries are the largest consumers of the dyes (Franciscon *et al.*, 2009). World Bank estimates that about one fifth of global industrial water pollution is sourced from dyeing of textiles and wastewater treatment. Following agricultural industry polluting agents of fresh water, originate from textile industry worldwide (Mani and Bharagava, 2018). This is because industrial wastewater are discharged with or without treatment to the environment (Al-Muzaini, 1998). After their discharge to the environment, their components including dyes can be easily washed away by rains to water streams just like pesticides on agricultural soils. Dyes can also get to water streams because of sewage pipes blockage or breakdown which are connected to the drains onto which domestic wastewater is disposed. Moreover, dyes usage has also been reported in battery industry (dye-sensitised solar cell) meaning that the disposal of their products also counts in dye transportation to the environment. As mentioned above, dyes end up in the environment through different ways. When industrial wastewater which mostly contains dyes are used to wet agricultural lands they harden the soil and make it difficult for plants to grow and for root penetration (Chandra *et al.*, 2009). Dye containing effluents when reached up to fresh water blocks the sunlight penetration, which is required for the photosynthesis of aquatic flora and fauna, and by doing so; it decreases oxygen, which is necessary for respiration of aquatic organisms (Carmen and Daniela, 2012). Since dyes reach water streams with many other organic substances, which are water insoluble, they sometimes form a layer above water surface, which blocks oxygen transfer present in water-air interface (Mani and Bharagava, 2018). Dye containing wastes may also lead to death of aquatic organisms including fish, which are food to human beings hence causing some imbalance in food chain. Sometimes, fish may carry the toxic



University of Fort Hare
Together in Excellence

substances constituted in wastewater specifically dyes and pass them to human beings and other living organisms through the food chain (Puvaneswari *et al.*, 2006). As a result these dyes have been reported to cause sporadic fever, cramps, hypertension, renal damages, etc (Puvaneswari *et al.*, 2006). These substances were also associated with cancer because of their carcinogenicity (Decouple, 1979).

2.5. Removal of pesticides from wastewater

Different conventional processes used to treat pesticides in wastewater have been reported, they include adsorption, oxidation, ultrasound techniques, and photo-catalytic removal (Matouq *et al.*, 2008). Yu *et al.* (2014) also mentioned biological treatment, coagulation/flocculation, ion exchange and membrane separation. However, conventional methods such as activated ion-exchange method, carbon adsorption and biological treatments still have their own disadvantages and limitations (Gao *et al.*, 2010; Verma *et al.*, 2012). Worthy of note, Matouq *et al.* (2008) reported that while a process is considered suitable for a specific application, it might not be suitable for others. Ahmad *et al.* (2010) defined adsorption process, as a surface phenomenon depending heavily on the available active sites, specific adsorptive surface area and porosity of adsorbent together with various types of interactions. Generally, carbonaceous materials have a unique place in the main adsorbents for their long time application in adsorption of various organic compounds (Ahmad *et al.*, 2010). According to Kyriakopoulos and Doulia (2006) granular activated carbon (GAC) and powder activated carbons (PAC) forms are the most widely used as they are said to be very effective and capable materials for the adsorption of a wide range of pesticides. Gupta *et al.* (2011) studied adsorption for the removal of pesticides using activated carbon prepared from waste rubber tire. Due to high cost of fragile activated carbons, polymeric resins were synthesized as one of potential alternatives to activated carbon (Ahmad *et al.*, 2010). Based on the properties of nanoparticles such as large adsorptive surface area, chemical and physical stabilities (Saharan *et al.*, 2014), they have also been used for pollutants removal in the

past few decades (Kyriakopoulos and Doulia, 2006). Conde-Avila *et al.* (2020) studied the biodegradation of pesticides by immobilization of microorganism. Ha *et al.* (2009) also used the same method specifically by using bacteria. To remove pesticides from aqueous solutions, Lafi and Al-Qodah (2006) used advanced oxidation and biological treatment techniques at the same time. Fiorenza *et al.* (2020) made use of molecular imprinting on TiO₂ photocatalysts to remove pesticides from water.

2.6. Dye removal techniques from polluted water

Treatment methods of industrial wastewater are divided into four stages (i.e. preliminary, followed by primary, then secondary, and tertiary processes) (Sonune *et al.*, 2014). The first two stages involve the elimination of coarse pollutants which are visible to the eyes (i.e. cloths, plastics, wood, papers, grits and more) and solids that froth by skimming and eradication of inorganic and organic materials which can be settled by flotation and sedimentation (Mashkoo and Nasar, 2020). However, secondary treatment includes microbial application to degrade colloidal and dissolved organic matter, which improve waste components stabilities (Stasinakis *et al.*, 2013). Biological (anaerobic, aerobic, facultative or anoxic or a combination of these), chemical (ozonation, chemical precipitation, ion exchange, oxidation, photocatalysis process) or physical (sedimentation, coagulation-flocculation, filtration, reverse osmosis, adsorption) techniques are used in advanced and tertiary treatments (Ye *et al.*, 2019; Ye *et al.*, 2017).

These treatment types are considered to remove pollutants that cannot be eliminated in the secondary treatment. Biological treatments are no longer of interest since dyes possess antimicrobial activity as mentioned earlier. The chemical processes have some short falls, which include low efficiency, high cost, and less flexibility. Therefore, the focus will be on physical techniques. Due to small particle size of dye molecules sedimentation is no longer of great use in dye removal. Coagulation-flocculation is the most commonly used physical method for dyes' elimination from water because of possibility of complete recovery of coagulating agents from

treated wastewater, high efficiency and ease of operation. Nevertheless, there are still concerns regarding it such as inapplicability in water-soluble dyes and its toxic sludge production (Singh and Arora, 2011; Crini and Lichtfouse, 2019). Filtration is suitable for classes of dyes as filter sizes can reach up to nano-filters and ultrafilters but its usage has limitations such as considerable consumption of energy, generation of concentrated sludge, high operational pressure, short life span and high membrane cost (Ahmed *et al.*, 2017; Saini, 2017; Koyuncu and Güney, 2013). Reverse osmosis has been reported to be effective in desalting due to maximum salt elimination and decolourizing. However, its use is limited due its high-pressure usage, operation cost and common membrane clogging (Saini, 2017; Koyuncu and Güney, 2013). Adsorption is known to be easy and has wide application, highly effective and economical. Adsorbents may be tailored from wastes and possess the possibility of regeneration and flexibility in enhancing its efficiency by chemical modifications (e.g. functionalization) (Saini, 2017; Nasar and Mashkoo, 2019). These are the reasons why is it highly studied by researchers.



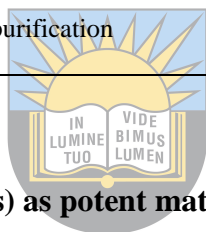
2.7. Zinc oxide nanoparticles global industrial usage

Zinc oxide nanoparticles' production has rapidly expanded in the past two decades. Thus, in 2015 they were counted the third highly produced nanoparticles among titanium oxide and silicon dioxide (Kaya *et al.*, 2015). Their production falls between hundred to thousand tons annually (Abdel-Daim *et al.*, 2019). Abdel-Daim *et al.* (2019) further reported that, their annual production can reach up to hundred times more compared to other nanomaterials in exception of the two mentioned. Their high and growing production is associated with their exceptional physicochemical properties (Jiang *et al.*, 2018). These properties include their photocatalytic property, high thermal and chemical stabilities due to their wide band gap, resistance to corrosion, biomedical activity; as they are crucial ingredients in production of ointments, enzymes and sunscreens for itch and pain relief (Siddiqi and Husen, 2018). Another crucial properties of these nanoparticles is their high surface area to volume ratio (Abdel-Daim *et al.*, 2019), which

contributes more in all the aforementioned properties. Due to these exceptional properties, ZnO NPs has earned much attention of the global industries. Table 2.5 show some of common global applications of zinc oxide nanoparticles.

Table 2.5: Some of the common global industrial usage of zinc oxide nanoparticles.

Name of nanoparticles	Industrial application	Reference
Zinc oxide	Antimicrobial application	(Venkataraju <i>et al.</i> , 2014)
	Food packaging	(Espitia <i>et al.</i> , 2012)
	Biomedical application	(Mirzaei and Darroudi, 2017)
	Cosmetics production	(Smijs and Pavel, 2011)
	Glass ionomer cement production	(Panahandeh <i>et al.</i> , 2018)
	Rubber production	(Xu <i>et al.</i> , 2019)
	Paint production	(Rohani <i>et al.</i> , 2022)
	Water purification	(Spoială <i>et al.</i> , 2021)



2.8. Metallic nanoparticles (MNPs) as potent materials for pesticides and dyes removal

Metallic nanoparticles are indeed among the most extensively studied materials in nano-science (Astruc, 2008). Metallic nanoparticles include metal nanoparticles, bimetallic nanoparticles, metal oxide nanoparticles, composite nanoparticles, etc. (Table 2.6 - 2.7). This is because they bridge the gap between atomic or molecular and bulk materials structures (Thakkar *et al.*, 2010). Normally, bulk metallic materials possess constant physical properties irrespectively of their size, however when they are nano-sized it is not the case (Thakkar *et al.*, 2010). Nanoparticles are microscopic particles having at least one dimension, which is less than 100 nm (Thakkar *et al.*, 2010). Generally, nanoparticles have large surface areas compared to micrometre and larger particles of the same mass (Bottero *et al.*, 2011) hence, they have greater sorption capacities. This is what makes metallic nanoparticles potent for pesticides and dyes removal from aqueous solutions.

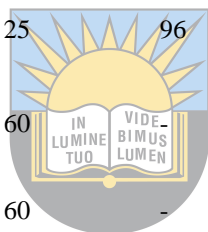
Table 2.6: Some commonly used metallic nanoparticles for the removal of pesticides from wastewater.

Name of metallic nanoparticles	Target pesticide	Contact time (min)	Adsorbed Amount (%)	Adsorption capacity (mg/g)	Reference
Laccase immobilized magnetic iron nanoparticles	Chlorpyrifos	720	99	-	(Das <i>et al.</i> , 2017)
Bimetallic Ni/Fe	DDT	1440	> 90	-	(Tian <i>et al.</i> , 2009)
Iron oxide	Lindane, DDT and aldrin	720	81, 100, and 79	-	(Shoiful <i>et al.</i> , 2016)
Chitosan-zinc oxide nanoparticles	Permethrin	180	99	-	(Dehaghi <i>et al.</i> , 2014)
Tungsten oxide doped zinc oxide nanoparticles	Diazinon	180	93.2	-	(Maleki <i>et al.</i> , 2020)
magnetic nanospheres coated with polystyrene	lindane, aldrin, dieldrin and endrin	20	-	10.2, 24.7, 21.3 and 33.5	(Lan <i>et al.</i> , 2014)
Fe ₃ O ₄ /graphene nanocomposite	ametryn	60	93.6	54.8	(Boruah <i>et al.</i> , 2017)
Copper chitosan nanocomposite	malathion	-	-	322.6	(Jaiswal <i>et al.</i> , 2012)
graphene oxide based silica coated magnetic nanoparticles functionalized with 2-phenylethylamine	Parathion Malathion and Chlorpyrifos	15	-	135, 61.9 and 25.6	(Wanjeri <i>et al.</i> , 2018)
BMTF-IL and CTAB functionalized Zinc oxide nanoparticles, and bare nanoparticles	Naphthalene	40	-	148.3, 89.96 and 66.80	(Kaur <i>et al.</i> , 2017)

Hence, smaller particles, precisely nanoparticles, are said to have more active sites. It has also been noticed that structure and other properties of nanoparticles change as particle size decreases (Waychunas and Zhang, 2008). A practical example would be the case of gamma-Al₂O₃ that becomes energetically stable when particle surface area exceeds 125 m²g⁻¹ compared to alpha-Al₂O₃ (McHale *et al.*, 1997).

Table 2.7: Some of previously reported adsorbents for various dyes' removal.

Name of metallic nanoparticles	Target dye	Contact time (minutes)	Maximum adsorbed Amount (%)	Adsorption capacity (mg/g)	Reference
Nickel oxide nanoparticles-modified diatomite	Basic red 46	60	84.49	105.61	(Sheshdeh <i>et al.</i> , 2014)
nanoparticle-modified polymeric adsorbent	Basic red 46	20	96.92	-	(Rahimi <i>et al.</i> , 2018)
SiO ₂ -coated Fe ₃ O ₄ magnetic nanoparticles	Methyl red	-	-	49.50	(Shariati-Rad <i>et al.</i> , 2014)
biofabricated crystalline α -MnO ₂ nanoparticles	Methyl red	60	100	74.02	(Srivastava and Choubey, 2021)
magnetite nanoparticles loaded Azolla	Crystal violet	25	-	30.21	(Alizadeh <i>et al.</i> , 2017)
magnetite nanoparticles loaded Fig leaves	Crystal violet	25	-	53.47	(Alizadeh <i>et al.</i> , 2017)
Cobalt nanoparticles	Rhodamine b	25	96	468	(Tang <i>et al.</i> , 2014)
MnFe ₂ O ₄ nanoparticles	Rhodamine b	60	-	9.30	(Lamdab <i>et al.</i> , 2018)
Zero-valent Fe NPs	Acid orange 7	60	-	66.6	(Zaheer <i>et al.</i> , 2019)
Fe-Mn binary oxide nanoparticles	Methylene blue	720	-	72.32	(Lu <i>et al.</i> , 2019)
NiO nanoparticles and CuO nanoparticles	Methyl orange	720	-	188.68 and 121.95	(Darwish <i>et al.</i> , 2019)
Flower shaped ZnO nanoparticles	Brilliant green and congo red	-	-	238 and 71.4	(Kataria and Garg, 2017)
Collagen-g-p(AA-co-NVP)/Fe ₃ O ₄ @SiO ₂	Brilliant green	220	96	-	(Salem <i>et al.</i> , 2016)
Bimetallic Fe-Zn nanoparticles	Congo red	60	-	28.56	(Gautam <i>et al.</i> , 2015)
silver nanoparticles	Malachite green	-	≥ 90	-	(Pandian <i>et al.</i> , 2017)
Bimetallic nanoparticles	Fe-Zn Malachite green	60	-	21.74	(Gautam <i>et al.</i> , 2015)



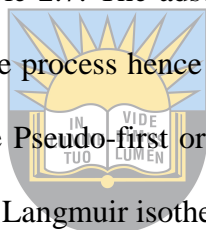
University of Fort Hare
Together in Excellence

Moreover, electronic properties and band gaps of nanoparticles versus their larger counterparts are different as a result of decreased size (Madden and Hochella Jr, 2005). The reactivity of metal-

oxide nanoparticles also can change with decreasing particle size (Brown Jr and Calas, 2012). Previous studies also showed that the potency of MNPs can also be improved via surface modifications (i.e. surface coating (Saravaia *et al.*, 2021), ligand exchange (Chen *et al.*, 2017) and functionalization (Chatterjee *et al.*, 2020)). Nanoparticles' surface coating enhances both the physical and chemical properties of nano-materials, which is key for their successful applications including adsorption (Hong *et al.*, 2006). Posthumus *et al.* (2004) observed improved compatibility of oxidic nanoparticles with organic matrices after 3-methacryloxypropyltrimethoxysilane coating. Grasset *et al.* (2003) used aminopropyltriethoxysilane to coat commercial ZnO nanoparticles under different conditions, and they realised that the coating was controllable, modification could not change the ZnO transmittance spectra, the particle size remains almost constant, and the aminosilane coating could increase their photo-stability. Another surface coating effect was observed in a study by Min *et al.* (2003), where conformal Al₂O₃ layer was deposited on ZnO nanorods and covered them without changing their properties. Even though, smaller particles are favourable in adsorption, metal nanoparticles have a tendency to agglomerate irreversibly (Caragheorgheopol and Checkik, 2008). This agglomeration can be reduced by coating with an additional protective layer of organic ligands. As a result of high curvature and high surface area of smaller nanoparticles, the number of protecting ligands is quite large for different cores (Caragheorgheopol and Checkik, 2008).

In this case, protecting ligands are the ones exposed to external reagents and used solvents. Therefore, nanoparticle properties (i.e. chemical reactivity, solubility and supramolecular binding) are determined by the protecting ligand structures (Caragheorgheopol and Checkik, 2008). In the case of pesticides adsorption, protecting ligand should have great affinity to the targeted pesticides if not; it must be substituted with the suitable one. In this way adsorption capacity would have been improved. Functionalization of surfaces of inorganic nanoparticles signifies a fundamental method for modifying their chemical properties and enhancing their

colloidal stability (Ghosh Chaudhuri and Paria, 2012). Ideally, chemical functionalization is accomplished by covalent grafting of molecular building blocks having a suitable anchor group (Zeininger *et al.*, 2015). However, such chemical alterations are mostly based on substitution reactions of covalently bound ligands on the nanoparticles' surface (Zeininger *et al.*, 2015). Due to the fact that desorption of the initial ligand creates a gap in the shell, partially free and highly reactive nanoparticle surfaces can stimulate permanent changes to the nanoparticles, such as aggregation and growth, substituting ligands can be problematic (Boal *et al.*, 2002). Zeininger *et al.* (2015) reported shell-by-shell (SbS) coating with functional, tailor-designed amphiphiles of inorganic nanoparticles. Table 2.6 shows some of the commonly used metallic nanoparticles for pesticides' removal while the commonly used metallic nanoparticles for the removal of dyes from aqueous solutions are presented in Table 2.7. The adsorption kinetics gives the dynamics and rate-determining step information of the process hence data obtained from this process is often fitted into different models such as the Pseudo-first order (Table 2.8). Adsorption data is also fitted into adsorption isotherms such as Langmuir isotherm (Table 2.9).



University of Fort Hare

Table 2.8: Commonly used adsorption kinetic models. *in Excellence*

Model	Equation	Parameters*	Reference
Pseudo-first order	$q_t = q_{eq} (1 - e^{-K_1 t})$	q_{eq}, K_1	(Ho, 2003)
Pseudo-second order	$q_t = (K_2 q_{eq}^2 t) / (1 + K_2 q_{eq} t)$	K_2, q_{eq}	(Lin and Wang, 2009)
Intraparticle diffusion	$q_t = K_{id} \sqrt{t} + l$	K_{id}, l	(Demirbas <i>et al.</i> , 2004)

* q_t - quantity of adsorbate adsorbed at time t ($\text{mg} \cdot \text{g}^{-1}$); q_{eq} - quantity of adsorbate adsorbed at equilibrium ($\text{mg} \cdot \text{g}^{-1}$); K_1 - pseudo-first order rate constant (min^{-1}); K_2 - pseudo second order rate constant ($\text{g} \cdot \text{mg}^{-1} \cdot \text{min}^{-1}$); k_{id} - intraparticle diffusion rate constant ($\text{mg} \cdot \text{g}^{-1} \cdot \text{min}^{0.5}$) and l - is a constant related to the thickness of the boundary layer ($\text{mg} \cdot \text{g}^{-1}$).

Table 2.9: Commonly used adsorption isotherms.

Isotherm	Equation	Parameters*	Reference
Langmuir	$1/q_e = (1/K_L q_{max})(1/C_e) + (1/q_{max})$	K_L and q_{max}	(Zhou <i>et al.</i> , 2011)
Freundlich	$\log q_e = \log K_F + (1/n) \log C_e$	K_F and n	(Zhou <i>et al.</i> , 2011)
Temkin	$q_e = B \ln K_T + B \ln C_e$	K_T and B	(Jinendra <i>et al.</i> , 2019)

* q_e - adsorption capacity at equilibrium; K_L - Langmuir constant; q_{max} - maximum adsorption capacity; C_e - adsorbate concentration at equilibrium; K_F - Freundlich constant; n - heterogeneity factor; B - Temkin constant and K_T - equilibrium binding constant.

2.9. Metallic nanoparticles synthesis methods

2.9.1. Sol – gel method

Sol–gel method includes hydrolysis and condensation of metal alkoxides resulting in metal oxide particles being dispersed in a sol after which gelling or drying is done through solvent removal or a chemical reaction (Oh and Park, 2011). Normally an acid or a base is used for alkoxide hydrolysis process (Ladj *et al.*, 2013). The obtained nanoparticles (NPs) properties depend on the speed of hydrolysis-condensation process, temperature, solution composition and pH of the reaction medium (Oh and Park, 2011). Disadvantage of this method is the post-treatment of the products due to by-products contamination (Oh and Park, 2011).

2.9.2. Co-precipitation method

Co-precipitation includes the production of metallic hydroxide from the solution of the starting salt such as metal nitrate or metal chloride in water using a precipitating medium. This method is commonly used in MNPs synthesis such as magnetite usually using NaOH and NH₄OH aqueous solution as precipitating medium (Mascolo *et al.*, 2013). The nature of alkali, pH, the rate of addition of alkaline solution and the drying conditions of the precipitate affect the paramagnetic properties, size and the extent of agglomeration of magnetite nanoparticles. These have been revealed through the use of NaOH, KOH and (C₂H₅)₄NOH solutions as precipitating media (Mascolo *et al.*, 2013). Even though this method is commonly used in magnetic nanoparticles synthesis, it can also be used for the synthesis of other nanoparticles. Low cost, simplicity, moderate reaction conditions at low synthesis temperature and ease of scale-up are the benefits of this method (Mukhtar *et al.*, 2012).

2.9.3. Sonothermal method

Sonothermal method as one competitive alternative has been broadly employed to produce new material with unique features (Tsaytler *et al.*, 2011). In this method, starting material solution (e.g. metallic salt solution) is exposed to live intensified ultrasonic vibrations capable of breaking

the compounds' chemical bonds. The ultrasound waves causes alternate compression and relaxation on the solution subjected to (Stankic *et al.*, 2016). Through that, metallic nanoparticles are formed. This method requires pressure of about 1800 atm, working temperatures of about 5000 K and cooling speed of above 1010 K/s (Solans *et al.*, 2005). The excessive cooling high speed is found to affect the crystallization and formation of the products (Gendanken, 2003). The advantage of this method is that it is fast, simple, convenient, economical, and environmentally friendly (Dhas and Suslick, 2005). However, there is still a barrier on its use, which is high-energy consumption in order to attain very high transient temperatures and cooling rates.

2.9.4. Microemulsion

This method involves two unmixing phases like oil and water, which are separated by a monolayer of molecules called surfactant, resulting into two binary systems—water/surfactant and oil/surfactant to allow the oil-soluble tails of the surfactant molecules to be dissolved in the oil phase and vice versa for the water-soluble heads (Bang and Suslick, 2007). In this method, appropriate amounts of oil, metallic precursor and water are mixed at room temperature to form homogenized phase (Sanchez-Dominguez *et al.*, 2009). Precipitating/oxidizing/reducing agents are then added, under vigorous stirring, to allow sedimentation of the formed nanoparticles (Stankic *et al.*, 2016). Further stabilization as a result of aggregation and impurity of products are the disadvantages of this method (Wu *et al.*, 2008). However, the ability to control the formation of various kinds of core-shell structures with sub-nanometric resolution is the major benefit of this method (Stankic *et al.*, 2005).

2.9.5. Green synthesis

Usually in green synthesis, plant materials are used (i.e. seeds, stem, roots, leaves and roots) due to their unique phytochemicals (Agarwal *et al.*, 2017). In addition, micro-organisms are also used at times (Raliya and Tarafdar, 2014). Metal oxide nanoparticles synthesis from plant materials are synthesis through extraction method. Plant extraction synthesis method is a very eco-friendly

and highly affordable process; intermediate based groups are not involved during the process (Agarwal *et al.*, 2017). It does not use expensive precursors and equipment; it is also less time consuming and gives high yield of high purity (Lee *et al.*, 2015). Generally, leave or flower extracts for ZnO NPs are obtained by washing the materials thoroughly under running tap water, followed by sterilization using distilled or double distilled water (Lee *et al.*, 2015). To facilitate the process, plant materials of larger surface areas are used. Larger surface area can be obtained by crushing the dried plant materials using mortar and pestle. Plant extracts are mixed with the precursor solution under stirring at prescribed temperature in order to obtain metal oxide nanoparticles (Zheng *et al.*, 2015).

2.10. Most common metal oxide nanoparticles characterization techniques

Metal oxide nanoparticles are usually characterized by various techniques for different reason. One of the most important characterizations are carried out for material formation confirmation. Usually this is done using spectroscopy techniques most commonly with Raman Spectroscopy whereas some researchers use FTIR (Mohammadian *et al.*, 2018; Inbasekaran *et al.*, 2014) and it is indicated by a strong peak or two in the finger print regions of FTIR. However, the strongest vibrational band represents metal-oxygen bond in Raman spectrum (Chassaing *et al.*, 2007; Inbasekaran *et al.*, 2014). Even though these observations are noticed, it cannot be concluded that metal oxide nanoparticles have been synthesised because some elements might as well be present in sufficient proportions. Therefore, researchers further consider more techniques SEM combined together with EDX. In this characterization technique chemical/elemental composition can be determined using EDX spectrum (Rekha *et al.*, 2010). Moreover, particle geometry can be determined by SEM images (Vanathi *et al.*, 2014) and it is also possible to determine particle sizes with this technique but it can only be accurate when there is completely no agglomeration. The particle size and shape are usually clearly determined with TEM (Becheri *et al.*, 2008). However, some researchers determine shape using XRD as well as average particle size

(Kumar *et al.*, 2013). XRD is also used to determine crystallinity of metal oxide nanoparticles (Kumar *et al.*, 2013). In some cases, these nanoparticles are modified with organic materials to fulfil certain desires and these modifications are usually confirmed with FTIR (Tu *et al.*, 2011). More characterization techniques are considered for some properties of these materials which are not of much interest in this study hence they are not discussed. For the determination of the purity and thermal stability of these materials, TGA is employed.

References

- Abel, A., 2012. The history of dyes and pigments: From natural dyes to high performance pigments. *Colour Design*, pp. 557-587.
- Agarwal, H., Kumar, S.V. and Rajeshkumar, S., 2017. A review on green synthesis of zinc oxide nanoparticles—An eco-friendly approach. *Resource-Efficient Technologies*, 3(4), pp.406-413.
- Ahmad, T., Rafatullah, M., Ghazali, A., Sulaiman, O., Hashim, R. and Ahmad, A., 2010. Removal of pesticides from water and wastewater by different adsorbents: a review. *Journal of Environmental Science and Health, Part C*, 28(4), pp.231-271.
- Ahmed, M.B., Zhou, J.L., Ngo, H.H., Guo, W., Thomaidis, N.S. and Xu, J., 2017. Progress in the biological and chemical treatment technologies for emerging contaminant removal from wastewater: a critical review. *Journal of Hazardous Materials*, 323, pp.274-298.
- Ahmed, R., Seth, V., Pasha, S.T. and Banerjee, B.D., 2000. Influence of dietary ginger (*Zingiber officinale* Rosc) on oxidative stress induced by malathion in rats. *Food and Chemical Toxicology*, 38(5), pp.443-450.
- Alizadeh, N., Shariati, S. and Besharati, N., 2017. Adsorption of crystal violet and methylene blue on azolla and fig leaves modified with magnetite iron oxide nanoparticles. *International Journal of Environmental Research*, 11(2), pp.197-206.
- Al-Muzaini, S., 1998. Industrial wastewater management in Kuwait. *Desalination*, 115(1), pp.57-62.

Amaral, A.F., 2014. Pesticides and asthma: challenges for epidemiology. *Frontiers in Public Health*, 2, pp.6.

Anand, P., Kunnumakara, A.B., Sundaram, C., Harikumar, K.B., Tharakan, S.T., Lai, O.S., Sung, B. and Aggarwal, B.B., 2008. Cancer is a preventable disease that requires major lifestyle changes. *Pharmaceutical Research*, 25(9), pp.2097-2116.

Arapoglou, D., Vlyssides, A., Israilides, C., Zorpas, A. and Karlis, P., 2003. Detoxification of methyl-parathion pesticide in aqueous solutions by electrochemical oxidation. *Journal of Hazardous Materials*, 98(1-3), pp.191-199.

Astruc, D., 2008. Transition-metal nanoparticles in catalysis: from historical background to the state-of-the art. *Nanoparticles and Catalysis*, 16, pp.1-48.

Azab, H.A. and Kamel, R.M., 2016. Binding of chlorfenvinphos and malathion with DNA and their detection using new sensitive luminescent Tb (III) complex probe. *Journal of Luminescence*, 170, pp.671-678.



Bang, J.H. and Suslick, K.S., 2007. Sonochemical synthesis of nanosized hollow hematite. *Journal of the American Chemical Society*, 129(8), pp.2242-2243.

Together in Excellence

Becheri, A., Dürr, M., Nostro, P.L. and Baglioni, P., 2008. Synthesis and characterization of zinc oxide nanoparticles: application to textiles as UV-absorbers. *Journal of Nanoparticle Research*, 10(4), pp.679-689.

Benkhaya, S., M'rabet, S. and El Harfi, A., 2020. A review on classifications, recent synthesis and applications of textile dyes. *Inorganic Chemistry Communications*, 115, p.107891.

Berradi, M., Hsissou, R., Khudhair, M., Assouag, M., Cherkaoui, O., El Bachiri, A. and El Harfi, A., 2019. Textile finishing dyes and their impact on aquatic environs. *Heliyon*, 5(11), p.e02711.

Bhuvaneshwari, R., Padmanaban, K. and Babu Rajendran, R., 2015. Histopathological alterations in muscle, liver and gill tissues of zebra fish *Danio rerio* due to environmentally relevant concentrations of organochlorine pesticides (OCPs) and heavy metals. *International Journal of Environmental Research*, 9(4), pp.1365-1372.

Bleiberg, J., Wallen, M., Brodtkin, R. and Applebaum, I.L., 1964. Industrially acquired porphyria. *Archives of Dermatology*, 89(6), pp.793-797.

Boal, A.K., Das, K., Gray, M. and Rotello, V.M., 2002. Monolayer exchange chemistry of γ -Fe₂O₃ nanoparticles. *Chemistry of Materials*, 14(6), pp.2628-2636.

Boruah, P.K., Sharma, B., Hussain, N. and Das, M.R., 2017. Magnetically recoverable Fe₃O₄/graphene nanocomposite towards efficient removal of triazine pesticides from aqueous solution: investigation of the adsorption phenomenon and specific ion effect. *Chemosphere*, 168, pp.1058-1067.

Bottero, J.Y., Auffan, M., Rose, J., Mouneyrac, C., Botta, C., Labille, J., Masion, A., Thill, A. and Chaneac, C., 2011. Manufactured metal and metal-oxide nanoparticles: Properties and perturbing mechanisms of their biological activity in ecosystems. *Comptes Rendus Geoscience*, 343(2-3), pp.168-176.

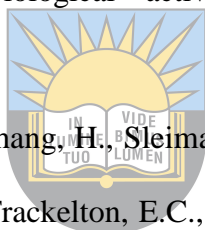
Bradfield, J.P., Qu, H.Q., Wang, K., Zhang, H., Sleiman, P.M., Kim, C.E., Mentch, F.D., Qiu, H., Glessner, J.T., Thomas, K.A. and Frackelton, E.C., 2011. A genome-wide meta-analysis of six type 1 diabetes cohorts identifies multiple associated loci. *Public Library of Science Genetics*, 7(9), pp.1002293.

Brown Jr, G.E. and Calas, G., 2012. Section 14. Does Size Matter? The Effect of Size on Nanoparticle Structure and Properties. *Geochemical Perspectives*, 1(4-5), pp.611-627.

Cahill, D.P., Kinzler, K.W., Vogelstein, B. and Lengauer, C., 1999. Genetic instability and darwinian selection in tumours. *Trends in Cell Biology*, 9(12), pp.M57-M60.

California Weed Conference, 1985. Principles of weed control in California. *Thomson Publications*.

Caragheorghopol, A. and Chechik, V., 2008. Mechanistic aspects of ligand exchange in Au nanoparticles. *Physical Chemistry Chemical Physics*, 10(33), pp.5029-5041.



University of Fort Hare
Together in Excellence

Carmen, Z. and Daniela, S., 2012. *Textile organic dyes-characteristics, polluting effects and separation/elimination procedures from industrial effluents-a critical overview* (Vol. 3, pp. 55-86). Rijeka: IntechOpen.

Chandra, R. and Bharagava, R.N., 2013. Bacterial degradation of synthetic and kraft lignin by axenic and mixed culture and their metabolic products. *Journal of Environmental Biology*, 34(6), pp.991.

Chandra, R., Bharagava, RN., Yadav, S., and Mohan, D. 2009. Accumulation and distribution of toxic metals in wheat (*Triticum aestivum* L.) and Indian mustard (*Brassica campestris* L.) irrigated with distillery and tannery effluents. *Journal of Hazardous Materials*, 162, pp. 1514–1521.

Chassaing, P.M., Demangeot, F., Paillard, V., Zwick, A., Combe, N., Pagès, C., Kahn, M.L., Maisonnat, A. and Chaudret, B., 2007. Raman study of E 2 and surface phonon in zinc oxide nanoparticles surrounded by organic molecules. *Applied Physics Letters*, 91(5), pp.053108.

Chatterjee, S., Guha, N., Krishnan, S., Singh, A.K., Mathur, P. and Rai, D.K., 2020. Selective and recyclable Congo red dye adsorption by spherical Fe₃O₄ nanoparticles functionalized with 1, 2, 4, 5-benzenetetracarboxylic acid. *Scientific Reports*, 10(1), pp.1-11.

Chen, K.C., Wu, J.Y., Liou, D.J. and Hwang, S.C.J., 2003. Decolorization of the textile dyes by newly isolated bacterial strains. *Journal of Biotechnology*, 101(1), pp.57-68.

Chen, Q., Zhou, K., Chen, Y., Wang, A. and Liu, F., 2017. Removal of ammonia from aqueous solutions by ligand exchange onto a Cu (II)-loaded chelating resin: kinetics, equilibrium and thermodynamics. *Royal Society of Chemistry Advances*, 7(21), pp.12812-12823.

Conde-Avila, V., Ortega-Martínez, L.D., Loera, O., El Kassis, E.G., Dávila, J.G., Valenzuela, C.M. and Armendáriz, B.P., 2020. Pesticides degradation by immobilised microorganisms. *International Journal of Environmental Analytical Chemistry*, pp.1-31.

Crini, G. and Lichtfouse, E., 2019. Advantages and disadvantages of techniques used for wastewater treatment. *Environmental Chemistry Letters*, 17(1), pp.145-155.

Darwish, A.A.A., Rashad, M. and AL-Aoh, H.A., 2019. Methyl orange adsorption comparison on nanoparticles: Isotherm, kinetics, and thermodynamic studies. *Dyes and Pigments*, 160, pp.563-571.

Das, A., Singh, J. and Yogalakshmi, K.N., 2017. Laccase immobilized magnetic iron nanoparticles: fabrication and its performance evaluation in chlorpyrifos degradation. *International Biodeterioration & Biodegradation*, 117, pp.183-189.

Dayan, F.E., Duke, S.O. and Grossmann, K., 2010. Herbicides as probes in plant biology. *Weed Science*, 58(3), pp.340-350.

de Boer, J., Dao, Q.T., van Leeuwen, S.P., Kotterman, M.J. and Schobben, J.H., 2010. Thirty year monitoring of PCBs, organochlorine pesticides and tetrabromodiphenylether in eel from The Netherlands. *Environmental Pollution*, 158(5), pp.1228-1236.

Decouple, P., 1979. Cancer risks associated with employment in the leather and leather products industry. *Archives of Environmental Health: An International Journal*, 34(1), pp.33-37.

Dehaghi, S.M., Rahmanifar, B., Moradi, A.M. and Azar, P.A., 2014. Removal of permethrin pesticide from water by chitosan–zinc oxide nanoparticles composite as an adsorbent. *Journal of Saudi Chemical Society*, 18(4), pp.348-355.

Demirbas, E., Kobya, M., Senturk, E. and Ozkan, T., 2004. Adsorption kinetics for the removal of chromium (VI) from aqueous solutions on the activated carbons prepared from agricultural wastes. *Water Science*, 30(4), pp.533-539.

Dhas, N.A. and Suslick, K.S., 2005. Sonochemical preparation of hollow nanospheres and hollow nanocrystals. *Journal of the American Chemical Society*, 127(8), pp.2368-2369.

Diagne, M., Oturan, N. and Oturan, M.A., 2007. Removal of methyl parathion from water by electrochemically generated Fenton's reagent. *Chemosphere*, 66(5), pp.841-848.

Dich, J., Zahm, S.H., Hanberg, A. and Adami, H.O., 1997. Pesticides and cancer. *Cancer Causes & Control*, 8(3), pp.420-443.

dos Santos Silva, P.M., Fiaschitello, T.R., de Queiroz, R.S., Freeman, H.S., da Costa, S.A., Leo, P., Montemor, A.F. and da Costa, S.M., 2020. Natural dye from *Croton urucurana* Baill. bark: Extraction, physicochemical characterization, textile dyeing and color fastness properties. *Dyes and Pigments*, 173, pp.107953.

El Qada, E.N., Allen, S.J. and Walker, G.M., 2008. Adsorption of basic dyes from aqueous solution onto activated carbons. *Chemical Engineering Journal*, 135(3), pp.174-184.

Eren, E. and Afsin, B., 2007. Investigation of a basic dye adsorption from aqueous solution onto raw and pre-treated sepiolite surfaces. *Dyes and Pigments*, 73(2), pp.162-167.

Eren, E. and Afsin, B., 2009. Removal of basic dye using raw and acid activated bentonite samples. *Journal of Hazardous Materials*, 166(2-3), pp.830-835.

Espitia, P.J.P., Soares, N.D.F.F., Coimbra, J.S.D.R., de Andrade, N.J., Cruz, R.S. and Medeiros, E.A.A., 2012. Zinc oxide nanoparticles: synthesis, antimicrobial activity and food packaging applications. *Food and Bioprocess Technology*, 5(5), pp.1447-1464.

Evangelou, E., Ntritsos, G., Chondrogiorgi, M., Kavvoura, F.K., Hernández, A.F., Ntzani, E.E. and Tzoulaki, I., 2016. Exposure to pesticides and diabetes: a systematic review and meta-analysis. *Environment International*, 91, pp.60-68.

Fenik, J., Tankiewicz, M. and Biziuk, M., 2011. Properties and determination of pesticides in fruits and vegetables. *TrAC Trends in Analytical Chemistry*, 30(6), pp.814-826.

Feo, M.L., Eljarrat, E. and Barceló, D., 2010. Determination of pyrethroid insecticides in environmental samples. *TrAC Trends in Analytical Chemistry*, 29(7), pp.692-705.

Ferreira, E.S., Hulme, A.N., McNab, H. and Quye, A., 2004. The natural constituents of historical textile dyes. *Chemical Society Reviews*, 33(6), pp.329-336.

Fiorenza, R., Di Mauro, A., Cantarella, M., Iaria, C., Scalisi, E.M., Brundo, M.V., Gulino, A., Spitaleri, L., Nicotra, G., Dattilo, S. and Carroccio, S.C., 2020. Preferential removal of pesticides from water by molecular imprinting on TiO₂ photocatalysts. *Chemical Engineering Journal*, 379, pp.122309.

Forgacs, E., Cserháti, T. and Oros, G., 2004. Removal of synthetic dyes from wastewaters: a review. *Environment International*, 30(7), pp.953-971.

Franciscon, E., Zille, A., Fantinatti-Garboggini, F., Silva, I.S., Cavaco-Paulo, A. and Durrant, L.R., 2009. Microaerophilic–aerobic sequential decolourization/biodegradation of textile azo dyes by a facultative *Klebsiella* sp. strain VN-31. *Process Biochemistry*, 44(4), pp.446-452.

Fröse, A., Schmidtke, K., Sukmann, T., Junger, I.J. and Ehrmann, A., 2019. Application of natural dyes on diverse textile materials. *Optik*, 181, pp.215-219.

Gao, S., Du, M., Tian, J., Yang, J., Yang, J., Ma, F. and Nan, J., 2010. Effects of chloride ions on electro-coagulation-flotation process with aluminum electrodes for algae removal. *Journal of Hazardous Materials*, 182(1-3), pp.827-834.

Gascón, J., 1998. Monitoring of organonitrogen pesticides in the Ebro river. Preliminary loadings estimates. *Analyst*, 123(5), pp.941-945.

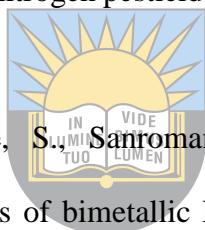
Gautam, R.K., Rawat, V., Banerjee, S., Sanroman, M.A., Soni, S., Singh, S.K. and Chattopadhyaya, M.C., 2015. Synthesis of bimetallic Fe–Zn nanoparticles and its application towards adsorptive removal of carcinogenic dye malachite green and Congo red in water. *Journal of Molecular Liquids*, 212, pp.227-236.

Gavrilescu, M., 2005. Fate of pesticides in the environment and its bioremediation. *Engineering in Life Sciences*, 5(6), pp.497-526.

Gedanken, A., 2003. Sonochemistry and its application to nanochemistry. *Current Science*, pp.1720-1722.

Gershon, H. and Shanks, L., 1975. Fungitoxicity of 1, 4-naphthoquinones to *Candida albicans* and *Trichophyton mentagrophytes*. *Canadian Journal of Microbiology*, 21 (9), pp. 1317-1321.

Ghosh Chaudhuri, R. and Paria, S., 2012. Core/shell nanoparticles: classes, properties, synthesis mechanisms, characterization, and applications. *Chemical Reviews*, 112(4), pp.2373-2433.



University of Fort Hare
Together in Excellence

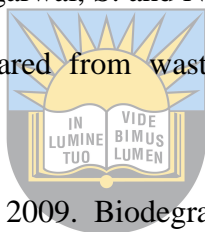
Gong, D.C., 2013. Pyrethroids pesticides residues and their behavior in a multimediu environment of Liangtan River Basin. *School of Environment and Civil Engineering, Chongqing Unviersity, Chongqing, 93*.

Grasset, F., Saito, N., Li, D., Park, D., Sakaguchi, I., Ohashi, N., Haneda, H., Roisnel, T., Mornet, S. and Duguet, E., 2003. Surface modification of zinc oxide nanoparticles by aminopropyltriethoxysilane. *Journal of Alloys and Compounds, 360(1-2)*, pp.298-311.

Gullino, M.L., Leroux, P. and Smith, C.M., 2000. Uses and challenges of novel compounds for plant disease control. *Crop Protection, 19(1)*, pp.1-11.

Gupta, R.C., Mukherjee, I.R.M., Malik, J.K., Doss, R.B., Dettbarn, W.D. and Milatovic, D., 2019. Insecticides. *Biomarkers in Toxicology*, pp.455-475.

Gupta, V.K., Gupta, B., Rastogi, A., Agarwal, S. and Nayak, A., 2011. Pesticides removal from wastewater by activated carbon prepared from waste rubber tire. *Water Research, 45(13)*, pp.4047-4055.



Ha, J., Engler, C.R. and Wild, J.R., 2009. Biodegradation of coumaphos, chlorferon, and diethylthiophosphate using bacteria immobilized in Ca-alginate gel beads. *Bioresource Technology, 100(3)*, pp.1138-1142.

University of Fort Hare
Together in Excellence

Hanahan, D. and Weinberg, R.A., 2000. The hallmarks of cancer. *Cell, 100(1)*, pp.57-70.

Hernández, A.F., Parrón, T. and Alarcón, R., 2011. Pesticides and asthma. *Current Opinion in Allergy and Clinical Immunology, 11(2)*, pp.90-96.

Hindson, C. and Diffey, B., 1984. Phototoxicity of glyphosate in a weedkiller. *Contact Dermatitis, 10(1)*, pp.51-52.

Ho, Y.S., 2003. Removal of copper ions from aqueous solution by tree fern. *Water Research, 37(10)*, pp.2323-2330.

Hong, R., Pan, T., Qian, J. and Li, H., 2006. Synthesis and surface modification of ZnO nanoparticles. *Chemical Engineering Journal, 119(2-3)*, pp.71-81

Huang, Z. and Lee, H.K., 2015. Micro-solid-phase extraction of organochlorine pesticides using porous metal-organic framework MIL-101 as sorbent. *Journal of Chromatography A*, 1401, pp.9-16.

Hunger, K., 2007. *Industrial dyes: chemistry, properties, applications*. John Wiley & Sons.

Hussein, S.A., Barakat, H.H., Merfort, I. and Nawwar, M.A., 1997. Tannins from the leaves of *Punica granatum*. *Phytochemistry*, 45(4), pp.819-823.

IARC Working Group, 1991. Occupational exposures in spraying and application of insecticides. *IARC Monographs on the Evaluation of the Carcinogenic Risk of Chemicals to Humans*, 53, pp.45-92.

Inbasekaran, S., Senthil, R., Ramamurthy, G. and Sastry, T.P., 2014. Biosensor using zinc oxide nanoparticles. *International Journal of Innovative Research in Science, Engineering and Technology*, 3(1), pp.8601-8606.

Isegbe, V., Habib, M., Obaje, J., Ekor, S. and Solomon, S., 2016. Residues of Organochlorine Pesticide in Dried Beans (*Vigna unguiculata*) Originating from Nigeria. *International Journal of Innovative Food, Nutrition & Sustainable Agriculture* 4 (4), pp.25-30.

Jaffrezic-Renault, N., 2001. New trends in biosensors for organophosphorus pesticides. *Sensors*, 1(2), pp.60-74.

Jaiswal, M., Chauhan, D. and Sankararamakrishnan, N., 2012. Copper chitosan nanocomposite: synthesis, characterization, and application in removal of organophosphorous pesticide from agricultural runoff. *Environmental Science and Pollution Research*, 19(6), pp.2055-2062.

Jarrah, N., 2017. Competitive adsorption isotherms of rhodium 6G and methylene blue on activated carbon prepared from residual fuel oil. *Journal of Environmental Chemical Engineering*, 5(5), pp.4319-4326.

Jemal, A., Siegel, R., Ward, E., Murray, T., Xu, J. and Thun, M.J., 2007. Cancer statistics, 2007. *CA: A Cancer Journal for Clinicians*, 57(1), pp.43-66.



University of Fort Hare
Together in Excellence

Jiao, S., Liu, P., Liu, Y., Zou, R., Zhao, Y., Liu, Y., Zhu, G. and Guo, Y., 2018. Binding properties of broad-specific monoclonal antibodies against three organophosphorus pesticides by a direct surface plasmon resonance immunosensor. *Analytical and Bioanalytical Chemistry*, 410(28), pp.7263-7273.

Jinendra, U., Kumar, J., Nagabhushana, B.M., Raghu, A.V. and Bilehal, D., 2019. Facile synthesis of CoFe₂O₄ nanoparticles and application in removal of malachite green dye. *Green Materials*, 7(3), pp.137-142.

Jokanović, M., 2009. Medical treatment of acute poisoning with organophosphorus and carbamate pesticides. *Toxicology Letters*, 190(2), pp.107-115.

Kanthasamy, A.G., Kitazawa, M., Kanthasamy, A. and Anantharam, V., 2005. Dieldrin-induced neurotoxicity: relevance to Parkinson's disease pathogenesis. *Neurotoxicology*, 26(4), pp.701-719.

Karami-Mohajeri, S. and Abdollahi, M., 2011. Toxic influence of organophosphate, carbamate, and organochlorine pesticides on cellular metabolism of lipids, proteins, and carbohydrates: a systematic review. *Human & Experimental Toxicology*, 30(9), pp.1119-1140.

Kataria, N. and Garg, V.K., 2017. Removal of Congo red and Brilliant green dyes from aqueous solution using flower shaped ZnO nanoparticles. *Journal of Environmental Chemical Engineering*, 5(6), pp.5420-5428.

Kaya, H.K. and Vega, F.E., 2012. Scope and basic principles of insect pathology. *Insect Pathology*. Academic Press, London, United Kingdom, pp.1-12.

Kim, J.H. and Smith, A., 2001. Distribution of organochlorine pesticides in soils from South Korea. *Chemosphere*, 43(2), pp.137-140.

Kim, K.H., Kabir, E. and Jahan, S.A., 2017. Exposure to pesticides and the associated human health effects. *Science of the Total Environment*, 575, pp.525-535.

Kosikowska, M. and Biziuk, M., 2010. Review of the determination of pesticide residues in ambient air. *TrAC Trends in Analytical Chemistry*, 29(9), pp.1064-1072.



University of Fort Hare
Together in Excellence

Koutros, S., Silverman, D.T., Alavanja, M.C., Andreotti, G., Lerro, C.C., Heltshe, S., Lynch, C.F., Sandler, D.P., Blair, A. and Beane Freeman, L.E., 2016. Occupational exposure to pesticides and bladder cancer risk. *International Journal of Epidemiology*, 45(3), pp.792-805.

Koyuncu, I. and Güney, K., 2013. Membrane-Based Treatment of Textile Industry Wastewaters. *Encyclopedia of Membrane Science and Technology*, pp.1-12.

Kughur, P.G., 2012. The effects of herbicides on crop production and environment in Makurdi Local Government Area of Benue State, Nigeria. *Journal of Sustainable Development in Africa*, 14(4), pp.23-29.

Kumar, S.S., Venkateswarlu, P., Rao, V.R. and Rao, G.N., 2013. Synthesis, characterization and optical properties of zinc oxide nanoparticles. *International Nano Letters*, 3(1), pp.1-6.

Kyriakopoulos, G. and Doulia, D., 2006. Adsorption of pesticides on carbonaceous and polymeric materials from aqueous solutions: a review. *Separation & Purification Reviews*, 35(3), pp.97-191.



Ladj, R., Bitar, A., Eissa, M., Mugnier, Y., Le Dantec, R., Fessi, H. and Elaissari, A., 2013. Individual inorganic nanoparticles: preparation, functionalization and in vitro biomedical diagnostic applications. *Journal of Materials Chemistry B*, 1(10), pp.1381-1396.

Lafi, W.K. and Al-Qodah, Z., 2006. Combined advanced oxidation and biological treatment processes for the removal of pesticides from aqueous solutions. *Journal of Hazardous Materials*, 137(1), pp.489-497.

Lambrecht, B.N. and Hammad, H., 2015. The immunology of asthma. *Nature Immunology*, 16(1), pp.45-56.

Lamdab, U., Wetchakun, K., Kangwansupamonkon, W. and Wetchakun, N., 2018. Effect of a pH-controlled co-precipitation process on rhodamine B adsorption of MnFe₂O₄ nanoparticles. *Royal Society of Chemistry Advances*, 8(12), pp.6709-6718.

Lan, J., Cheng, Y. and Zhao, Z., 2014. Effective organochlorine pesticides removal from aqueous systems by magnetic nanospheres coated with polystyrene. *Journal of Wuhan University of Technology-Materials Science Edition*, 29(1), pp.168-173.

Latchoumycandane, C. and Mathur, P., 2002. Induction of oxidative stress in the rat testis after short-term exposure to the organochlorine pesticide methoxychlor. *Archives of Toxicology*, 76(12), pp.692-698.

Lee, D.H., Steffes, M.W., Sjödin, A., Jones, R.S., Needham, L.L. and Jacobs Jr, D.R., 2010. Low dose of some persistent organic pollutants predicts type 2 diabetes: a nested case-control study. *Environmental Health Perspectives*, 118(9), pp.1235-1242.

Lee, D.H., Steffes, M.W., Sjödin, A., Jones, R.S., Needham, L.L. and Jacobs Jr, D.R., 2011. Low dose organochlorine pesticides and polychlorinated biphenyls predict obesity, dyslipidemia, and insulin resistance among people free of diabetes. *Public Library of Science 1*, 6(1), p.e15977.

Lee, P.K., Choi, B. Y. and Kang, M.J., 2015. Assessment of mobility and bio-availability of heavy metals in dry depositions of Asian dust and implications for environmental risk. *Chemosphere*, 119, pp.1411-1421.

Lin, J. and Wang, L., 2009. Comparison between linear and non-linear forms of pseudo-first-order and pseudo-second-order adsorption kinetic models for the removal of methylene blue by activated carbon. *Frontiers of Environmental Science & Engineering in China*, 3(3), pp.320-324.

Lin, T., Hu, L., Shi, X., Li, Y., Guo, Z. and Zhang, G., 2012. Distribution and sources of organochlorine pesticides in sediments of the coastal East China Sea. *Marine Pollution Bulletin*, 64(8), pp.1549-1555.

Lu, K., Wang, T., Zhai, L., Wu, W., Dong, S., Gao, S. and Mao, L., 2019. Adsorption behavior and mechanism of Fe-Mn binary oxide nanoparticles: adsorption of methylene blue. *Journal of Colloid and Interface Science*, 539, pp.553-562.

Madden, A.S. and Hochella Jr, M.F., 2005. A test of geochemical reactivity as a function of mineral size: Manganese oxidation promoted by hematite nanoparticles. *Geochimica et Cosmochimica Acta*, 69(2), pp.389-398.

Mahajan, R., Blair, A., Lynch, C.F., Schroeder, P., Hoppin, J.A., Sandler, D.P. and Alavanja, M.C., 2006. Fonofos exposure and cancer incidence in the agricultural health study. *Environmental Health Perspectives*, 114(12), pp.1838-1842.

Maleki, A., Moradi, F., Shahmoradi, B., Rezaee, R. and Lee, S.M., 2020. The photocatalytic removal of diazinon from aqueous solutions using tungsten oxide doped zinc oxide nanoparticles immobilized on glass substrate. *Journal of Molecular Liquids*, 297, p.111918.

Mani, S. and Bharagava, R.N., 2018. Textile industry wastewater: environmental and health hazards and treatment approaches. *Recent Advances in Environmental Management*, pp.47-69

Mansouriieh, N., Sohrabi, M.R. and Khosravi, M., 2019. Optimization of profenofos organophosphorus pesticide degradation by zero-valent bimetallic nanoparticles using response surface methodology. *Arabian Journal of Chemistry*, 12(8), pp.2524-2532.

Mascolo, M.C., Pei, Y. and Ring, T.A., 2013. Room temperature co-precipitation synthesis of magnetite nanoparticles in a large pH window with different bases. *Materials*, 6(12), pp.5549-5567.

Mashkoo, F. and Nasar, A., 2020. Magsorbents: Potential candidates in wastewater treatment technology—A review on the removal of methylene blue dye. *Journal of Magnetism and Magnetic Materials*, 500, pp.166408.

Matouq, M.A., Al-Anber, Z.A., Tagawa, T., Aljbour, S. and Al-Shannag, M., 2008. Degradation of dissolved diazinon pesticide in water using the high frequency of ultrasound wave. *Ultrasonics Sonochemistry*, 15(5), pp.869-874.

McHale, J.M., Auroux, A., Perrotta, A.J. and Navrotsky, A., 1997. Surface energies and thermodynamic phase stability in nanocrystalline aluminas. *Science*, 277(5327), pp.788-791.

Mendoza, F., Farinas, I.S., Gascon, M.P. and Salazar, L.P., 2008. Erythema-multiforme like eruption: Irritant contact dermatitis from a glyphosate pesticide. *Contact Dermatitis*, 59, pp.5456.

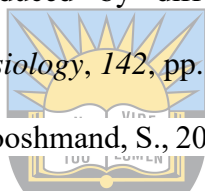
Min, B., Lee, J.S., Hwang, J.W., Keem, K.H., Kang, M.I., Cho, K., Sung, M.Y., Kim, S., Lee, M.S., Park, S.O. and Moon, J.T., 2003. Al₂O₃ coating of ZnO nanorods by atomic layer deposition. *Journal of Crystal Growth*, 252(4), pp.565-569.

Mirzaei, H. and Darroudi, M., 2017. Zinc oxide nanoparticles: Biological synthesis and biomedical applications. *Ceramics International*, 43(1), pp.907-914.

Mo, W.Y. and He, H.W., 2005. Development of herbicidal-activitive materials from plants. *Chemical and Biological Engineering*, 8.

Mohamed, H.I. and Akladios, S.A., 2017. Changes in antioxidants potential, secondary metabolites and plant hormones induced by different fungicides treatment in cotton plants. *Pesticide Biochemistry and Physiology*, 142, pp.117-122.

Mohammadian, M., Es'haghi, Z. and Hooshmand, S., 2018. Green and chemical synthesis of zinc oxide nanoparticles and size evaluation by UV-vis spectroscopy. *Journal of Nanomedicine Research*, 7(1), pp.00175.



University of Fort Hare
Together in Excellence

Morris, A.P., Voight, B.F., Teslovich, T.M., Ferreira, T., Segre, A.V., Steinthorsdottir, V., Strawbridge, R.J., Khan, H., Grallert, H., Mahajan, A. and Prokopenko, I., 2012. Large-scale association analysis provides insights into the genetic architecture and pathophysiology of type 2 diabetes. *Nature Genetics*, 44(9), pp.981.

Mossa, A.T.H., Mohafrash, S.M. and Chandrasekaran, N., 2018. Safety of natural insecticides: toxic effects on experimental animals. *BioMedicine Research International*, 2018.

Mostafalou, S., Eghbal, M.A., Nili-Ahmadabadi, A., Baeri, M. and Abdollahi, M., 2012. Biochemical evidence on the potential role of organophosphates in hepatic glucose metabolism toward insulin resistance through inflammatory signaling and free radical pathways. *Toxicology and Industrial Health*, 28(9), pp.840-851.

Mothemela, M., 2010. Pesticides and dermatoses: allergies in the workplace. *Current Allergy & Clinical Immunology*, 23(1), pp.37-39.

Mukhtar, M., Munisa, L. and Saleh, R., 2012. Co-precipitation synthesis and characterization of nanocrystalline zinc oxide particles doped with Cu²⁺ ions.

Nasar, A. and Mashkoor, F., 2019. Application of polyaniline-based adsorbents for dye removal from water and wastewater—a review. *Environmental Science and Pollution Research*, 26(6), pp.5333-5356.

Ndlovu, V., Dalvie, M.A. and Jeebhay, M.F., 2014. Asthma associated with pesticide exposure among women in rural Western Cape of South Africa. *American Journal of Industrial Medicine*, 57(12), pp.1331-1343.

Nguyen, T.A. and Juang, R.S., 2013. Treatment of waters and wastewaters containing sulfur dyes: a review. *Chemical Engineering Journal*, 219, pp.109-117.

Nolan, C.J., Damm, P. and Prentki, M., 2011. Type 2 diabetes across generations: from pathophysiology to prevention and management. *The Lancet*, 378(9786), pp.169-181.

Nozet, H. and Majault, J., 1976. *Textiles Chimiques: Fibres Modernes*. Eyrolles.

Oh, J.K. and Park, J.M., 2011. Iron oxide-based superparamagnetic polymeric nanomaterials: design, preparation, and biomedical application. *Progress in Polymer Science*, 36(1), pp.168-189.

Omer, S.M., Georghiou, G.P. and Irving, S.N., 1980. DDT/pyrethroid resistance inter-relationships in *Anopheles stephensi*. *Mosquito News*, 40, pp.200-209.

Panahandeh, N., Torabzadeh, H., Aghae, M., Hasani, E. and Safa, S., 2018. Effect of incorporation of zinc oxide nanoparticles on mechanical properties of conventional glass ionomer cements. *Journal of Conservative Dentistry: JCD*, 21(2), p.130.

Pandey, A., Singh, P. and Iyengar, L., 2007. Bacterial decolorization and degradation of azo dyes. *International Biodeterioration & Biodegradation*, 59(2), pp.73-84.

Pandian, A.M.K., Karthikeyan, C. and Rajasimman, M., 2017. Isotherm and kinetic studies on adsorption of malachite green using chemically synthesized silver nanoparticles. *Nanotechnology for Environmental Engineering*, 2(1), pp.2.

Penagos, H., Ruepert, C., Partanen, T. and Wesseling, C., 2004. Pesticide patch test series for the assessment of allergic contact dermatitis among banana plantation workers in panama. *Dermatitis: Contact, Atopic, Occupational, Drug*, 15(3), pp.137-145.

Posthumus, W., Magusin, P.C.M.M., Brokken-Zijp, J.C.M., Tinnemans, A.H.A. and Van der Linde, R., 2004. Surface modification of oxidic nanoparticles using 3-methacryloxypropyltrimethoxysilane. *Journal of Colloid and Interface Science*, 269(1), pp.109-116.

Pourfaraj, R., Fatemi, S.J., Kazemi, S.Y. and Biparva, P., 2017. Synthesis of hexagonal mesoporous MgAl LDH nanoplatelets adsorbent for the effective adsorption of Brilliant Yellow. *Journal of Colloid and Interface Science*, 508, pp.65-74

Puvaneswari, N., Muthukrishnan, J. and Gunasekaran, P., 2006. Toxicity assessment and microbial degradation of azo dyes.



Qasem, J.R., 2011. *Herbicides applications: problems and considerations*. IntechOpen.

Quinete, N.S., de Oliveira, E.D.S., Fernandes, D.R., de Souza Avelar, A. and Santelli, R.E., 2011. Assessment of organochlorine pesticide residues in Atlantic Rain Forest fragments, Rio de Janeiro, Brazil. *Environmental Pollution*, 159(12), pp.3604-3612.

Quinn, L., de Vos, J., Fernandes-Whaley, M., Roos, C., Bouwman, H., Kylin, H., Pieters, R. and van den Berg, J., 2011. Pesticide Use in South Africa: One of the Largest Importers of Pesticides in Africa. *Pesticides in the Modern World*, pp.49-96.

Raanan, R., Harley, K.G., Balmes, J.R., Bradman, A., Lipsett, M. and Eskenazi, B., 2015. Early-life exposure to organophosphate pesticides and pediatric respiratory symptoms in the CHAMACOS cohort. *Environmental Health Perspectives*, 123(2), pp.179-185.

Rademaker, M., 1998. Occupational contact dermatitis among New Zealand farmers. *Australasian Journal of Dermatology*, 39(3), pp.164-167.

Rahimi, K., Mirzaei, R., Akbari, A. and Mirghaffari, N., 2018. Preparation of nanoparticle-modified polymeric adsorbent using wastage fuzzes of mechanized carpet and its application in dye removal from aqueous solution. *Journal of Cleaner Production*, 178, pp.373-383.

Raliya, R. and Tarafdar, J.C., 2014. Biosynthesis and characterization of zinc, magnesium and titanium nanoparticles: an eco-friendly approach. *International Nano Letters*, 4(1), p.93.

Reddy, A.B., Jaafar, J., Majid, Z.A., Aris, A., Umar, K., Talib, J. and Madhavi, G., 2015. Relative efficiency comparison of carboxymethyl cellulose (CMC) stabilized Fe⁰ and Fe⁰/Ag nanoparticles for rapid degradation of chlorpyrifos in aqueous solutions. *Digest Journal of Nanomaterials & Biostructures (DJNB)*, 10(2), pp. 331–340.

Rekha, K., Nirmala, M., Nair, M.G. and Anukaliani, A., 2010. Structural, optical, photocatalytic and antibacterial activity of zinc oxide and manganese doped zinc oxide nanoparticles. *Physica B: Condensed Matter*, 405(15), pp.3180-3185.

Ren, X.L., Lai, X.H., Zhu, K.J., Sun, Y. and He, D.L., 2016. Removal of acid turquoise blue 2G from aqueous solution by adsorbent derived from sludge and straw: kinetic, isotherm and thermodynamic study. *Desalination and Water Treatment*, 57(1), pp.440-448.

Roex, E.W., Keijzers, R. and Van Gestel, C.A., 2003. Acetylcholinesterase inhibition and increased food consumption rate in the zebrafish, *Danio rerio*, after chronic exposure to parathion. *Aquatic Toxicology*, 64(4), pp.451-460.

Rohani, R., Dzulkharnien, N.S.F., Harun, N.H. and Ilias, I.A., 2022. Green Approaches, Potentials, and Applications of Zinc Oxide Nanoparticles in Surface Coatings and Films. *Bioinorganic Chemistry and Applications*, 2022.

Roselló-Márquez, G., Fernández-Domene, R.M., Sánchez-Tovar, R., García-Carrión, S., Lucas-Granados, B. and Garcia-Anton, J., 2019. Photoelectrocatalyzed degradation of a pesticides

mixture solution (chlorfenvinphos and bromacil) by WO₃ nanosheets. *Science of The Total Environment*, 674, pp.88-95.

Ryoo, K.S., Jung, S.Y., Sim, H. and Choi, J.H., 2013. Comparative study on adsorptive characteristics of diazinon in water by various adsorbents. *Bulletin of the Korean Chemical Society*, 34(9), pp.2753-2759.

Saharan, p., Chaudhary, G.R., Mehta, S.K. and Umar, A., 2014. Removal of water contaminants by iron oxide nanomaterials. *Journal of Nanoscience and Technology*, 14(1), pp.627-643.

Saini, R.D., 2017. Textile organic dyes: polluting effects and elimination methods from textile waste water. *International Journal of Chemical Engineering Research*, 9(1), pp.121-136.

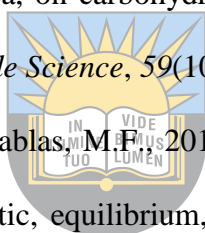
Saladin, G., Magné, C. and Clément, C., 2003. Effects of fludioxonil and pyrimethanil, two fungicides used against *Botrytis cinerea*, on carbohydrate physiology in *Vitis vinifera* L. *Pest Management Science: formerly Pesticide Science*, 59(10), pp.1083-1092.

Salem, M.A., Elsharkawy, R.G. and Hablas, M.F., 2016. Adsorption of brilliant green dye by polyaniline/silver nanocomposite: kinetic, equilibrium, and thermodynamic studies. *European Polymer Journal*, 75, pp.577-590.

Salleh, M.A.M., Mahmoud, D.K., Karim, W.A.W.A. and Idris, A., 2011. Cationic and anionic dye adsorption by agricultural solid wastes: a comprehensive review. *Desalination*, 280(1-3), pp.1-13.

Sanborn, M., Kerr, K.J., Sanin, L.H., Cole, D.C., Bassil, K.L. and Vakil, C., 2007. Non-cancer health effects of pesticides: systematic review and implications for family doctors. *Canadian Family Physician*, 53(10), pp.1712-1720.

Sanchez-Dominguez, M., Boutonnet, M. and Solans, C., 2009. A novel approach to metal and metal oxide nanoparticle synthesis: the oil-in-water microemulsion reaction method. *Journal of Nanoparticle Research*, 11(7), pp.1823-1829.



University of Fort Hare
Together in Excellence

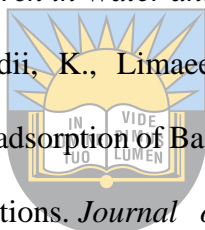
Saratale, R.G., Saratale, G.D., Chang, J.S. and Govindwar, S.P., 2011. Bacterial decolorization and degradation of azo dyes: a review. *Journal of the Taiwan Institute of Chemical Engineers*, 42(1), pp.138-157.

Saravaia, H., Ramanuj, R. and Chanchpara, A., 2021. Mesoporous silica-coated α -Fe₂O₃/C nanoparticles as an efficient adsorbent for cationic dye removal. *Journal of the Iranian Chemical Society*, pp.1-11.

Savitt, L.E., 1972. Contact dermatitis due to benomyl insecticide. *Archives of Dermatology*, 105(6), pp.926-927.

Shariati-Rad, M., Irandoust, M., Amri, S., Feyzi, M. and Ja'fari, F., 2014. Removal, preconcentration and determination of methyl red in water samples using silica coated magnetic nanoparticles. *Journal of Applied Research in Water and Wastewater*, 1(1), pp.6-12.

Sheshdeh, R.K., Nikou, M.R.K., Badii, K., Limaee, N.Y. and Golkarnarenji, G., 2014. Equilibrium and kinetics studies for the adsorption of Basic Red 46 on nickel oxide nanoparticles-modified diatomite in aqueous solutions. *Journal of the Taiwan Institute of Chemical Engineers*, 45(4), pp.1792-1802.



University of Fort Hare
Together in Excellence

Shoiful, A., Ueda, Y., Nugroho, R. and Honda, K., 2016. Degradation of organochlorine pesticides (OCPs) in water by iron (Fe)-based materials. *Journal of Water Process Engineering*, 11, pp.110-117.

Siddiqi, K.S. and Husen, A., 2018. Properties of zinc oxide nanoparticles and their activity against microbes. *Nanoscale Research Letters*, 13(1), pp.1-13.

Singh, K. and Arora, S., 2011. Removal of synthetic textile dyes from wastewaters: a critical review on present treatment technologies. *Critical Reviews in Environmental Science and Technology*, 41(9), pp.807-878.

Siva, R., 2007. Status of natural dyes and dye-yielding plants in India. *Current Science*, pp.916-925.

Slama, H.B., Chenari Bouket, A., Pourhassan, Z., Alenezi, F.N., Silini, A., Cherif-Silini, H., Oszako, T., Luptakova, L., Golinska, P. and Belbahri, L., 2021. Diversity of Synthetic Dyes from Textile Industries, Discharge Impacts and Treatment Methods. *Applied Sciences*, 11(14), pp.6255.

Smijs, T.G. and Pavel, S., 2011. Titanium dioxide and zinc oxide nanoparticles in sunscreens: focus on their safety and effectiveness. *Nanotechnology, Science and applications*, 4, p.95.

Solans, C., Izquierdo, P., Nolla, J., Azemar, N. and Garcia-Celma, M.J., 2005. Nano-emulsions. *Current Opinion in Colloid & Interface Science*, 10(3-4), pp.102-110.

Sonune, A. and Ghate, R., 2004. Developments in wastewater treatment methods. *Desalination*, 167, pp.55-63.

Śpiewak, R., 2001. Pesticides as a cause of occupational skin diseases in farmers. *Annals of Agricultural and Environmental Medicine*, 8(1), pp.1-5.

Spoială, A., Ilie, C.I., Trușcă, R.D., Oprea, O.C., Surdu, V.A., Vasile, B.Ș., Ficai, A., Ficai, D., Andronescu, E. and Dițu, L.M., 2021. Zinc Oxide Nanoparticles for Water Purification. *Materials*, 14(16), p.4747.

Srivastava, V. and Choubey, A.K., 2021. Study of adsorption of anionic dyes over biofabricated crystalline α -MnO₂ nanoparticles. *Environmental Science and Pollution Research*, 28(12), pp.15504-15518.

Stankic, S., Sterrer, M., Hofmann, P., Bernardi, J., Diwald, O. and Knözinger, E., 2005. Novel optical surface properties of Ca²⁺ doped MgO nanocrystals. *Nano Letters*, 5(10), pp.1889-1893.

Stankic, S., Suman, S., Haque, F. and Vidic, J., 2016. Pure and multi metal oxide nanoparticles: synthesis, antibacterial and cytotoxic properties. *Journal of Nanobiotechnology*, 14(1), pp.1-20.

Stasinakis, A.S., Thomaidis, N.S., Arvaniti, O.S., Asimakopoulos, A.G., Samaras, V.G., Ajibola, A., Mamais, D. and Lekkas, T.D., 2013. Contribution of primary and secondary treatment on the removal of benzothiazoles, benzotriazoles, endocrine disruptors, pharmaceuticals and

perfluorinated compounds in a sewage treatment plant. *Science of the Total Environment*, 463, pp.1067-1075.

Tamang, D., Nath, R. and Sengupta, K., 2015. Effect of herbicide application on weed management in green gram [*Vigna radiata* (L.) Wilczek]. *Advances in Crop Science and Technology*.

Tang, L., Cai, Y., Yang, G., Liu, Y., Zeng, G., Zhou, Y., Li, S., Wang, J., Zhang, S., Fang, Y. and He, Y., 2014. Cobalt nanoparticles-embedded magnetic ordered mesoporous carbon for highly effective adsorption of rhodamine B. *Applied Surface Science*, 314, pp.746-753.

Tang, W., Wang, D.I., Wang, J., Wu, Z., Li, L., Huang, M., Xu, S. and Yan, D., 2018. Pyrethroid pesticide residues in the global environment: an overview. *Chemosphere*, 191, pp.990-1007.

Tankiewicz, M., Fenik, J. and Biziuk, M., 2011. Solventless and solvent-minimized sample preparation techniques for determining currently used pesticides in water samples: A review. *Talanta*, 86, pp.8-22.



Thakkar, K.N., Mhatre, S.S. and Parikh, R.Y., 2010. Biological synthesis of metallic nanoparticles. *Nanomedicine: Nanotechnology, Biology and Medicine*, 6(2), pp.257-262.

Thurman, E.M. and Meyer, M.T., 1996. Herbicide metabolites in surface water and groundwater: introduction and overview.

Tian, H., Li, J., Mu, Z., Li, L. and Hao, Z., 2009. Effect of pH on DDT degradation in aqueous solution using bimetallic Ni/Fe nanoparticles. *Separation and Purification Technology*, 66(1), pp.84-89.

Tsaytler, P., Harding, H.P., Ron, D. and Bertolotti, A., 2011. Selective inhibition of a regulatory subunit of protein phosphatase 1 restores proteostasis. *Science*, 332(6025), pp.91-94.

Tu, W., Lei, J., Wang, P. and Ju, H., 2011. Photoelectrochemistry of Free-Base-Porphyrin-Functionalized Zinc Oxide Nanoparticles and Their Applications in Biosensing. *Chemistry—A European Journal*, 17(34), pp.9440-9447.

United States Environmental Protection Agency. 1999. Fonofos Registration Eligibility Document Facts. Washington, DC: US Environmental Protection Agency. Available: <http://www.epa.gov/oppsrrd1/REDS/factsheets/0105fact.pdf> [accessed: 29 June 2021]

Vanathi, P., Rajiv, P., Narendhran, S., Rajeshwari, S., Rahman, P.K. and Venckatesh, R., 2014. Biosynthesis and characterization of phyto mediated zinc oxide nanoparticles: a green chemistry approach. *Materials Letters*, 134, pp.13-15.

Vazquez-Ortega, F., Lagunes, I. and Trigos, A., 2020. Cosmetic dyes as potential photosensitizers of singlet oxygen generation. *Dyes and Pigments*, 176, p.108248.

Velić, N., Pavlović, H., Gorenšek, J., Kezerle, A., Mastanjević, K. and Velić, D., 2017. Screening of new fungal isolates for synthetic dyes decolourisation ability.

Venkataraman, J.L., Sharath, R., Chandraprabha, M.N., Neelufar, E., Hazra, A. and Patra, M., 2014. Synthesis, characterization and evaluation of antimicrobial activity of zinc oxide nanoparticles. *Journal of Biochemical Technology*, 3(5), pp.151-154.

Verma, A.K., Dash, R.R. and Bhunia, P., 2012. A review on chemical coagulation/flocculation technologies for removal of colour from textile wastewaters. *Journal of Environmental Management*, 93(1), pp.154-168.

Wagner, H., Kreher, B., Lotter, H., Hamburger, M.O. and Cordell, G.A., 1989. Structure determination of new isomeric naphtho [2, 3-b] furan-4, 9-diones from *Tabebuia avellanedae* by the selective-INEPT technique. *Helvetica Chimica Acta*, 72(4), pp.659-667.

Wang, X., Mao, H., Huang, W., Guan, W., Zou, X., Pan, J. and Yan, Y., 2011. Preparation of magnetic imprinted polymer particles via microwave heating initiated polymerization for selective enrichment of 2-amino-4-nitrophenol from aqueous solution. *Chemical Engineering Journal*, 178, pp.85-92.

Wanjeri, V.W.O., Sheppard, C.J., Prinsloo, A.R.E., Ngila, J.C. and Ndungu, P.G., 2018. Isotherm and kinetic investigations on the adsorption of organophosphorus pesticides on graphene oxide

based silica coated magnetic nanoparticles functionalized with 2-phenylethylamine. *Journal of Environmental Chemical Engineering*, 6(1), pp.1333-1346.

Waychunas, G.A. and Zhang, H., 2008. Structure, chemistry, and properties of mineral nanoparticles. *Elements*, 4(6), pp.381-387.

Whiting, D.R., Guariguata, L., Weil, C. and Shaw, J., 2011. IDF diabetes atlas: global estimates of the prevalence of diabetes for 2011 and 2030. *Diabetes Research and Clinical Practice*, 94(3), pp.311-321.

Wu, Q., Zhou, X., Li, Y., Zang, X., Wang, C. and Wang, Z., 2009. Application of dispersive liquid-liquid microextraction combined with high-performance liquid chromatography to the determination of carbamate pesticides in water samples. *Analytical and Bioanalytical Chemistry*, 393(6), pp.1755-1761.

Wu, W., He, Q. and Jiang, C., 2008. Magnetic iron oxide nanoparticles: synthesis and surface functionalization strategies. *Nanoscale Research Letters*, 3(11), pp.397-415.

Xia, X.J., Huang, Y.Y., Wang, L., Huang, L.F., Yu, Y.L., Zhou, Y.H. and Yu, J.Q., 2006. Pesticides-induced depression of photosynthesis was alleviated by 24-epibrassinolide pretreatment in *Cucumis sativus* L. *Pesticide Biochemistry and Physiology*, 86(1), pp.42-48.

Xiao, P., Mori, T. and Kondo, R., 2011. Biotransformation of the organochlorine pesticide trans-chlordane by wood-rot fungi. *New Biotechnology*, 29(1), pp.107-115.

Xu, Z., Zheng, L., Wen, S. and Liu, L., 2019. Graphene oxide-supported zinc oxide nanoparticles for chloroprene rubber with improved crosslinking network and mechanical properties. *Composites Part A: Applied Science and Manufacturing*, 124, p.105492.

Yamagami, A., Kawano, K., Futaki, S., Kuramochi, K. and Tsubaki, K., 2017. Syntheses and properties of second-generation V-shaped xanthene dyes with piperidino groups. *Tetrahedron*, 73(50), pp.7061-7066.

Yang, D., Wang, F., Yang, X., Wu, Y. and Zhu, S., 2015. Water's effect of benzene hexachloride. *Advances in Computer Science Research*, 2352, pp.198-204.

Yao, Y., Xu, F., Chen, M., Xu, Z. and Zhu, Z., 2010. Adsorption behavior of methylene blue on carbon nanotubes. *Bioresource Technology*, 101(9), pp.3040-3046.

Yao, Y., Xu, F., Chen, M., Xu, Z. and Zhu, Z., 2010. Adsorption behavior of methylene blue on carbon nanotubes. *Bioresource Technology*, 101(9), pp.3040-3046.

Ye, F., Xie, Z., Wu, X. and Lin, X., 2006. Determination of pyrethroid pesticide residues in vegetables by pressurized capillary electrochromatography. *Talanta*, 69(1), pp.97-102.

Ye, S., Yan, M., Tan, X., Liang, J., Zeng, G., Wu, H., Song, B., Zhou, C., Yang, Y. and Wang, H., 2019. Facile assembled biochar-based nanocomposite with improved graphitization for efficient photocatalytic activity driven by visible light. *Applied Catalysis B: Environmental*, 250, pp.78-88.

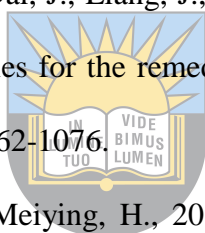
Ye, S., Zeng, G., Wu, H., Zhang, C., Dai, J., Liang, J., Yu, J., Ren, X., Yi, H., Cheng, M. and Zhang, C., 2017. Biological technologies for the remediation of co-contaminated soil. *Critical Reviews in Biotechnology*, 37(8), pp.1062-1076.

Ying, X., Shaohua, C., Wei, H. and Meiyong, H., 2012. New progress and prospect for the microbial degradation of pyrethroid pesticides. *Chinese Agricultural Science Bulletin*, 27.

Yoo, M., Lim, Y.H., Kim, T., Lee, D. and Hong, Y.C., 2016. Association between urinary 3-phenoxybenzoic acid and body mass index in Korean adults: 1 st Korean National Environmental Health Survey. *Annals of Occupational and Environmental Medicine*, 28(1), pp.1-8.

Yu, J.G., Zhao, X.H., Yang, H., Chen, X.H., Yang, Q., Yu, L.Y., Jiang, J.H. and Chen, X.Q., 2014. Aqueous adsorption and removal of organic contaminants by carbon nanotubes. *Science of the Total Environment*, 482, pp.241-251.

Yu, M., Han, Y., Li, J. and Wang, L., 2017. CO₂-activated porous carbon derived from cattail biomass for removal of malachite green dye and application as supercapacitors. *Chemical Engineering Journal*, 317, pp.493-502



University of Fort Hare
Together in Excellence

Yu, S., Cui, J., Wang, J., Zhong, C., Wang, X. and Wang, N., 2020. Facile fabrication of Cu (II) coordinated chitosan-based magnetic material for effective adsorption of reactive brilliant red from aqueous solution. *International Journal of Biological Macromolecules*, 149, pp.562-571.

Zaheer, Z., Bawazir, W.A., Al-Bukhari, S.M. and Basaleh, A.S., 2019. Adsorption, equilibrium isotherm, and thermodynamic studies to the removal of acid orange 7. *Materials Chemistry and Physics*, 232, pp.109-120.

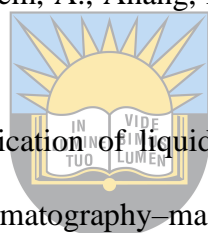
Zeininger, L., Petzi, S., Schönamsgruber, J., Portilla, L., Halik, M. and Hirsch, A., 2015. Very Facile Polarity Umpolung and Noncovalent Functionalization of Inorganic Nanoparticles: A Tool Kit for Supramolecular Materials Chemistry. *Chemistry – a European Journal*, 21, pp.14030-14035.

Zerin, I., Farzana, N., Muhammad Sayem, A., Anang, D.M. and Haider, J., 2019. Potentials of natural dyes for textile applications.

Zhang, J. and Lee, H.K., 2006. Application of liquid-phase microextraction and on-column derivatization combined with gas chromatography–mass spectrometry to the determination of carbamate pesticides. *Journal of Chromatography A*, 1117(1), pp.31-37.

Zheng, Y., Fu, L., Han, F., Wang, A., Cai, W., Yu, J., Yang, J. and Peng, F., 2015. Green biosynthesis and characterization of zinc oxide nanoparticles using *Corymbia citriodora* leaf extract and their photocatalytic activity. *Green Chemistry Letters and Reviews*, 8(2), pp.59-63.

Zhou, L., Jin, J., Liu, Z., Liang, X. and Shang, C., 2011. Adsorption of acid dyes from aqueous solutions by the ethylenediamine-modified magnetic chitosan nanoparticles. *Journal of Hazardous Materials*, 185(2-3), pp.1045-1052.



University of Fort Hare
Together in Excellence

Chapter Three

Adsorption of simazine herbicide from aqueous solution by novel pyrene functionalized zinc oxide nanoparticles: Kinetics and isotherm studies

Abstract

This study reports on the synthesis of functionalized novel zinc oxide nanoparticles for the removal of simazine from aqueous solution. This functionalized zinc oxide nanoparticles was synthesized via a simple co-precipitation method. The nanoparticles were then functionalized with 1-(4-hydroxyphenyl)-4-phenyl-2,3-diazobutadiene via covalent coupling in order to obtain the novel adsorbent. The synthesized materials were characterized with several techniques including; Fourier transform infrared spectroscopy (FTIR), scanning electron microscope (SEM), energy dispersive x-ray spectroscopy (EDX), X-ray diffraction analysis (XRD) and thermogravimetric analysis (TGA) and found that the materials were successfully synthesized. Because the characteristic stretch for Zn-O was observed in both bare and functionalized nanoparticles in the range $500 - 450 \text{ cm}^{-1}$. XRD analysis showed the characteristic reflections of ZnO nanoparticles for both bare and functionalized nanoparticles (i.e. 31.8° , 34.5° , 36.3° , 47.6° , 56.6° , 62.9° , 66.5° , 68.0° and 69.2°). In addition, the EDX spectra only showed the expected elements in all synthesized materials. The novel material's adsorption performance was evaluated through batch adsorption experiments for the removal of simazine from aqueous solution. From all batch adsorption experiments conducted, the adsorbent showed effectiveness and high adsorption capacity for the removal of simazine with maximum adsorption capacity of 137 mg/g (solution $\text{pH} = 2$, adsorbent dose at approximately $= 20.0 \text{ mg}$, adsorbate concentration $= 0.312 \text{ mg/L}$ and temperature $= 20 \pm 2^\circ\text{C}$ and shaking period $= 60$ minutes). Kinetics of the adsorption favoured pseudo-first order. The most applicable isotherm was Temkin isotherm. However, Langmuir isotherm could also be employed to describe the adsorption process. The material also showed reusability of up to three runs indicating that this material can be regenerated

and re-used. The result from this study showed that this functionalized material can serve as new substitute material for the removal of herbicides such as simazine from aqueous solutions and can be explored to real life situations.

Keywords: Simazine; adsorption; desorption; herbicides; GC-ECD and SPE.



University of Fort Hare
Together in Excellence

3.1. Introduction

Environmental pollution by pesticides has been of noticeable interest for researchers especially in water ecosystems. Because of heavy usage and environmental persistence, many pesticides have been detected in both ground and surface waters (Katsumata *et al.*, 2006). Thus, considered a treat to aquatic life and human beings as well. This is because some pesticides including simazine have estrogenic effect meaning they are endocrine disruptors (Katsumata *et al.*, 2006). Hayes *et al.* (2006) reported s-triazines to have carcinogenic potential. Simazine with the IUPAC name 2-chloro-4,6-bis(ethylamino)-s-triazine (Figure 3.1) is a synthetic s-triazazine herbicide which has been in use since 1956 (Flores *et al.*, 2009). This herbicide works by inhibiting the photosynthetic electron transport processes in plant leaves (Paul *et al.*, 2010). Extensive use of this herbicide has been on pre-emergence control of broadleaf weeds, non-crop fields and annual grasses in agricultural fields (Gunasekara *et al.*, 2007). It is also used for weed removal from corn, banana, sorghum, pineapple, sugarcane and tea gardens (Paul *et al.*, 2010). Arias-Estévez *et al.* (2008) reported that major fraction of pesticides are lost to the environment, and contaminates the soil, air and water. This could also be expected for the aforementioned herbicides, which are externally applied to targeted herb. Hence, Troiano *et al.* (2001) reported simazine to be the second commonly found pesticide in ground and surface water in the United States, Australia and Europe. This herbicide can be transported to non-target areas through runoffs similar to fertilizers (Beck *et al.*, 1993).

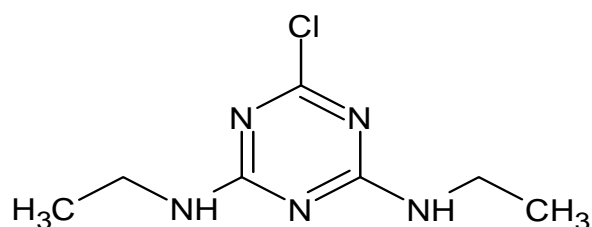


Figure 3.1: Chemical structure of simazine.

Because of the aforementioned negative effects of pesticides, scientists have developed and applied various methods for their removal including; adsorption (Esposito *et al.*, 2013; Paul *et al.*, 2010; Sannino *et al.*, 2013; Zhou *et al.*, 2006), membrane filtration (Scutariu *et al.*, 2018), oxidation (Beltrán *et al.*, 2000), photocatalytic degradation (Meriam Suhaimy *et al.*, 2018; Flores *et al.*, 2020; Chu *et al.*, 2009; López-Muñoz *et al.*, 2011), coagulation (Jiang and Adams, 2006). From these removal methods, adsorption has been of great interest owing to its efficiency, intrinsic simplicity and low costs. Therefore, many adsorbents have been developed and applied for this technology for the removal of pesticides in water. These adsorbents include corn straw biochars (Zhang *et al.*, 2011), porous silica (Sannino *et al.*, 2013), acid-activated beidellite (Paul *et al.*, 2010), zeolite H-Y (Sannino *et al.*, 2012), acid activated natural clinoptilolite (Salvestrini *et al.*, 2015), granular activated carbon (Fulazzaky, 2012), and both conventional activated carbon and surface modified activated carbons (Chingombe *et al.*, 2006). In spite of the existence of these adsorbents, there have been notable drawbacks including low adsorption capacity, high cost of preparation, inability to re-use these adsorbents and generation of secondary contaminants.

Zinc oxide nanoparticles have shown adsorption ability for several contaminants (organic and inorganic) in water. Even though they have been mainly used for the removal of dyes in water (Debnath and Mondal, 2020; Zhang *et al.*, 2013; Monsef Khoshhesab and Souhani, 2018) and toxic metals (Gu *et al.*, 2020; Primo *et al.*, 2020; Sheela *et al.*, 2012), they have shown efficiency in the few occasions that they were employed for the removal of pesticides from wastewater (Jangwan *et al.*, 2021; Sabir *et al.*, 2014).

Their ability to remove the previously mentioned contaminants from aqueous solutions have been due to their large surface area, high thermal and chemical stabilities. Pyrene ligands are naturally electron rich in nature therefore their interactions are usually easier with electrophiles due to opposite charge attractions. However, when coupled to nanoparticles to attract other electron rich chemical species, their surface charge can be altered by pH effect. Thus making it possible for nanoparticles functionalized with these ligands to adsorb both electron rich and electron deficient

chemical species in water. Hence, in this study, a novel pyrene functionalized zinc oxide nanoparticles was developed and evaluated for the removal of a recalcitrant herbicide, simazine from aqueous solution. This material is made up of zinc oxide nanoparticles backbone and its adsorption capacity was improved with pyrene ligand, 1-(4-hydroxyphenyl)-4-pyrenyl-2,3-diaza-1,3-butadiene with multiple nitrogen functionalities where other groups including simazine can attach. To the best of our knowledge, this is the first study to report on the functionalization of zinc oxide nanoparticles with pyrene ligand for the removal of simazine herbicide from aqueous solution. In addition, this study also examined the kinetics and isotherm models that would best describe the adsorption of simazine from aqueous solution using this novel material. Lastly, desorption studies were conducted to determine if this material can be re-used.

3.2. Experimental

3.2.1. Materials and chemicals

4-hydroxybenzaldehyde (purity $\geq 98\%$), 1-pyrenecarboxyaldehyde (purity $\geq 99\%$) and hydrazine hydrate (purity $\geq 99\%$) used in pyrene ligand synthesis were bought from Sigma-Aldrich, United Kingdom, Croatia and China respectively. Zinc nitrate hexahydrate (purity $\geq 98\%$) was also purchased from Sigma-Aldrich, China. Sodium chloride and Sodium hydroxide of purities of 98% and above were purchased from associated chemical enterprises. Tetraethylorthosilicate (purity $\geq 98\%$), 4-dimethylaminopyridine (purity $\geq 98\%$) and 99% solution of 3-aminopropyltriethoxysilane were purchased from Sigma-Aldrich, China as well. Absolute ethanol and 32% hydrochloric acid solution were bought from Merck Chemicals, Gauteng, South Africa. Dicyclohexylcarbodiimide and succinic anhydride of purities 98% and above were bought from Merck Chemicals, Germany, whereas, Sodium chloride and Sodium hydroxide of purities 98% and above were bought from associated chemical enterprises. Simazine (99%) was



purchased from Sigma-Aldrich, China. These materials and chemicals were used as received from the suppliers.

3.2.2. Synthesis

3.2.2.1. Synthesis of 1-(4-hydroxyphenyl)-4-phenyl-2,3-diazabutadiene (Pyrene)

Pyrene ligand was synthesized according to the method of Wang *et al.* (2010). This was done by adding 50 mL of $\text{H}_6\text{N}_2\text{O}$ solution dropwise into 150 mL absolute ethanol containing 9.40 g of 1-pyrenecarboxyaldehyde and 18.8 g of 4-hydroxybenzaldehyde. The resulting solution was then refluxed at 55°C for 10 h (Figure 3.2). The final product was obtained after filtering, washed with distilled water and dried. IR (ATR, cm^{-1}) 3360, 3050, 2920, 2620, 1550 (Figure 3.4); ^1H NMR (DMSO, Bruker TopSpin) δ (ppm): 8.35, 8.32, 8.30, 8.28, 8.25, 8.22, 8.20, 8.16, 8.14, 8.09, 8.07, 8.05, 7.86, 7.84, 4.40, 2.50, 1.06 (Figure A-I.1); ^{13}C NMR (DMSO, Bruker TopSpin) δ (ppm): 163.38, 161.82, 160.73, 160.41, 160.33, 159.43, 130.58, 130.15, 128.84, 126.20, 125.94, 39.73, 39.52, 39.31 (Figure A-I.2).

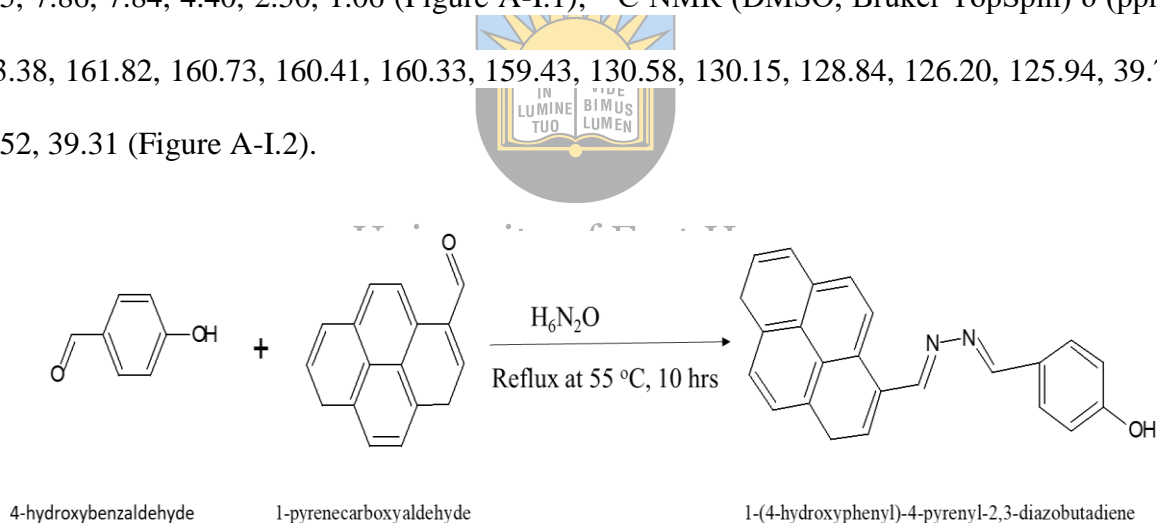


Figure 3.2: Synthesis of 1-(4-hydroxyphenyl)-4-pyrenyl-2,3-diaza-1,3-butadiene.

3.2.2.2. Synthesis of zinc oxide nanoparticles (ZnO NPs)

ZnO NPs were prepared via co-precipitation method with some slight adjustments (Wu *et al.*, 2006). This was accomplished by adding slowly 15.2 g solution of $\text{Zn}(\text{NO}_3)_2 \cdot 6\text{H}_2\text{O}$ into 4.07 g solution of NaOH prepared in separate 50 mL distilled water using 250 mL conical flasks. After the $\text{Zn}(\text{NO}_3)_2 \cdot 6\text{H}_2\text{O}$ solution has been totally added, the solution was further stirred for 2 h. After which the solution was separated by centrifugation. The white precipitate was washed several

times with absolute ethanol and distilled water. The washed precipitate was then dried over night at 70°C in an oven. The dried white precipitate was then calcined at 450°C to obtain the off-white zinc oxide nanoparticles.

3.2.2.3. Zinc oxide nanoparticles functionalization

The functionalization of zinc oxide nanoparticles was done through several steps (Figure 3.3). Firstly, the surface of the ZnO NPs was coated with silica by adding 30 mL of tetraorthosilicate (TEOS) into 11.0 g of ZnO NPs dispersed in 50 mL of absolute ethanol and refluxed at 60°C for 6 h (Ojemaye *et al.*, 2017). The resultant solution was separated, washed with ethanol and distilled water and dried in an oven at 70°C. Following this, similar treatment was made with 3-aminopropyltriethoxysilane (APTES) but the time was reduced to 5 h (Ojemaye *et al.*, 2018). After 5 h, the zinc oxide nanoparticles were converted to carboxylic functionalized zinc oxide nanoparticles by adding 5.64 g succinic anhydride previously dissolved in dry dimethylformamide (DMF) and stirred further for 48 h. Before the functionalization with pyrene ligand, carboxylic acid functionalized zinc oxide nanoparticles were activated with 4.001 g of dicyclohexylcarbodiimide (DCC) previously dissolved in 25 mL of dry DMF with continuous stirring in the dark for 24 h. Then this activated carboxylic acid functionalized ZnO NPs in dry DMF was slowly added into a stirring solution of 8.02 g of 1-(4-hydroxyphenyl)-4-pyrenyl-2,3-diaza-1,3-butadiene in the presence of 2.08 g of 4-dimethylaminopyridine (DMAP). The reaction mixture was allowed to stir further for 24 h before separation with centrifugation. The product was washed a couple of times with distilled water and the product was dried at 75°C in an oven.

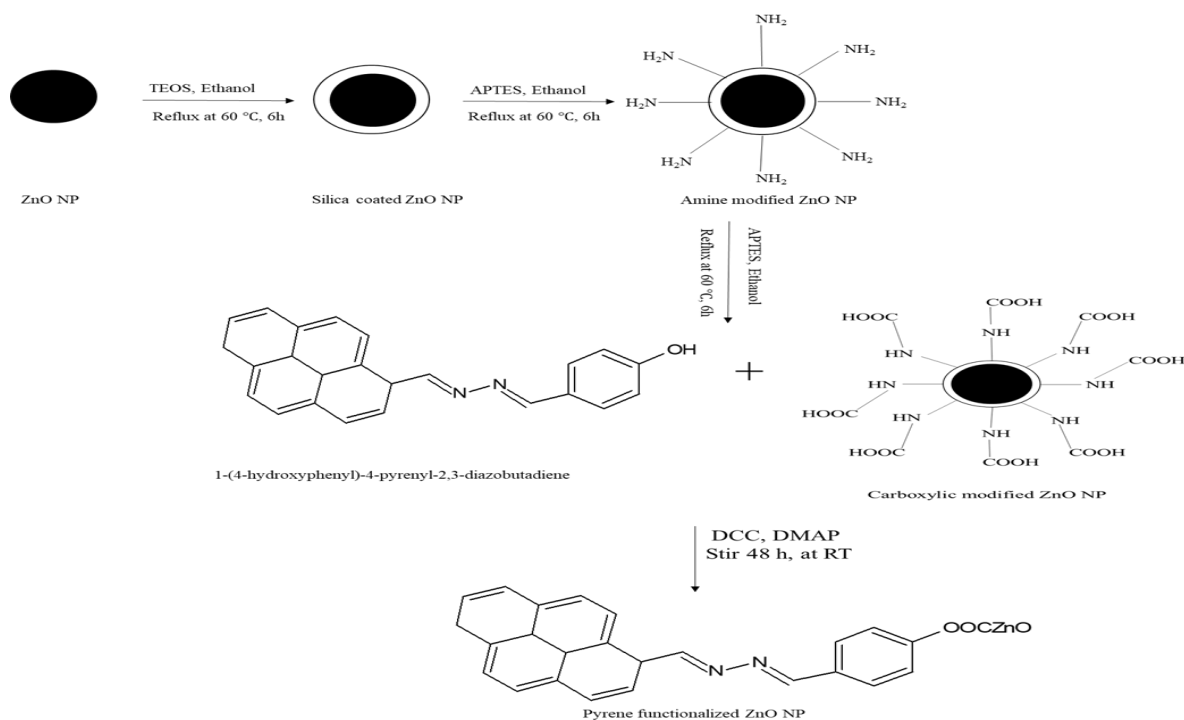


Figure 3.3: Preparation of novel pyrene functionalized ZnO NPs.

3.2.3. Characterization

Characterization of the nanoparticles was done with BET, XRD, SEM, EDX, TGA and FTIR. XRD (Bruker D8 Advanced XRD) was used to determine the crystal phase information of the materials. Surface morphologies and elemental/chemical composition were determined using SEM/EDX (JOEL JSM-6390 LVSEM). The percentage of volatile compounds present in the samples, purity and thermal resistances of the prepared samples were determined using TGA (Perkin Elmer TGA 4000 analyzer). FTIR (Perkin-Elmer Universal ATR) was used for functional group identification and confirmation of functionalization. Transmission electron microscope (JOEL 1210 transmission electron microscope) was used to determine particle size and to confirm particles geometry. Hydrogen and carbon framework of the ligand were determined using proton nuclear magnetic resonance (¹H NMR) and carbon 13 nuclear magnetic resonance (¹³C NMR) spectrometer (DMSO, Bruker TopSpin NMR). FTIR, EDX and SEM were also performed for the ligand.

3.2.4. Adsorbate preparation

A stock solution of simazine (1000 mg/L) was prepared by dissolving a specific amount of simazine in a specific volume of methanol. Series of standard concentrations and working solution were then prepared from the stock solution by dilution in water.

3.2.5. Surface charge determination

Surface charge determination was evaluated before the commencement of batch adsorption experiments via salt addition method (Kataria and Garg, 2017). This was done using 2 mg of the adsorbent in eight 20 mL solutions of 0.1 N NaCl with different initial pH values (pH_i) between 2 and 9. The adjustment of pH was done using 0.1 N HCl or 0.1N NaOH. The glass bottle containing the different solutions were agitated for 6 hr at room temperature using an orbital shaker at a speed of 150 rpm. Thereafter, final pH values (pH_f) were determined.

3.2.6. Adsorption studies



The herbicide's removal was done using batch adsorption experiments as reported by ul Haq *et al.* (2020) by varying pH, adsorbate concentration, contact time and adsorbent dose. Adsorption was performed in 100 mL glass bottles with screw caps and the agitation was done with an orbital shaker at 150 rotations per minute in the dark to avoid photodegradation. Initial and final concentrations of the herbicide were measured by means of a gas chromatograph equipped with electron capture detector (GC/ECD). Each of the aforementioned parameters was evaluated by keeping all others fixed. For pH adjustments, 0.1 N HCl and NaOH solutions were used as appropriate. The pH effect was investigated between pH 2 and 10. The contact time effect was studied between 0 and 360 minutes. The effect of adsorbent dose and adsorbate amount were evaluated at four different concentrations. The adsorption efficiency (% adsorbed) and adsorption capacity (q_e) were calculated by using equations 3.1 and 3.2 respectively:

$$\text{Adsorption efficiency (\% adsorbed)} = \left(\frac{c_i - c_{eq}}{c_i} \right) \times 100 \quad (3.1)$$

$$\text{Adsorption capacity } (q_e) = \frac{(c_i - c_{eq})V}{m} \quad (3.2)$$

Where, c_i = initial simazine concentration in mg/L

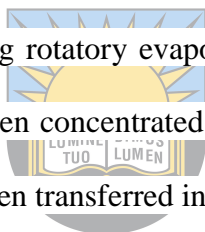
c_{eq} = equilibrium concentration of the simazine in mg/L

q_e = adsorption capacity in mg/g

m = mass of the adsorbent (g) and V = volume of the adsorbate solution used (L).

3.2.7. Solid phase extraction (SPE)

Unlike standards, samples were subjected to SPE prior to their injection into GC/ECD. This was done to ensure the removal of water and other particulates including traces of the adsorbent. Initially the SPE cartridges were preconditioned with 10 mL of ethyl acetate, methanol and distilled water respectively. The elution of the analytes was then carried out with 10 mL of ethyl acetate followed by concentrating using rotatory evaporator. In the concentrating process, the elute was evaporated to dryness and then concentrated in a millimeter of methanol. The 1 mL methanol concentrated analytes were then transferred into GC sample vials for injection.



University of Fort Hare
Together in Excellence

3.2.8. GC/ECD analysis

Quantification of the herbicide was done by means of an Agilent 7820A Gas Chromatograph equipped with Micro Electron Capture Detector (GC/ μ ECD with a column, Agilent 19091J-413: 1 HP-5 and dimension, 30 m length x 320 μ m diameter x 0.25 μ m film). Using nitrogen and helium as make-up and carrier gases respectively. The temperature programming of the oven was done similarly to Vassilakis *et al.* (1998). The initial temperature was set at 80°C and fixed for a minute before being changed to 218°C at 8°C/min. The oven temperature was then changed to 250°C at 4°C/min and maintained for 10 min. The injection was carried out splitless at 250°C with injection volume of 1 μ l.

3.2.9. Quality Assurance

The determination of limit of detection (LOD) and limit of quantification (LOQ), precision, accuracy and linearity were carried out using five concentration levels and details are shown in Table 3.1 and Figure A-I.3.

Table 3.1: Calibration data and quality assurance parameters.

Concentration level (s)	1	2	3	4	5	R ² = 0.9944
Area (A.U)	69039	100650	122320	143040	170030	Intercept = 47704.2 Slope = 24437.2
Precision (%)	113.7193	LOD (mg/L)	0.001062	LOQ (mg/L)	0.003219	Linear equation y = 24437x + 47704

3.2.10. Desorption and reusability studies

For reusability studies, three runs of adsorption were considered for a run period of 6 h. This was done to ascertain the reusability of the adsorbent for cost effectiveness. After each run of adsorption, the loaded adsorbent was separated by centrifugation, dried in a fume hood and dispersed in three 20 mL methanol solutions with solution pH 9 and stirred for the equivalent period as in adsorption. However, in the reusability studies the adsorbent was used successively for three 6h runs without desorption. Further, separation was also performed using centrifugation. At the end of desorption and reusability experiments, the concentration of the adsorbate was measured using GC/ECD. Desorption efficiency (% desorbed) was calculated using equation 3.3:

$$\text{Desorption efficiency (\% desorbed)} = \left(\frac{c_d}{c_a}\right) \times 100 \quad (3.3)$$

Where C_d = adsorbate concentration desorbed and C_a = adsorbate concentration adsorbed both in mg/L.

3.2.11. Data analysis

The data obtained from this study was statistically analysed and plotted using OriginPro 2021b.

3.3. Results and discussion

3.3.1. Characterization

3.3.1.1. FTIR analysis

The FTIR analysis was carried to obtain FTIR spectra of the materials and to verify if functionalization of the adsorbent was successful. The obtained spectra of the ZnO, and ZnO-Pyrene synthesized nanoparticles clearly showed the Zn-O stretch between 500 and 450 cm^{-1} (Figure 3.4). The stretch between 800 and 700 cm^{-1} in the ZnO spectrum could be interpreted as motion of hydrogen atoms parallel to the connection line of the two adjacent metal ions originating from the atmosphere during the analysis (Lutz *et al.*, 1998). Between 1400 and 1300 cm^{-1} alcohol O-H bending was observed, which might have resulted from atmospheric moisture (Ahmed *et al.*, 2020). In the ZnO-Pyrene spectrum, -OH alcohol appeared at 3360 cm^{-1} .

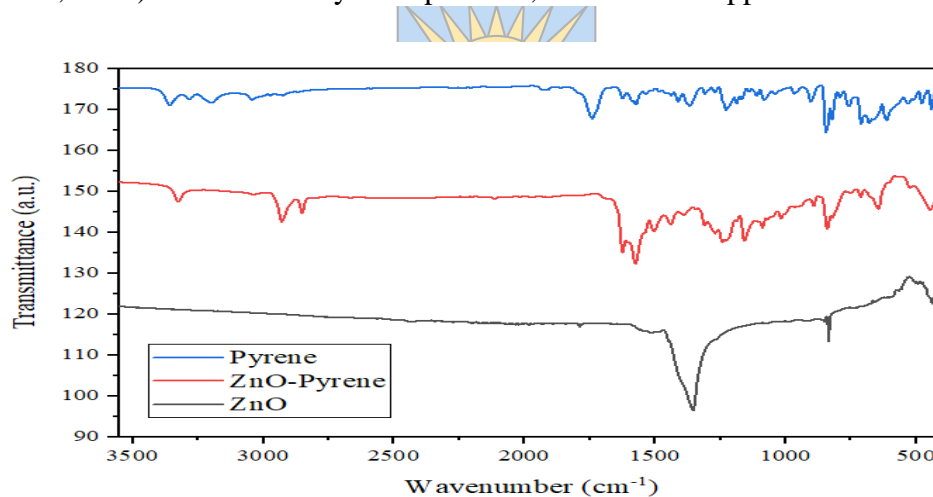


Figure 3.4: FTIR spectra of ZnO, ZnO-Pyrene and Pyrene ligand.

The strong stretches between 1700 and 1300 cm^{-1} attributed to carboxyl group of ester (Wang *et al.*, 2011) resulted from the functionalization. The weak peak observed between 3100 and 3000 cm^{-1} corresponds to C-H stretch aromatic followed by two alkane C-H stretches between 2990 and 2850 cm^{-1} (Zhuo *et al.*, 2000; Mahendra *et al.*, 2017). In the pyrene ligand spectrum, additional peaks appeared adjacent to the -OH, this might have resulted from the traces of water that were present hence that -OH stretch appeared like -OH stretch of carboxylic acid. A strong peak corresponding to C=C also appeared in pyrene spectrum in the region 1700 cm^{-1} – 1600 cm^{-1} .

¹ (Marshall *et al.*, 2005). These results are similar to those reported by Gnanasangeetha and Saralathambavani (2013) and Winiarski *et al.* (2018). From these observations, it can be said that zinc oxide nanoparticles were successfully synthesized and functionalized with pyrene ligand.

3.3.1.2. EDX analysis

EDX analysis was carried to determine the chemical/elemental composition of the materials for purity determination and to verify the successful syntheses of the materials. In the analysis, clear peaks corresponding to Zn were observed in three intervals, 0.8 - 1.2 keV, 8.4 - 8.8 keV, and 9.4 - 9.8 keV respectively in both ZnO and ZnO-Pyrene spectra (Figure 3.5 (a)-(b)). A peak corresponding to oxygen was also observed between 0.4 and 0.6 keV in both spectra. In the ZnO-Pyrene spectrum, there were additional peaks corresponding to C and N between 0.2 and 0.4 keV. These observations were also noticed in the EDX spectrum of pyrene ligand with the exception of Zn peaks. From the EDX spectra, it can be deduced that the samples were of high purity as no unwanted elements were observed (Zhang *et al.*, 2016). Further, the nanoparticles showed an approximation of 50/50 atomic percentage of Zn/O. This indicated that the precursor was successfully converted to the novel adsorbent.

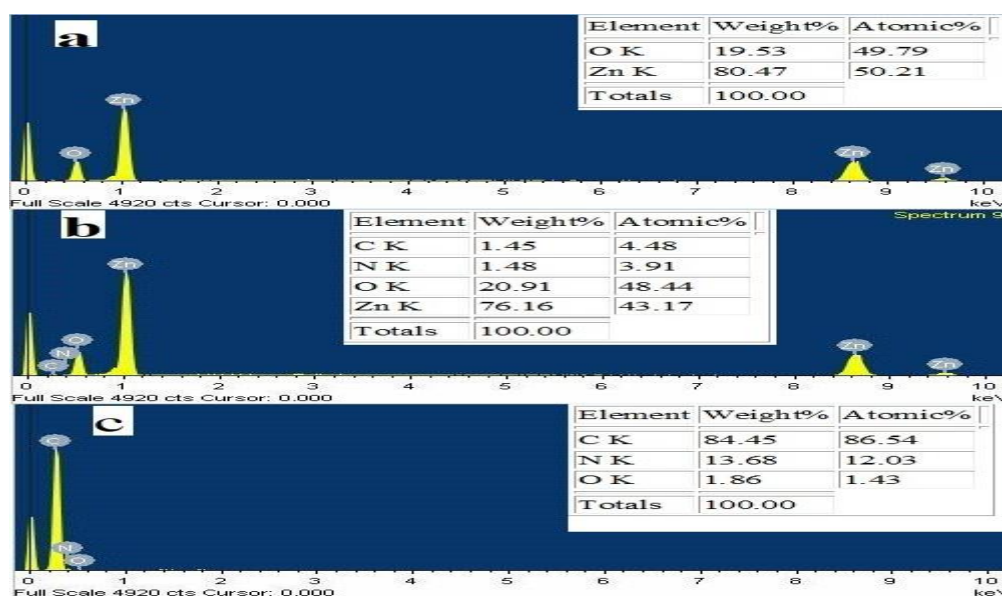


Figure 3.5: EDX spectra of (a) ZnO (b) ZnO-Pyrene and (c) Pyrene ligand.

3.3.1.3. SEM analysis

SEM analysis was carried to determine the morphology of the materials, which also play a crucial role in adsorption. This was performed under the same magnification. In the analysis, a crystalline morphology of ZnO NPs was observed as shown in Figure 3.6 (a) (Zafar *et al.*, 2019). Its morphology was maintained even after functionalization with pyrene (Figure 3.6 (b)); this is an indication that the core properties of this nanoparticle were maintained (Cho *et al.*, 2015). Further, aggregation was improved in the novel adsorbent. Upon further magnification of SEM images the spherical geometry could be anticipated even though it was not fully conclusive hence, further analysis was done with TEM. Pyrene ligand possessed flake-like particles (Figure 3.6 (c)), indicating an amorphous morphology.

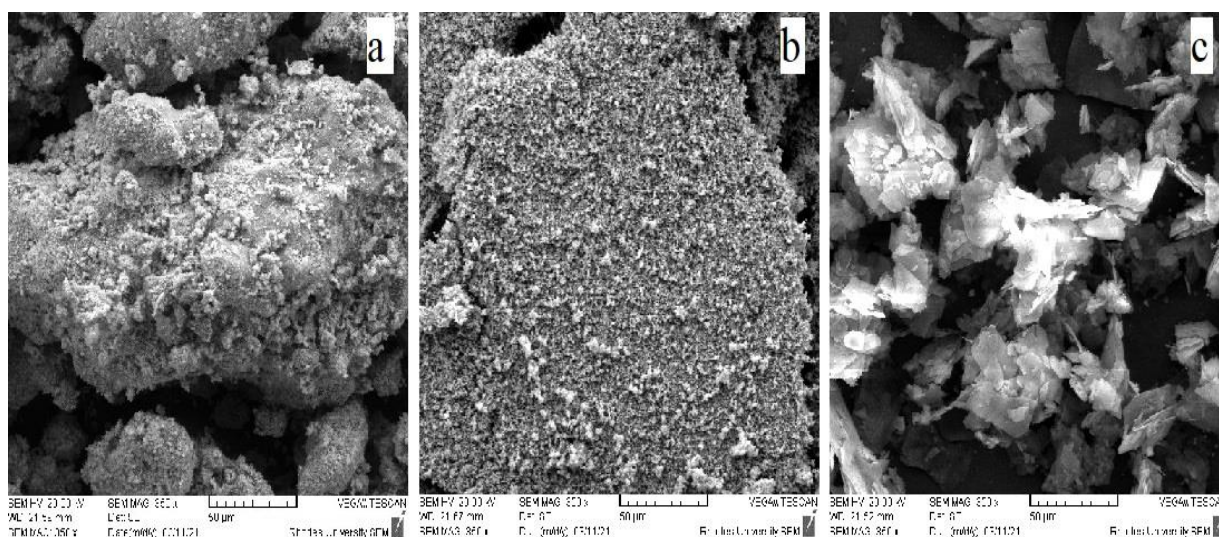


Figure 3.6: SEM images of (a) ZnO (b) ZnO-Pyrene and (c) Pyrene ligand.

3.3.1.4. TEM analysis

TEM images of the synthesized materials are presented in Figure 3.7. In Figure 3.7(a), spherically shaped material with little agglomeration was observed to have been synthesized with an average size of 290 nm. This result compliments the result obtained from the SEM analysis (Figure 3.6).

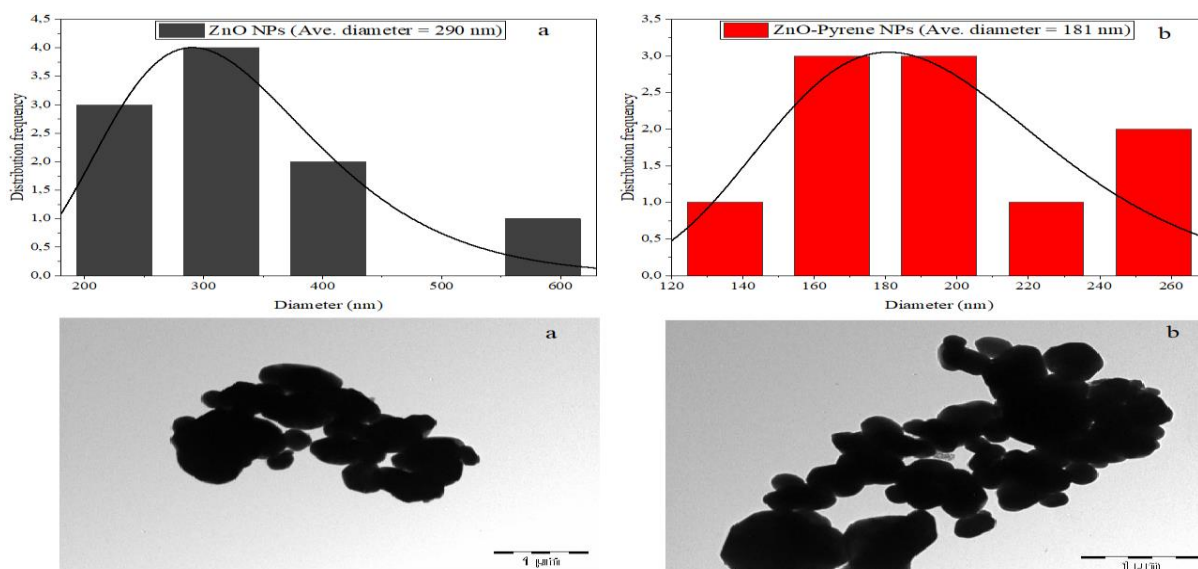


Figure 3.7: Synthesized NPs TEM images (a) ZnO NPs and (b) ZnO-Pyrene NPs and their particle size distributions.

Upon functionalization of zinc oxide nanoparticles with pyrene ligand, it was observed that average (Ave.) particle size of the functionalized material decreased to 180 nm. Reason being that the introduction of the ligand decreased the particle aggregation via electron-electron repulsions between the functionalized nanoparticles as a result more smaller particles were detected in the novel adsorbent. Ojemaye *et al.* (2017) also published a similar result.

3.3.1.5. XRD analysis

In order to know the crystal information of the synthesized materials, XRD analysis was carried out. In the XRD diffractogram of ZnO nanoparticles, nine diffraction reflections were observed at 31.8° , 34.5° , 36.3° , 47.6° , 56.6° , 62.9° , 66.5° , 68.0° and 69.2° (Figure 3.8). These reflections were assigned to the following miller indices: (100), (002), (101), (102), (110), (103), (200), (112) and (201) respectively. Mohan and Renjanadevi (2016) reported similar results. The XRD reflections of ZnO were preserved in the novel material (ZnO-Pyrene). This implied that the structure was maintained throughout. Moreover, this is another implication that functionalization was successful and that functionalization does not affect the inner core structure of the bulk

material. The absence of other undesired reflections indicated purity of the materials. Further confirmation of the purity of the materials was done with TGA (Figure 3.9).

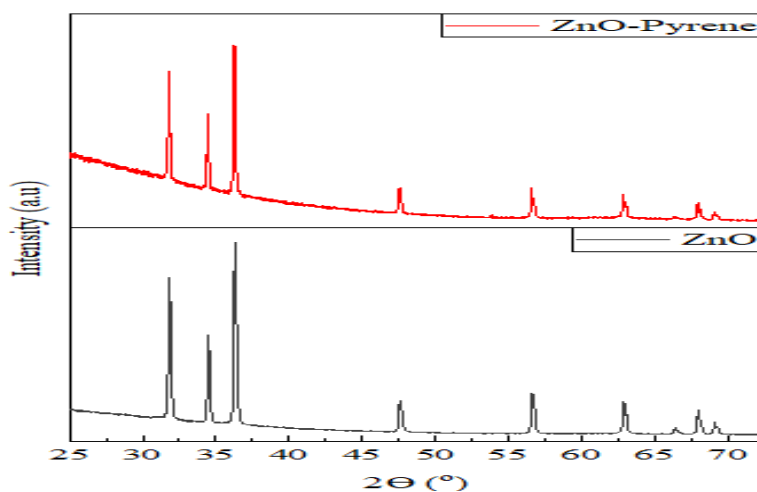


Figure 3.8: XRD diffractograms of ZnO and pyrene functionalized ZnO nanoparticles.

3.3.1.6. TGA analysis



TGA analysis was performed in order to determine the percentage of organic compounds present in the samples, thermal stability and purity of the samples. In the TGA graph of pure ZnO nanoparticles, there were two weight losses observed (Figure 3.9 (a)). First weight loss (3 wt%) was observed between 95 and 350°C, and can be assigned to loss of water present in the sample. This water might have originated from the solvent used during the analysis. The second weight loss (17 wt%) was observed between 510 and 800°C due to thermal decomposition of $\text{Zn}(\text{OH})_x$, which resulted from the presence of water during the analysis to ZnO. In ZnO-Pyrene TGA curve, the weight loss (2.22 wt%) between 625 and 800°C was a result of thermal decomposition of the addition shells which result from functionalization. In this analysis, it was also noted that the thermal stability of ZnO was improved by functionalization due to more resulted residue (Figure 3.9 (b)).

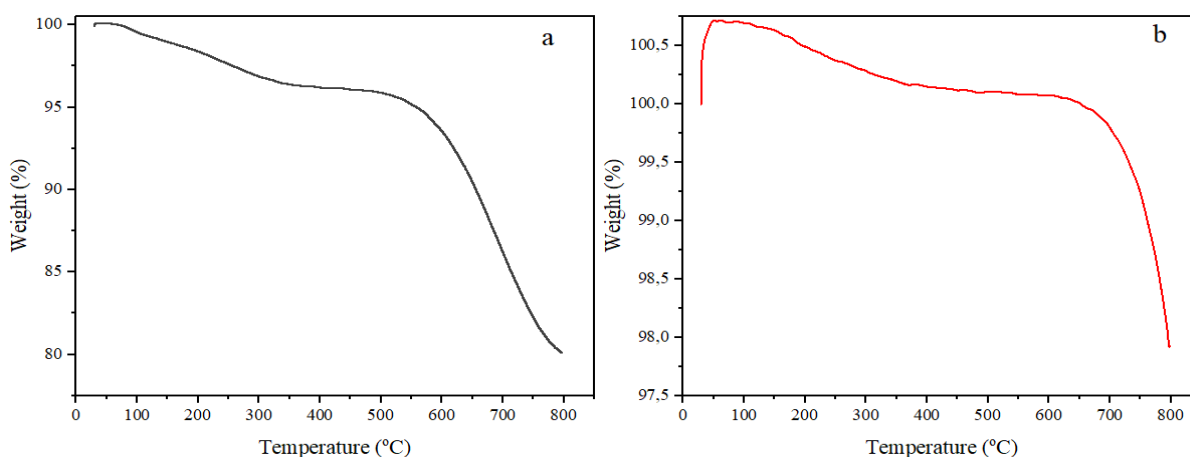


Figure 3.9: TGA curves of (a) ZnO and (b) ZnO-Pyrene nanoparticles.

3.3.2. Adsorption studies

3.3.2.1. pH effect

The point of zero charge of the adsorbent was found to be 6 (Figure 3.10 (a)) and data showing the point of zero charge is presented in Table A-I.1. This was accomplished with solution volume of 20 mL, salt solution concentration of 0.1 M, adsorbent dose of approximately 2 mg, temperature of $20 \pm 2^\circ\text{C}$ and shaking period of 6 h. It was also found that below the point of zero charge the adsorbent bare a positive charge and vice versa for pH values above the point of zero charge. This implied that the adsorbent would adsorb more adsorbate at lower pH values due to the nature of the adsorbate. The nature of the adsorbate is such that it has two nitrogen atoms that are outside its ring (Figure 3.1), which allows it to behave as a nucleophile. Worthy of mention is that the highest adsorption was noticed at pH 2 (Figure 3.10 (b)). Also, there is a common phenomenon with triazine class of compounds under acidic conditions in which C-Cl bond undergo hydrolysis. This might have also affected the concentration of the contaminant. Nevertheless, despite two exceptions, pH 5 and 7, it was observed that adsorption was decreasing with increasing pH. The pH effect was evaluated between pH 2 and 9 while keeping the adsorbate concentration at 0.313 mg/L, adsorbent dose approximately at 20.0 mg, temperature at $20 \pm 2^\circ\text{C}$ and shaking time at 360 minutes.

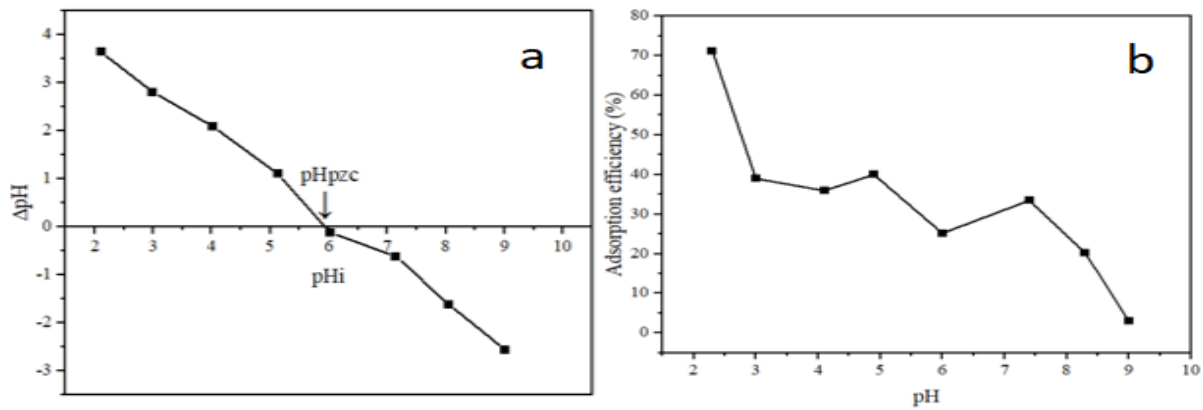


Figure 3.10: (a) Point of zero charge curve of ZnO-Pyrene nanoparticles and (b) pH effect.

3.3.2.2. Effect of contact time

Contact time effect was evaluated at five time intervals between 0 and 60 minutes (Figure 3.11).

This was accomplished by fixing the solution pH at 2, adsorbent dose at approximately 20.0 mg,

adsorbate concentration at 0.281 mg/L and the temperature at $20 \pm 2^\circ\text{C}$. It was noticed that the

material adsorbs more at lower contact times as observed at 5 minutes shaking period. At higher contact time, the adsorption capacity decreased. This implies that the adsorption was physical as

the adsorbate would attach and detach on the adsorbent while shaking. The optimum time was

Together in Excellence

noticed from 15 minutes even though the curve was not completely constant for the

aforementioned reason. However, 60 minutes was considered for further experiments.

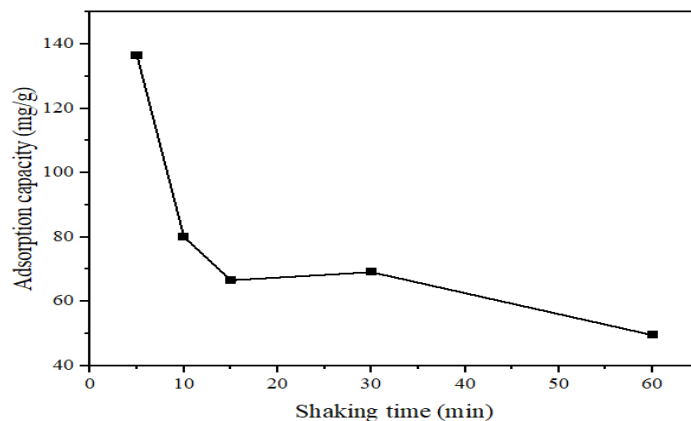


Figure 3.11: Effect of contact time.

3.3.2.3. Effect of adsorbent amount

Effect of adsorbent amount was evaluated at four different adsorbent weights i.e. 10.0, 20.0, 30.0 and 40.0 mg (Figure 3.12). This was carried out while keeping other parameters constant (pH = 2, Temperature = $20 \pm 2^\circ\text{C}$, adsorbate concentration = 0.312 mg/L and shaking time = 60.0 minutes). It was noticed that the adsorption efficiency was increasing with increasing adsorbent amount. This is because the more the adsorbent, the more the active adsorptive sites available to adsorb the contaminant.

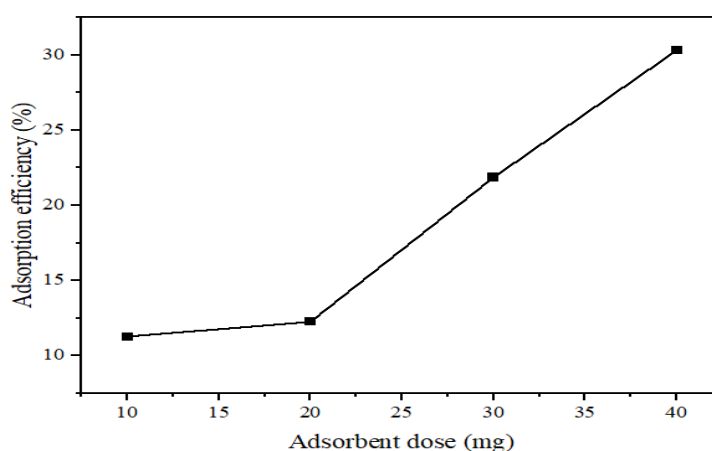


Figure 3.12: Effect of adsorbent amount.
University of Fort Hare
Together in Excellence

3.3.2.4. Effect of adsorbate concentration

Four adsorbate concentrations were considered in the evaluation of effect of adsorbate concentration (0.118, 0.179, 0.244 and 0.302 mg/L) (Figure 3.13). This was accomplished by keeping constant all other parameters (Temperature = $20 \pm 2^\circ\text{C}$, adsorbent dose approximately = 20 mg, pH = 2 and shaking period = 60 minutes). It was noticed that the adsorption capacity was increasing with increasing adsorbate concentration. At lower concentrations the adsorption capacity was increasing sharply because there were more active sites on the adsorbent available for adsorption of simazine but fewer adsorbate molecules, therefore at every collision there was adsorption. As the concentration of adsorbate increases, the adsorption capacity was decreasing and becoming steady. Between 0.244 and 0.302 mg/L there was no major change in adsorption capacity hence further concentrations were not considered.

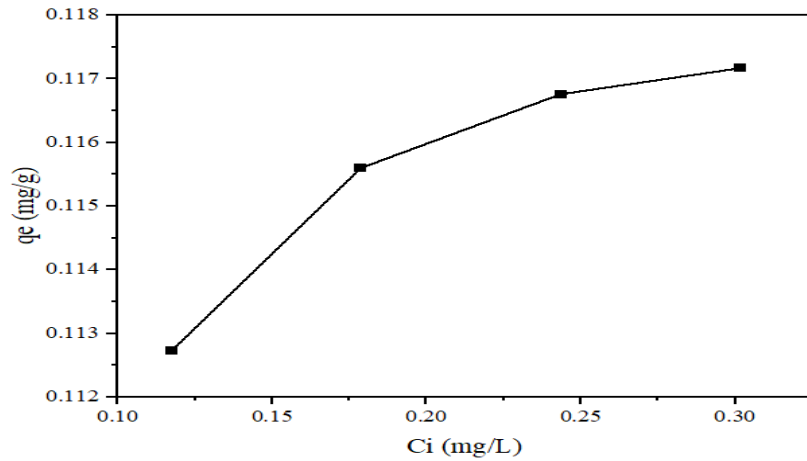


Figure 3.13: Effect of adsorbate concentration.

3.3.3. Adsorption isotherms

The adsorption data were fitted into three different adsorption isotherms; Langmuir, Freundlich and Temkin isotherm expressed in equations (3.4), (3.5) and (3.6) respectively:

$$\frac{1}{q_e} = \left(\frac{1}{K_L q_{max}} \right) \left(\frac{1}{c_e} \right) + \left(\frac{1}{q_{max}} \right) \quad (3.4)$$

$$\log q_e = \log K_F + \left(\frac{1}{n} \right) \log c_e \quad (3.5)$$

$$q_e = B \ln K_T + B \ln c_e \quad (3.6)$$

Where, q_{max} (mg/g) symbolises maximum adsorption capacity, K_L (L/mg), the Langmuir constant and q_e , the adsorption capacity (mg/g). K_F (mg/g(L/mg)^{1/n}) denotes Freundlich constant and n the heterogeneity factor whereas c_e is the dye concentration at equilibrium time. B (J mol⁻¹) is the Temkin constant, which indicates the heat of adsorption, and K_T (L.g⁻¹) is equilibrium binding constant. Adsorption parameters were obtained using linear form of Langmuir adsorption isotherm (Equation 3.4) by plotting a graph of $1/q_e$ against $1/c_e$. The linear plot of $\log q_e$ versus $\log c_e$ (Equation 3.5) was used to determine the Freundlich isotherms parameter values. However, q_e versus $\ln c_e$ (Equation 3.6) was used for Temkin parameters determination. The correlation coefficients and isotherm parameter values of simazine are listed in Table 3.2 and presented in Figure A-I.8.

Table 3.2: Simazine adsorption isotherms' parameters.

Adsorption isotherms	Parameters	Values
Langmuir isotherm	K_L (L/mg)	6.59×10^4
	q_{max} (mg/g)	0.117
	R^2	0.918
Freundlich isotherm	K_F (mg/g(L/mg) ^{1/n})	0.119
	n	98.0
	R^2	0.995
Temkin isotherm	K_T (L/mg)	0.888
	B (J.mol ⁻¹)	848.65
	R^2	0.991

*The numerical values in this table are presented in three significant figures.

From the obtained results, Freundlich possessed the closest R^2 value to 1 meaning that there was a possibility that the data could be better fitted to this model. However, since the n value was above 10, the isotherm was discarded. Temkin isotherm showed the second closest R^2 value to 1, which makes it acceptable for this data. Moreover, B value was positive meaning that the adsorption process was exothermic. Even though the R^2 value of Langmuir isotherm was not that close to 1, it can be considered a better fit compared to Freundlich isotherm because q_{max} was greater than zero. The applicability of Langmuir isotherm implies that the adsorption of simazine onto the novel material was monolayer in nature. The Temkin applicability and positive B value implies that the process was exothermic. Previously published studies did not report on isotherm studies of simazine onto various adsorbents. Therefore, there are no possible comparison with the result obtained in this study. However, this study serves a baseline and provided an insight by which knowledge can be derived for new applications of various adsorbents as well as the currently reported adsorbent for simazine and other contaminants.

3.3.4. Adsorption kinetics

Three kinetics models (pseudo-first order, pseudo-second order and intraparticle diffusion kinetic models) were considered for the determination of rate mechanism of simazine adsorption onto the novel adsorbent (Kataria and Garg, 2017). The equations for these models are expressed in equations 3.7, 3.8 and 3.9 respectively:

$$\ln(q_e - q_t) = \ln q_e - K_1 t \quad (3.7)$$

$$\frac{t}{q_t} = \frac{1}{K_2 q_e^2} + \frac{t}{q_e} \quad (3.8)$$

$$q_t = K_{id} t^{1/2} + C \quad (3.9)$$

Where, q_e denotes adsorption capacity at equilibrium time, q_t (mg/g) is the adsorption capacity at time t , K_1 and K_2 (min^{-1}) are pseudo-first order kinetic rate constant and pseudo-second order rate constant respectively, t denotes time in minutes, K_{id} is the intra-particle diffusion rate constant usually expressed in $\text{mg g}^{-1} \text{min}^{-0.5}$ and C is the thickness of boundary layer expressed in mg/g. All kinetic parameters are presented in Table 3.3 together with their R^2 values. Only pseudo-second order gave an accepted R^2 value. However, the q_e was far greater from the experimental value meaning this was not conclusive.

Table 3.3: Simazine adsorption onto the novel adsorbent kinetic models' parameters.

Kinetic models	Parameters	Values of parameters
Pseudo-first order	K_1 (min^{-1})	2.70×10^{-4}
	q_e (cal)	0.0178
	R^2	0.768
Pseudo-second order	K_2 (g/mg.min)	1.06×10^{-3}
	q_e (cal)	4.04
	R^2	0.992
Intraparticle diffusion	K_{id} ($\text{mg.g}^{-1} \text{min}^{-0.5}$)	-1.58×10^{-3}
	C	0.135
	R^2	0.632
Experimental data	q_e (exp)	0.117

*The numerical values in this table are presented in three significant figures.

Pseudo-first order showed the second closest R^2 value to 1. Even though the R^2 was not the closest to 1, it can be considered a better fit because it showed the closest q_e value to the experimental value in comparison with the pseudo-second order. Intra-particle diffusion could not be considered a better fit as a result of its low R^2 value and the fact that C was not equal to zero meaning its curve was not passing through the origin. The applicability of the pseudo-first order implies that the adsorption process was physisorption. This means that the simazine

particles were physically attached to the novel adsorbent through the multiple nitrogen ends of the pyrene ligand.

3.3.5. Reusability and desorption studies

The reusability studies were carried out three times by shaking for 60 minutes, with 20 mg adsorbent dose and 5 mg/L adsorbate concentration at room temperature (Figure 3.14).

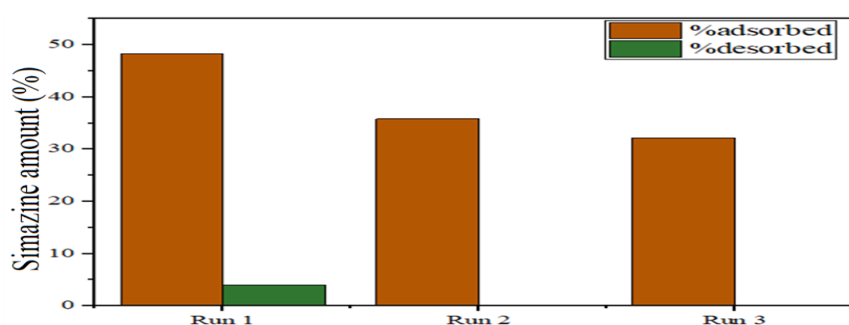


Figure 3.14: Reusability and desorption studies.

It was noticed that as number of runs increases, adsorption efficiency was decreasing. This was due to the decrease in the number of sites on the adsorbent available for the adsorption of simazine from aqueous solution as the number of runs increases. In desorption experiments only one experiment showed desorption and others did not give any detectable results. In the two other experiments, there might be no desorption or strong possibility that the amount of simazine present in solution was below the limit of quantification.

3.4. Conclusion

In this study, the synthesis of pyrene functionalized zinc oxide was carried out for the removal of simazine herbicide from aqueous solution. The result of characterization showed that the synthesis of the novel adsorbent was successful. SEM reveal a crystalline morphology and TEM analysis revealed a spherical geometry of the novel material. Functionalization of bare zinc oxide nanoparticles indicated a decrease in the particle size from 290 nm for bare zinc oxide nanoparticles to 181 nm for pyrene functionalized zinc oxide nanoparticles. The latter result means that the grafting of the ligand onto zinc oxide nanoparticles will improve the performance

of bare material since small particle size enhances adsorption efficiency. The material showed high adsorption capacity from all batch adsorption experiments conducted in this study. The adsorption data was better fitted to Temkin isotherm and Temkin constant (B) was found positive, which led to a conclusion that the adsorption process for the removal of simazine from aqueous solution by using this novel material is exothermic in nature. Also, Langmuir isotherm was also applicable. The kinetics of the adsorption process favoured pseudo-first order. These results is an indication that this material can be considered as an alternative adsorbent for the removal of simazine and other organic contaminants from wastewater and can be explored to real life scenerios.

References

Ahmed, D.S., Mohammed, M.R. and Mohammed, M.K., 2020. Synthesis of multi-walled carbon nanotubes decorated with ZnO/Ag nanoparticles by co-precipitation method. *Nanoscience & Nanotechnology-Asia*, 10(2), pp.127-133.

Arias-Estévez, M., López-Periago, E., Martínez-Carballo, E., Simal-Gándara, J., Mejuto, J.C. and García-Río, L., 2008. The mobility and degradation of pesticides in soils and the pollution of groundwater resources. *Agriculture, Ecosystems & Environment*, 123(4), pp.247-260.

Beck, A.J., Johnston, A.J. and Jones, K.C., 1993. Movement of nonionic organic chemicals in agricultural soils. *Critical Reviews in Environmental Science and Technology*, 23(3), pp.219-248.

Beltrán, F.J., García-Araya, J.F., Rivas, J., Álvarez, P.M. and Rodriguez, E., 2000. Kinetics of simazine advanced oxidation in water. *Journal of Environmental Science & Health Part B*, 35(4), pp.439-454.

Cho, K.Y., Yeom, Y.S., Seo, H.Y., Kumar, P., Lee, A.S., Baek, K.Y. and Yoon, H.G., 2015. Ionic block copolymer doped reduced graphene oxide supports with ultra-fine Pd nanoparticles: strategic realization of ultra-accelerated nanocatalysis. *Journal of Materials Chemistry A*, 3(41), pp.20471-20476.

Chu, W., Rao, Y. and Hui, W.Y., 2009. Removal of simazine in a UV/TiO₂ heterogeneous system. *Journal of Agricultural and Food Chemistry*, 57(15), pp.6944-6949.

Debnath, P. and Mondal, N.K., 2020. Effective removal of congo red dye from aqueous solution using biosynthesized zinc oxide nanoparticles. *Environmental Nanotechnology, Monitoring & Management*, 14, pp.100320.

Esposito, S., Sannino, F., Pansini, M., Bonelli, B. and Garrone, E., 2013. Modes of interaction of simazine with the surface of model amorphous silicas in water. *The Journal of Physical Chemistry C*, 117(21), pp.11203-11210.

Flores, C., Morgante, V., González, M., Navia, R. and Seeger, M., 2009. Adsorption studies of the herbicide simazine in agricultural soils of the Aconcagua valley, central Chile. *Chemosphere*, 74(11), pp.1544-1549.

Flores, K., Valdes, C., Ramirez, D., Eubanks, T.M., Lopez, J., Hernandez, C., Alcoutlabi, M. and Parsons, J.G., 2020. The effect of hybrid zinc oxide/graphene oxide (ZnO/GO) nano-catalysts on the photocatalytic degradation of simazine. *Chemosphere*, 259, p.127414.

Fulazzaky, M.A., 2012. Analysis of global and sequential mass transfers for the adsorption of atrazine and simazine onto granular activated carbons from a hydrodynamic column. *Analytical Methods*, 4(8), pp.2396-2403.

Gnanasangeetha, D. and SaralaThambavani, D., 2013. One pot synthesis of zinc oxide nanoparticles via chemical and green method. *Journal of Materials Science Research*, 2320, pp.6055.

Gu, M., Hao, L., Wang, Y., Li, X., Chen, Y., Li, W. and Jiang, L., 2020. The selective heavy metal ions adsorption of zinc oxide nanoparticles from dental wastewater. *Chemical Physics*, 534, pp.110750.

Gunasekara, A.S., Troiano, J., Goh, K.S. and Tjeerdema, R.S., 2007. Chemistry and fate of simazine. *Reviews of Environmental Contamination and Toxicology*, pp.1-23.

Hayes, T.B., Case, P., Chui, S., Chung, D., Haeffele, C., Haston, K., Lee, M., Mai, V.P., Marjuoa, Y., Parker, J. and Tsui, M., 2006. Pesticide mixtures, endocrine disruption, and amphibian declines: are we underestimating the impact?. *Environmental Health Perspectives*, 114(1), pp.40-50.

Jangwan, J.S., Kumar, G., Kumar, V. and Kumar, A., 2021. Abatement of organic and inorganic pollutants from drinking water by using commercial and laboratory-synthesized zinc oxide nanoparticles. *SN Applied Sciences*, 3(3), pp.1-12.

Jiang, H. and Adams, C., 2006. Treatability of chloro-s-triazines by conventional drinking water treatment technologies. *Water Research*, 40(8), pp.1657-1667.

Kataria, N. and Garg, V.K., 2017. Removal of Congo red and Brilliant green dyes from aqueous solution using flower shaped ZnO nanoparticles. *Journal of Environmental Chemical Engineering*, 5(6), pp.5420-5428.



Katsumata, H., Kaneco, S., Suzuki, T. and Ohta, K., 2006. Determination of atrazine and simazine in water samples by high-performance liquid chromatography after preconcentration with heat-treated diatomaceous earth. *Analytica Chimica Acta*, 577(2), pp.214-219.

López-Muñoz, M.J., Aguado, J. and Revilla, A., 2011. Photocatalytic removal of s-triazines: Evaluation of operational parameters. *Catalysis Today*, 161(1), pp.153-162.

Lutz, H.D., Jung, C., Mörtel, R., Jacobs, H. and Stahl, R., 1998. Hydrogen bonding in solid hydroxides with strongly polarising metal ions, β -Be(OH)₂ and ϵ -Zn(OH)₂. *Spectrochimica Acta Part A: Molecular and Biomolecular Spectroscopy*, 54(7), pp.893-901.

Mahendra, C., Murali, M., Manasa, G., Ponnamma, P., Abhilash, M.R., Lakshmeesha, T.R., Satish, A., Amruthesh, K.N. and Sudarshana, M.S., 2017. Antibacterial and antimutagenic potential of bio-fabricated zinc oxide nanoparticles of *Cochlospermum religiosum* (L.). *Microbial Pathogenesis*, 110, pp.620-629.

Meriam Suhaimy, S.H., Lai, C.W., Tajuddin, H.A., Samsudin, E.M. and Johan, M.R., 2018. Impact of TiO₂ nanotubes' morphology on the photocatalytic degradation of simazine pollutant. *Materials*, 11(11), p.2066.

Mohan, A.C. and Renjanadevi, B., 2016. Preparation of zinc oxide nanoparticles and its characterization using scanning electron microscopy (SEM) and X-ray diffraction (XRD). *Procedia Technology*, 24, pp.761-766.

Monsef Khoshhesab, Z. and Souhani, S., 2018. Adsorptive removal of reactive dyes from aqueous solutions using zinc oxide nanoparticles. *Journal of the Chinese Chemical Society*, 65(12), pp.1482-1490.

Ojemaye, M.O., Okoh, O.O. and Okoh, A.I., 2017. Adsorption of Cu²⁺ from aqueous solution by a novel material; azomethine functionalized magnetic nanoparticles. *Separation and Purification Technology*, 183, pp.204-215.



Ojemaye, M.O., Okoh, O.O. and Okoh, A.I., 2018. Uptake of Zn²⁺ and As³⁺ from wastewater by adsorption onto imine functionalized magnetic nanoparticles. *Water*, 10(1), pp.36.

Paul, B., Yang, D., Yang, X., Ke, X., Frost, R. and Zhu, H., 2010. Adsorption of the herbicide simazine on moderately acid-activated beidellite. *Applied Clay Science*, 49(1-2), pp.80-83.

Primo, J.D.O., Bittencourt, C., Acosta, S., Sierra-Castillo, A., Colomer, J.F., Jaerger, S., Teixeira, V.C. and Anaissi, F.J., 2020. Synthesis of zinc oxide nanoparticles by ecofriendly routes: adsorbent for copper removal from wastewater. *Frontiers in Chemistry*, 8, pp.1100.

Sabir, S., Arshad, M. and Chaudhari, S.K., 2014. Zinc oxide nanoparticles for revolutionizing agriculture: synthesis and applications. *The Scientific World Journal*, 2014.

Salvestrini, S., Vanore, P., Iovino, P., Leone, V. and Capasso, S., 2015. Adsorption of simazine and boscalid onto acid-activated natural clinoptilolite. *Environmental Engineering Management Journal*, 14, pp.1705-1712.

Sannino, F., Ruocco, S., Marocco, A., Esposito, S. and Pansini, M., 2013. Simazine removal from waters by adsorption on porous silicas tailored by sol-gel technique. *Microporous and Mesoporous Materials*, 180, pp.178-186.

Sannino, F., Ruocco, S., Marocco, A., Esposito, S. and Pansini, M., 2012. Cyclic process of simazine removal from waters by adsorption on zeolite HY and its regeneration by thermal treatment. *Journal of Hazardous Materials*, 229, pp.354-360.

Scutariu, R.E., Iancu, V., Nechifor, G., Radu, G.L., Simion, M. and Niculescu, M., 2018. Membrane filtration efficiency on triazine herbicides in organic and aqueous solutions.

Sheela, T., Nayaka, Y.A., Viswanatha, R., Basavanna, S. and Venkatesha, T.G., 2012. Kinetics and thermodynamics studies on the adsorption of Zn (II), Cd (II) and Hg (II) from aqueous solution using zinc oxide nanoparticles. *Powder Technology*, 217, pp.163-170.

Troiano, J., Weaver, D., Marade, J., Spurlock, F., Pepple, M., Nordmark, C. and Bartkowiak, D., 2001. Summary of well water sampling in California to detect pesticide residues resulting from nonpoint-source applications. *Journal of Environmental Quality*, 30(2), pp.448-459.

ul Haq, A., Saeed, M., Usman, M., Naqvi, S.A.R., Bokhari, T.H., Maqbool, T., Ghaus, H., Tahir, T. and Khalid, H., 2020. Sorption of chlorpyrifos onto zinc oxide nanoparticles impregnated pea peels (*Pisum sativum* L): Equilibrium, kinetic and thermodynamic studies. *Environmental Technology & Innovation*, 17, pp.100516.

Vassilakis, I., Tsipi, D. and Scoullou, M., 1998. Determination of a variety of chemical classes of pesticides in surface and ground waters by off-line solid-phase extraction, gas chromatography with electron-capture and nitrogen-phosphorus detection, and high-performance liquid chromatography with post-column derivatization and fluorescence detection. *Journal of Chromatography A*, 823(1-2), pp.49-58.

Wang, X., Mao, H., Huang, W., Guan, W., Zou, X., Pan, J. and Yan, Y., 2011. Preparation of magnetic imprinted polymer particles via microwave heating initiated polymerization for

selective enrichment of 2-amino-4-nitrophenol from aqueous solution. *Chemical Engineering Journal*, 178, pp.85-92.

Wang, Y., Li, B., Zhang, L., Liu, L., Zuo, Q. and Li, P., 2010. A highly selective regenerable optical sensor for detection of mercury (II) ion in water using organic–inorganic hybrid nanomaterials containing pyrene. *New Journal of Chemistry*, 34(9), pp.1946-1953.

Winiarski, J., Tylus, W., Winiarska, K., Szczygieł, I. and Szczygieł, B., 2018. XPS and FT-IR characterization of selected synthetic corrosion products of zinc expected in neutral environment containing chloride ions. *Journal of Spectroscopy*, 2018.

Wu, C., Qiao, X., Chen, J., Wang, H., Tan, F. and Li, S., 2006. A novel chemical route to prepare ZnO nanoparticles. *Materials Letters*, 60(15), pp.1828-1832.

Zafar, M.N., Dar, Q., Nawaz, F., Zafar, M.N., Iqbal, M. and Nazar, M.F., 2019. Effective adsorptive removal of azo dyes over spherical ZnO nanoparticles. *Journal of Materials Research and Technology*, 8(1), pp.713-725.



Zhang, F., Lan, J., Yang, Y., Wei, T., Tan, R. and Song, W., 2013. Adsorption behavior and mechanism of methyl blue on zinc oxide nanoparticles. *Journal of Nanoparticle Research*, 15(11), pp.1-10.

Zhang, G., Zhang, Q., Sun, K., Liu, X., Zheng, W. and Zhao, Y., 2011. Sorption of simazine to corn straw biochars prepared at different pyrolytic temperatures. *Environmental Pollution*, 159(10), pp.2594-2601.

Zhang, Z., Xin, X., Yan, Q., Li, Q., Yang, Y. and Ren, T.L., 2016. Two-step heating synthesis of sub-3 millimeter-sized orthorhombic black phosphorus single crystal by chemical vapor transport reaction method. *Science China Materials*, 59(2), pp.122-134.

Zhou, Q., Xiao, J., Wang, W., Liu, G., Shi, Q. and Wang, J., 2006. Determination of atrazine and simazine in environmental water samples using multiwalled carbon nanotubes as the adsorbents for preconcentration prior to high performance liquid chromatography with diode array detector. *Talanta*, 68(4), pp.1309-1315.

Zhuo, Y., Lemaigen, L., Chatzakis, I.N., Reed, G.P., Dugwell, D.R. and Kandiyoti, R., 2000.

An attempt to correlate conversions in pyrolysis and gasification with FT-IR spectra of coals. *Energy & Fuels*, 14(5), pp.1049-1058.



University of Fort Hare
Together in Excellence

Chapter Four

Zinc oxide nanoparticles functionalized with chelating nitrogenous groups for the adsorption of methyl violet in aqueous solutions

Abstract

In this study, a potent material for adsorption of methyl violet (one of the hazardous organic pollutants) in water was developed. This material was synthesized from silica coated zinc oxide nanoparticles. The material was obtained after functionalization of silica coated zinc oxide nanoparticles with pyrene ligand. Fourier transform infrared spectrometer (FTIR), energy dispersive x-ray spectrometer (EDX), scanning electron microscope (SEM), X-ray diffractometer (XRD) and thermogravimetric analyser (TGA) were used for characterization of the synthesized materials. Moreover, the ligand was initially characterized with ^1H NMR and ^{13}C NMR. The results showed Zn-O stretch in the characteristic region of 500 and 450 cm^{-1} in all the synthesized nanoparticles with additional organic stretches due to functionalization. In addition, 62.4% particle size decrease and about 100°C thermal stability increase were revealed by TEM and TGA analysis respectively as a result of functionalization. The potent adsorbent showed high efficiency for the removal of methyl violet (MV) in all batch adsorption experiments and a reasonable adsorption maximum capacity (q_{max}) (31.5 mg/g) in comparison with other MV adsorbents was achieved. The highest adsorption efficiency of 87.7 % was attained with adsorbent dose approximately = 40 mg, MV concentration = 14.6 mg/L, contact time = 360 min and temperature = $20 \pm 2^\circ\text{C}$ whereas the highest adsorption capacity was found to be with (adsorbent dose approximately = 40 mg, adsorbate concentration = 25.9 mg/L, pH = 6.5 and temperature = $20 \pm 2^\circ\text{C}$). Kinetic and isotherm studies indicated that the process for the removal of this pollutant with the new material proceeded via pseudo-first order and Langmuir isotherm models respectively. These results indicated that this material could serve as alternate adsorbent to the already established materials for the removal of recalcitrant organic pollutants from aqueous solutions.

Keywords: Adsorption, isotherm, zinc oxide, methyl violet, desorption, reusability.



University of Fort Hare
Together in Excellence

4.1. Introduction

Dyes as constituents of wastewater from industries such as plastic, food processing, leather, pharmaceutical, dye manufacturing and textile are the major pollutants in surface water. Usually dyes are synthesized and have complex structures, their complex structures are what makes them photo and oxidation stable as well as biodegradable resistant (Ofomaja and Ho, 2008; Aksu, 2005). Therefore, their occurrence interferes with sunlight transmission and disturb the biological processes resulting in harm to aquatic communities in the ecosystem (Hameed and Ahmad, 2009; Royer *et al.*, 2009). Through direct exposure or through food chain, these pollutants negatively affect the human health. Therefore, to meet the environmental regulations, industries using dye substances should reduce their levels in effluents prior to their discharge into the environment (Liu *et al.*, 2011). Their mutagenic and carcinogenic properties have made dyes to be associated with negative human health effects including kidney dysfunction, reproductive complications, central nervous system, liver and brain damages (Ajji and Ali, 2007; Kadirvelu *et al.*, 2003). Methyl violet is a basic/cationic dye, which possess harmful effects on living organism even in short period exposure (Chen *et al.*, 2010). MV is highly recalcitrant to biological oxidation, conventional physical treatments, and resistant to biodegradation owing to its complex aromatic structure (Figure 4.1).

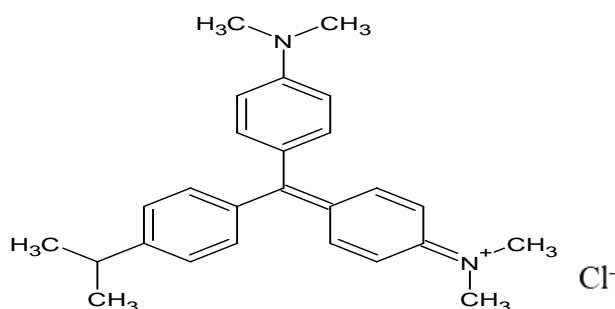
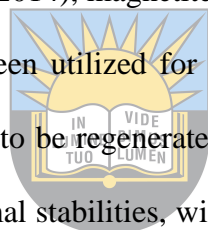


Figure 4.1: Chemical structure of methyl violet.

Because of the aforementioned negative effects of this dye, various chemical, biological and physical techniques have been reported and applied for their removal. These techniques include

electrocoagulation (Mbacké *et al.*, 2016; Ghosh *et al.*, 2008; Durango-Usuga *et al.*, 2010; Vidya Vijay *et al.*, 2019; Moneer *et al.*, 2018), photocatalytic degradation (Jiang *et al.*, 2015; Ameen *et al.*, 2013; Rashad *et al.*, 2019; Sathiyavimal *et al.*, 2020; Abdelrahman *et al.*, 2019), advanced oxidation (Jana *et al.*, 2010; Jiani *et al.*, 2020; Abdi *et al.*, 2020) and adsorption (Liu *et al.*, 2011; Aji and Ali, 2007; Chen *et al.*, 2010; Şolpan and Kölge, 2006; Azizian *et al.*, 2009; Cengiz and Cavas, 2010; Xu *et al.*, 2011; Mittal *et al.*, 2016; Musyoka *et al.*, 2014; Mahini *et al.*, 2018; Maity and Ray, 2014). Among these techniques, adsorption is an innovative and economical reasonable alternative technique due to its ease of operation and high removal performance (Dotto *et al.*, 2016; Hayati *et al.*, 2017).

Also, it is worthy of mention that numerous materials such as activated charcoal (Iqbal and Ashiq, 2007), montmorillonite (Aladağ *et al.*, 2014), magnetite (Bonetto *et al.*, 2015), titanium dioxide (Jafari *et al.*, 2011) and more have been utilized for the removal of methyl violet but these materials are limited by their inability to be regenerated, high production cost and so on. ZnO NPs have excellent chemical and thermal stabilities, wide band gap and high excitation binding energy at room temperature (Özgür *et al.*, 2005). This imply that ZnO NPs can adsorb other chemical species without any chemical bonding at room temperature. However, Zabihi *et al.* (2011) stated that their high surface energy might result in agglomeration of particles, as it is the case in other nanoparticle when dispersed in organic solvents and matrices. Functionalization of ZnO NPs will prevent this negative effect and maintain other desired properties such as large surface area and chelating capabilities. Therefore, this study aims to synthesize a highly efficient material for methyl violet removal from wastewater. This material will be obtained from the functionalization of zinc oxide nanoparticles with pyrene ligand. To the best of our knowledge, no report on the functionalization of zinc oxide nanoparticles with pyrene nitrogen chelating groups for the removal of methyl violet from aqueous solution has been published. It is believed that the functionalization of the zinc nanoparticles will improve its adsorption efficiency and capacity as the used ligand will provide an additional shell from which other functionalities may



University of Fort Hare
Together in Excellence

be attached. It is also believed that functionalization will improve zinc oxide nanoparticles physical properties such as thermal stability, which will permit their use even at higher temperatures. Also, the kinetics and isotherm studies of the adsorption process was evaluated through batch adsorption process involving effect of varying contact time, pH and adsorbate concentration.

4.2. Methodology

4.2.1. Materials and reagents

Tetraethylorthosilicate (purity $\geq 98\%$), 4-dimethylaminopyridine (purity $\geq 98\%$) and 99% solution of 3-aminopropyltriethoxysilane were purchased from Sigma-Aldrich, China. However, 4-hydroxybenzaldehyde (purity $\geq 98\%$) was also bought from Sigma-Aldrich, United Kingdom together with 1-pyrenecarboxyaldehyde (purity $\geq 99\%$). Absolute ethanol and 32% solution hydrochloric acid were bought from Merck Chemicals, Gauteng, South Africa. Dicyclohexylcarbodiimide and succinic anhydride of purities of 98% and above were purchased from Merck Chemicals, Germany, whereas, sodium chloride and sodium hydroxide of purities of 98% and above were bought from Associated Chemical Enterprises, South Africa. Hydrazine hydrate (purity $\geq 99\%$) was also purchased from Sigma-Aldrich, China, while methyl violet dye was purchased from Saarchem pty Ltd, South Africa. These materials and reagents were used as received from the suppliers.

4.2.2. Syntheses of materials

4.2.2.1. Silica coated zinc oxide nanoparticles (ZnO-Si NPs)

In order to obtain ZnO-Si NPs, zinc oxide nanoparticles (ZnO NPs) were coated with silica. This was accomplished by adding 30 mL of tetraorthosilicate (TEOS) to ZnO NPs previously dispersed in 50 mL of absolute ethanol and refluxed for 6 hrs at 60°C under constant stirring following a method by Ojemaye *et al.* (2017) (Figure 4.2). The resultant solution was separated by centrifugation, washed and dried in oven over night.

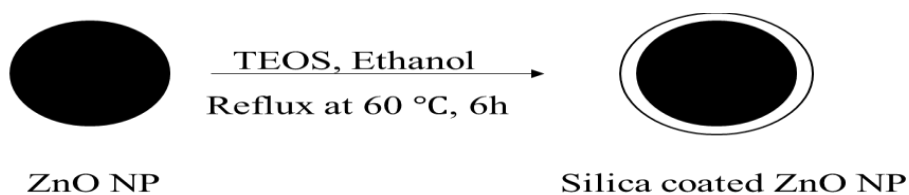


Figure 4.2: Preparation of silica coated ZnO NPs.

4.2.2.2. 1-(4-hydroxyphenyl)-4-pyrenyl-2,3-diazabutadiene (Pyrene) synthesis

1-(4-hydroxyphenyl)-4-pyrenyl-2,3-diazobutadiene was synthesized following Wang *et al.* (2010) procedure with slight modification. 50 mL hydrazine hydrate solution was added drop wise into 150 mL absolute ethanol solution with 0.154 mol of 4-hydroxybenzaldehyde and 0.0408 mol of 1-pyrenecarboxyaldehyde as constituents and then refluxed for 10 hrs at 55°C (Figure 4.3). The suspension was washed and filtered to yield 1-(4-hydroxyphenyl)-4-pyrenyl-2,3-diaza-1,3-butadiene. IR (ATR, cm^{-1}) 1550, 2620, 2920, 3050, 3360 (Figure 4.7); ^1H NMR (DMSO, Bruker TopSpin) δ (ppm): 1.06, 2.50, 4.40, 7.84, 7.86, 8.05, 8.07, 8.09, 8.14, 8.16, 8.20, 8.22, 8.25, 8.28, 8.30, 8.32, 8.35 (Figure A-I.1); ^{13}C NMR (DMSO, Bruker TopSpin) δ (ppm): 39.31, 39.52, 39.73, 125.94, 126.20, 128.84, 130.15, 130.58, 159.43, 160.33, 160.41, 160.73, 161.82, 163.38 (Figure A-I.2). Proton NMR signals' assignment (^1H NMR (DMSO, TopSpin)), δ (ppm): 7.16 (2H, d), 8.14 (2H, d), 8.20 (1H, d), 8.22–8.26 (4H, m), 8.29 (1H, t), 8.37 (1H, d), 8.41(1H, d), 8.69 (1H, s), 8.72 (1H, d), 8.76 (1H, s).

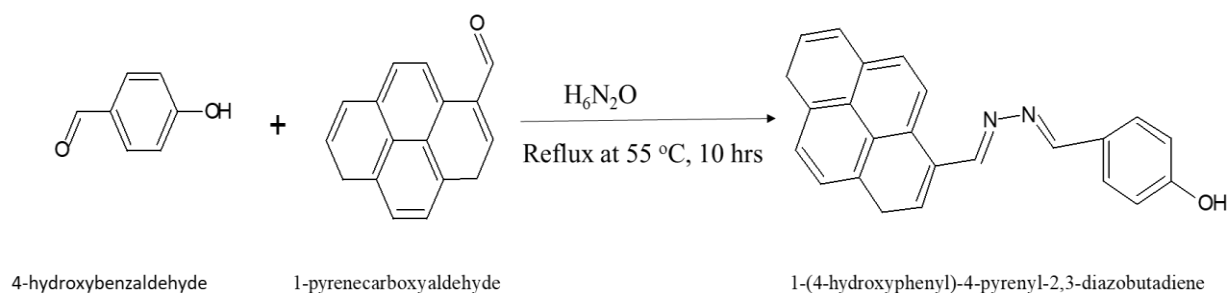


Figure 4.3: Synthesis of 1-(4-hydroxyphenyl)-4-pyrenyl-2,3-diaza-1,3-butadiene.

4.2.2.3. Pyrene grafted onto zinc oxide nanoparticles (ZnO-Pyrene NPs) synthesis

9.726 g of dried ZnO-Si NPs were first converted to amine modified ZnO NPs (ZnO-NH₂ NPs) by adding 30 mL of 3-aminopropyltriethoxysilane (APTES) to their 50 mL solution of absolute ethanol and refluxed for 5 hrs at 60°C as reported by Ojemaye *et al.* (2018) (Figure 4.4).

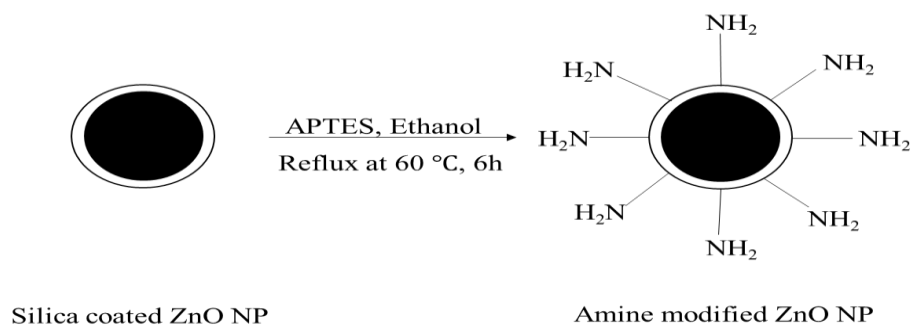


Figure 4.4: Preparation of amine modified ZnO NPs.

Dry ZnO-NH₂ NPs (9.60 g) were then converted to carboxylic functionalized zinc oxide nanoparticles (ZnO-COOH NPs) by adding previously dispersed ZnO-NH₂ NPs (8.601 g) in dry dimethylformamide (DMF) into a stirring solution of succinic anhydride (0.0563 mol) in dry DMF. The reaction mixture was allowed to further stir for 48 hrs as shown in (Figure 4.5) before centrifugation. Washing was done using ethanol and the product was allowed to dry in an oven at 70°C to obtain carboxylic functionalized zinc oxide nanoparticles (ZnO-COOH NPs).

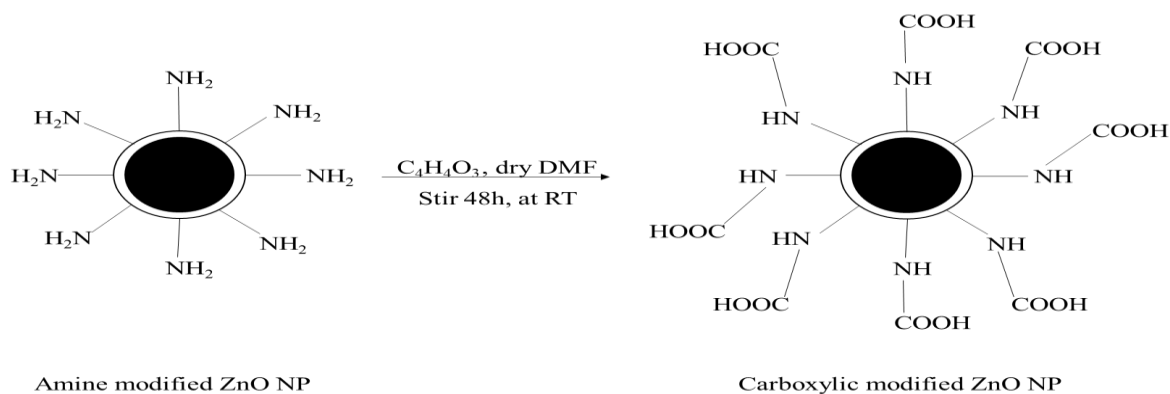


Figure 4.5: Preparation of carboxylic modified ZnO NPs.

ZnO-COOH NPs (8.012 g) in 25 mL of dry DMF was activated with 0.0194 mol of dicyclohexylcarbodiimide (DCC) in 25 mL of dry DMF with continuous stirring in the dark for 24 hrs. Then the activated carboxylic acid functionalized ZnO NPs in 50 mL dry DMF was added slowly to the stirring solution of 8.024 g of pyrene ligand in ethanol in the presence of 0.017 mol of 4-dimethylaminopyridine (DMAP). The suspension was then further stirred for 24 hrs (Figure 4.6) and separated through centrifugation, washed severally with deionized water and allowed to dry at 75°C for 24 hrs in an oven. After that, pyrene grafted onto zinc oxide nanoparticles was obtained.

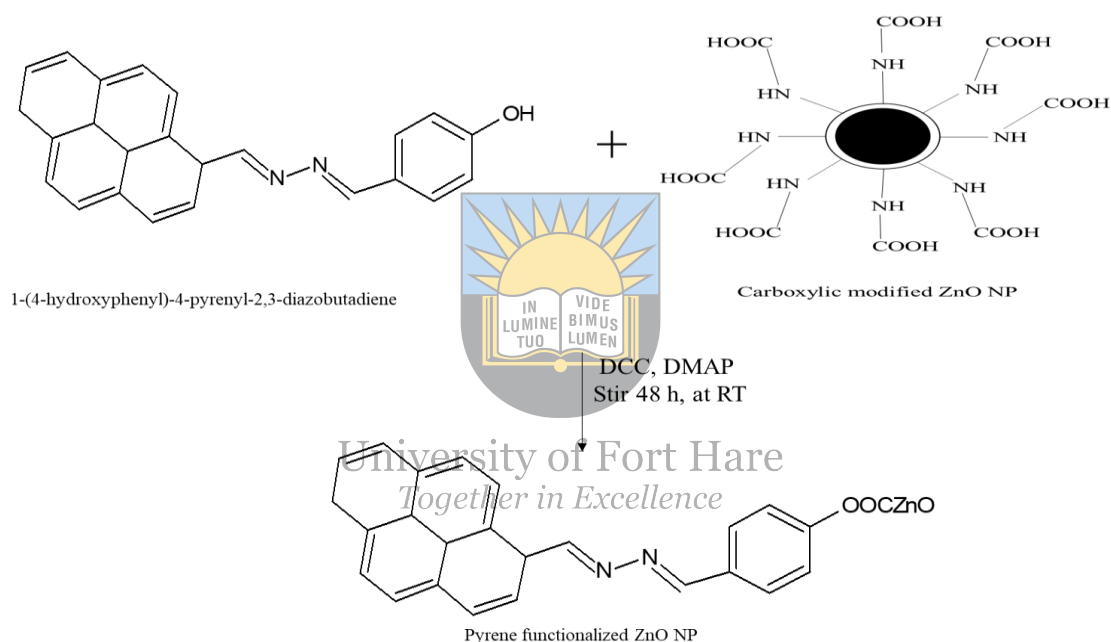


Figure 4.6: Preparation of pyrene grafted onto ZnO NPs.

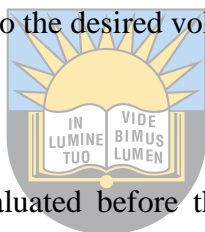
4.2.3. Characterization

Characterization of the materials was performed with X-ray diffractometer (XRD), scanning electron microscopy (SEM), energy dispersive x-ray (EDX), thermogravimetric analyser (TGA) and fourier-transform infrared spectroscopy (FTIR) and nuclear magnetic resonance spectroscopy (NMR). XRD (Bruker D8 Advanced XRD) was used to determine the crystal phase information of the materials. Surface morphologies and elemental/chemical composition were determined using SEM/EDX (JOEL JSM-6390 LVSEM). The percentage of organic compounds

present in the samples, purity and thermal resistances of the prepared samples were determined using TGA (Perkin Elmer TGA 4000 analyzer). FTIR (Perkin-Elmer Universal ATR) was used for functional group identification and confirmation of functionalization. Transmission electron microscope (JOEL 1210 transmission electron microscope) was used to determine particle size and to confirm particles geometry. Proton nuclear magnetic resonance (^1H NMR) was used to determine hydrogen framework, whereas, carbon 13 nuclear magnetic resonance (^{13}C NMR) was used to determine carbon framework (DMSO, Bruker TopSpin NMR) of the ligand.

4.2.4. Adsorbate preparation

Stock solution (1000 mg/L) of methyl violet was prepared by dissolving 1.000 g into 1000 mL of distilled water. Working solutions were then prepared from the stock solution by taking specific volumes of stock solution and diluting to the desired volumes in separate volumetric flasks.



4.2.5. Surface charge determination

Surface charge determination was evaluated before the commencement of batch adsorption experiments via salt addition method (Katarina and Garg, 2017). This was done using 2 mg of the adsorbent in eight 20 mL solutions of 0.1 M NaCl with different initial pH values (pH_i) between 2 and 9. The adjustment of pH was done using 0.1 N HCl or 0.1N NaOH as the case may be. The glass bottle containing the different solutions were shaken for 6 hr at room temperature using an orbital shaker at a speed of 150 rpm. Thereafter, final pH values (pH_f) were determined by means of a pH meter.

4.2.6. Adsorption studies

The removal of methyl violet was done using batch adsorption experiments as reported by ul Haq *et al.* (2020) by varying pH, temperature, adsorbate concentration, contact time and adsorbent dose. Adsorption was performed in 100 mL glass bottles with screw caps and the agitation was done with an orbital shaker at 150 rotations per minute. Initial and final

concentrations of the dye was measured with Ultra Violet-Visible light spectrophotometer (UV-Vis) at $\lambda_{\max} = 585$ nm. Each of the aforementioned parameters was evaluated by keeping all the others fixed. For pH adjustments, 0.1 M HCl and NaOH solutions were used as appropriate. The pH effect was investigated between pH 2 and 10. The contact time effect was studied between 0 and 360 minutes. The effect of adsorbent dose and adsorbate amount were evaluated at four different concentrations (i.e. 10.4, 19.8, 40.6 and 80.2 mg, and, 7.25, 21.2, 40.2 and 54.2 mg/L respectively). The adsorption efficiency (% adsorbed) and adsorption capacity (q_e) were calculated by using equations 4.1 and 4.2 respectively:

$$\text{Adsorption efficiency (\% adsorbed)} = \left(\frac{c_i - c_{eq}}{c_i} \right) \times 100 \quad (4.1)$$

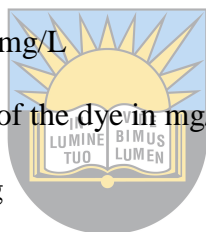
$$\text{Adsorption capacity } (q_e) = \frac{(c_i - c_{eq})V}{m} \quad (4.2)$$

Where, c_i = initial BG concentration in mg/L

c_{eq} = equilibrium concentration of the dye in mg/L

q_e = adsorption capacity in mg/g

m = mass of the adsorbent (g) and, V = volume of the adsorbate solution used (L).



University of Port Harcourt
Together in Excellence

4.2.7. Desorption and reusability studies

For reusability studies, three runs of adsorption were considered for a run period of 6 h successively without desorption. After, each run separation was done by means of centrifugation. This was done to check the reusability of the adsorbent for cost effectiveness. However, in the desorption studies after each run of adsorption the loaded adsorbent was separated by centrifugation, dried in an oven at 70°C and dispersed in three 0.1 N HNO₃ solutions and stirred for the equivalent period as in adsorption. At the end of reusability/desorption experiments concentration was measured at $\lambda_{\max} = 585$ nm using UV/Visible spectrophotometer. Desorption efficiency (% desorbed) was calculated using equation 4.3:

$$\text{Desorption efficiency (\% desorbed)} = \left(\frac{c_d}{c_a} \right) \times 100 \quad (4.3)$$

Where C_d = dye concentration desorbed and C_a = dye concentration adsorbed both in mg/dm^3 .

4.2.8. Data analysis

The data obtained from this study was statistically analysed and plotted using OriginPro 2021b.

4.3. Results and discussion

4.3.1. Characterization

4.3.1.1. Functional group identification

The FTIR analysis was carried to obtain vibrational spectra of the materials and to verify if functionalization occurred or not. The obtained spectra of the ZnO-Si, ZnO-NH₂, ZnO-COOH and ZnO-Pyrene synthesized nanoparticles clearly showed the Zn-O stretch between 500 and 450 cm^{-1} (Figure 4.7); (Gnanasangeetha and Saralathambavani, 2013; Winiarski *et al.*, 2018). The stretch between 800 and 700 cm^{-1} in the ZnO-Si and ZnO-NH₂ spectra could be a result of hydrogen atoms motion parallel to the connection line of the two nearest metal ions (Lutz *et al.*, 1998). Between 1400 and 1300 cm^{-1} , alcohol O-H bending was also observed in these spectra, which might have resulted from atmospheric moisture (Ahmed *et al.*, 2020). In addition, Si-O stretch at 988 cm^{-1} was also noticed in both spectra and Zn-N stretch between 450 and 400 cm^{-1} in ZnO-NH₂ spectrum which appeared to interfere with the Zn-O stretch hence the peak is more pronounced (El-Nahhal *et al.*, 2016; Hu *et al.*, 2011).

The C-N non-aromatic amine bending was also observed between 1100 and 1200 cm^{-1} in ZnO-NH₂ spectrum (Nasrollahi *et al.*, 2018). Same observations were noticed in ZnO-COOH spectrum with the appearance of two stretches (i.e C-O stretch, between 1400 and 1300 cm^{-1} and C=O stretch, between 1700 and 1500 cm^{-1}), which arose from the introduction of carboxyl group (Wang *et al.*, 2011). In the ZnO-Pyrene spectrum, -OH alcohol appeared at 3360 cm^{-1} , this might have emerged from pyrene ligand. The strong peaks between 1700 and 1300 cm^{-1} attributed to carboxyl group of ester (Wang *et al.*, 2011) resulted from the functionalization with pyrene ligand. Weak peak between 3100 and 3000 cm^{-1} corresponds to C-H aromatic stretch followed

by two C-H stretches of alkane between 2990 and 2850 cm^{-1} . These peaks were conspicuously missing from the peaks of silica coated zinc oxide nanoparticles. From these observations, it can be deduced that silica coated zinc oxide nanoparticles were successfully synthesized and functionalised with pyrene ligand.

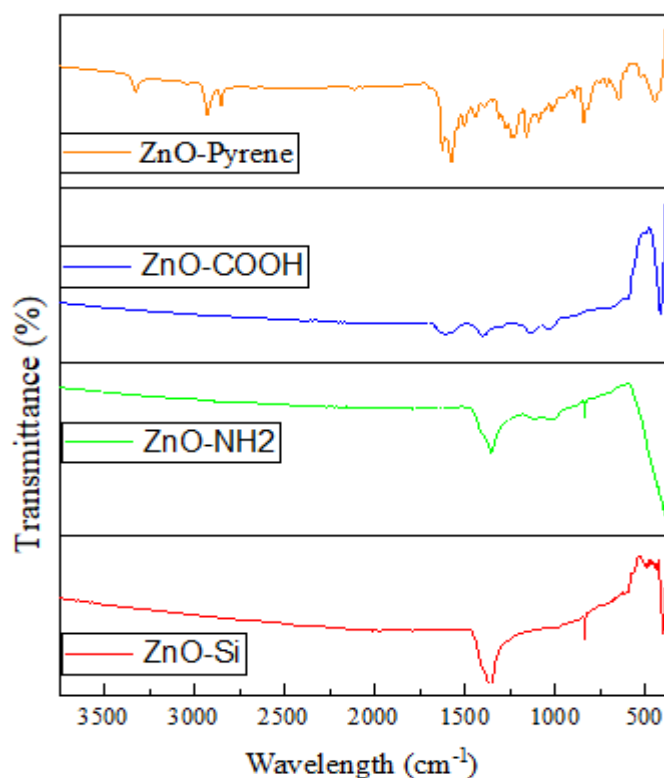


Figure 4.7: FTIR spectra of ZnO-Si, ZnO-NH₂, ZnO-COOH and ZnO-Pyrene.

4.3.1.2. Morphology and composition of synthesized materials

SEM analysis was performed to determine the morphology of the materials as this plays a crucial role in adsorption. In the analysis, which was carried out at the same magnification, crystalline morphology was observed for ZnO-Si NPs (Figure 4.8 (a)). A similar morphology was also determined for the uncoated ZnO nanoparticles in chapter three. The morphology was retained from (Figure 4.8 (b) – (d)) for ZnO-NH₂, ZnO-COOH and ZnO-Pyrene NPs respectively, this is an indication that the core properties were maintained after successive surface modifications. The geometry determination was inconclusive with the SEM analysis due to low resolution, which

might have been due to particles aggregation. Thus, TEM analysis was considered for geometry determination. The elemental composition was determined using EDX in order to ascertain the purity of the synthesized materials and to verify if the syntheses of the materials were successful. In the analysis, clear peaks corresponding to Zn were observed in three intervals, 0.8 - 1.2 keV, 8.4 - 8.8 keV, and 9.4 - 9.8 keV respectively (Figure 4.9 (a) - (d)).

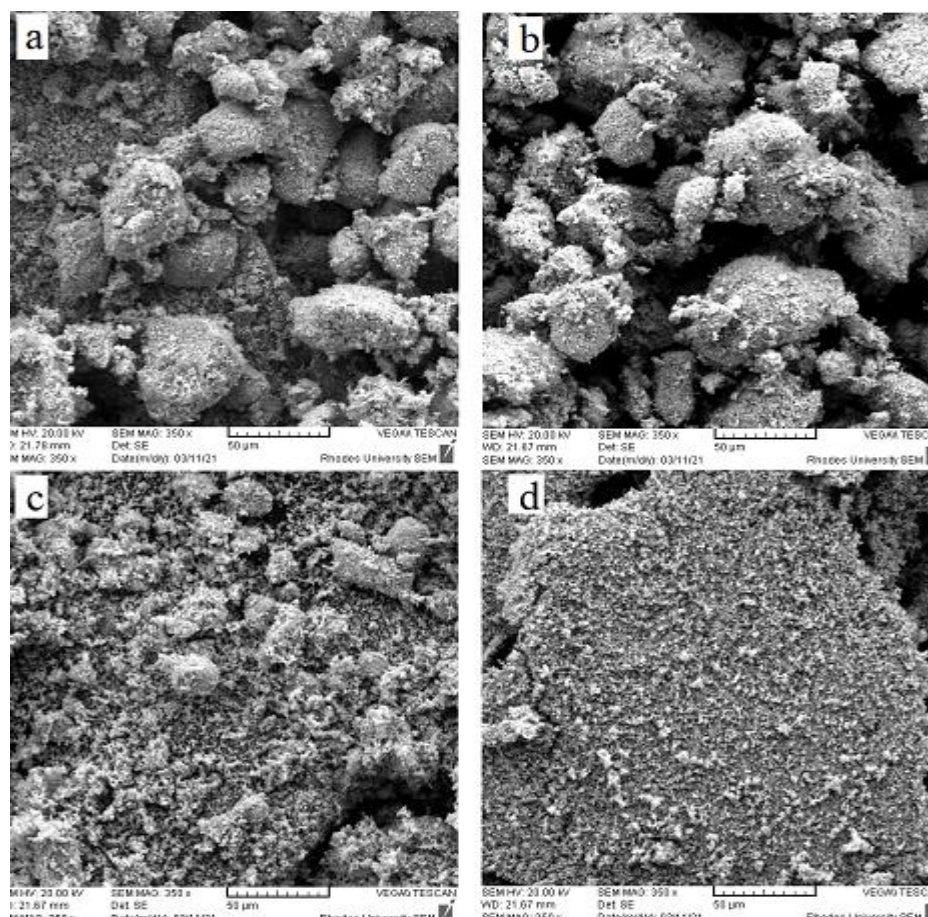


Figure 4.8: SEM images of (a) ZnO-Si, (b) ZnO-NH₂, (c) ZnO-COOH and (d) ZnO-Pyrene NPs.

A peak corresponding to O was also observed between 0.4 and 0.6 keV in the nanoparticles (NPs) spectra. All synthesized NPs spectra showed peaks corresponding to Zn and O, in similar regions as reported in a work reported by Alam *et al.* (2012) with an additional peak corresponding to Si between 1.6 and 1.8 keV in Figure 4.9 (a) (Ramasamy *et al.*, 2014). After functionalization with amine, Si peak disappeared due to its low proportion compared to other elements and an additional peak of N was noted in Figure 4.9 (b) between 0.2 and 0.4 keV for ZnO-NH₂. The

same observations were also noticed for N in Figure 4.9 (c) and an addition of C was noted between 0.2 and 0.4 keV for ZnO-COOH. In Figure 4.9 (d), an additional peak of nitrogen and carbon which originated from the introduced pyrene ligand was obtained between 0.2 and 0.6 keV and 0.2 and 0.4 keV respectively for ZnO-Pyrene NPs were noticed. From the EDX spectra, it can be deduced that the samples were of high purity as no foreign or unwanted elements appeared. The high ratios of Zn and O atoms imply that the substrate material was ZnO. Followed by coating and functionalization. Also, the addition of specifically the atoms that form the introduced functional groups mean that only the functional groups were taken from their sources to the substrate material. For purity confirmation, further analysis was done with TGA.

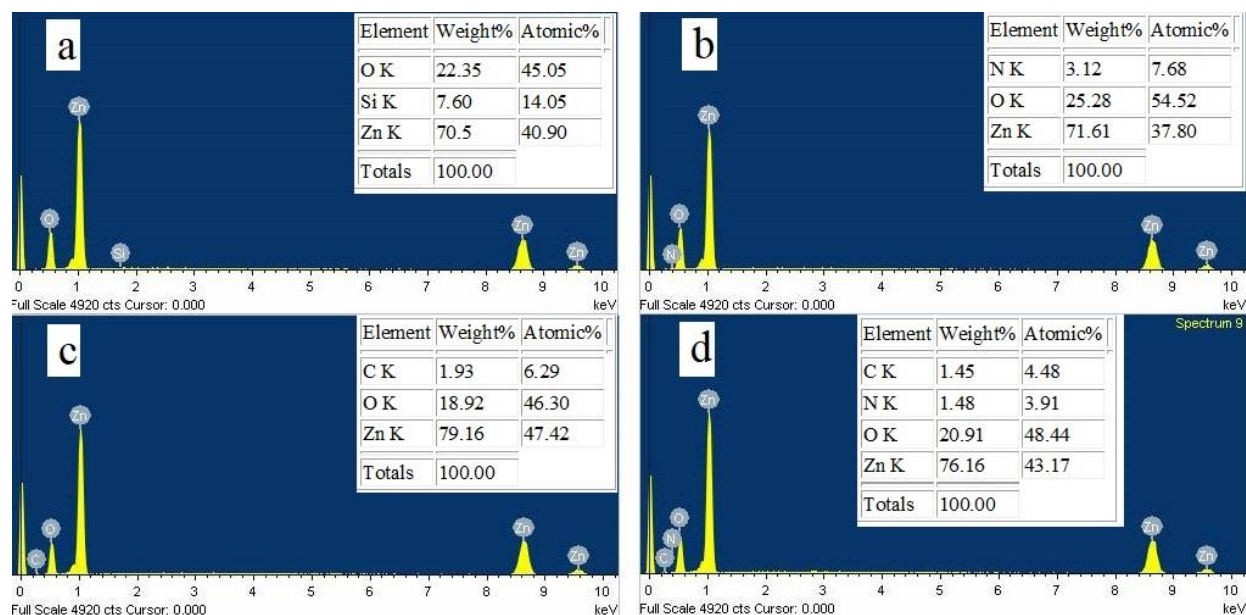


Figure 4.9: EDX spectra of (a) ZnO-Si, (b) ZnO-NH₃, (c) ZnO-COOH and (d) ZnO-Pyrene NPs.

4.3.1.3. Particle size determination and shape confirmation

Figure 4.10 shows the TEM images of (a) ZnO-Si (b) ZnO-NH₂ (c) ZnO-COOH and (d) ZnO-Pyrene NPs at same magnification and also their particle size distributions. It can be noticed from all four TEM images that a spherical shape was observed and maintained similarly to the crystallinity observed in the SEM analysis. It can also be deduced that the particle size was decreasing as functionalization proceeded (Figure 4.10). The particle size decreased from 276 to

181 nm on average (Figure 4.10). This observation was due to decreased particles aggregation because of functionalization due to electron-electron repulsion brought by the ligand in the novel adsorbent.

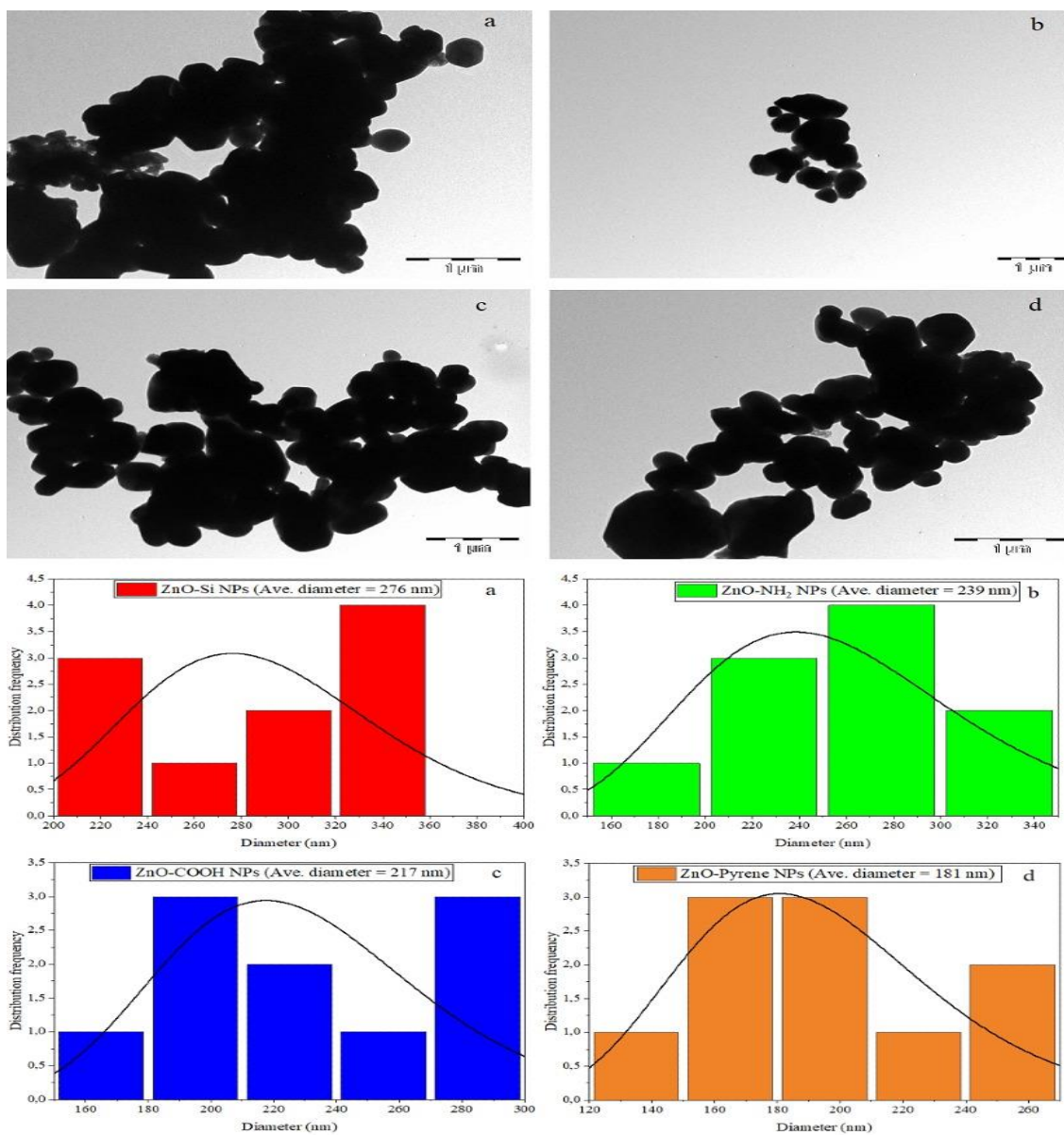


Figure 4.10: TEM images of (a) ZnO-Si, (b) ZnO-NH₂, (c) ZnO-COOH and ZnO-Pyrene nanoparticles and their particle distributions.

4.3.1.4. Crystal information determination

In order to determine the crystal and phase information of the synthesized materials, XRD analysis was carried out. In the XRD diffractogram of ZnO-Si NPs nine reflections were observed

at 31.8 °, 34.5 °, 36.3 °, 47.6 °, 56.6 °, 62.9 °, 66.5 °, 68.0 ° and 69.2 ° (Figure 4.11). These XRD reflections were assigned to the following miller indices respectively, (100), (002), (101), (102), (110), (103), (200), (112) and (201). These results were similar to the results of Mohan and Renjanadevi (2016). The reflections were maintained from ZnO-Si up to the novel material (ZnO-Pyrene NPs) meaning that the core structure was maintained throughout. In addition, the diffractogram of ZnO-Pyrene showed amorphous nature of the ligand used for grafting ZnO NPs as the roughness of the diffractogram was observed.

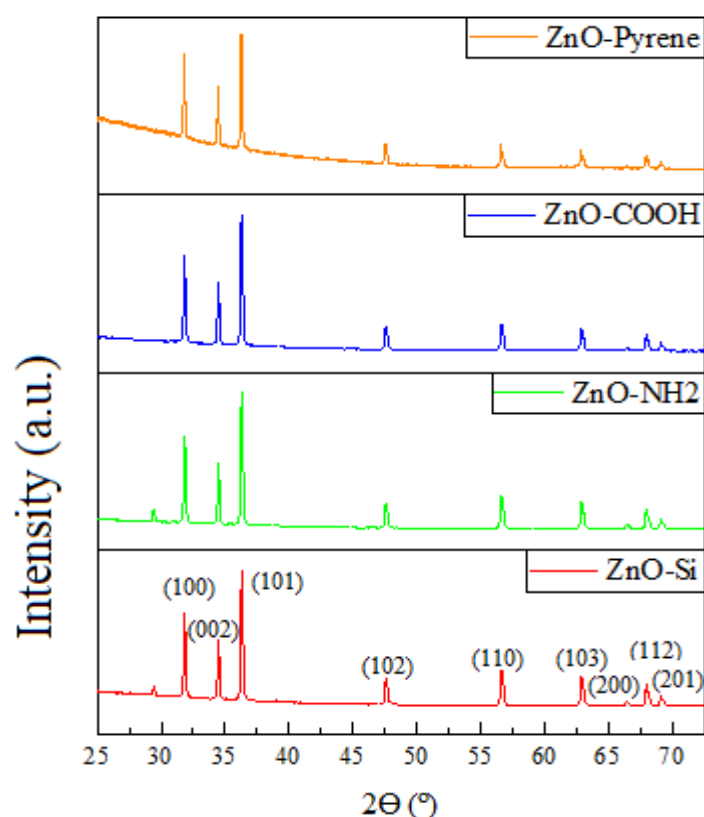


Figure 4.11: XRD spectra of ZnO-Si, ZnO-NH₂, ZnO-COOH and ZnO-Pyrene.

Moreover, this is another implication that functionalization was successful and that functionalization is a surface effect as there were no alterations in the core structure of the starting material.

4.3.1.5. Purity and thermal stability of the materials

TGA analysis was carried out to determine the percentage of organic compounds present in the samples, thermal stabilities and purities of the samples. Two weight losses were observed in ZnO-Si TGA curve, 2 wt% between 50 and 150°C, 55 wt% between 350 and 800°C (Figure 4.12 (a)). The first weight loss was due to loss of solvent and traces of water that might have been initial present and the second one attributes to the loss of the silica layer.

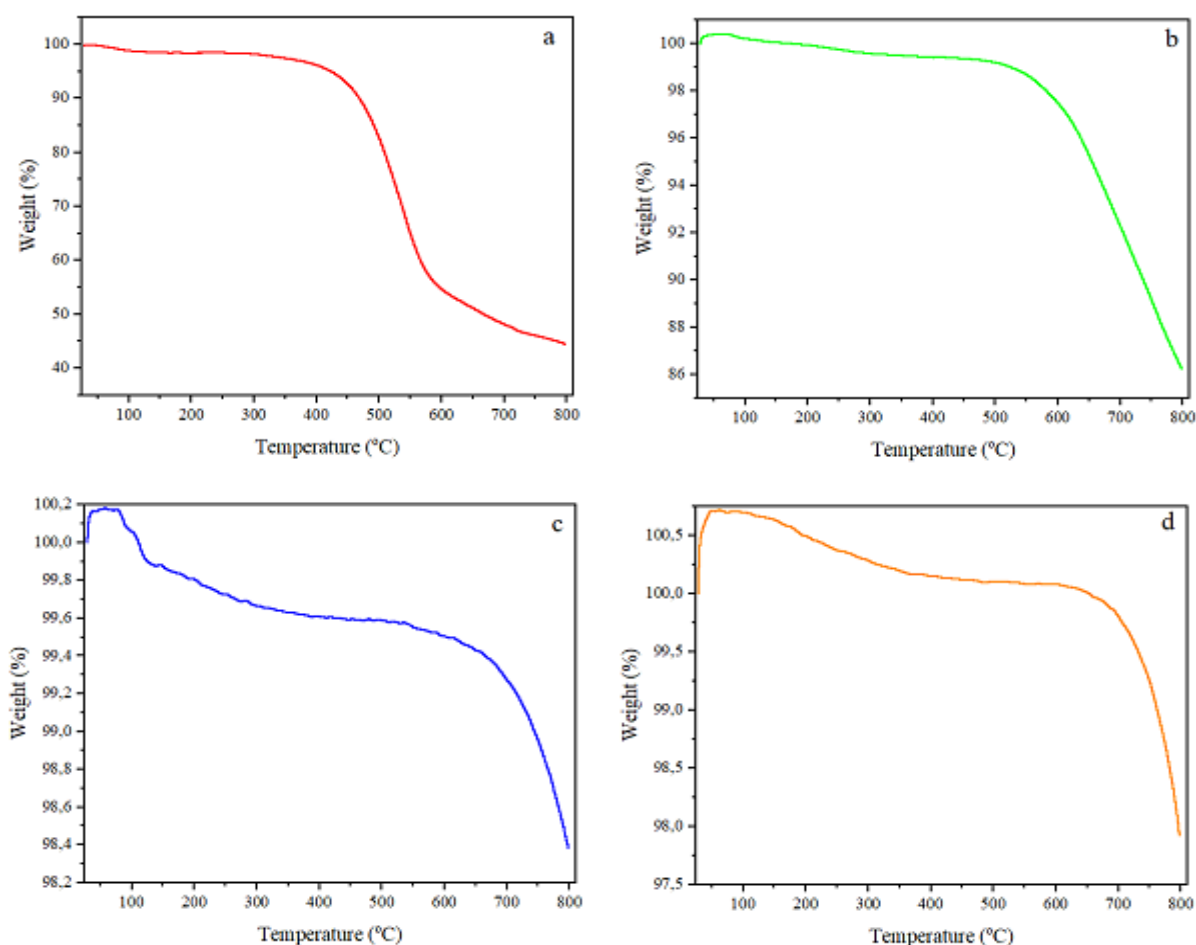


Figure 4.12: TGA curve of (a) ZnO-Si (b) ZnO-NH₂ (c) ZnO-COOH and (d) ZnO-Pyrene NPs.

The loss of amine functionality occurred with the loss of water due to the high solubility of NH₃ gas in water in ZnO-NH₂ TGA curve (Figure 4.12 (b)). The latter occurred between 100 – 300°C, followed by the thermal decomposition of silica layer. The 0.1 wt% weight loss in ZnO-COOH TGA curve between 80 and 125°C attributed to the loss of hydrocarbons (including the carboxylic

functionality) and water traces that were initially present (Figure 4.12 (c)). Weight loss between 125 and 550°C attributed to the loss from the remaining water traces and silica layer. The last weight loss in ZnO-COOH TGA curve between 550 and 800°C can be attributed to thermal decomposition $Zn(OH)_x$, which might have evolved from the initial presence of water. In ZnO-Pyrene TGA curve, the weight loss (2.22 wt%) between 625 and 800°C was a result of the additional shells resulted from coating and functionalization (Figure 4.12 (d)). The weight additions, which occurred initially from Figure 4.12 (b - d), were caused by atmospheric moisture.

4.3.2. Adsorption studies

4.3.2.1. pH effect

To evaluate the effect of the solution pH on adsorption, contact time, adsorbent dose and adsorbate concentration were kept constant. This was done in pH interval 2-10. In the experiment, it was noticed that adsorption was increasing with increasing pH (Figure 4.13) similar to the report of Xu *et al.* (2011). Lower adsorption at pH values below the pH_{pzc} was due to the electrostatic repulsions between MV molecules and ZnO-Pyrene since they both bare a positive charge at those pH values. The opposite was observed for pH values above the pH_{pzc} . From pH 2 to 4, the adsorption was increasing sharply, however, from pH 4 to 9 it was becoming constant and that was an indication of the optimum pH. On that note, 6.5 was adopted as the pH for subsequent adsorption experiment.

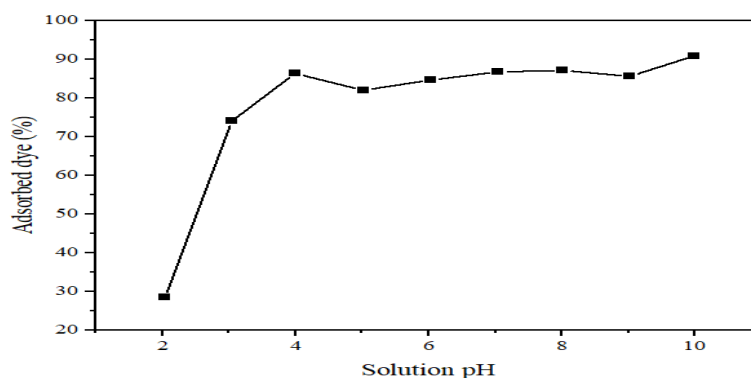


Figure 4.13: pH effect curve on MV adsorption (Dose approximately = 40 mg, MV concentration = 14.6 mg/L, contact time = 360 min and temperature = $20 \pm 2^\circ\text{C}$).

4.3.2.2. Effect of contact time

Although there were some fluctuations in the adsorption capacity when contact time was varied, overall, the adsorption was increasing with increase in contact time (Figure 4.14). This observation is similar to the result reported by Rahchamani *et al.* (2011). The increase in adsorption capacity was not sharp at low time intervals viz., (5, 15, 30, 60 and 105 min); this might have been due to low adsorbent dispersion in the solution in those contact time intervals.

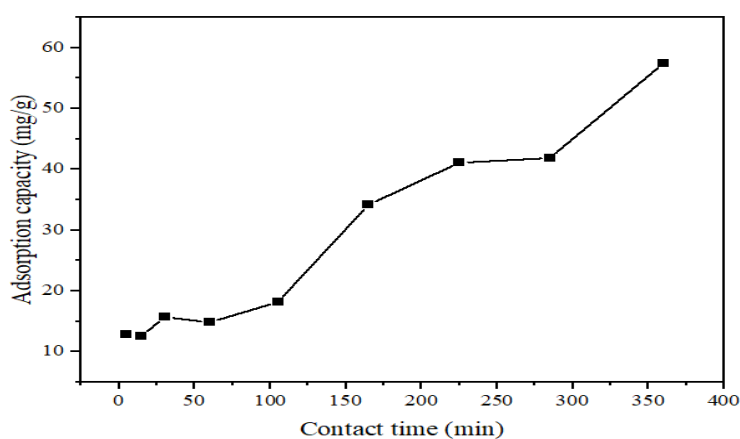


Figure 4.14: Contact time effect curve on MV adsorption capacity (dose approximately= 40 mg, concentration = 25.9 mg/L, pH = 6.5 and temperature = $20 \pm 2^\circ\text{C}$).

However, it was the opposite from 105 to 360 min. However, 360 min was adopted since it is the time at which maximum adsorption was observed.

4.3.2.3. Dose effect

In this experiment, the pH, adsorbate concentration, contact time and temperature were kept constant. It was observed that the adsorption of MV increased with an increase in adsorbent amount (Figure 4.15). Adsorption increased from 22.41 to 79.09 % with adsorbent dose from 5 to 40 mg respectively. The maximum adsorption was observed at 40.1 mg. This was due to the fact that the more the adsorbent dose the more the surface active sites available for the adsorption of MV from aqueous solution, thus higher adsorption efficiency was observed at higher adsorbent dose.

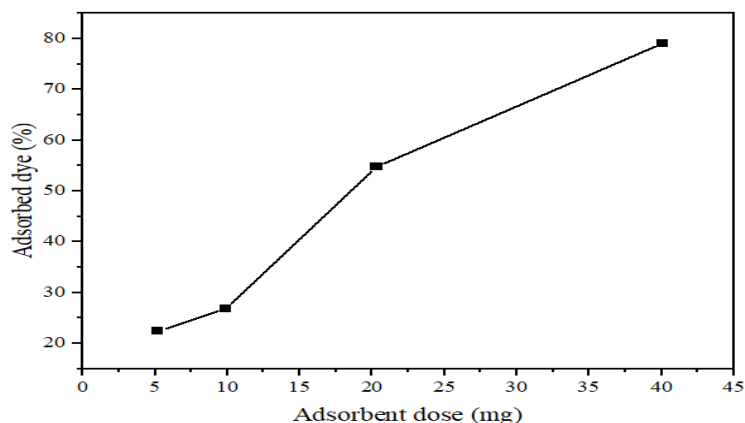


Figure 4.15: Adsorbent dose effect curve on MV adsorption (MV concentration = 30.0 mg/L, pH= 6.5, temperature = $20 \pm 2^\circ\text{C}$ and contact time = 360 min).

4.3.2.4. Effect of dye concentration

The initial concentration effect on the adsorption of MV by ZnO-Pyrene was studied at four different dye concentrations. During this experiment, other parameters were kept constant. Adsorption capacity increased from 15.1 to 50.7 mg/g until adsorption attained equilibrium (Figure 4.16). Chen *et al.* (2010) also reported similar observation on the effect of adsorbate concentration on zinc oxide nanoparticles. This behaviour may be as a result of fewer adsorbent-adsorbate collisions at lower dye concentrations hence q_e was low and vice versa for higher concentrations.

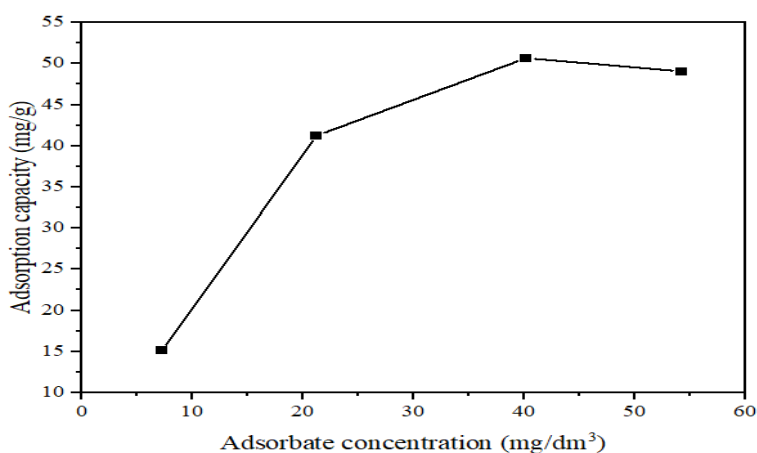


Figure 4.16: Adsorbate concentration effect on adsorption capacity of MV onto the adsorbent (contact time = 360 min, dose approximately = 40 mg temperature = $20 \pm 2^\circ\text{C}$ and pH = 6.5).

The insignificant difference between the last two concentrations in adsorption capacity means that the active sites of the adsorbent were used up or almost used up.

4.3.3. Kinetic studies

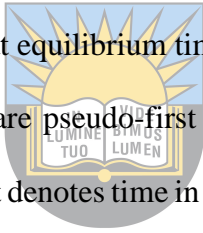
Three kinetics models were considered in the rate mechanism determination of the adsorption of methyl violet by ZnO-Pyrene viz., (pseudo-first order, pseudo-second order and intraparticle diffusion kinetic models). These models are expressed in equations (4.4), (4.5) and (4.6) respectively:

$$\ln(q_e - q_t) = \ln q_e - K_1 t \tag{4.4}$$

$$\frac{t}{q_t} = \frac{1}{K_2 q_e^2} + \frac{t}{q_e} \tag{4.5}$$

$$q_t = K_{id} t^{1/2} + C \tag{4.6}$$

Where, q_e denotes adsorption capacity at equilibrium time, q_t (mg/g) is the adsorption capacity at time t , K_1 (min^{-1}) and K_2 (g/mg.min) are pseudo-first order kinetic rate constant and pseudo-second order rate constant respectively, t denotes time in minutes, K_{id} is the intra-particle diffusion rate constant usually expressed in $\text{mg.g}^{-1}.\text{min}^{-0.5}$ and C is the thickness of boundary layer normally expressed in mg/g. All the values of the kinetic parameters are presented in Table 4.1 together with their R^2 values.



University of Fort Hare
Together in Excellence

Table 4.1: MV adsorption onto the novel adsorbent kinetic models' parameters.

Kinetic models	Parameters	Values of parameters
Pseudo-first order	K_1 (min^{-1})	-1.84×10^{-5}
	q_e (cal)	23.2
	R^2	0.931
Pseudo-second order	K_2 (g/mg.min)	1.06×10^{-10}
	q_e (cal)	3.24×10^4
	R^2	0.0473
Intraparticle diffusion	K_{id} ($\text{mg.g}^{-1}.\text{min}^{1/2}$)	0.0756
	C	1.43
	R^2	0.893
Experimental data	q_e (exp)	20.6

*The numerical values in this table are presented in three significant figures.

Since $C \neq 0$ it can be concluded that intraparticle diffusion model was unapplicable to explain the adsorption of MV by ZnO-Pyrene nanoparticles (Rahchamani *et al.*, 2011). The value of the

adsorption capacity for the adsorption of MV at equilibrium for the pseudo-first order was closer to experimental value. The fact that the R^2 value of the data when fitted to pseudo-first order was the closest to 1 implied that the data could be better described by pseudo-first order. This means that the adsorption was physisorption.

4.3.4. Adsorption isotherms

Four adsorbate concentrations in the intervals 7.25; 21.2; 40.2 and 54.2 mg/L were considered for removal of MV from aqueous solution by ZnO-Pyrene nanoparticles (Figure 4.16). The interaction between MV and ZnO-Pyrene molecules was explained using three adsorption isotherms. Langmuir adsorption isotherm, Freundlich adsorption isotherm and Temkin adsorption isotherm expressed as equations (4.7), (4.8) and (4.9) respectively:

$$\frac{1}{q_e} = \left(\frac{1}{K_L q_{max}} \right) \left(\frac{1}{c_e} \right) + \left(\frac{1}{q_{max}} \right) \quad (4.7)$$

$$\log q_e = \log K_F + \left(\frac{1}{n} \right) \log c_e \quad (4.8)$$

$$q_e = B \ln K_T + B \ln c_e \quad (4.9)$$

q_{max} (mg/g) is the maximum adsorption capacity, K_L (L/mg) is the Langmuir constant and q_e is the adsorption capacity in (mg/g), K_F (mg/g(L/mg)^{1/n}) denotes Freundlich constant and n is the heterogeneity factor, c_e is the dye concentration at equilibrium time, B (J mol⁻¹) is the Temkin constant which indicates the adsorption heat and K_T (L.g⁻¹) is equilibrium binding constant. Adsorption parameters were obtained using linear form of Langmuir adsorption isotherm from a graph of between $1/q_e$ versus $1/c_e$ (equation 4.7) for Langmuir adsorption isotherm. The linear plot of $\log q_e$ versus $\log c_e$ (equation 4.8) was used to determine the Freundlich isotherms parameter values. The values of Temkin parameters were determined from a graph of q_e versus $\ln c_e$ (equation 4.9). The correlation coefficients and isotherm parameter values of MV are listed in Table 4.2. For a favourable adsorption process, in the Freundlich isotherm the value of n should be between 1 and 10, which indeed was the case in this study. However, the R^2 was not closer to 1 in comparison with Temkin and Langmuir isotherms. Therefore, it was discarded. Even though

the Temkin's isotherm R^2 was better than that of Freundlich isotherm it was also discarded since it was far from 1 in comparison to Langmuir isotherm. Therefore, the interaction between MV molecules and ZnO-Pyrene nanoparticles can be best explained using Langmuir isotherm. Meaning that the adsorption was limited to a single layer. This result is similar to the data reported by Doğan and Alkan (2003). The material showed quite high maximum adsorption capacity in comparison to some other adsorbents previously reported in literature (Table 4.3), therefore it could be a considerable alternative for MV removal from aqueous solution.

Table 4.2: MV adsorption isotherms' parameters.

Adsorption isotherms	Parameters	Values
Langmuir isotherm	K_L (L/mg)	0.253
	q_{max} (mg/g)	31.5
	R^2	0.980
Freundlich isotherm	K_F (mg/g(L/mg) ^{1/n})	8.56
	n	2.89
	R^2	0.809
Temkin isotherm	K_T (L/mg)	1.19×10^3
	B	0.168
	R^2	0.864

*The numerical values in this table are presented in three significant figures.

Table 4.3: Comparison of adsorption capacities of various MV adsorbents from aqueous medium.

Adsorbent	Adsorbate	q_{max} (mg/g)	References
ZnO-NRs-AC	MV	81.6	(Dil <i>et al.</i> , 2017)
Bagasse fly ash	MV	26.3	(Mall <i>et al.</i> , 2006)
TiO ₂ (B)	MV	3.00	(Jafari <i>et al.</i> , 2012)
AgI/ TiO ₂ (B)	MV	4.12	(Jafari <i>et al.</i> , 2012)
Sepiolite	MV	10.2	(Özdemir <i>et al.</i> , 2006)
Mansonia sawdust	MV	16.1	(Ofomaja, 2008)
ZnO-Pyrene	MV	31.5	Current study

*The numeric values are presented in three significant values.

4.3.5. Desorption and reusability studies

From cycle 1 to 2, the efficiency was decreasing. However, from cycle 2 to 3 efficiency was increasing. Nevertheless, overall it was noticed that the adsorption efficiency was decreasing as the runs proceeded because there was no much difference between cycle 2 and 3 (Figure 4.17). This was due to the decreasing number of adsorptive sites as the cycle numbers were increasing. It was also noticed that desorption was increasing as number of cycles was increasing.

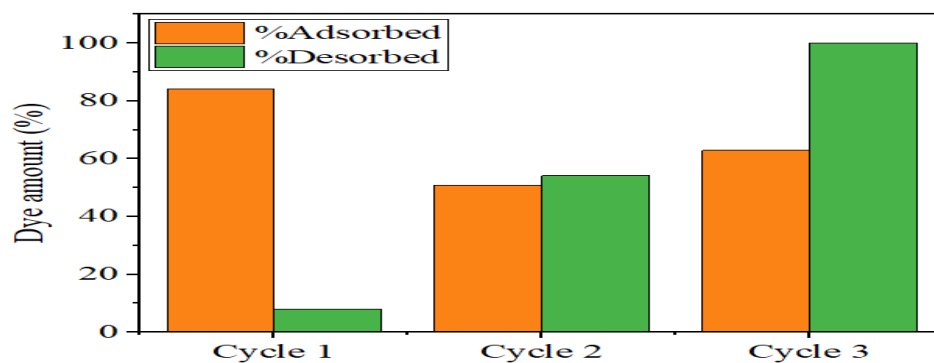


Figure 4.17: Adsorption and desorption of methyl violet.

This was due to the fact that there were more adsorbed dye molecules in the higher cycles thus making it easy to desorb.

4.4. Conclusion

Pyrene grafted onto ZnO NPs (ZnO-Pyrene) were synthesized successfully as proven by characterization results. The FTIR analysis proved that the functionalization was successful. These synthesized materials were of high purity as there were no unwanted elements in their EDX spectra. This was also proven by the TGA analysis, which showed high residuals at different temperature range. Through the functionalization process, the inner core properties such as shape were maintained and proof to that is the XRD result. The morphology and shape of the particles were crystalline and spherical as observed on the SEM and TEM analyses respectively. The particle size was reduced from 290 to 181 nm as a result of functionalization. The novel material showed high efficiency and capacity for the removal of MV compared to some known adsorbent reported in literature for MV removal and its potency was highly influenced by pH, adsorbent dose, contact time and adsorbate concentrations from batch adsorption experiments. These results are indication of the excellent adsorptive properties of ZnO-Pyrene for the removal of stubborn contaminants such as methyl violet from aqueous solution.

References

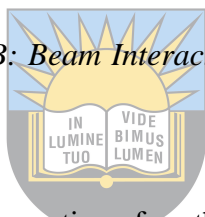
Abdelrahman, E.A., Hegazey, R.M., Kotp, Y.H. and Alharbi, A., 2019. Facile synthesis of Fe₂O₃ nanoparticles from Egyptian insecticide cans for efficient photocatalytic degradation of

methylene blue and crystal violet dyes. *Spectrochimica Acta Part A: Molecular and Biomolecular Spectroscopy*, 222, p.117195.

Abdi, M., Balagabri, M., Karimi, H., Hossini, H. and Rastegar, S.O., 2020. Degradation of crystal violet (CV) from aqueous solutions using ozone, peroxone, electroperoxone, and electrolysis processes: a comparison study. *Applied Water Science*, 10(7), pp.1-10.

Ahmed, D.S., Mohammed, M.R. and Mohammed, M.K., 2020. Synthesis of multi-walled carbon nanotubes decorated with ZnO/Ag nanoparticles by co-precipitation method. *Nanoscience & Nanotechnology-Asia*, 10(2), pp.127-133.

Ajji, Z. and Ali, A.M., 2007. Adsorption of methyl violet and brilliant blue onto poly (vinyl alcohol) membranes grafted with N-vinyl imidazole/acrylic acid. *Nuclear Instruments and Methods in Physics Research Section B: Beam Interactions with Materials and Atoms*, 265(1), pp.362-365.



Aksu, Z., 2005. Application of biosorption for the removal of organic pollutants: a review. *Process Biochemistry*, 40(3-4), pp.997-1026.

University of Fort Hare
Together in Excellence

Aladağ, E., Fil, B.A., Boncukcuoğlu, R., Sözüdoğru, O. and Yılmaz, A.E., 2014. Adsorption of methyl violet dye, a textile industry effluent onto montmorillonite—batch study. *Journal of Dispersion Science and Technology*, 35(12), pp.1737-1744.

Alam, S.N., Poloju, M., Sahu, S., Kumar, M. and Singh, A., 2012. SEM, EDX & XRD of zinc oxide nanostructures synthesized by zinc oxidation. *Microscopy and Analysis*, 26(4), pp.11-14.

Ameen, S., Akhtar, M.S., Nazim, M. and Shin, H.S., 2013. Rapid photocatalytic degradation of crystal violet dye over ZnO flower nanomaterials. *Materials Letters*, 96, pp.228-232.

Azizian, S., Haerifar, M. and Bashiri, H., 2009. Adsorption of methyl violet onto granular activated carbon: Equilibrium, kinetics and modeling. *Chemical Engineering Journal*, 146(1), pp.36-41.

Bonetto, L.R., Ferrarini, F., De Marco, C., Crespo, J.S., Guégan, R. and Giovanela, M., 2015. Removal of methyl violet 2B dye from aqueous solution using a magnetic composite as an adsorbent. *Journal of Water Process Engineering*, 6, pp.11-20.

Cengiz, S. and Cavas, L., 2010. A promising evaluation method for dead leaves of *Posidonia oceanica* (L.) in the adsorption of methyl violet. *Marine Biotechnology*, 12(6), pp.728-736.

Chen, S., Zhang, J., Zhang, C., Yue, Q., Li, Y. and Li, C., 2010. Equilibrium and kinetic studies of methyl orange and methyl violet adsorption on activated carbon derived from *Phragmites australis*. *Desalination*, 252(1-3), pp.149-156.

Dil, E.A., Ghaedi, M. and Asfaram, A., 2017. The performance of nanorods material as adsorbent for removal of azo dyes and heavy metal ions: application of ultrasound wave, optimization and modeling. *Ultrasonics Sonochemistry*, 34, pp.792-802.



University of Fort Hare
Together in Excellence

Doğan, M. and Alkan, M., 2003. Adsorption kinetics of methyl violet onto perlite. *Chemosphere*, 50(4), pp.517-528.

Dotto, G.L., Rodrigues, F.K., Tanabe, E.H., Fröhlich, R., Bertuol, D.A., Martins, T.R. and Foletto, E.L., 2016. Development of chitosan/bentonite hybrid composite to remove hazardous anionic and cationic dyes from colored effluents. *Journal of Environmental Chemical Engineering*, 4(3), pp.3230-3239.

Durango-Usuga, P., Guzmán-Duque, F., Mosteo, R., Vazquez, M.V., Peñuela, G. and Torres-Palma, R.A., 2010. Experimental design approach applied to the elimination of crystal violet in water by electrocoagulation with Fe or Al electrodes. *Journal of Hazardous Materials*, 179(1-3), pp.120-126.

El-Nahhal, I.M., Salem, J.K., Kuhn, S., Hammad, T., Hempelmann, R. and Al Bhaisi, S., 2016. Synthesis & characterization of silica coated and functionalized silica coated zinc oxide nanomaterials. *Powder Technology*, 287, pp.439-446.

Ghosh, D., Medhi, C.R., Solanki, H. and Purkait, M.K., 2008. Decolorization of crystal violet solution by electrocoagulation. *Journal of Environmental Protection Science*, 2(1), pp.25-35.

Gnanasangeetha, D. and SaralaThambavani, D., 2013. One pot synthesis of zinc oxide nanoparticles via chemical and green method. *Materials Science Research Journal*, 2320, pp.6055.

Hameed, B.H. and Ahmad, A.A., 2009. Batch adsorption of methylene blue from aqueous solution by garlic peel, an agricultural waste biomass. *Journal of Hazardous Materials*, 164(2-3), pp.870-875.



Hayati, B., Maleki, A., Najafi, F., Daraei, H., Gharibi, F. and McKay, G., 2017. Adsorption of Pb²⁺, Ni²⁺, Cu²⁺, Co²⁺ metal ions from aqueous solution by PPI/SiO₂ as new high performance adsorbent: Preparation, characterization, isotherm, kinetic, thermodynamic studies. *Journal of Molecular Liquids*, 237, pp.428-436.

Hu, Y., Kazemian, H., Rohani, S., Huang, Y. and Song, Y., 2011. In situ high pressure study of ZIF-8 by FTIR spectroscopy. *Chemical Communications*, 47(47), pp.12694-12696.

Iqbal, M.J. and Ashiq, M.N., 2007. Adsorption of dyes from aqueous solutions on activated charcoal. *Journal of Hazardous Materials*, 139(1), pp.57-66.

Jafari, S., Azizian, S. and Jaleh, B., 2011. Adsorption kinetics of methyl violet onto TiO₂ nanoparticles with different phases. *Colloids and Surfaces A: Physicochemical and Engineering Aspects*, 384(1-3), pp.618-623.

Jafari, S., Azizian, S. and Jaleh, B., 2012. Enhancement of methyl violet removal by modification of TiO₂ nanoparticles with AgI. *Journal of Industrial and Engineering Chemistry*, 18(6), pp.2124-2128.

Jana, S., Purkait, M.K. and Mohanty, K., 2010. Removal of crystal violet by advanced oxidation and microfiltration. *Applied Clay Science*, 50(3), pp.337-341.

Jiang, Y.R., Lin, H.P., Chung, W.H., Dai, Y.M., Lin, W.Y. and Chen, C.C., 2015. Controlled hydrothermal synthesis of BiO_xCl_y/BiO_mIn composites exhibiting visible-light photocatalytic degradation of crystal violet. *Journal of Hazardous Materials*, 283, pp.787-805.

Jiani, L., Zhicheng, X., Hao, X., Dan, Q., Zhengwei, L., Wei, Y. and Yu, W., 2020. Pulsed electrochemical oxidation of acid Red G and crystal violet by PbO₂ anode. *Journal of Environmental Chemical Engineering*, 8(3), pp.103773.

Kadirvelu, K., Kavipriya, M., Karthika, C., Radhika, M., Vennilamani, N. and Pattabhi, S., 2003. Utilization of various agricultural wastes for activated carbon preparation and application for the removal of dyes and metal ions from aqueous solutions. *Bioresource Technology*, 87(1), pp.129-132.

Kataria, N. and Garg, V.K., 2017. Removal of Congo red and Brilliant green dyes from aqueous solution using flower shaped ZnO nanoparticles. *Journal of Environmental Chemical Engineering*, 5(6), pp.5420-5428.

Liu, R., Zhang, B., Mei, D., Zhang, H. and Liu, J., 2011. Adsorption of methyl violet from aqueous solution by halloysite nanotubes. *Desalination*, 268(1-3), pp.111-116.

Lutz, H.D., Jung, C., Mörtel, R., Jacobs, H. and Stahl, R., 1998. Hydrogen bonding in solid hydroxides with strongly polarising metal ions, β -Be(OH)₂ and ϵ -Zn(OH)₂. *Spectrochimica Acta Part A: Molecular and Biomolecular Spectroscopy*, 54(7), pp.893-901.



University of Fort Hare
Together in Excellence

Mahini, R., Esmaeili, H. and Foroutan, R., 2018. Adsorption of methyl violet from aqueous solution using brown algae *Padina sanctae-crucis*. *Turkish Journal of Biochemistry*, 43(6), pp.623-631.

Maity, J. and Ray, S.K., 2014. Enhanced adsorption of methyl violet and congo red by using semi and full IPN of polymethacrylic acid and chitosan. *Carbohydrate Polymers*, 104, pp.8-16.

Mall, I.D., Srivastava, V.C. and Agarwal, N.K., 2006. Removal of Orange-G and Methyl Violet dyes by adsorption onto bagasse fly ash—kinetic study and equilibrium isotherm analyses. *Dyes and Pigments*, 69(3), pp.210-223.

Mbacké, M.K., Kane, C., Diallo, N.O., Diop, C.M., Chauvet, F., Comtat, M. and Tzedakis, T., 2016. Electrocoagulation process applied on pollutants treatment-experimental optimization and fundamental investigation of the crystal violet dye removal. *Journal of Environmental Chemical Engineering*, 4(4), pp.4001-4011.



Mittal, H., Kumar, V. and Ray, S.S., 2016. Adsorption of methyl violet from aqueous solution using gum xanthan/Fe₃O₄ based nanocomposite hydrogel. *International Journal of Biological Macromolecules*, 89, pp.1-11.

University of Fort Hare
Together in Excellence

Mohan, A.C. and Renjanadevi, B., 2016. Preparation of zinc oxide nanoparticles and its characterization using scanning electron microscopy (SEM) and X-ray diffraction (XRD). *Procedia Technology*, 24, pp.761-766.

Moneer, A.A., El-Sadaawy, M.M., El-Said, G.F. and Morsy, F.A., 2018. Modeling adsorption kinetic of crystal violet removal by electrocoagulation technique using bipolar iron electrodes. *Water Science and Technology*, 77(2), pp.323-336.

Musyoka, S.M., Mittal, H., Mishra, S.B. and Ngila, J.C., 2014. Effect of functionalization on the adsorption capacity of cellulose for the removal of methyl violet. *International Journal of Biological Macromolecules*, 65, pp.389-397.

Nasrollahi, N., Aber, S., Vatanpour, V. and Mahmoodi, N.M., 2018. The effect of amine functionalization of CuO and ZnO nanoparticles used as additives on the morphology and the permeation properties of polyethersulfone ultrafiltration nanocomposite membranes. *Composites Part B: Engineering*, 154, pp.388-409.

Ofomaja, A.E. and Ho, Y.S., 2008. Effect of temperatures and pH on methyl violet biosorption by *Mansonia* wood sawdust. *Bioresource Technology*, 99(13), pp.5411-5417.

Ofomaja, A.E., 2008. Kinetic study and sorption mechanism of methylene blue and methyl violet onto *Mansonia* (*Mansonia altissima*)^{wood} sawdust. *Chemical Engineering Journal*, 143(1-3), pp.85-95.

Ojemaye, M.O., Okoh, O.O. and Okoh, A.I., 2017. Adsorption of Cu²⁺ from aqueous solution by a novel material; azomethine functionalized magnetic nanoparticles. *Separation and Purification Technology*, 183, pp.204-215.



Ojemaye, M.O., Okoh, O.O. and Okoh, A.I., 2018. Uptake of Zn²⁺ and As³⁺ from wastewater by adsorption onto imine functionalized magnetic nanoparticles. *Water*, 10(1), pp.36.

University of Fort Hare
Together in Excellence

Özdemir, Y., Doğan, M. and Alkan, M., 2006. Adsorption of cationic dyes from aqueous solutions by sepiolite. *Microporous and Mesoporous Materials*, 96(1-3), pp.419-427.

Özgür, Ü., Alivov, Y.I., Liu, C., Teke, A., Reshchikov, M., Doğan, S., Avrutin, V.C.S.J., Cho, S.J. and Morkoç, A.H., 2005. A comprehensive review of ZnO materials and devices. *Journal of Applied Physics*, 98(4), pp.11.

Rahchamani, J., Mousavi, H.Z. and Behzad, M., 2011. Adsorption of methyl violet from aqueous solution by polyacrylamide as an adsorbent: Isotherm and kinetic studies. *Desalination*, 267(2-3), pp.256-260.

Ramasamy, M., Kim, Y.J., Gao, H., Yi, D.K. and An, J.H., 2014. Synthesis of silica coated zinc oxide–poly (ethylene-co-acrylic acid) matrix and its UV shielding evaluation. *Materials Research Bulletin*, 51, pp.85-91.

Rashad, S., Zaki, A.H. and Farghali, A.A., 2019. Morphological effect of titanate nanostructures on the photocatalytic degradation of crystal violet. *Nanomaterials and Nanotechnology*, 9, pp.1847980418821778.

Royer, B., Cardoso, N.F., Lima, E.C., Macedo, T.R. and Airoidi, C., 2009. Sodic and acidic crystalline lamellar magadiite adsorbents for the removal of methylene blue from aqueous solutions: Kinetic and equilibrium studies. *Separation Science and Technology*, 45(1), pp.129-141.

Sathiyavimal, S., Vasantharaj, S., Shanmugavel, M., Manikandan, E., Nguyen-Tri, P., Brindhadevi, K. and Pugazhendhi, A., 2020. Facile synthesis and characterization of hydroxyapatite from fish bones: Photocatalytic degradation of industrial dyes (crystal violet and Congo red). *Progress in Organic Coatings*, 148, pp.105890.



University of East Africa
Together in Excellence

Şolpan, D. and Kölge, Z., 2006. Adsorption of methyl violet in aqueous solutions by poly (N-vinylpyrrolidone-co-methacrylic acid) hydrogels. *Radiation Physics and Chemistry*, 75(1), pp.120-128.

ul Haq, A., Saeed, M., Usman, M., Naqvi, S.A.R., Bokhari, T.H., Maqbool, T., Ghaus, H., Tahir, T. and Khalid, H., 2020. Sorption of chlorpyrifos onto zinc oxide nanoparticles impregnated pea peels (*Pisum sativum* L): Equilibrium, kinetic and thermodynamic studies. *Environmental Technology & Innovation*, 17, pp.100516.

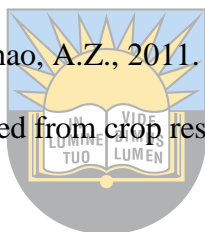
Vidya Vijay, E.V., Jerold, M., Sankar, R., Lakshmanan, S. and Sivasubramanian, V., 2019. Electrocoagulation using commercial grade aluminium electrode for the removal of crystal violet from aqueous solution. *Water Science and Technology*, 79(4), pp.597-606.

Wang, X., Mao, H., Huang, W., Guan, W., Zou, X., Pan, J. and Yan, Y., 2011. Preparation of magnetic imprinted polymer particles via microwave heating initiated polymerization for selective enrichment of 2-amino-4-nitrophenol from aqueous solution. *Chemical Engineering Journal*, 178, pp.85-92.

Wang, Y., Li, B., Zhang, L., Liu, L., Zuo, Q. and Li, P., 2010. A highly selective regenerable optical sensor for detection of mercury (II) ion in water using organic–inorganic hybrid nanomaterials containing pyrene. *New Journal of Chemistry*, 34(9), pp.1946-1953.

Winiarski, J., Tylus, W., Winiarska, K., Szczygieł, I. and Szczygieł, B., 2018. XPS and FT-IR characterization of selected synthetic corrosion products of zinc expected in neutral environment containing chloride ions. *Journal of Spectroscopy*, 2018.

Xu, R.K., Xiao, S.C., Yuan, J.H. and Zhao, A.Z., 2011. Adsorption of methyl violet from aqueous solutions by the biochars derived from crop residues. *Bioresource Technology*, 102(22), pp.10293-10298.



Zabihi, O., Mostafavi, S.M., Ravari, F., Khodabandeh, A., Hooshafza, A., Zare, K. and Shahizadeh, M., 2011. The effect of zinc oxide nanoparticles on thermo-physical properties of diglycidyl ether of bisphenol A/2, 2'-Diamino-1, 1'-binaphthalene nanocomposites. *Thermochimica Acta*, 521(1-2), pp.49-58.

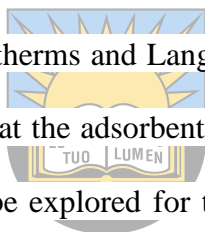
Zafar, M.N., Dar, Q., Nawaz, F., Zafar, M.N., Iqbal, M. and Nazar, M.F., 2019. Effective adsorptive removal of azo dyes over spherical ZnO nanoparticles. *Journal of Materials Research and Technology*, 8(1), pp.713-725.

Chapter Five

Pyrene ligand grafted onto zinc oxide nanoparticles for the removal of brilliant green from aqueous solutions

Abstract

Herein, previously synthesized pyrene grafted onto zinc oxide nanoparticles (ZnO-Pyrene NPs) were used for brilliant green (BG) dye removal from aqueous solutions. The efficiency of pyrene grafted onto zinc oxide nanoparticles was evaluated through batch adsorption experiments. The maximum adsorption efficiency of 88.8% was accomplished with 79.8 mg at pH 6.50 and constant room temperature. BG adsorption rate mechanism was determined using three kinetic models and was best explained by the pseudo-first order kinetic model. Dye adsorption behaviour was explained using three different isotherms and Langmuir isotherm was the most applicable. Reusability of the adsorbent showed that the adsorbent is still efficient after 3 runs. This study indicates that this novel material can be explored for the removal of dyes and vast variety of contaminants from real wastewater considering its high adsorption efficiency and recyclability.

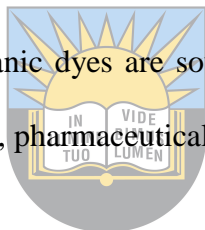


Together in Excellence

Keywords: Adsorption, 1-(4-hydroxyphenyl)-4-pyrenyl-2,3-diaza-1,3-butadiene, isotherm, silica, grafted, zinc oxide

5.1. Introduction

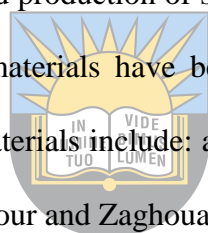
Water covers about 70% of the earth's surface. However, worldwide, supply of water fails to match up with the rapid growing demand, due to water quality deterioration, industrialization, etc (Abdin and Gaafar, 2009; Blomquist *et al.*, 2012; Qu *et al.*, 2013). Water quality deterioration mostly arise from discharges of toxic heavy metals, organic and inorganic pollutants since water is their principal receiver (Kataria and Garg, 2017). Organic contaminants are carbon-based chemicals like pharmaceuticals, solvents, dyes and pesticides (Alexander *et al.*, 2012; Bond *et al.*, 2012; Delgado *et al.*, 2012; Wankhade Atul *et al.*, 2013), which end up in water streams as a result of farmlands runoff (Reichenberger *et al.*, 2007) or factories discharge (Guasmi *et al.*, 2010). The occurrence of the latter substances changes the chemical and physical properties of water and causes a significant threat to human well-being (Saharan *et al.*, 2014). As a typical example of organic contaminants, organic dyes are sourced from various industries including textile, pulp and paper, leather, printing, pharmaceutical etc (Hanafi and Sapawe, 2020; Saharan *et al.*, 2014).



These industries use dyes for different desires (Rehman *et al.*, 2013). Furthermore the quality and quantity of dyes vary from industry to industry, and from use to use (Rehman *et al.*, 2013). Dyes are broadly grouped into anionic and cationic dyes, in comparison anionic dyes are more toxic (Nandi *et al.*, 2009). Nevertheless, brilliant green as cationic dye has been associated with a number of health problems such as skin irritation, diarrhoea, eye irritation, difficult breathing, vomiting, nausea, coughing, etc (Rehman *et al.*, 2013). They are also associated with lung and kidney failure (Bhattacharya *et al.*, 2019; Chatterjee and Dasgupta, 2005; Forgacs *et al.*, 2004). Therefore, it can be considered as one of the environment threats. Its health problems are a result of its carcinogenic, allergenic and mutagenic characteristics (Kishor *et al.*, 2021; Rehman *et al.*, 2013). These negative health effects imply that pre-treatment of industrial wastewater constituting dyes is crucial prior to their discharge. Many techniques have been discovered and used for the removal of recalcitrant pollutants like brilliant green in water. These techniques

include electrocoagulation (Hashim *et al.*, 2019; Mariah and Pak, 2020; Nandi and Patel, 2017; Nandi and Patel, 2014), photo-degradation (Bhattacharya *et al.*, 2019; Chen *et al.*, 2008; Hassan and Mannaa, 2016; Khan *et al.*, 2020; Shambharkar and Chowdhury, 2016; Sood *et al.*, 2015), advance oxidation process (Ju *et al.*, 2013; Rehman *et al.*, 2018), adsorption (Kismir and Aroguz, 2011; Kobiraj *et al.*, 2012; Mane and Babu, 2011; Nandi *et al.*, 2009; Rehman *et al.*, 2013; Salem *et al.*, 2016). Among these, adsorption technique is an innovative and economical reasonable alternative owing that to its ease of application and high removal performance (Ali and Gupta, 2007; Patil *et al.*, 2020) more especially with nanomaterials.

Although other techniques have also shown high removal efficiency, their worldwide application is limited due to certain economical and technical limitations associated with their use such as high cost, high energy consumption and production of sludge after water treatment (Asgher and Bhatti, 2012). In addition, different materials have been extensively used as adsorbents for water/wastewater treatments. These materials include: activated carbon (Asadullah *et al.*, 2010; Ghaedi *et al.*, 2011), natural clay (Aichour and Zaghouane-Boudiaf, 2019; Rehman *et al.*, 2013), carbon nanotubes (Kumar *et al.*, 2014), magnetic nanoparticles (Zhang *et al.*, 2017) and so on. These materials have shown to possess uncharacteristic removal efficiency, inadequate active sites, and no re-usability abilities which results into seeking alternate materials that can effectively take care of these disadvantages. Zinc oxide nanoparticles are excellent materials with adsorption and photocatalytic properties. Therefore, this study seeks to develop for the first time economically reasonable and highly effective adsorbent; pyrene grafted onto zinc oxide nanoparticles. As a potent alternative for BG removal from aqueous solution, it is highly characterized by great chemical and thermal stabilities of zinc oxide core with an enhanced chelating capabilities brought about by the presence of pyrene nitrogen functionalities on the surface of zinc oxide nanoparticles. Thus, improving the adsorption efficiency as well, by providing a scaffold where other functionalities can be attached. In addition, batch adsorption removal involving influence of pH, time, brilliant green concentration and adsorbent amount were



University of Fort Hare
Together in Excellence

evaluated in other to ascertain the best possible condition for the removal of this contaminant from water using the novel material.

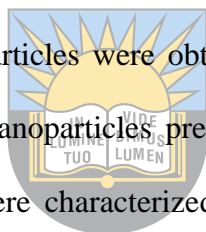
5.2. Methodology

5.2.1. Materials and chemicals

32% hydrochloric acid analar was bought from Merck Chemicals, Gauteng, South Africa. Sodium chloride and sodium hydroxide of purities of 98% and above were bought from Associated Chemical Enterprises (South Africa). Brilliant green dye was purchased from Baird & Tatlock Ltd, London, England. This dye and chemicals were used as received from the suppliers.

5.2.2. Synthesis and characterization of pyrene grafted zinc oxide nanoparticles

The pyrene grafted zinc oxide nanoparticles were obtained after covalent grafting of pyrene ligand on the surface of zinc oxide nanoparticles previously synthesized by co-precipitation method. The synthesized materials were characterized via several techniques; details of the synthesis and characterization of the synthesized materials were previously discussed in Chapters 3 and 4.



University of East West Africa
Together in Excellence

5.2.3. Preparation of adsorbate solutions

BG (1 g) was dissolved in enough distilled water in 1000 mL volumetric flask. After the solute was totally dissolved, distilled water was added to the mark up volume (1000 mL). Standard and working solutions were then obtained from the stock solution by diluting to the desired concentration in separate volumetric flasks.

5.2.4. Point of zero charge

Point of zero charge (pH_{pzc}) was evaluated before the commencement of batch adsorption experiments via salt addition method (Kataria and Garg, 2017). This was accomplished by adding 2 mg of ZnO-Pyrene in eight 20 mL solutions of 0.1 M NaCl with different initial pH values (pH_i)

ranging from 2-9. The adjustment of pH of the solutions was done using 0.1 M HCl or NaOH solutions as the case may be. Glass bottles containing the different solutions were shaken for 6 hrs at room temperature using an orbital shaker at a speed of 150 rpm. Thereafter, final pH values (pH_f) were determined. The p*H*_{pzc} of ZnO-Pyrene was calculated from a plot of ΔpH versus p*H*_i.

5.2.5. Adsorbate removal experiment

BG removal from aqueous solution was carried out via batch adsorption experiments as earlier reported by ul Haq *et al.* (2020) with little adjustments, considering the effect of adsorbate concentration, pH, contact time and adsorbent dose. This was done using 100 mL glass bottles with screw caps and orbital shaker for adsorption at 150 rpm. Separation of adsorption solution was done by means of centrifugation after each time interval and the remaining dye concentration was determined with UV-Visible spectrophotometer (UV-Vis) at λ_{max} = 625 nm. The effect of solution pH on the adsorption process was investigated from pH 2-10 by changing the initial solution pH to the desired pH using 0.1M hydrochloric acid or sodium hydroxide solutions. The contact time effect was evaluated for the time interval 0 to 360 minutes whereas the effect of adsorbent dose and adsorbate concentration was carried out at four different concentrations. The adsorption efficiency also presented as % adsorbed and adsorption capacity denoted as *q_e* were determined using equations 5.1 and 5.2 respectively:

$$\text{Adsorption efficiency (\% adsorbed)} = \left(\frac{c_i - c_{eq}}{c_i} \right) \times 100 \quad (5.1)$$

$$\text{Adsorption capacity (} q_e \text{)} = \frac{(c_i - c_{eq})V}{m} \quad (5.2)$$

Where, C_i = BG concentration (mg L⁻¹)

C_{eq} = BG concentration at equilibrium (mg L⁻¹)

q_e = equilibrium adsorption capacity (mg g⁻¹)

m = adsorbent mass (g)

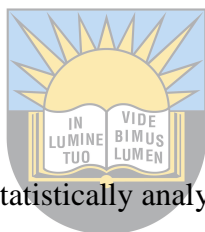
and *V* = volume of the adsorbate solution used (L).

5.2.6. Reusability and desorption studies

Three runs were considered for reusability and desorption studies and each run was 6 hrs. This was done to check the reusability of the adsorbent for cost effectiveness. The loaded adsorbent was separated by centrifugation after each run of adsorption, dried in an oven at 70°C and dispersed in three 0.1M HNO₃ solutions and stirred for the same period as was for adsorption. At the end of reusability and desorption experiments, concentration was measured at $\lambda_{\text{max}} = 625$ nm using UV-Visible spectrophotometer. Desorption efficiency (% desorbed) was calculated using equation 5.3:

$$\text{Desorption efficiency (\% desorbed)} = \left(\frac{c_d}{c_a} \right) \times 100 \quad (5.3)$$

Where C_d = dye concentration desorbed and C_a = dye concentration initially adsorbed both in (mg/L).



5.2.7. Data analysis

The data obtained from this study was statistically analysed and plotted using OriginPro 2021b.

University of Fort Hare
Together in Excellence

5.3. Results and discussion

5.3.1. Characterization

The characterization of this novel material using analytical instruments/equipments such as FTIR, SEM-EDX, TEM, XRD, TGA and BET indicates that this material was successfully synthesized. FTIR spectra showed distinct peaks at about 500 cm⁻¹ ascribed to Zn-O stretch as well as the other peaks from pyrene ligand. In addition, a crystalline morphology and spherical shape of the material was observed from the SEM and TEM micrographs respectively, which are characteristics of zinc oxide nanoparticles. Detailed result of characterization of this material has been discussed in the preceding chapters of this study (Chapters 3 and 4).

5.3.2. Adsorption studies

5.3.2.1. Influence of pH

The solution pH and BG removal relationship was evaluated in the pH range 2-9. In this experiment all other four parameters were fixed viz., (contact time = 6 h, adsorbent dose approximately = 40.0 mg, adsorbate concentration = 34.6 mg/L and temperature = $20 \pm 2^\circ\text{C}$). Prior to this investigation, pH_{pzc} was determined and found to be 6 (Figure 5.1 (a)). During that course it was deduced that at pH values below the pH_{pzc} , the adsorbent surface charge was positive. The latter was a result of protonation (H^+). BG dye is also positive in aqueous solution therefore more electrostatic repulsions between positively charged molecules (ZnO-Pyrene and BG) resulted in lower removal efficiency. However, above the pH_{pzc} the removal was higher due to electrostatic attractions between ZnO-Pyrene and BG molecules. Contaminant removal increased from 51.07 to 98.03 % in pH range 2-9 (Figure 5.1 (b)). This result was similar to the data reported by Kataria and Garg (2017). Even below the pH_{pzc} the removal was high implying that ZnO-Pyrene is a potent material for BG removal. From as low as pH 4 the removal began to become constant signifying the optimum pH even though there were slight fluctuations. However, pH 6.5, a pH just above pH_{pzc} , was considered for further adsorption experiments on this material.

5.3.2.2. Influence of contact time

Contact time and dye removal relationship was evaluated to explore the optimum equilibrium time for BG removal. This was conducted for time intervals from 5-360 min while the pH = 6.5, adsorbent dose approximately = 40 mg, adsorbate concentration = 40.4 mg/L and temperature = $20 \pm 2^\circ\text{C}$ were fixed (Figure 5.1 (c)). Overall, it was noticed that adsorption efficiency was increasing with time as it was reported in the study of Abbas (2020). At low time intervals 5, 15, 30 and 60 minutes the increase in adsorption capacity was not sharp, this might have been due to low adsorbent dispersion in the solution in those contact time intervals. However, it was the opposite from 60 to 225 min. From 225 to 360 min the gradient decreased as the adsorption

capacity was becoming constant, this was an indication of the optimum equilibrium time for BG removal and 360 min was adopted. This decision was made because 360 minutes showed the highest adsorption capacity in comparison to other time intervals.

5.3.2.3. Influence of adsorbent dose

The adsorbent dose and adsorption relationship was carried at four levels viz., 10, 19.6, 39.6 and 79.8 mg while keeping other parameters constant (Figure 5.1 (d)). Solution pH was kept at pH = 6.5, adsorbate concentration = 40.0 mg/L, contact time = 360 min and temperature = $20 \pm 2^\circ\text{C}$. The removal efficiency increased from 10 to 79.8 mg and the maximum adsorption was found to be 88.83 % with 79.8 mg. These results were similar to the ones reported by (Kataria and Garg, 2017). 10 mg possessed the lowest adsorption as a result of a lesser number of active sites whereas 79.8 mg possessed a highest adsorption due to a large number of present active sites compared to others. However, from 39.6 to 79.8 mg the adsorption was almost constant as a result of many packed sites which might have led to electrostatic repulsions after sometime between the adsorbent and adsorbate molecules. Since the adsorption started to become constant from 39.6 mg, 39.6 mg was kept for further experiments.

5.3.2.4. Influence of adsorbate concentration

Four different concentrations were considered for the adsorbate concentration and adsorption capacity relationship study. During this experiment pH = 6.5, contact time = 360 min, adsorbent dose approximately = 40.0 mg and temperature = $20 \pm 2^\circ\text{C}$ were kept constant. In this experiment, it can be noticed that the adsorption capacity was increasing with concentration from 10.2 – 65.0 mg/L (Figure 5.1 (e)). The increase was due to the fact that at high concentrations there were more adsorbent-adsorbate collisions as a result of excess adsorbate molecules. Abbas (2020) also reported similar results.

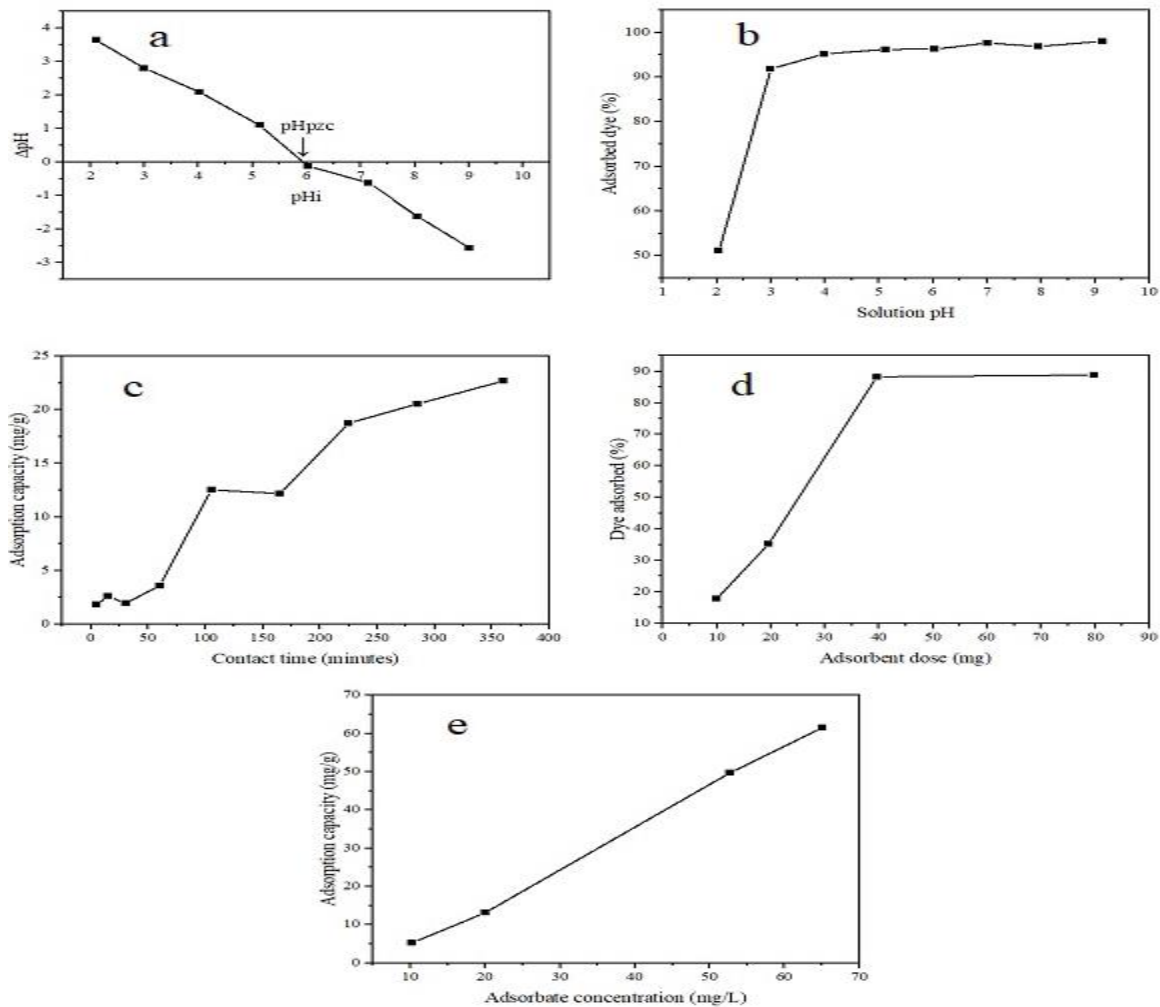


Figure 5.1: (a) Point of zero charge (b) influence of pH (c) influence of contact time (d) influence of adsorbent dose and (e) influence of adsorbate concentration.

5.3.3. Kinetic studies

The rate mechanism of brilliant green removal process was evaluated using both the pseudo-first order (equation 5.4) (Kataria and Garg, 2017) and pseudo second order (equation 5.5) (Ho *et al.*, 2000) in addition to intraparticle diffusion (equation 5.6) (Kataria and Garg, 2017) kinetic models. These models can be expressed as follows:

$$\ln(q_e - q_t) = \ln q_e - K_1 t \quad (5.4)$$

$$\frac{t}{q_t} = \frac{1}{K_2 q_e^2} + \frac{t}{q_e} \quad (5.5)$$

$$q_t = K_{id} t^{1/2} + C \quad (5.5)$$

Where, q_e and q_t (mg/g) denote adsorption capacity at equilibrium time and time (t) respectively, K_1 (min^{-1}) and K_2 (g/mg.min) are kinetic rate constant and pseudo-second order rate constant respectively, t is time in minutes, K_{id} ($\text{mg g}^{-1} \text{min}^{-0.5}$) denotes the intra-particle diffusion rate constant whereas the boundary layer thickness is denoted by C (mg/g) . Table 5.1 gives a summary of kinetic parameters and R^2 values of the kinetic models. The pseudo-first order kinetic model's kinetic rate constant and equilibrium adsorption capacity were determined from a graph of $\ln(q_e - q_t)$ versus t. The equilibrium adsorption capacity and R^2 of the pseudo-first order kinetic model were greater than those of the pseudo-second order kinetic model. These far lesser values implied non-applicability of the pseudo-second order in comparison with the pseudo-first order. The parameters of pseudo-second order kinetic model were determined from a plot of t/q_t versus t. Moreover, the equilibrium adsorption capacity of pseudo-first order was the closest to the experimental equilibrium adsorption capacity.

Therefore, the data was better fitted to pseudo-first order equation. A plot of q_t versus $t^{1/2}$ was used in intraparticle diffusion model to determine C , K_{id} , and R^2 values. Since the linear regression curve did not pass through the origin, intraparticle diffusion cannot be noted as the only rate determining step of the process (Dawood and Sen, 2012). Therefore, intraparticle diffusion model was not applicable to the adsorption of studied dye onto ZnO-Pyrene nanoparticles that was also indicated by the R^2 value that is far from 1. These results imply that the attachment of BG on the adsorbent was physically not chemically.

Table 5.1: Brilliant green adsorption onto ZnO-Pyrene nanoparticles kinetic models' parameters.

Kinetic models	Parameters	Values of parameters
Pseudo-first order	K_1 (min^{-1})	-8.84×10^{-5}
	q_e (cal)	7.83
	R^2	0.903
Pseudo-second order	K_2 (g/mg.min)	3.68×10^{-10}
	q_e (cal)	1.14×10^4
	R^2	0.0224
Intraparticle diffusion	K_{id} ($\text{mg.g}^{-1}.\text{min}^{-0.5}$)	0.0368
	C	-2.67
	R^2	0.796
	q_e (exp)	6.58

*The numerical values in this table are presented in three significant figures.

5.3.4. Adsorption isotherms

Adsorption capacity of BG dye onto ZnO-Pyrene NPs was determined using four different adsorbate concentration in the range 10.2 – 65.0 mg/L (Figure 5.1 (e)). Adsorption behaviour between adsorbate and ZnO-Pyrene NPs was explained using three adsorption isotherms. Langmuir adsorption isotherm expressed as equation (5.7), Freundlich adsorption isotherm expressed as equation (5.8) and Temkin adsorption isotherm expressed as equation (5.9):

$$\frac{1}{q_e} = \left(\frac{1}{K_L q_{max}} \right) \left(\frac{1}{c_e} \right) + \left(\frac{1}{q_{max}} \right) \quad (5.7)$$

$$\log q_e = \log K_F + \left(\frac{1}{n} \right) \log c_e \quad (5.8)$$

$$q_e = B \ln K_T + B \ln c_e \quad (5.9)$$

In equation (5.7), q_{max} (mg/g) is the maximum adsorption capacity, K_L (L/mg) is the Langmuir constant. Adsorption parameters were obtained using linear form of Langmuir adsorption isotherm equation (5.7) from a graph of between $1/q_e$ versus $1/C_e$ and listed with the correlation coefficient in Table 5.2. In equation (5.8), K_F (mg/g(L/mg)^{1/n}) denotes Freundlich constant and n is the heterogeneity factor. The linear plot of $\log q_e$ versus $\log C_e$ was used to determine the parameter values. The n value should be between 1 and 10 for a favourable adsorption process. Freundlich isotherms correlation coefficient and parameters are presented in Table 5.2. In equation (5.9), B (J mol⁻¹) is the Temkin constant, which indicates the adsorption heat and K_T (L g⁻¹) is equilibrium binding constant. Temkin parameters' values were determined from a graph of q_e versus $\ln C_e$. The correlation coefficient and Temkin parameter values of BG are listed in Table 5.2. Comparing the adsorption isotherms' R^2 values it can be deduced that the rate mechanism of BG adsorption may be best explained by Langmuir isotherm (Mane *et al.*, 2007). Even though the R^2 of Freundlich isotherm is acceptable, it is not applicable due to n value that is less than 1. Therefore, these observations imply that the adsorption of brilliant green was limited to monolayer.

Table 5.2: BG adsorption isotherms' parameters.

Adsorption isotherms	Parameters	Values
Langmuir isotherm	K_L (L/mg)	-0.0633
	q_{max} (mg/g)	-8.60
	R^2	0.988
Freundlich isotherm	K_F (mg/g(L/mg) ^{1/n})	0.0275
	n	0.348
	R^2	0.956
Temkin isotherm	K_T (L/mg)	0.163
	B	64.4
	R^2	0.815

*The numerical values in this table are presented in three significant figures.

5.3.5. Reusability and desorption studies

For reusability study, adsorption was performed three times for 6 hrs per run. After each run the used adsorbent was separated through centrifugation and dried before it was used for the following run. The concentration was determined using UV-Visible spectrophotometer at $\lambda_{max} = 625$ nm. It was noticed that the adsorption efficiency was decreasing as the runs proceeded (Figure 5.2). This was due to the decreasing number of present adsorptive sites of the adsorbent. In the third run, the efficiency was 12.1 %, which is not a good efficiency at all. However, in the second run the efficiency was 65.6 %, which is substantial. These observations implied that the material can be used to a maximum of two runs. Another evidence to the latter is the undefinable desorption observed at run 3. This was done to minimize cost, unlike using these potent materials only once and dispose them. In the desorption experiments, the recovered packed adsorbents from each run were dispersed in 50 mL of 0.1N HNO₃ solutions. Each solution was stirred for 6 hrs. After stirring and separation, the concentration was determined using UV-Visible spectrophotometer at $\lambda_{max} = 625$ nm. It was noticed that at higher runs there was high desorption. This was so because at higher runs more BG particles were adsorbed to the adsorbent surface, thus, easy removal was expected due to dye particle-particle repulsion. This experiment was also done to ascertain the effectiveness of this adsorbent for cost reduction.

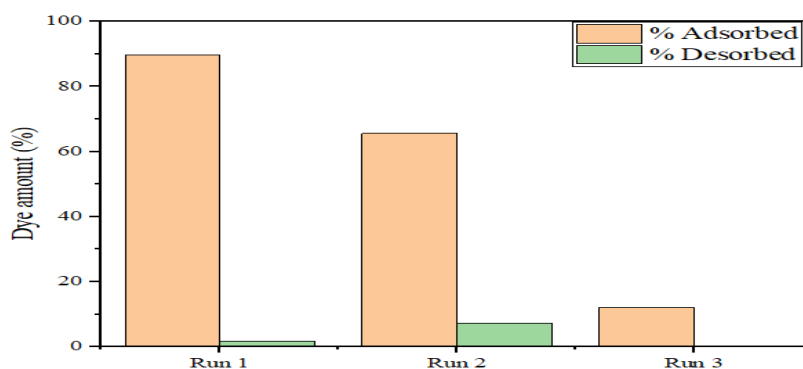


Figure 5.2: Adsorption and desorption of BG onto ZnO-Pyrene.

5.4. Conclusion

ZnO nanoparticles were successfully prepared and functionalized. This was confirmed by the FTIR analysis. The geometry of the nanoparticles was spherical as observed in the TEM images, and it was also confirmed by the retained crystallinity from XRD analysis. The synthesized materials were of high purity as no foreign elements were found in their EDX spectra and this was also confirmed by TGA with high amounts of residuals. The pyrene functionalized zinc oxide nanoparticles were able to remove BG and their efficiency was dependent on pH, adsorbent dose, contact time and adsorbate concentration. Their rate mechanism was best explained by pseudo-first order and their adsorption behaviour was best explained using Langmuir isotherm. The adsorbent showed quite a high reusability in the considered number of runs and run period. This study shows that this new material can serve as substitute material to already known materials for the removal of hazardous dyes from water.

References

- Abbas, M., 2020. Removal of brilliant green (BG) by activated carbon derived from medlar nucleus (ACMN)–Kinetic, isotherms and thermodynamic aspects of adsorption. *Adsorption Science & Technology*, 38(9-10), pp.464-482.
- Abdin, A.E. and Gaafar, I., 2009. Rational water use in Egypt. *Technological Perspectives for Rational Use of Water Resources in the Mediterranean Region*.

Aichour, A. and Zaghouane-Boudiaf, H., 2019. Highly brilliant green removal from wastewater by mesoporous adsorbents: kinetics, thermodynamics and equilibrium isotherm studies. *Microchemical Journal*, 146, pp.1255-1262.

Alexander, J.T., Hai, F.I. and Al-Aboud, T.M., 2012. Chemical coagulation-based processes for trace organic contaminant removal: Current state and future potential. *Journal of Environmental Management*, 111, pp.195-207.

Asadullah, M., Asaduzzaman, M., Kabir, M.S., Mostofa, M.G. and Miyazawa, T., 2010. Chemical and structural evaluation of activated carbon prepared from jute sticks for Brilliant Green dye removal from aqueous solution. *Journal of Hazardous Materials*, 174(1-3), pp.437-443.

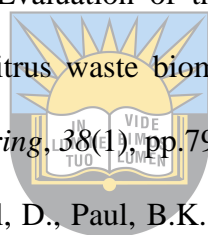
Asgher, M. and Bhatti, H.N., 2012. Evaluation of thermodynamics and effect of chemical treatments on sorption potential of Citrus waste biomass for removal of anionic dyes from aqueous solutions. *Ecological Engineering*, 38(1), pp.79-85.

Bhattacharya, D., Ghoshal, D., Mondal, D., Paul, B.K., Bose, N., Das, S. and Basu, M., 2019. Visible light driven degradation of brilliant green dye using titanium based ternary metal oxide photocatalyst. *Results in Physics*, 12, pp.1850-1858.

Blomquist, W., Cunniff, S., Fox, P., Furukawa, D., Garcia, M., Gritzuk, M. and Wolff, G., 2012. Desalination and water Purification technology roadmap: A report of the executive committee. *Desalination: Solutions and Roadmap for an Improved Water Supply*, pp.87-179.

Bond, T., Templeton, M.R. and Graham, N., 2012. Precursors of nitrogenous disinfection by-products in drinking water—a critical review and analysis. *Journal of Hazardous Materials*, 235, pp.1-16.

Chatterjee, D. and Dasgupta, S., 2005. Visible light induced photocatalytic degradation of organic pollutants. *Journal of Photochemistry and Photobiology C: Photochemistry Reviews*, 6(2-3), pp.186-205.



University of Fort Hare
Together in Excellence

Chen, C.C., Lu, C.S., Fan, H.J., Chung, W.H., Jan, J.L., Lin, H.D. and Lin, W.Y., 2008. Photocatalyzed N-de-ethylation and degradation of Brilliant Green in TiO₂ dispersions under UV irradiation. *Desalination*, 219(1-3), pp.89-100.

Dawood, S. and Sen, T.K., 2012. Removal of anionic dye Congo red from aqueous solution by raw pine and acid-treated pine cone powder as adsorbent: equilibrium, thermodynamic, kinetics, mechanism and process design. *Water Research*, 46(6), pp.1933-1946.

Delgado, L.F., Charles, P., Glucina, K. and Morlay, C., 2012. The removal of endocrine disrupting compounds, pharmaceutically activated compounds and cyanobacterial toxins during drinking water preparation using activated carbon—A review. *Science of the Total Environment*, 435, pp.509-525.

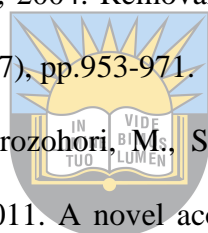
Forgacs, E., Cserhati, T. and Oros, G., 2004. Removal of synthetic dyes from wastewaters: a review. *Environment International*, 30(7), pp.953-971.

Ghaedi, M., Hossainian, H., Montazerzohori, M., Shokrollahi, A., Shojaipour, F., Soylak, M.U.S.T.A.F.A. and Purkait, M.K., 2011. A novel acorn based adsorbent for the removal of brilliant green. *Desalination*, 281, pp.226-233.

Guasmi, I., Kherici-Bousnoubra, H., Kherici, N. and Hadji, F., 2010. Assessing the organic pollution of surface water of Medjerda watershed (NE Algeria). *Environmental Earth Sciences*, 60(5), pp.985-992.

Hanafi, M.F. and Sapawe, N., 2020. A review on the water problem associated with organic pollutants derived from phenol, methyl orange, and remazol brilliant blue dyes. *Materials Today: Proceedings*, 31, pp.A141-A150.

Hashim, K.S., Al-Saati, N.H., Alquzweeni, S.S., Zubaidi, S.L., Kot, P., Kraidi, L., Hussein, A.H., Alkhaddar, R., Shaw, A. and Alwash, R., 2019, August. Decolourization of dye solutions by electrocoagulation: an investigation of the effect of operational parameters. In *IOP Conference Series: Materials Science and Engineering*, 584(1), pp.012024.



University of Fort Hare
Together in Excellence

Hassan, S.M. and Mannaa, M.A., 2016. Photocatalytic degradation of brilliant green dye by SnO₂/TiO₂ nanocatalysts. *International Journal Nano Material Science*, 5(1), pp.9-19.

Ho, Y.S., Ng, J.C.Y. and McKay, G., 2000. Kinetics of pollutant sorption by biosorbents. *Separation and purification methods*, 29(2), pp.189-232.

Ju, Y., Wang, X., Qiao, J., Li, G., Wu, Y., Li, Y., Zhang, X., Xu, Z., Qi, J., Fang, J. and Dionysiou, D.D., 2013. Could microwave induced catalytic oxidation (MICO) process over CoFe₂O₄ effectively eliminate brilliant green in aqueous solution?. *Journal of Hazardous Materials*, 263, pp.600-609.

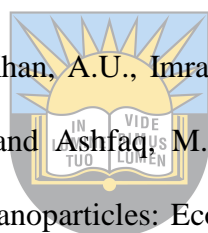
Kataria, N. and Garg, V.K., 2017. Removal of Congo red and Brilliant green dyes from aqueous solution using flower shaped ZnO nanoparticles. *Journal of Environmental Chemical Engineering*, 5(6), pp.5420-5428.

Khan, Z.U.H., Shah, N.S., Iqbal, J., Khan, A.U., Imran, M., Alshehri, S.M., Muhammad, N., Sayed, M., Ahmad, N., Kousar, A. and Ashfaq, M., 2020. Biomedical and photocatalytic applications of biosynthesized silver nanoparticles: Ecotoxicology study of brilliant green dye and its mechanistic degradation pathways. *Journal of Molecular Liquids*, 319, p.114114.

Kishor, R., Purchase, D., Saratale, G.D., Saratale, R.G., Ferreira, L.F.R., Bilal, M., Chandra, R. and Bharagava, R.N., 2021. Ecotoxicological and health concerns of persistent coloring pollutants of textile industry wastewater and treatment approaches for environmental safety. *Journal of Environmental Chemical Engineering*, pp.105012.

Kismir, Y. and Aroguz, A.Z., 2011. Adsorption characteristics of the hazardous dye Brilliant Green on Saklikent mud. *Chemical Engineering Journal*, 172(1), pp.199-206.

Kobiraj, R., Gupta, N., Kushwaha, A.K. and Chattopadhyaya, M.C., 2012. Determination of equilibrium, kinetic and thermodynamic parameters for the adsorption of Brilliant Green dye from aqueous solutions onto eggshell powder.



University of Fort Hare
Together in Excellence

Kumar, R., Ansari, M.O. and Barakat, M.A., 2014. Adsorption of brilliant green by surfactant doped polyaniline/MWCNTs composite: evaluation of the kinetic, thermodynamic, and isotherm. *Industrial & Engineering Chemistry Research*, 53(17), pp.7167-7175.

Mane, V.S. and Babu, P.V., 2011. Studies on the adsorption of Brilliant Green dye from aqueous solution onto low-cost NaOH treated saw dust. *Desalination*, 273(2-3), pp.321-329.

Mane, V.S., Mall, I.D. and Srivastava, V.C., 2007. Kinetic and equilibrium isotherm studies for the adsorptive removal of Brilliant Green dye from aqueous solution by rice husk ash. *Journal of Environmental Management*, 84(4), pp.390-400.

Mariah, G.K. and Pak, K.S., 2020. Removal of brilliant green dye from aqueous solution by electrocoagulation using response surface methodology. *Materials Today: Proceedings*, 20, pp.488-492.

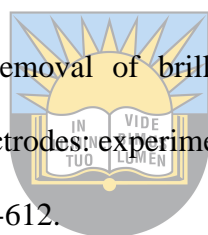
Nandi, B.K. and Patel, S., 2014. Removal of brilliant green from aqueous solution by electrocoagulation using aluminum electrodes: experimental, kinetics, and modeling. *Separation Science and Technology*, 49(4), pp.601-612.

Nandi, B.K. and Patel, S., 2017. Effects of operational parameters on the removal of brilliant green dye from aqueous solutions by electrocoagulation. *Arabian Journal of Chemistry*, 10, pp.S2961-S2968.

Nandi, B.K., Goswami, A. and Purkait, M.K., 2009. Adsorption characteristics of brilliant green dye on kaolin. *Journal of Hazardous Materials*, 161(1), pp.387-395.

Patil, C.S., Kadam, A.N., Gunjal, D.B., Naik, V.M., Lee, S.W., Kolekar, G.B. and Gore, A.H., 2020. Sugarcane molasses derived carbon sheet@ sea sand composite for direct removal of methylene blue from textile wastewater: Industrial wastewater remediation through sustainable, greener, and scalable methodology. *Separation and Purification Technology*, 247, p.116997.

Qu, X., Alvarez, P.J. and Li, Q., 2013. Applications of nanotechnology in water and wastewater treatment. *Water Research*, 47(12), pp.3931-3946.



University of Fort Hare
Together in Excellence

- Rehman, F., Sayed, M., Khan, J.A., Shah, N.S., Khan, H.M. and Dionysiou, D.D., 2018. Oxidative removal of brilliant green by UV/S₂O₈²⁻, UV/HSO₅⁻ and UV/H₂O₂ processes in aqueous media: a comparative study. *Journal of Hazardous Materials*, 357, pp.506-514.
- Rehman, M.S.U., Munir, M., Ashfaq, M., Rashid, N., Nazar, M.F., Danish, M. and Han, J.I., 2013. Adsorption of Brilliant Green dye from aqueous solution onto red clay. *Chemical Engineering Journal*, 228, pp.54-62.
- Reichenberger, S., Bach, M., Skitschak, A. and Frede, H.G., 2007. Mitigation strategies to reduce pesticide inputs into ground- and surface water and their effectiveness; a review. *Science of the Total Environment*, 384(1-3), pp.1-35.
- Saharan, P., Chaudhary, G.R., Mehta, S.K. and Umar, A., 2014. Removal of water contaminants by iron oxide nanomaterials. *Journal of Nanoscience and Nanotechnology*, 14(1), pp.627-643.
- Salem, M.A., Elsharkawy, R.G. and Hablas, M.F., 2016. Adsorption of brilliant green dye by polyaniline/silver nanocomposite: kinetic, equilibrium, and thermodynamic studies. *European Polymer Journal*, 75, pp.577-590.
- Shambharkar, B.H. and Chowdhury, A.P., 2016. Ethylene glycol mediated synthesis of Ag₈SnS₆ nanoparticles and their exploitation in the degradation of eosin yellow and brilliant green. *Royal Society of Chemistry Advances*, 6(13), pp.10513-10519.
- Sood, S., Umar, A., Mehta, S.K., Sinha, A.S.K. and Kansal, S.K., 2015. Efficient photocatalytic degradation of brilliant green using Sr-doped TiO₂ nanoparticles. *Ceramics International*, 41(3), pp.3533-3540.
- ul Haq, A., Saeed, M., Usman, M., Naqvi, S.A.R., Bokhari, T.H., Maqbool, T., Ghaus, H., Tahir, T. and Khalid, H., 2020. Sorption of chlorpyrifos onto zinc oxide nanoparticles impregnated pea peels (*Pisum sativum* L): Equilibrium, kinetic and thermodynamic studies. *Environmental Technology & Innovation*, 17, p.100516.



Wankhade Atul, V., Gaikwad, G.S., Dhonde, M.G., Khaty, N.T. and Thakare, S.R., 2013. Removal of organic pollutant from water by heterogenous photocatalysis: a review. *Research Journal Chemical Environment*, 17, pp.84-94.

Zhang, D., Zhu, M.Y., Yu, J.G., Meng, H.W. and Jiao, F.P., 2017. Effective removal of brilliant green from aqueous solution with magnetic Fe₃O₄@ SDBS@ LDHs composites. *Transactions of Nonferrous Metals Society of China*, 27(12), pp.2673-2681.



University of Fort Hare
Together in Excellence

Chapter Six

General conclusion and recommendations

In this study, 1-(4-hydroxyphenyl)-4-pyrenyl-2,3-diaza-1,3-butadiene grafted onto zinc oxide nanoparticles was successfully synthesized. This was confirmed with FTIR, EDX and XRD. The other properties such as morphology, shape and particle size were determined with SEM and TEM analyses. The crystallinity was also successfully evaluated using XRD instrument as the adsorbent showed reflections in their characteristic 2 Theta regions. The ligand used for functionalization was successfully synthesized and characterized with FTIR and NMR. In all the synthesised nanoparticles, Zn-O stretch appeared between 500 and 450 cm^{-1} , which is a characteristic stretch for ZnO nanoparticles. This indicated that the bare nanoparticles were successfully synthesized and the inner core properties were maintained throughout. The functionalization of the nanoparticles and the introduction of organic stretches at 3100 – 3000 cm^{-1} as well as 2990 and 2850 cm^{-1} were also confirmed by the latter. For the confirmation of the synthesis of this material, EDX analysis showed newly introduced peaks corresponding to C, N and O, which were not initially present in the bare nanoparticles.

Furthermore, the XRD analysis of the functionalized and unfunctionalized nanoparticles showed similar miller indices at similar regions implying that the core properties were maintained. However, in the diffractogram of the functionalized material (ZnO-Pyrene NPs), amorphous nature of the ligand introduced to ZnO NPs made the diffractogram to show some roughness. This layer provided an extra shell to which the contaminants were attached. Functionalization improved the thermal stability of the unfunctionalized nanoparticles. Functionalization decreased the particle size from 290 to 181 nm and by that improved the efficiency of the unfunctionalized materials for the removal of varying contaminants. The adsorbents showed high removal efficiency for all three contaminants in aqueous solution. The efficiency was more for dyes in comparison to simazine herbicide. This was revealed by the batch adsorption experiments of the

individual contaminants. The highest observed efficiencies for simazine, methyl violet and brilliant green were 71.3, 87.7 and 88.8% respectively. Moreover, the adsorbents also showed reusability and desorption capacity in all contaminants after three runs. These are ideal properties of good adsorbents. Therefore, this adsorbent can be considered as alternate adsorbents for these and other organic contaminants. Based on the results obtained in this study, application of this adsorbent to real industrial wastewater and for the removal of many more other organic contaminants from wastewater are recommended.



University of Fort Hare
Together in Excellence

Appendix I

Data for simazine removal

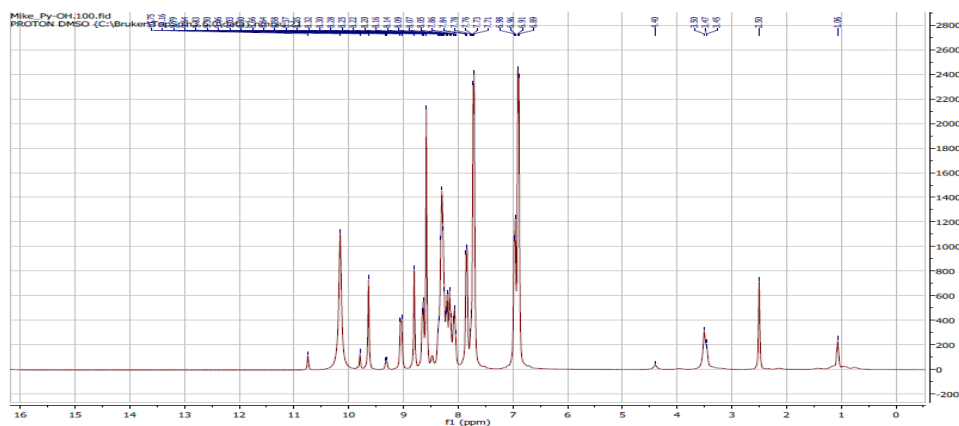


Figure A-I.1: ^1H NMR spectrum of pyrene ligand.

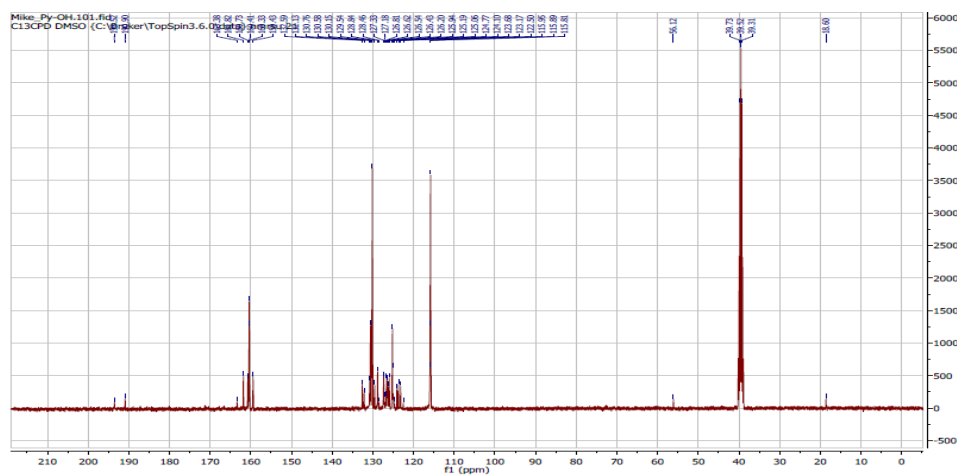


Figure A-I.2: ^{13}C NMR spectrum of pyrene ligand.

Table A-I.1: Data for point of zero charge (solution volume = 20 ml, salt concentration = 0.1M, adsorbent dose = approximately = 20 mg, temperature = $20 \pm 2^\circ\text{C}$ and shaking period = 6 hr).

pHi	ΔpH
2.11	3.64
2.99	2.81
4.02	2.09
5.13	1.10
6.02	-0.120
7.15	-0.620
8.05	-1.62
9.01	-2.56

Table A-I.2: Data for GC/ECD calibration

Concentration level	Area (A.U)
1	69039
2	100650
3	122320
4	143040
5	170030

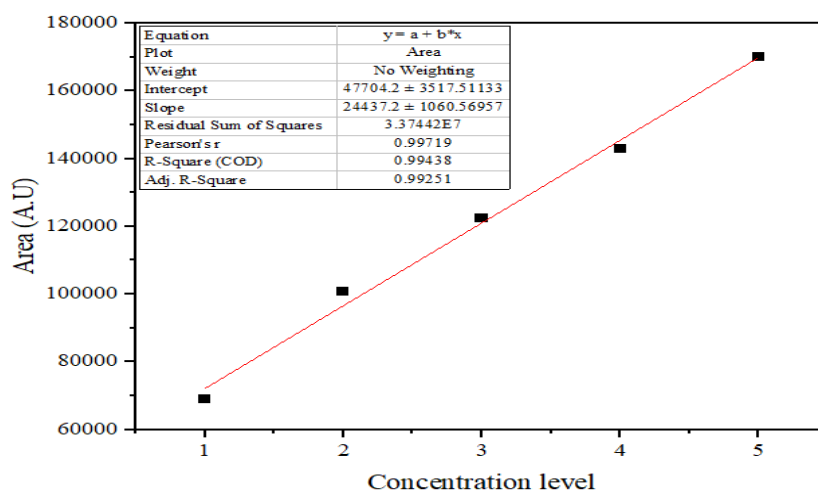


Figure A-I.3: GC/ECD calibration curve.

University of Fort Hare

Table A-I.3: pH effect data (adsorbate concentration = 0.313 mg/L, adsorbent dose at approximately = 20.0 mg, temperature = $20 \pm 2^\circ\text{C}$ and shaking time = 360 minutes).

pH	C _i (mg/L)	C _e (mg/L)	Dose (g)	Volume (L)	%adsorbed
2.30	0.313	0.0810	0.0200	0.0200	71.3
3.00	0.313	0.191	0.0204	0.0200	39.0
4.10	0.313	0.201	0.0198	0.0200	35.9
4.90	0.313	0.188	0.0195	0.0200	40.0
6.00	0.313	0.234	0.0200	0.0200	25.2
7.40	0.313	0.208	0.0201	0.0200	33.5
8.30	0.313	0.250	0.0204	0.0200	20.2
9.00	0.313	0.303	0.0199	0.0200	3.07

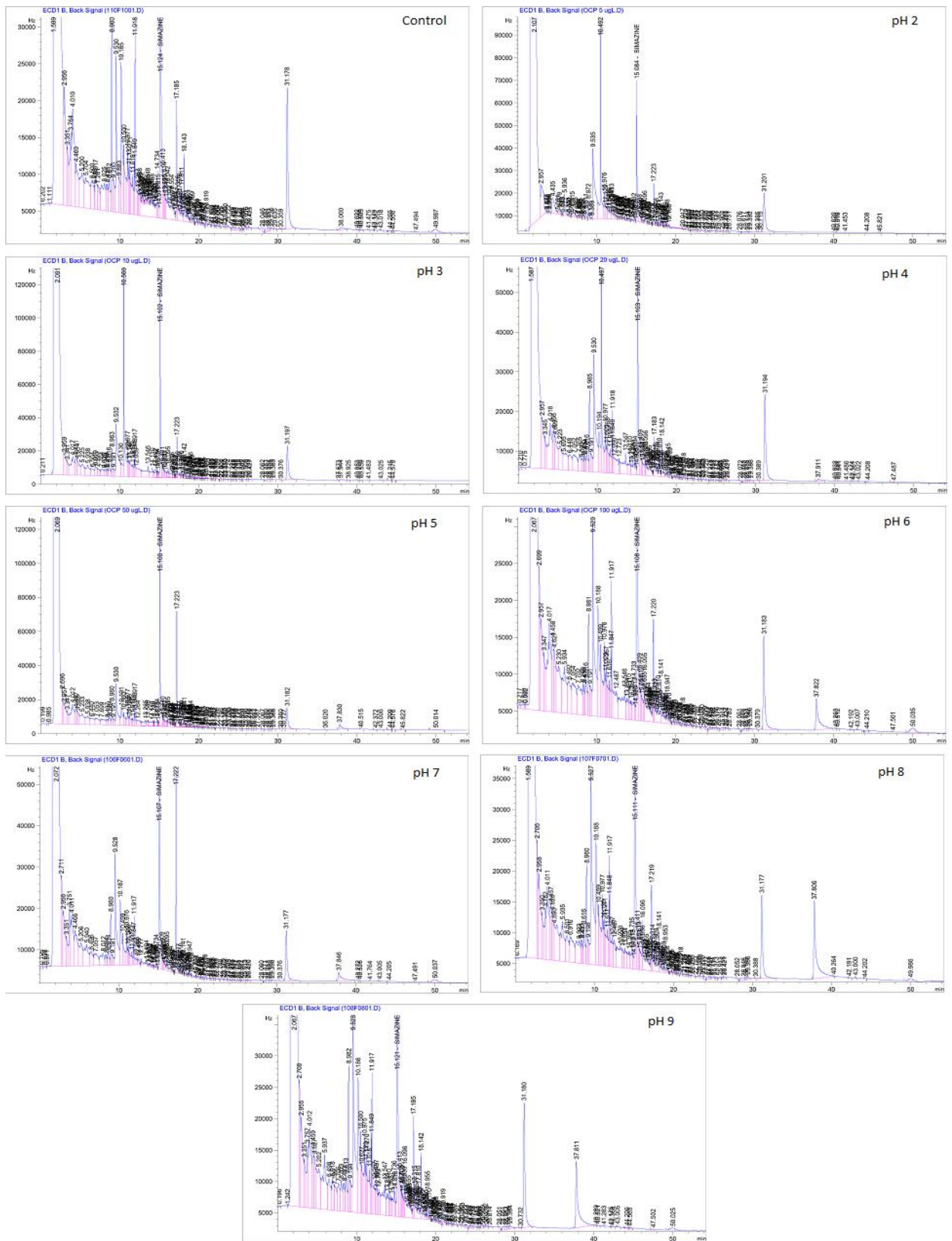


Figure A-I.4: Effect of pH chromatograms.

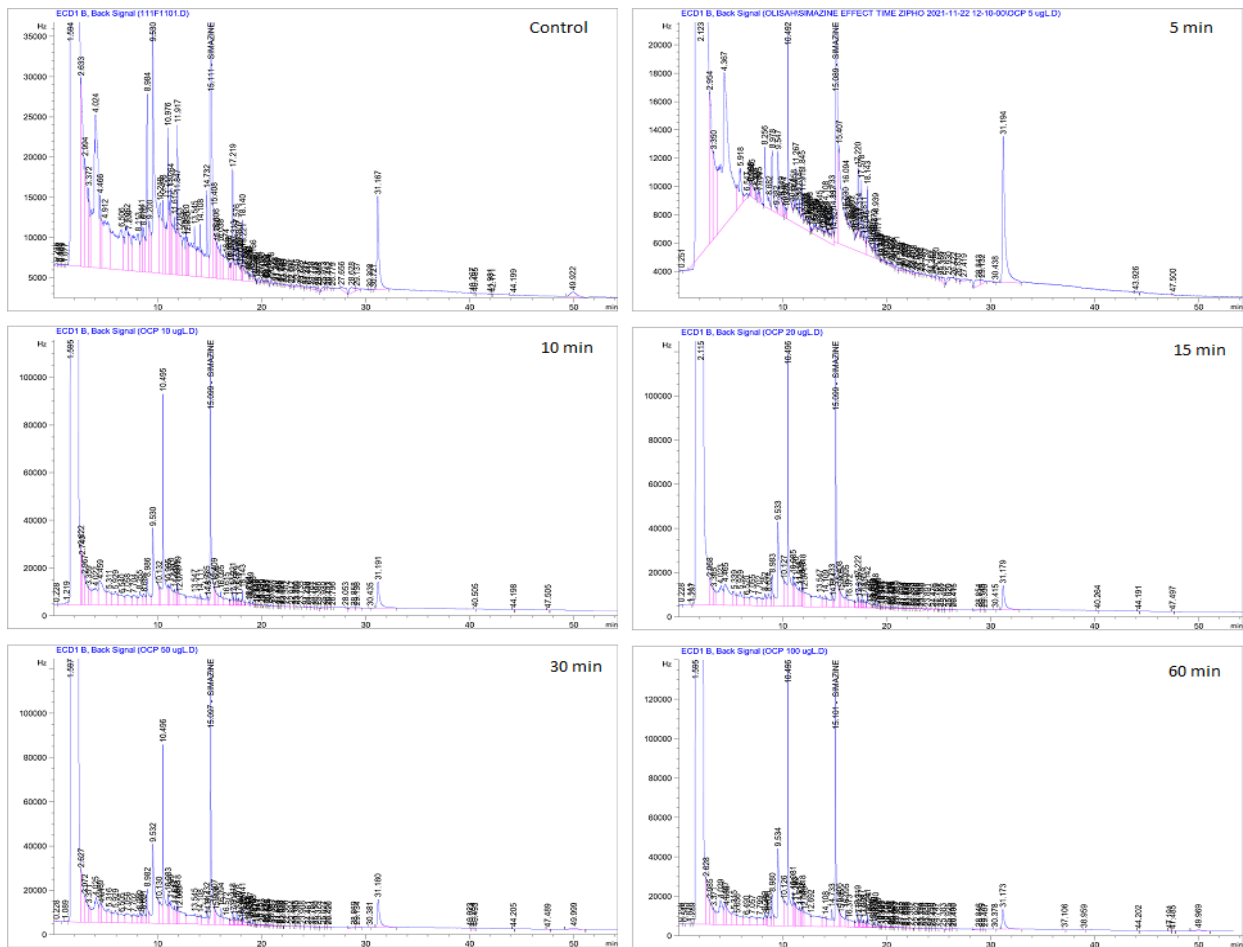
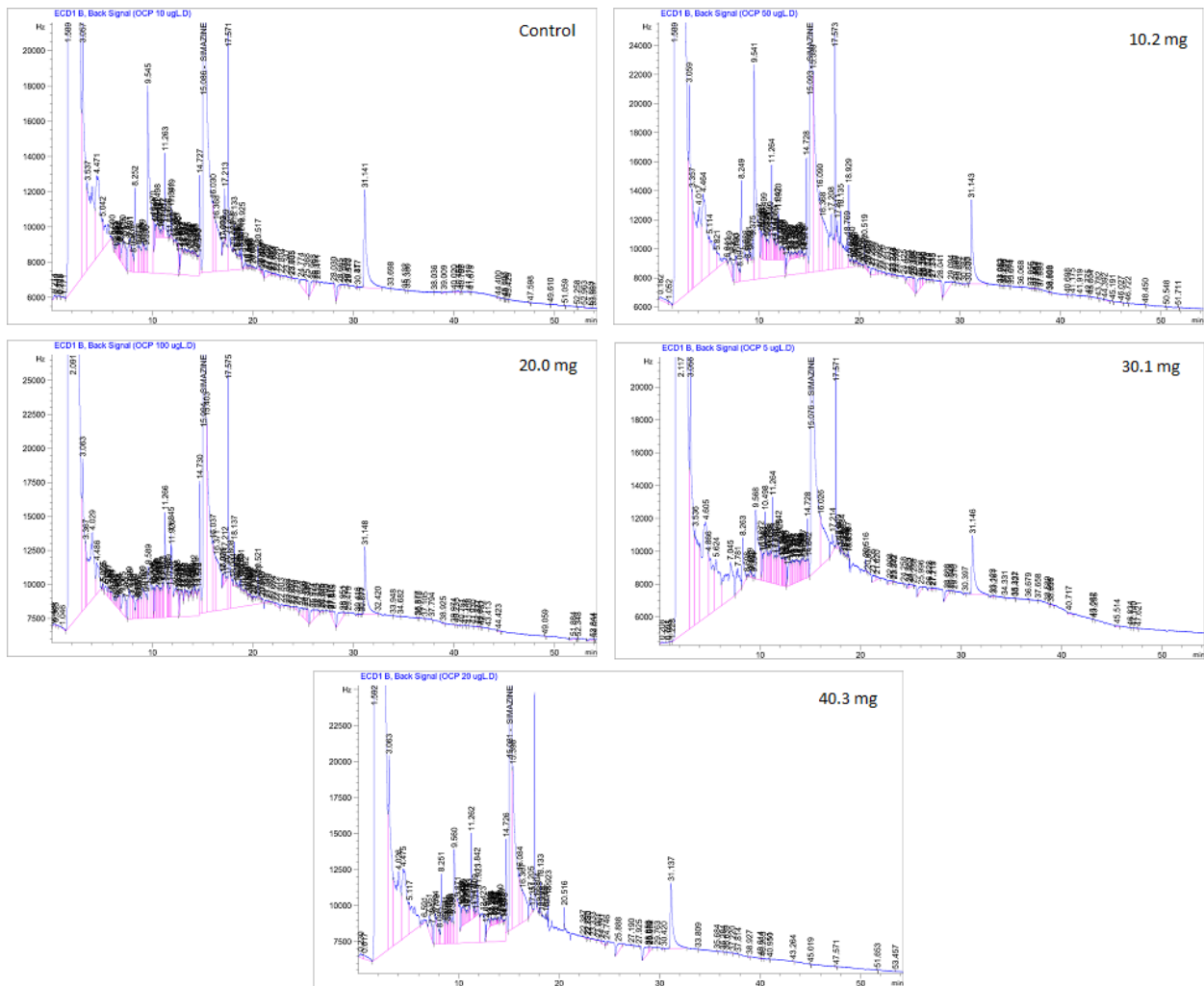


Figure A-I.5: Effect of contact time chromatograms.

University of Fort Hare
Together in Excellence

Table A-I.4: Effect of contact time data (solution pH = 2, adsorbent dose at approximately = 20.0 mg, adsorbate concentration = 0.281 mg/L and the temperature at $20 \pm 2^\circ\text{C}$).

Contact time (min)	C _i (mg/L)	C _e (mg/L)	Dose (g)	Volume (L)	Q _e (mg/g)
5.00	0.281	0.146	0.0199	0.0200	137
10.0	0.281	0.201	0.0201	0.0200	80.1
15.0	0.281	0.216	0.0196	0.0200	66.6
30.0	0.281	0.212	0.0201	0.0200	69.1
60.0	0.281	0.232	0.0198	0.0200	49.5



University of Fort Hare
Together in Excellence

Figure A-I.6: Effect of adsorbent amount chromatograms.

Table A-I.5: Effect of adsorbent amount data (solution pH = 2, Temperature = $20 \pm 2^\circ\text{C}$, adsorbate concentration = 0.312 mg/L and shaking time = 60 minutes).

Adsorbent amount (mg)	Ci (mg/L)	Ce (mg/L)	Volume (L)	%adsorbed
10.2	0.312	0.277	0.020	11.3
20.0	0.312	0.274	0.020	12.3
30.1	0.312	0.244	0.020	21.9
40.3	0.312	0.217	0.020	30.3

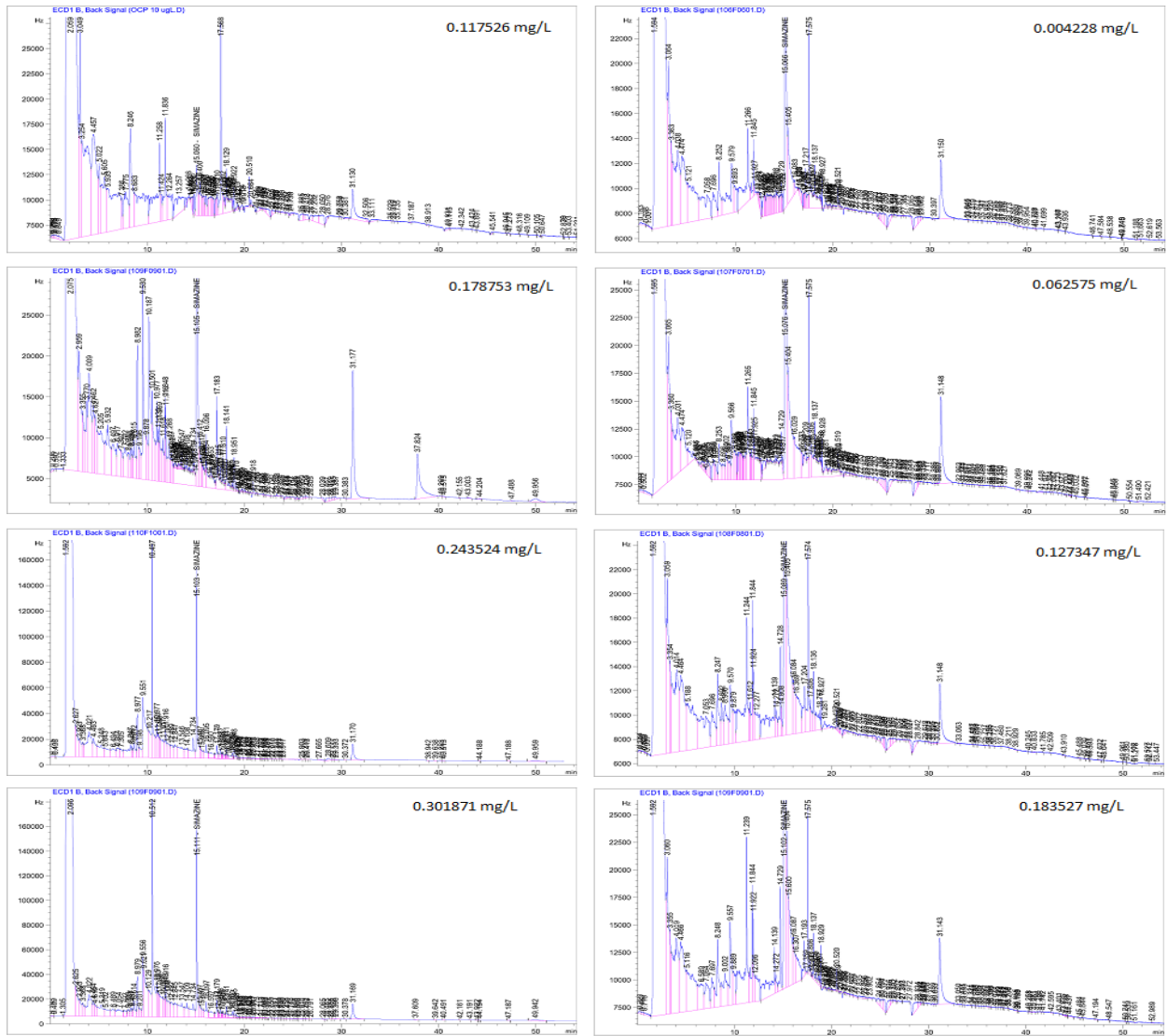


Figure A-I.7: Effect of adsorbate concentration chromatograms.

Table A-I.6: Effect of adsorbate concentration data ((Temperature = $20 \pm 2^\circ\text{C}$, shaking period = 60 minutes, adsorbent dose at approximately = 20 mg and pH = 2).

C_i (mg/L)	C_e (mg/L)	Dose (g)	Volume (L)	q_e (mg/g)
0.118	0.00423	0.0201	0.0200	0.113
0.179	0.0626	0.0201	0.0200	0.116
0.244	0.127	0.0199	0.0200	0.117
0.302	0.184	0.0202	0.0200	0.117

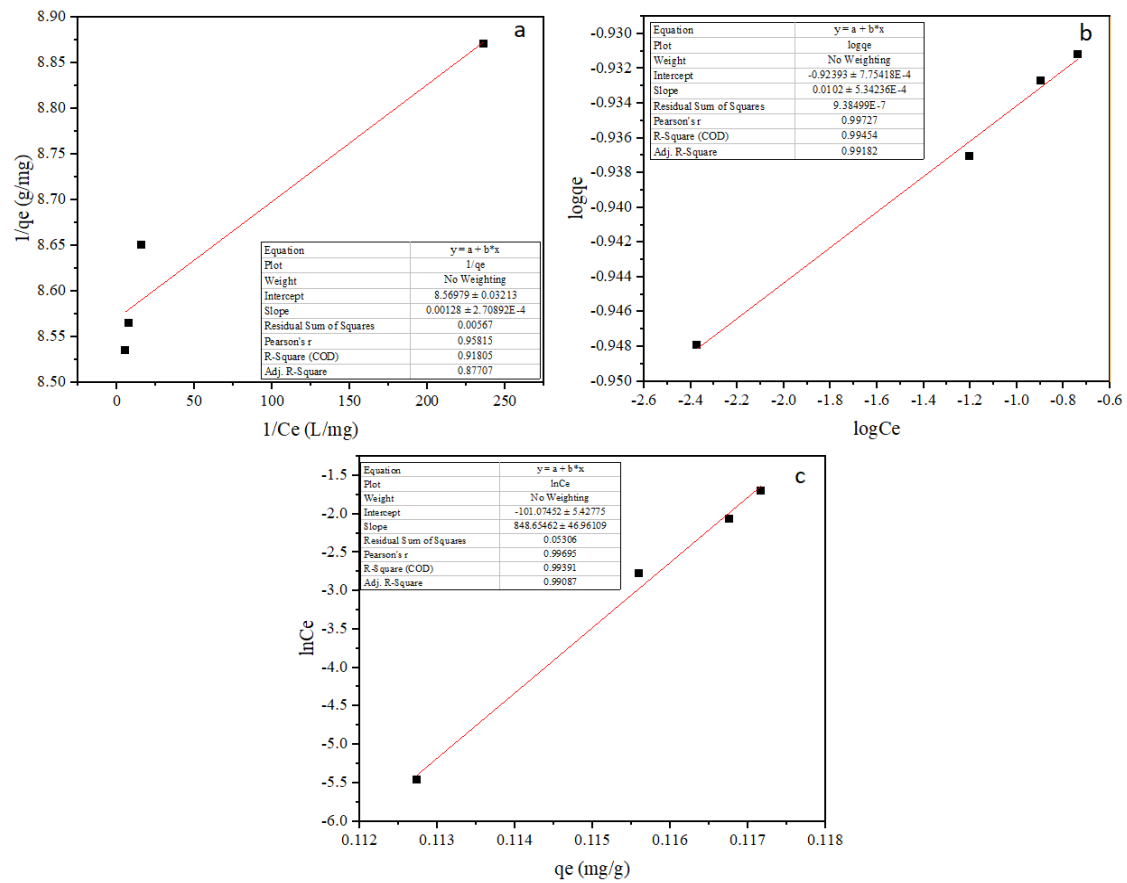


Figure A-I.8: Adsorption isotherm models curves.

University of Fort Hare
Together in Excellence

Table A-I.7: Adsorption isotherms data.

C_i (mg/L)	C_e (mg/L)	Dose (g)	Volume (L)	q_e (mg/g)	$1/C_e$ (L/mg)	$1/q_e$ (g/mg)	$\log C_e$	$\text{Log} q_e$	q_e (mg/g)	$\ln C_e$
0.118	0.00423	0.0201	0.0200	0.113	236	8.87	-2.37	-0.948	0.113	-5.47
0.179	0.0626	0.0201	0.0200	0.116	16.0	8.65	-1.20	-0.937	0.116	-2.77
0.244	0.127	0.0199	0.0200	0.117	7.85	8.56	-0.895	-0.933	0.117	-2.06
0.302	0.184	0.0202	0.0200	0.117	5.45	8.53	-0.736	-0.931	0.117	-1.70

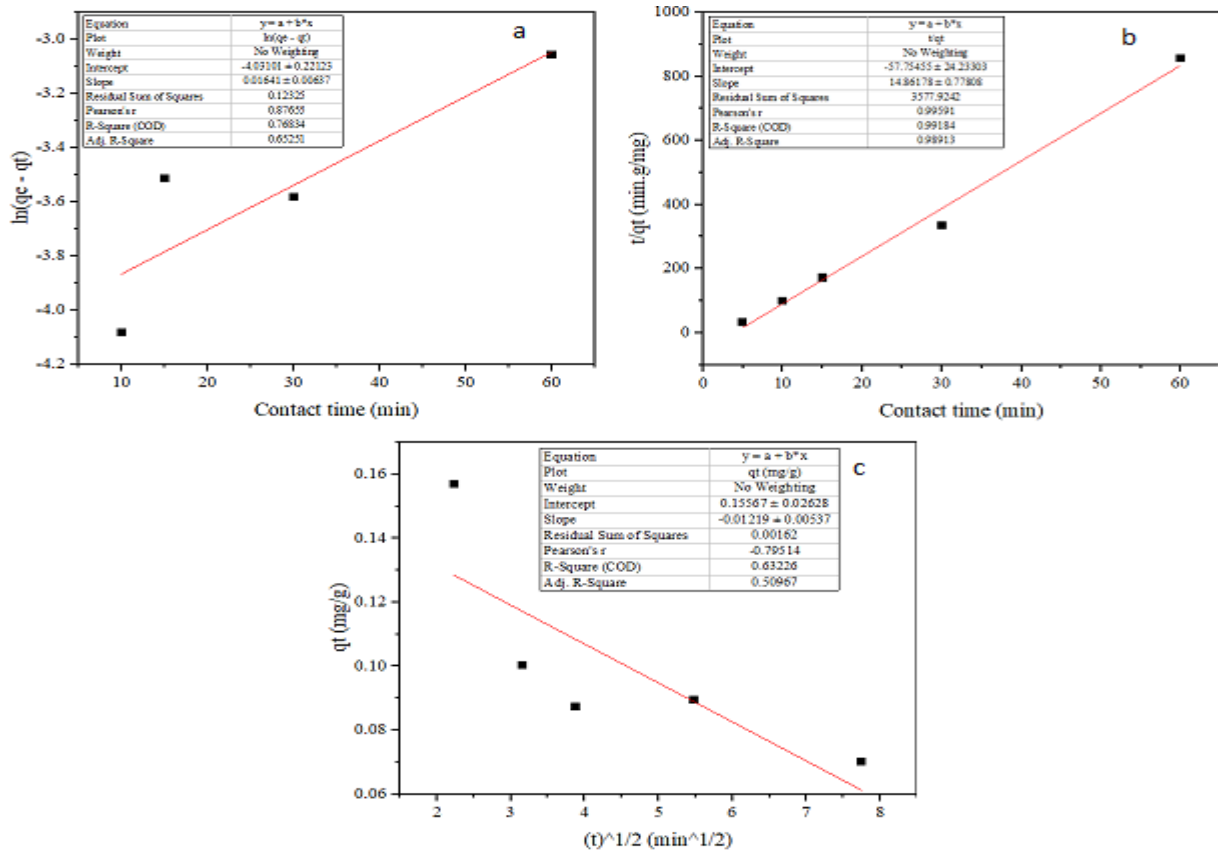


Figure A-I.9: Adsorption kinetic models curves.



University of Fort Hare

Table A-I.8: Adsorption kinetics models data.

Contact time (min)	C_i (mg/L)	C_e (mg/L)	Dose (g)	Volume (L)	q_t (mg/g)	q_e (mg/g)	$\ln(q_e - q_t)$	t/q_t (min.g/mg)	$t^{1/2}$ (min ^{1/2})
5	0.302	0.146	0.0199	0.0200	0.157	0.117	-	31.8	2.24
10	0.302	0.201	0.0201	0.0200	0.100	0.117	-4.08	99.7	3.16
15	0.302	0.216	0.0196	0.0200	0.0874	0.117	-3.51	172	3.87
30	0.302	0.212	0.0201	0.0200	0.0894	0.117	-3.58	336	5.48
60	0.302	0.232	0.0198	0.0200	0.0701	0.117	-3.06	856	7.75

Table A-I.9: Reusability and desorption studies data.

Ci (mg/L)	Ce (mg/L)	Ca (mg/L)	Dose (g)	Volume (L)	%adsorbed	Recovered dose (g)	Cd (mg/L)	%desorbed
0.473	0.245	0.229	0.0299	0.0200	48.26877	0.0299	0.00910	3.98
0.473	0.304	0.169	0.0299	0.0200	35.79497	0.0299	-	-
0.473	0.321	0.152	0.0300	0.0200	32.14462	0.0300	-	-



University of Fort Hare
Together in Excellence

Appendix II

Data for methyl violet removal.

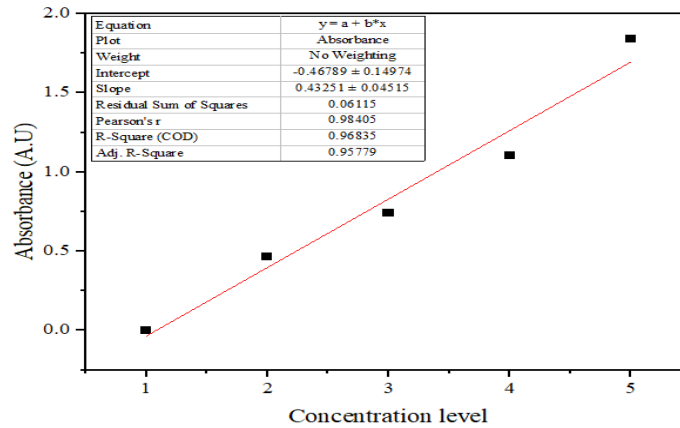


Figure A-II.1: pH effect calibration curve.

Table A-II.1: UV-Vis calibration data for pH effect.

Concentration level	Absorbance (A.U)
0	0.0001
5	0.4634
10	0.7394
15	1.1027
20	1.8428

Table A-II.2: pH effect data (dose at approximately = 40.0 mg, MV concentration = 40 mg/dm³, contact time = 360 min and temperature = 20 ± 2°C).

pH	Ci (mg/L)	Ce (mg/L)	Dose (g)	Volume (L)	% Adsorbed
2.04	14.6	10.46	0.0408	0.0500	28.5
3.04	14.6	3.80	0.0408	0.0500	74.1
3.99	14.6	1.99	0.0404	0.0500	86.4
5.01	14.6	0.264	0.0402	0.0500	82.0
6.03	14.6	2.24	0.0406	0.0500	84.7
7.04	14.6	1.94	0.0410	0.0500	86.8
8.01	14.6	1.88	0.0408	0.0500	87.2
9.02	14.6	2.10	0.0398	0.0500	85.7
9.99	14.6	1.32	0.0398	0.0500	91.0

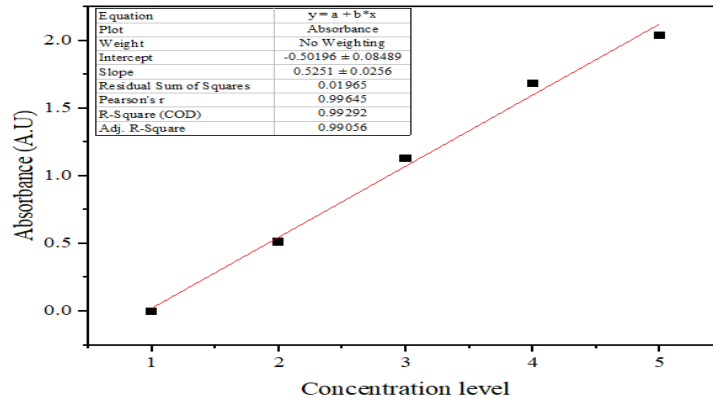


Figure A-II.2: Effect of contact time calibration curve.

Table A-II.3: UV-Vis calibration data for for contact time effect.

Concentration level	Absorbance (A.U)
1	0.0001
2	0.512
3	1.1307
4	1.6846
5	2.0393

Table A-II.4: Effect of contact time data (dose at approximately = 40.0 mg, concentration = 25.9 mg/dm³, pH = 6.5 and temperature = 20 ± 2°C).

contact time (min)	C _i (mg/L)	C _f (mg/L)	dose (g)	Volume (L)	q _e (mg/L)
5	25.9	20.8	0.0404	0.0500	6.40
15	25.9	20.8	0.0408	0.0500	6.3
30	25.9	19.6	0.0402	0.0500	7.85
60	25.9	20.1	0.0398	0.0500	7.4
105	25.9	18.8	0.0394	0.0500	9.1
165	25.9	12.0	0.0408	0.0500	17.1
225	25.9	9.10	0.0410	0.0500	20.6
285	25.9	9.11	0.0402	0.0500	21.0
360	25.9	3.20	0.0396	0.0500	28.7

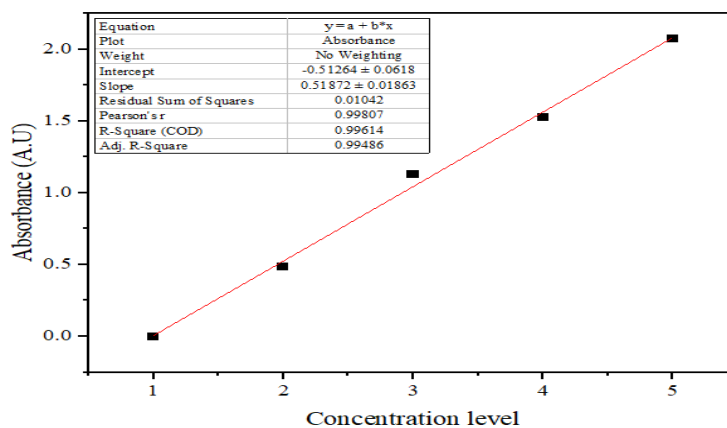


Figure A-II.3: Dose effect calibration curve.

Table A-II.5: UV-Vis calibration data for dose effect.

Concentration level	Absorbance (A.U)
0	-0.0002
5	0.4871
10	1.1307
15	1.5261
20	2.0739

Table A-II.6: Dose effect data (MV concentration = 30.0 mg/dm³, pH= 6.5, temperature = 20 ± 2°C and contact time = 360 min)

Adsorbent amount (mg)	C _i (mg/L)	C _e (mg/L)	Volume (L)	%adsorbed
80.2	30.0	6.22	0.050	71.25057
40.6	30.0	13.5	0.050	38.96009
19.8	30.0	21.8	0.050	35.93033
10.4	30.0	23.1	0.050	39.98177

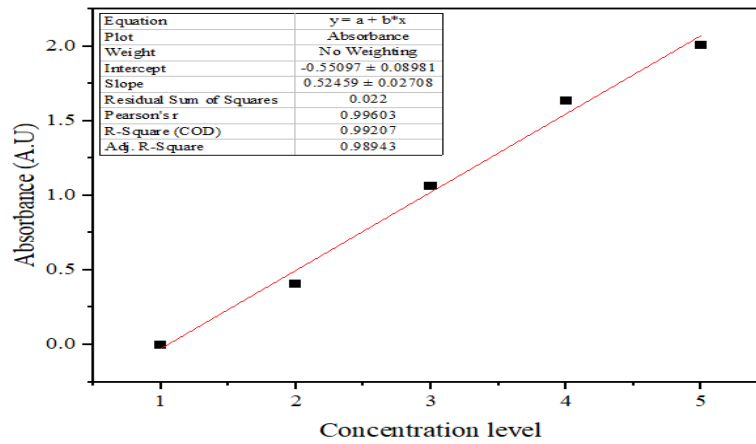


Figure A-II.4: Effect of adsorbate concentration calibration curve.

Table A-II.7: UV-Vis calibration data for adsorbate concentration effect.

Concentration level	Absorbance (A.U)
1	-0.0012
2	0.4094
3	1.0611
4	1.6365
5	2.0082
6	2.7124

University of Fort Hare
Together in Excellence

Table A-II.8: Effect of adsorbate concentration data (contact time = 360 min, dose at approximately = 40 mg temperature = 20 ± 2°C and pH = 6.5).

C _i (mg/L)	C _e (mg/L)	Dose (g)	Volume (L)	q _e (mg/g)
7.25	1.27	0.0400	0.0500	0.223
21.2	4.81	0.0408	0.0500	0.120
40.2	20.1	0.0396	0.0500	0.114
54.2	34.6	0.0390	0.0500	0.128

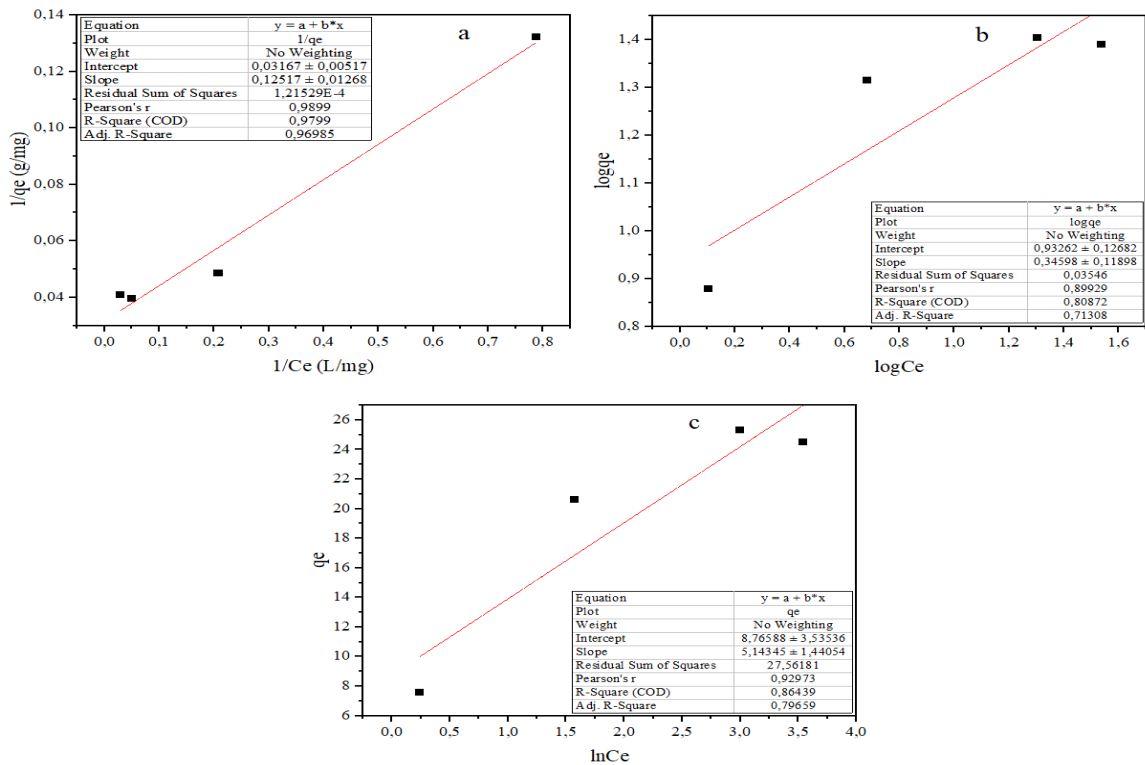


Figure A-II.5: Adsorption isotherms of (a) Langmuir (b) Freundlich and (c) Temkin.

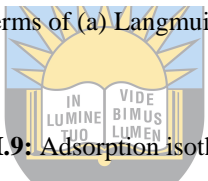


Table A-II.9: Adsorption isotherms data.

C _i (mg/L)	C _e (mg/L)	volume (L)	Dose (g)	q _e (mg/g)	1/C _e (L/mg)	1/q _e (g/mg)	logC _e	Logq _e	q _e (mg/g)	lnC _e
7.25	1.27	0.0500	0.0396	7.56	0.787	0.132	0.104	0.878	7.56	0.239
21.2	4.81	0.0500	0.0398	20.6	0.208	0.0485	0.682	1.31	20.6	1.57
40.2	20.1	0.0500	0.0396	25.3	0.0498	0.0395	1.30	1.40	25.3	3.00
54.2	34.6	0.0500	0.0400	24.5	0.0289	0.0408	1.54	1.39	24.5	3.54

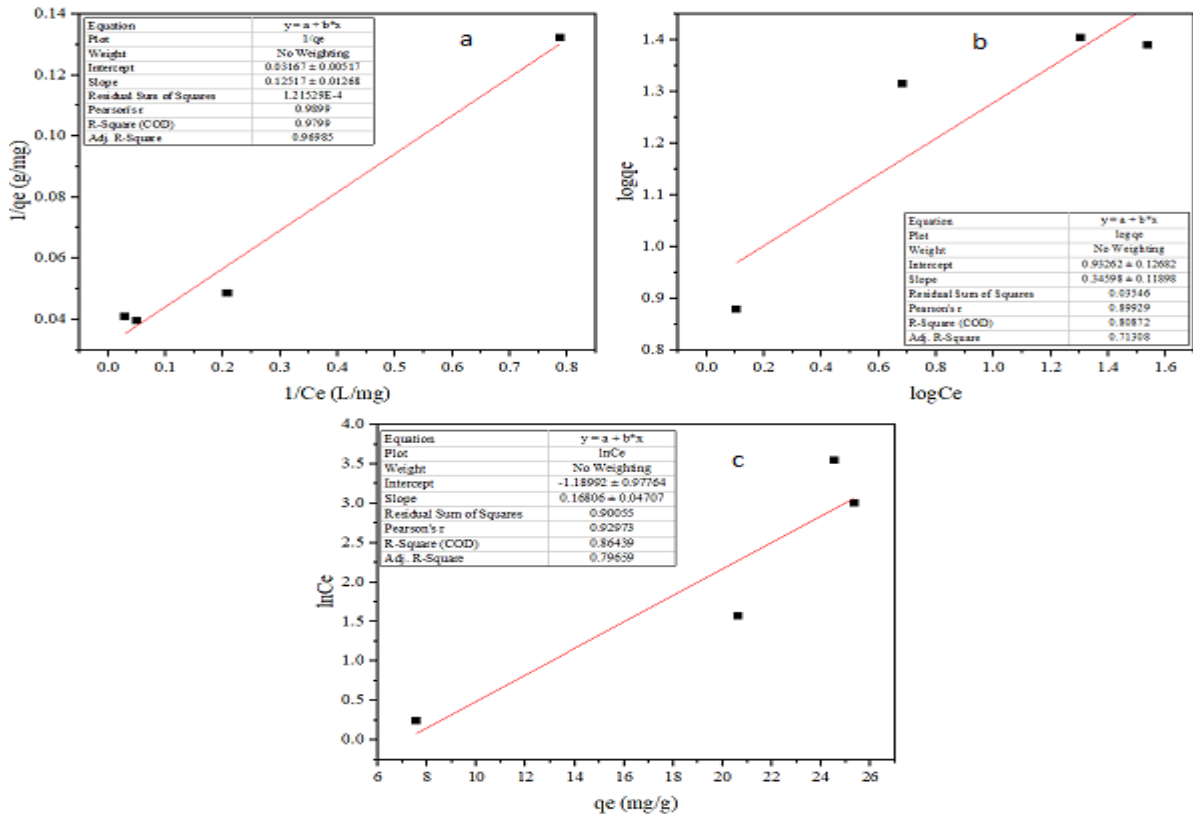


Figure A-II.6: Adsorption kinetic models curves.



Table A-II.10: Adsorption kinetic models data.

contact time	C_i (mg/L)	C_e (mg/L)	$C_i - C_e$ (mg/L)	volume (L)	Dose (g)	qt (mg/g)	q_e (mg/g)	$\ln(q_e - qt)$	t/qt (min.g/mg)	$t^{1/2}$ (min ^{1/2})
5	21.2	20.8	0.454	0.0500	0.0404	0.562	20.6	3.00	8.90	2.24
15	21.2	20.8	0.405	0.0500	0.0408	0.497	20.6	3.00	30.2	3.87
30	21.2	19.6	1.58	0.0500	0.0402	1.97	20.6	2.93	15.2	5.48
60	21.2	20.1	1.17	0.0500	0.0398	1.47	20.6	2.95	40.8	7.75
105	21.2	18.8	2.43	0.0500	0.0394	3.08	20.6	2.86	34.1	10.2
165	21.2	12.0	9.22	0.0500	0.0408	11.3	20.6	2.23	14.6	12.8
225	21.2	9.10	12.1	0.0500	0.0410	14.8	20.6	1.76	15.2	15.0
285	21.2	9.11	12.1	0.0500	0.0402	15.1	20.6	1.72	18.9	16.9
360	21.2	3.20	18.0	0.0500	0.0396	22.8	20.6	-	15.8	19.0

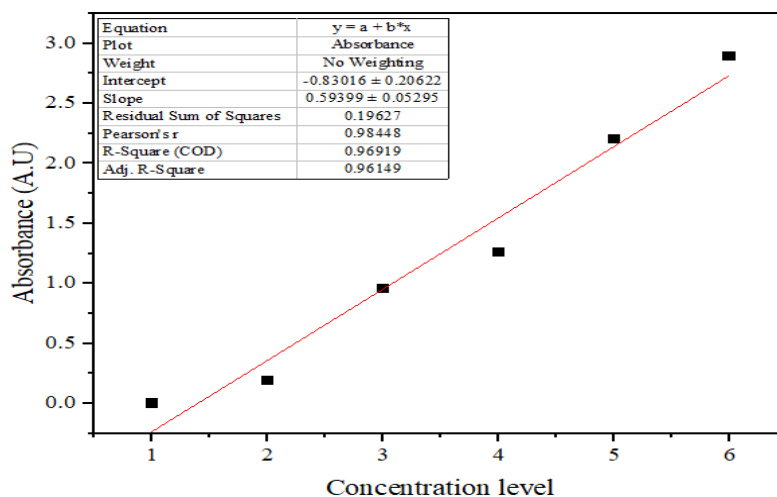


Figure A-II.7: UV-Vis reusability and desorption calibration curve.

Table A-II.11: UV-Vis reusability and desorption calibration data.

Concentration level	Absorbance (A.U)
1	-0.0004
2	0.1884
3	0.9571
4	1.2563
5	2.2017
6	2.8897

Table A-II.12: Reusability and desorption studies data.

C _i (mg/L)	C _e (mg/L)	C _i - C _e (mg/L)	Dose (g)	Volume (L)	%adsorbed	Recovered dose (mg)	C _d (mg/L)	%Desorbed
44.0	6.78	37.3	0.0392	0.0400	84.6	0.0374	3.14	8.43
44.0	20.9	23.3	0.0390	0.0400	52.8	0.02224	12.3	53.1
44.0	15.3	28.8	0.0392	0.0400	65.3	0.0312	28.8	100

Appendix III

Data for brilliant green removal

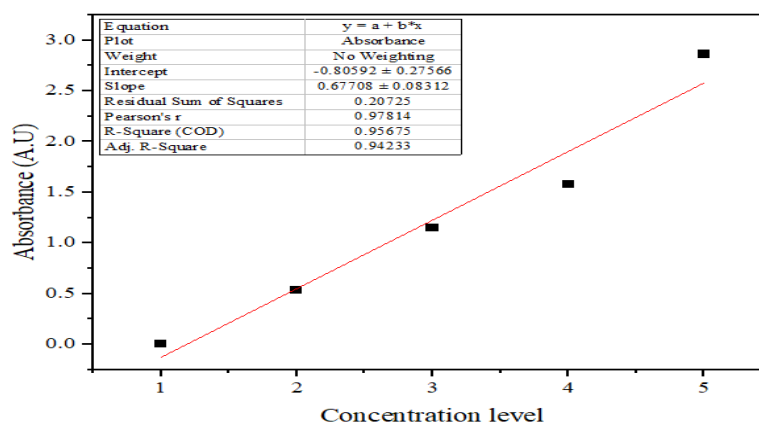


Figure A-III.1: Influence of pH calibration curve.

Table A-III.1: UV-Vis calibration data for pH influence.

concentration level	Absorbance (A.U)
1	0.0004
2	0.5363
3	1.1455
4	1.5809
5	2.8635

Table A-III.2: Influence of pH data (contact time = 6hr, adsorbent dose at approximately = 40 mg, adsorbate concentration = 34.6 mg/L and temperature = $20 \pm 2^\circ\text{C}$).

pH	Ci (mg/L)	Cf (mg/L)	dose (g)	Volume (L)	%adsorbed
2.04	34.6	16.9	0.0388	0.0500	51.1
3	34.6	2.83	0.0392	0.0500	91.8
3.99	34.6	1.67	0.0404	0.0500	95.2
5.13	34.6	1.31	0.0406	0.0500	96.2
6.03	34.6	1.30	0.0398	0.0500	96.2
7.01	34.6	0.816	0.0402	0.0500	97.6
7.95	34.6	1.09	0.039	0.0500	96.9
9.14	34.6	0.682	0.0408	0.0500	98.0

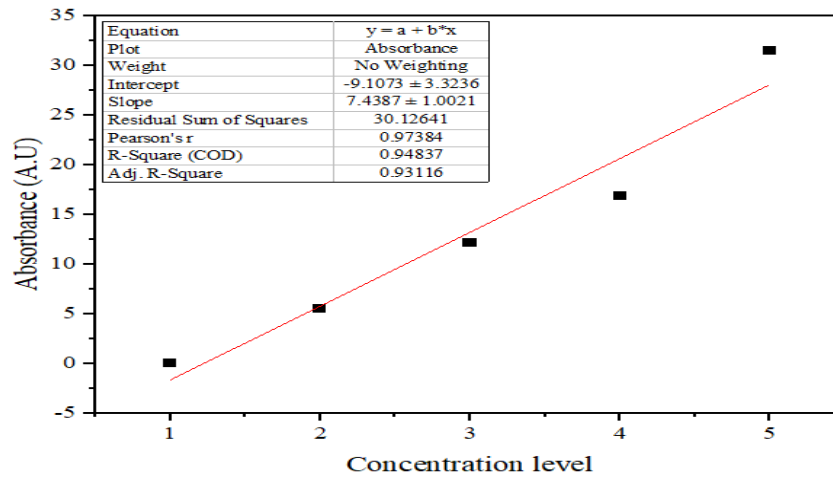


Figure A-III.2: Influence of contact time calibration curve.

Table A-III.3: UV-Vis calibration data for contact time influence.

concentration level	Absorbance (A.U)
1	0.002
2	5.531
3	12.114
4	16.872
5	31.525

Table A-III.4: Influence of contact time data (pH = 6.5, adsorbent dose approximately = 40 mg, adsorbate concentration = 40.4 mg/L and temperature = $20 \pm 2^\circ\text{C}$).

Contact time (min)	Ci (mg/L)	Cf (mg/L)	Dose (g)	Volume (L)	qe (mg/g)
5	40.4	37.4	0.0404	0.05	3.62
15	40.4	36.2	0.0396	0.05	5.22
30	40.4	37.3	0.0398	0.05	3.85
60	40.4	34.7	0.0396	0.05	7.18
105	40.34	20.3	0.04	0.05	25.0
165	40.4	20.6	0.0406	0.05	24.4
225	40.4	10.1	0.0404	0.05	37.5
285	40.4	6.5	0.0412	0.05	41.1
360	40.4	3.70	0.0404	0.05	45.4

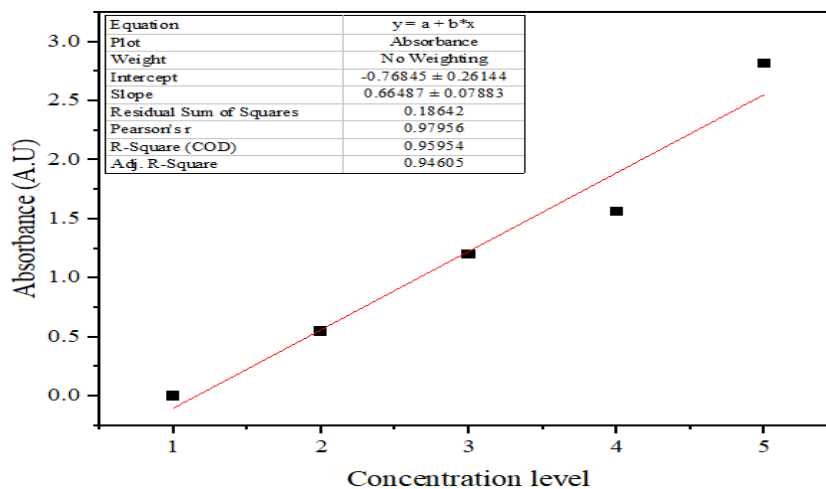


Figure A-III.3: Influence of adsorbent amount calibration curve.

Table A-III.5: UV-Vis calibration data for adsorbent amount influence.

concentration level	Absorbance (A.U)
1	0.0001
2	0.5474
3	1.2033
4	1.5637
5	2.8163

University of Fort Hare
Together in Excellence

Table A-III.6: Influence of adsorbent amount data (pH = 6.5, adsorbate concentration = 40 mg/L, contact time = 360 minutes and temperature = $20 \pm 2^\circ\text{C}$).

dose (mg)	C _i (mg/L)	C _f (mg/L)	volume (L)	%adsorbed
10	40.0	32.9	0.05002	17.8
19.6	40.0	25.9	0.0500	35.2
39.6	40.0	4.71	0.0500	88.2
79.8	40.0	4.47	0.0500	88.8

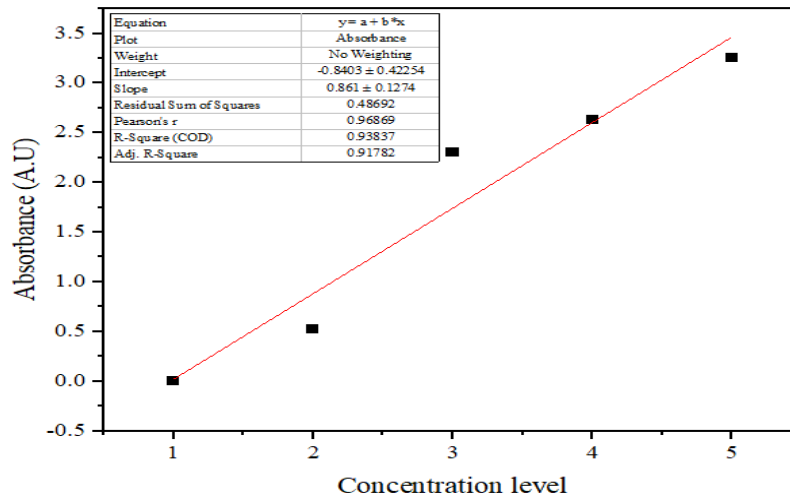


Figure A-III.4: Influence of adsorbate concentration calibration curve.

Table A-III.7: UV-Vis calibration data for adsorbate concentration influence.

concentration level	Absorbance (A.U)
1	0
2	0.5259
3	2.3022
4	2.6349
5	3.2505

Table A-III.8: Influence of adsorbate concentration data (pH = 6.5, contact time = 360 minutes, adsorbent dose at approximately = 40 mg and temperature = $20 \pm 2^\circ\text{C}$).

C_i (mg/L)	C_f (mg/L)	Dose (g)	volume (L)	% adsorbed	q_e (mg/g)
10.2	6.01	0.0400	0.0500	41.0	5.22
20.0	9.41	0.0402	0.0500	53.0	13.2
52.7	12.7	0.0402	0.0500	75.8	49.7
65.0	14.9	0.0408	0.0500	77.1	61.5

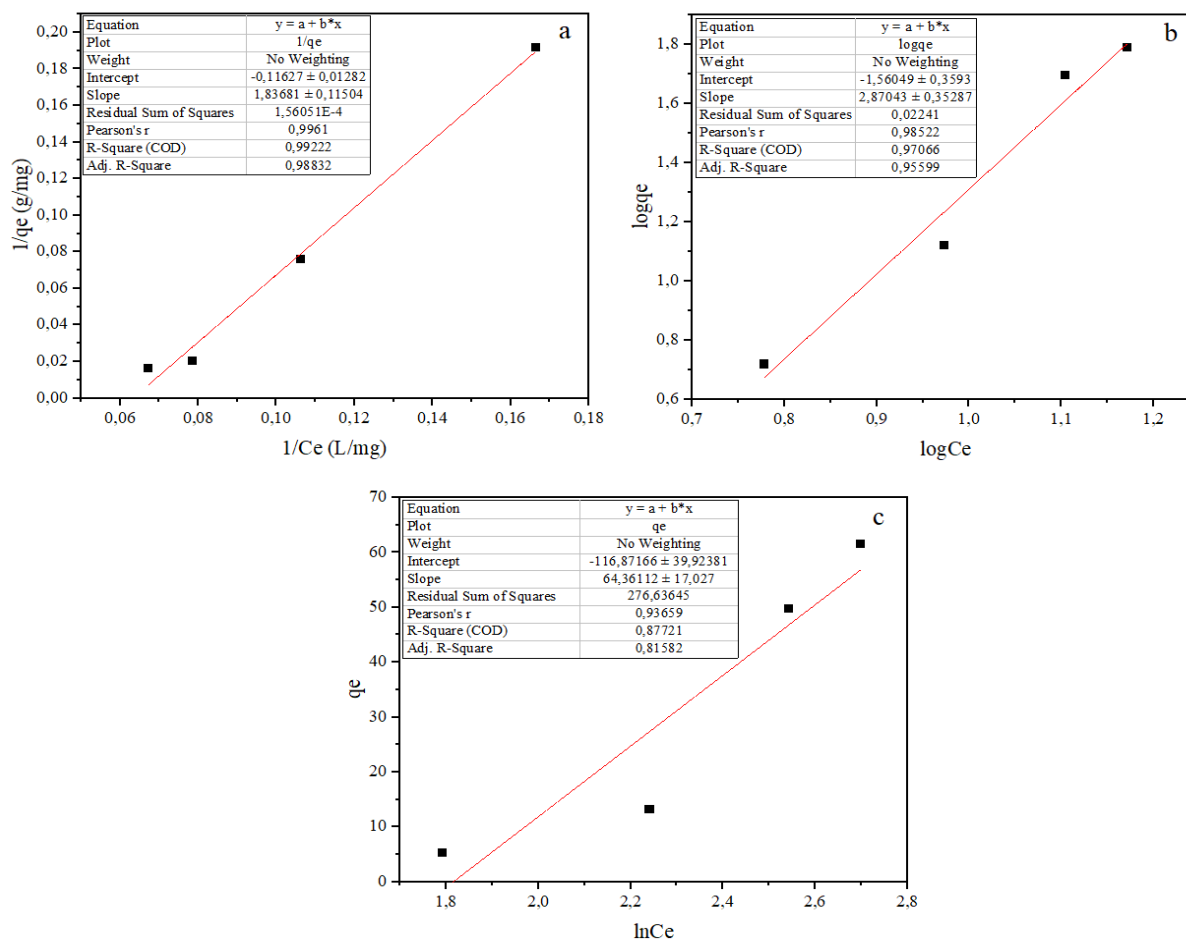


Figure A-III.5: Adsorption isotherms of (a) Langmuir (b) Freundlich and (c) Temkin.

Table A-III.9: Adsorption isotherms data.

C_i (mg/L)	C_e (mg/L)	Volume (L)	Dose (mg)	Q_e (mg/L)	$1/C_e$ (L/mg)	$1/q_e$ (g/mg)	$\log C_e$	$\log q_e$	q_e (mg/L)	$\ln C_e$
10.2	6.01	0.0500	0.0400	5.22	0.166	0.192	0.779	0.718	5.22	1.79
20.0	9.41	0.0500	0.0402	13.2	0.106	0.0759	0.973	1.12	13.2	2.24
52.7	12.7	0.0500	0.0402	49.7	0.0786	0.0201	1.10	1.70	49.7	2.54
65.0	14.9	0.0500	0.0408	61.5	0.0673	0.0163	1.17	1.79	61.5	2.70

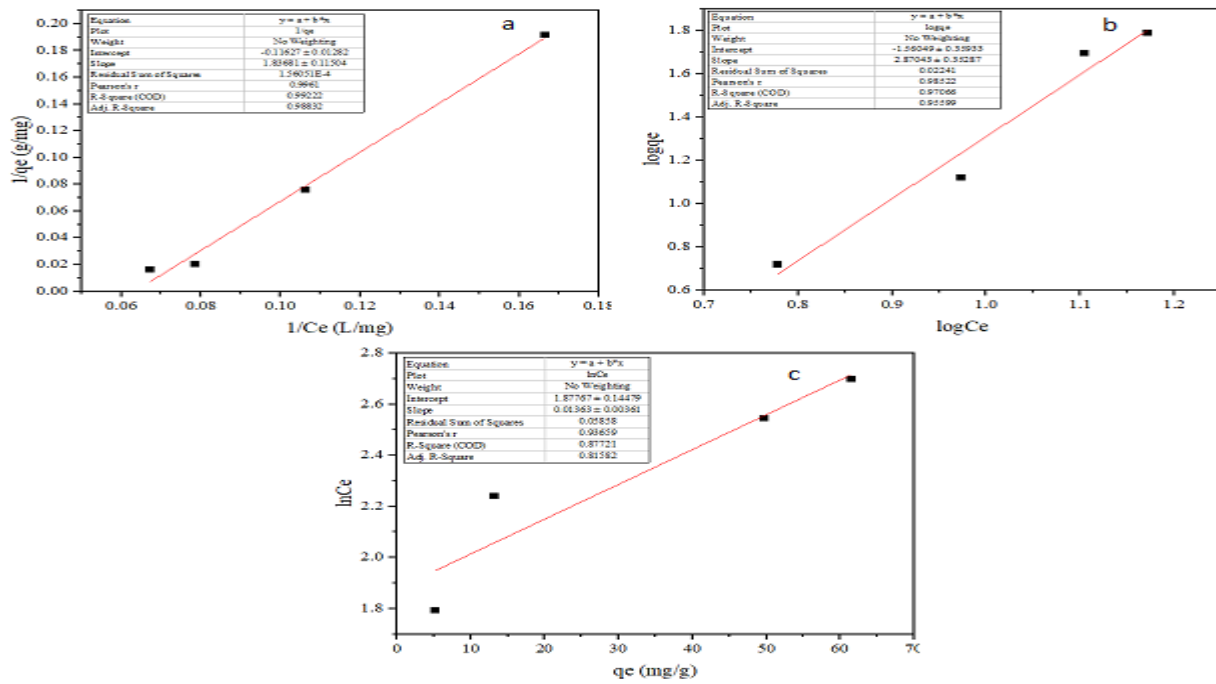


Figure A-III.6: Adsorption kinetic models curves.



Table A-III.10: Adsorption kinetics models data.

contact time (min)	Ci (mg/L)	Ce (mg/L)	volume (L)	Dose (g)	qt (mg/g)	qe (mg/g)	ln(qe - qt)	t/qt (min.g/mg)	t ^{1/2} (min ^{1/2})
5	20.0	18.7	0.0500	0.0404	1.59	13.2	2.45	3.15	2.24
15	20.0	18.1	0.0500	0.0396	2.38	13.2	2.38	6.30	3.87
30	20.0	18.6	0.0500	0.0398	1.70	13.2	2.44	17.7	5.48
60	20.0	17.3	0.0500	0.0396	3.36	13.2	2.28	17.8	7.75
105	20.0	10.2	0.0500	0.0400	12.3	13.2	0.130	8.54	10.2
165	20.0	10.3	0.0500	0.0406	12.0	13.2	0.194	13.8	12.8
225	20.0	5.03	0.0500	0.0404	18.5	13.2	-	12.1	15.0
285	20.0	3.25	0.0500	0.0412	20.3	13.2	-	14.0	16.9
360	20.0	1.85	0.0500	0.0404	22.5	13.2	-	16.0	19.0

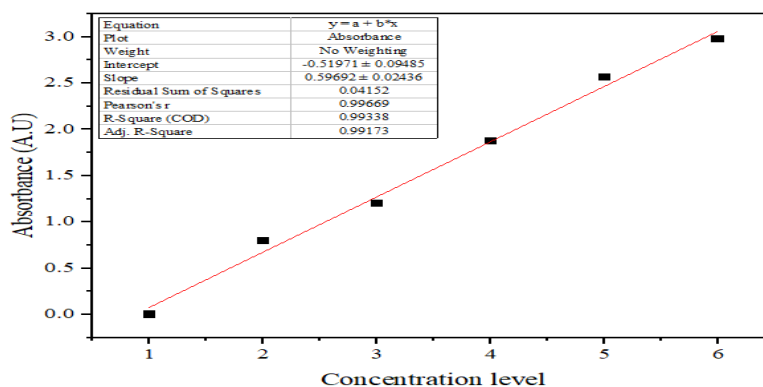


Figure A-III.7: UV-Vis reusability and desorption calibration curve.

Table A-III.11: Reusability and desorption studies data.

Concentration level	Absorbance (A.U)
1	-0.0002
2	0.7934
3	1.2031
4	1.8747
5	2.5653
6	2.9808

Table A-III.12: Reusability and desorption studies data.

C _i (mg/L)	C _e (mg/L)	C _i - C _e (mg/L)	Dose (g)	Volume (L)	%adsorbed	Recovered dose (g)	C _d (mg/L)	%desorbed
50.586	5.716	44.87	0.0396	0.04	88.70043	0.02668	0.648	2.143524
50.586	17.402	33.184	0.0404	0.04	65.59918	0.0404	2.44	7.352941
50.586	44.46	6.126	0.0410	0.04	12.11007	0.0354	-	-



University of Fort Hare
Together in Excellence

Ethics clearance

REC-270710-028-RA Level 01

Project Number: OKO021SSAM01

Project title: **Preparation and evaluation of pyrene grafted onto zinc oxide nanoparticles for the removal of organic contaminants from wastewater.**

Qualification: Masters in Chemistry (Full Dissertation)

Student name: Zipho Samuel

Registration number: 201607606

Supervisor: Prof O Okoh

Department: Chemistry

Co-supervisor: Dr M Ojemaye

On behalf of the University of Fort Hare's Research Ethics Committee (UREC) I hereby grant ethics approval for OKO021SSAM01. This approval is valid for 12 months from the date of approval. Renewal of approval must be applied for BEFORE termination of this approval period. Renewal is subject to receipt of a satisfactory progress report. The approval covers the undertakings contained in the above- mentioned project and research instrument(s). The research may commence as from the 03/11/20, using the reference number indicated above.

Note that should any other instruments be required or amendments become necessary, these require separate authorisation.

Please note that UREC must be informed immediately of

- Any material changes in the conditions or undertakings mentioned in the document;
- Any material breaches of ethical undertakings or events that impact upon the ethical conduct of the research.

The student must report to the UREC in the prescribed format, where applicable, annually, and at the end of the project, in respect of ethical compliance.

UREC retains the right to

- Withdraw or amend this approval if
 - Any unethical principal or practices are revealed or suspected;
 - Relevant information has been withheld or misrepresented;
 - Regulatory changes of whatsoever nature so require;
 - The conditions contained in the Certificate have not been adhered to.
- Request access to any information or data at any time during the course or after completion of the project.

Your compliance with Department of Health 2015 guidelines and any other applicable regulatory instruments and with UREC ethics requirements as contained in UREC policies and standard operating procedures is implied.

UREC wishes you well in your research.

Yours sincerely



Professor Renuka Vithal

Chairperson: University Research Ethics Committee

22 February 2021